REPORT NO. FAA-RD-72-128

MICROWAVE SCANNING BEAM APPROACH AND LANDING SYSTEM PHASED ARRAY ANTENNA

Volume I

R.M. Kalafus
G.J. Bishop
F.J. LaRussa
P.J. Pantano
W.R. Wade
R.S. Yatsko

FEBRUARY 1973
SECOND ANNUAL REPORT JULY 1971-JUNE 1972

Prepared for
DEPARTMENT OF TRANSPORTATION
FEDERAL AVIATION ADMINISTRATION
Systems Research and Development Service
Washington, D.C. 20591

TECHNICAL REPORT STANDARD TITLE PAGE

1. Report No.	2. Government Accession No.	3. Recipient's Catalog No.
FAA-RD-72-128 V.I		

4. Title and Subtitle	5. Report Date
Microwave Scanning Beam Approach and Landing System Phased Array Antenna Volume I	February 1973
	6. Performing Organization Code: TER
7. Author(s) R.M. Kalafus, G. J. Bishop, F.J. LaRussa, P.J. Pantano, W.R. Wade, R.S. Yatsko	8. Performing Organization Report No.: DOT-TSC-FAA-72-41
9. Performing Organization Name and Address Department of Transportation Transportation Systems Center Kendall Square Cambridge, MA. 02142	10. Work Unit No.: PPA-FA-209 11. Contract or Grant No.: R2104
12. Sponsoring Agency Name and Address Department of Transportation Federal Aviation Administration Systems Research and Development Service Washington, D.C. 20591	13. Type of Report and Period Covered: Annual Report July 1971-June 1972 14. Sponsoring Agency Code

15. Supplementary Notes

16. Abstract

The use of phased arrays for the proposed landing system (MLS) is discussed. Studies relating to ground reflections, near field focusing, and phased-array errors are presented. Two experimental antennas which were fabricated and tested are described. Complete component specifications as well as test results are included.

The first annual report, having the same title, was published in September 1971 as report number FAA-RD-71-87 (TSC-FAA-71-29).

This report, the second annual report, is printed in two volumes. Volume I contains sections 1 through 7.

17. Key Words	18. Distribution Statement
Aircraft Guidance; Cylindrical Arrays; Linear Arrays; Air Traffic Control; C-Band; Components; Stripline; Microstrip; Microwave Sources.	Document is available to the public through the National Technical Information Service, Springfield, Virginia 22151.

19. Security Classif. (of this report)	20. Security Classif. (of this page)	21. No. of Pages	22. Price
Unclassified	Unclassified	246	

Form DOT F 1700.7 (8-69)

PREFACE

The authors wish to acknowledge the efforts and assistance of G. G. Haroules, for his helpful discussions and guidance; J. A. Bottari, C. L. Dunne, J. W. Reardon, N. E. Rice, and W. J. Walsh for the fabrication, testing, and assembly of the antennas, components, and structure; I. Golini and D. Spangler, for the fabrication and testing of the control and logic equipment; and J. D. Owens for his computer programming assistance.

VOLUME I
CONTENTS

1. INTRODUCTION AND SUMMARY

CONTENTS

ILLUSTRATIONS

1.1 INTRODUCTION

The purpose of the work performed on this project is to assess the use of phased arrays for the microwave landing system (MLS), and to address the critical technological issues involved in the development of the system. The work has concentrated on C-band technology and the conventional scanning technique; however, many of the issues are the same for the Doppler scanning technique and Ku-band technology.

Phased arrays offer the potential of high reliability, variable scan and sweep rates, internal monitoring, long life and time-coding. The graceful degradation feature of phased arrays results in less down time. While the initial cost is higher than for mechanical scan, the long-term costs may be less.

During the first year, as reported in the first Annual Report, studies were performed which indicated that planar beams in azimuth are necessary; a circular array was found to satisfy the requirements, and a 4° azimuth antenna was designed with three candidate feed systems. Only one was intended to be carried through to the final stage, while the others were to be evaluated in terms of measured component behavior. Procurement difficulties dictated that a second antenna be also carried through to completion. The question of planar beams in elevation was not settled during the first year; a ground antenna configuration evolved during the second year which is believed to offer considerable improvement in system performance, and which allows either planar or conical beams to be used. This will be discussed in a separate report.

The antennas were designed not only to establish feasibility, but to address the critical issues. As such the arrays are designed to give variable scan and sweep rate, variable step size, variable sidelobe levels, sum or difference patterns, and are capable of being focused in the near field. It is anticipated that they will be used during the next year to perform critical experiments to help establish the system requirements.

Several documents are referred to repeatedly in this report, and are given in abbreviated form:

1. RTCA Report-"A New Guidance System for Approach and Landing", Radio Technical Commission for Aeronautics Special Committee 117 (RTCA SC-117), December, 1970 (Two volumes), DO-148.

2. First Annual Report-"Microwave Scanning Beam Approach and Landing System Phased Array Antenna", R. M. Kalafus, G. J. Bishop, P. Harris, G. G. Haroules, F. J. LaRussa, P. J. Pantano, B. Rubinger, and R. S. Yatsko, Report No. RD-71-87, September, 1971.

In the present report, a number of areas are covered. Studies were performed on the effect of phase and amplitude variations on beam pointing errors, near-field effects, the effect of ground reflections on the design of azimuth and elevation antennas, and monitoring. The design studies, component test results, and antenna range tests, static and dynamic, are given in the later chapters and appendices.

1.2 SUMMARY OF ACCOMPLISHMENTS

The major accomplishments of the program during FY 1972 were the following:

1. Design, procurement of components, testing of components, fabrication, assembly, and range testing of a lens-fed circular array. The range tests demonstrated the beam steering (step-scan) capability of the antenna as well as excellent beam shape and sidelobe levels.

2. Design, procurement of components, testing of components, fabrication and assembly of a continuous-scan electronic attenuator-fed circular array. As of the end of the fiscal year, assembly is 95% complete.

3. Successful procurement and acceptance of several state-of-the-art phased array components, at C-band, namely:

(a) Four-bit diode phase shifters with an average insertion loss of 1.8 dB; (b) Single-pole-two-throw RF switches; (c) Three-bit digital electronic attenuators with steps of 1.4 dB and a power-handling capability of 1 watt; (d) Transfer switches, having inputs on one side of stripline board, outputs on the other, an arrangement which allows for modularization of higher-order transfer matrices; (e) A solid state source having 2 watts output, and an amplifier giving 8 watts of power.

1.3 SUMMARY OF EVENTS AND DECISIONS

At the end of FY71 the procurement of components for two feed networks had reached the stage of contract awards, with deliveries scheduled for the end of September. Amendments were added on the switch and attenuator contracts to incorporate the logic drive circuitry, which added 4-6 weeks to the delivery schedule (phase shifters had drive circuitry in the original contract). By November it was apparent that the power divider, attenuator, and phase shifter procurements were in trouble, and termination proceedings were taken against the manufacturers of the power dividers and attenuators; new vendors were found, and new delivery schedules were for March and April, respectively. The phase shifters appeared to be heading for a late, but satisfactory delivery, but in February serious mechanical defects were found which the vendor was asked to correct.

The uncertainty of a satisfactory phase shifter shipment forced a decision to carry the lens-fed system through to the complete antenna assembly stage; originally it had been intended as a back-up position, to be carried through to the component stage only. This required a significant amount of manpower for designing logic for the antenna (manual and automatic), subsystem tests, cable design and procurement, and assembly. The reason this antenna could be developed was that a step-scan mode was possible which did not use phase shifters.

The elevation antenna had to be postponed for three reasons: The lateness of the phase shifters, the reprocurement of power dividers, and the fact that the key designer was removed from the project for 9 weeks due to higher priority requirements.

The phase shifters were delivered and accepted in June; the power dividers in May, and the attenuators in June. The logic for the attenuator-fed antenna was completed in June, leaving minor trouble shooting to be performed.

The loss of an engineer at mid-year caused the receiver assembly to be delayed. However, in June the receiver had been debugged and was performing statisfactorily in a time-code mode and was used for dynamic testing of the lens-fed antenna.

Range tests were performed during June. The tests involved about 200 static patterns, in order to test accuracy, sidelobe level, skew, near-field focusing, elevation patterns, variation with frequency, and fine scan. Dynamic patterns using the receiver were taken, and recorded on an X-Y plotter. These show the patterns which an aircraft receiver would see under ideal siting conditions. The results of the tests demonstrated the feasibility of C-band phased arrays for MLS application.

1.4 DISCUSSION OF WORK PERFORMED

The work performed during FY72 consisted of studies, design, procurement, fabrication, assembly, testing of antenna components and subsystems, and can be put into six categories: (1) Studies, (2) Lens-fed circular array, (3) Attenuator-fed circular array, (4) Linear array, (5) Receiver, and (6) Sources. These are discussed individually below.

1.4.1 Studies

These studies are an extension of work reported in the first annual report and address several of the critical issues raised by RTCA-SC-117.

A. Effects of Phase and Amplitude Variations on Beam Pointing Accuracy of Phased Arrays. A study was performed which yields the beam-pointing error resulting from phase and amplitude errors caused by quantization and random errors due to component imperfections. It was concluded that the resulting beam-pointing errors are not severe.

B. Performance of an R-2R Lens as a Phased Array Component. An experimental study was made of a circular, flat-plate, probe-fed cavity which serves as a lens in an R-2R antenna. Measured values indicate an insertion loss of about 1dB, r.m.s. phase fluctuation of 5°, and r.m.s. amplitude variation of 0.6dB. A surprising phenomenon occurred which is believed to be due to mutual coupling or curvature, namely that the phase center appears to be at the probes, rather than at the annular ring. It was concluded that the component is satisfactory, although in an antenna system it suffers from complexity.

C. Near-Field Effects. Near-field patterns of a linear array were computed which showed that the closest an aircraft can come to the antenna and maintain accurate guidance is $D^2/2\lambda$, where D is the effective linear dimension of the antenna, and λ is the wavelength. The question of focusing in the near-field was considered, and it was concluded that it is not a recommended procedure.

D. Ground-Reflection Effects and Antenna Height. Computations were performed on the effects of ground reflections on the performance of elevation and azimuth antennas. In the case of the azimuth antennas, reflections from the ground cause variation in the signal strength; the parameters in question are the receiver dynamic range and AGC time response. For the elevation antennas, the reflections cause errors in the angle

measurement. In both cases the antenna height is an important parameter. Guidelines have been derived which require experimental verification.

E. Monitoring. The effects of missing elements and elements with adverse phase conditions on the beam pointing error and sidelobe levels have been computed. A discussion of internal and external monitoring is given in section 5.

1.4.2 Lens-Fed Circular Array

The lens-fed circular array involves the following components: power divider, transfer switches, single-pole-four-throw switches, input cables, cavity lens, output cables, antenna structure, manual logic, automatic sweep logic, standard gain horn, reference, optical sighting instrument, and power supplies; additionally for the tests, mechanical attenuators were used to set up the distribution, and mechanical phase shifters used for tuning out cable errors and attenuator errors which would not exist in a prototype system. Component testing and subsystem testing were performed in preparation for range testing. Figure 1.4.1 is a front view of the antenna, showing antenna structure, elements, optical sighting mount, standard gain antenna, output cables and mechanical phase shifters as well as the antenna mount used. Figure 1.4.2 is a rear view showing power supplies, cavity lens, input cables, and manual logic box.

Range tests were performed at the Lincoln Laboratory Ground Reflection Range through the courtesy of the Antennas and Sites Group. This is an excellently equipped range, one which allowed a large number of reliable patterns to be obtained in a relatively short time. The results of the tests, static and dynamic, were considered to be quite satisfactory.

1.4.3 Attenuator-Fed Circular Array

The attenuator-fed circular array involves the following components: power dividers, four-bit diode phase shifters,

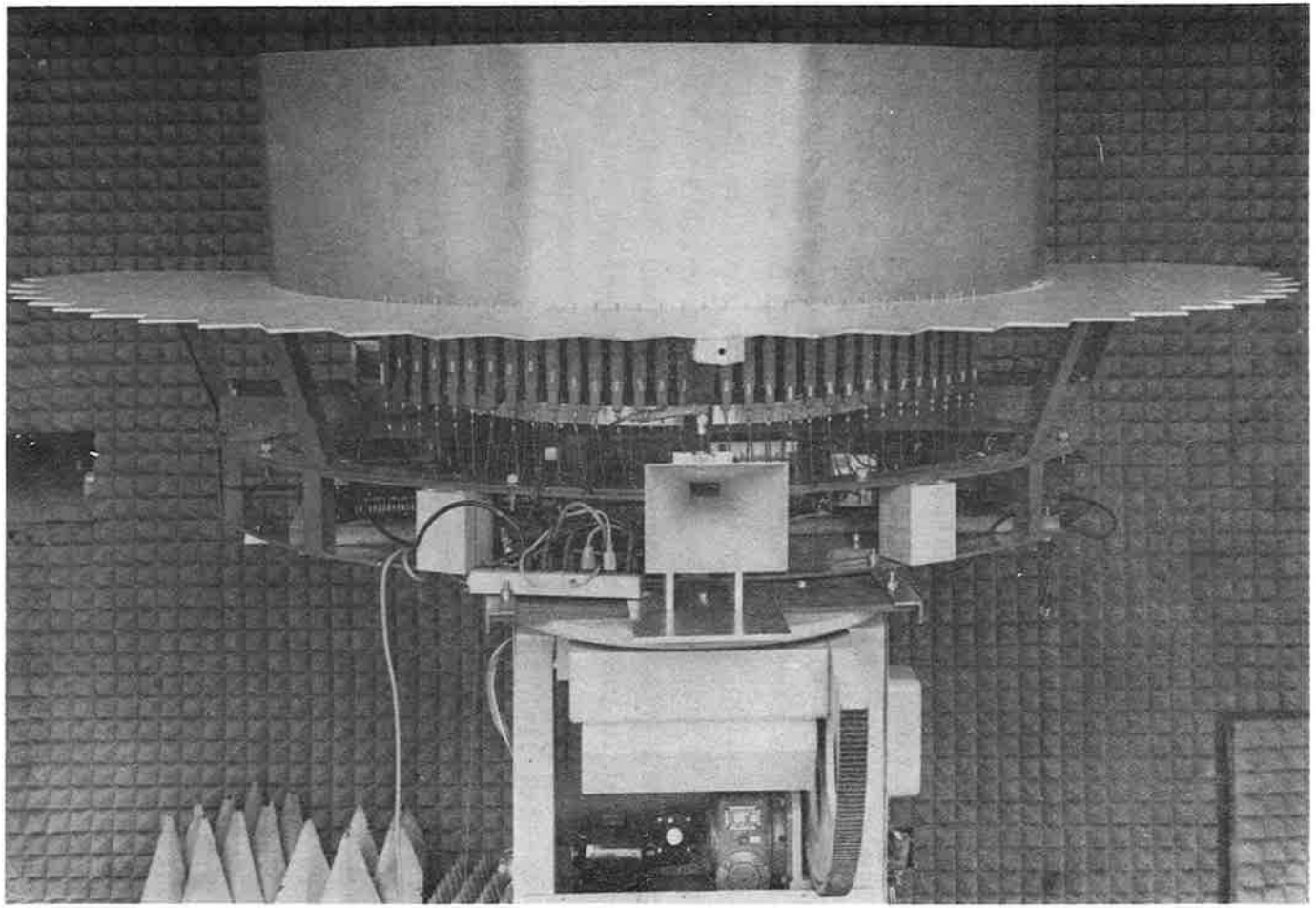

Figure 1.4.1 Front View of Lens-Fed Azimuth Antenna

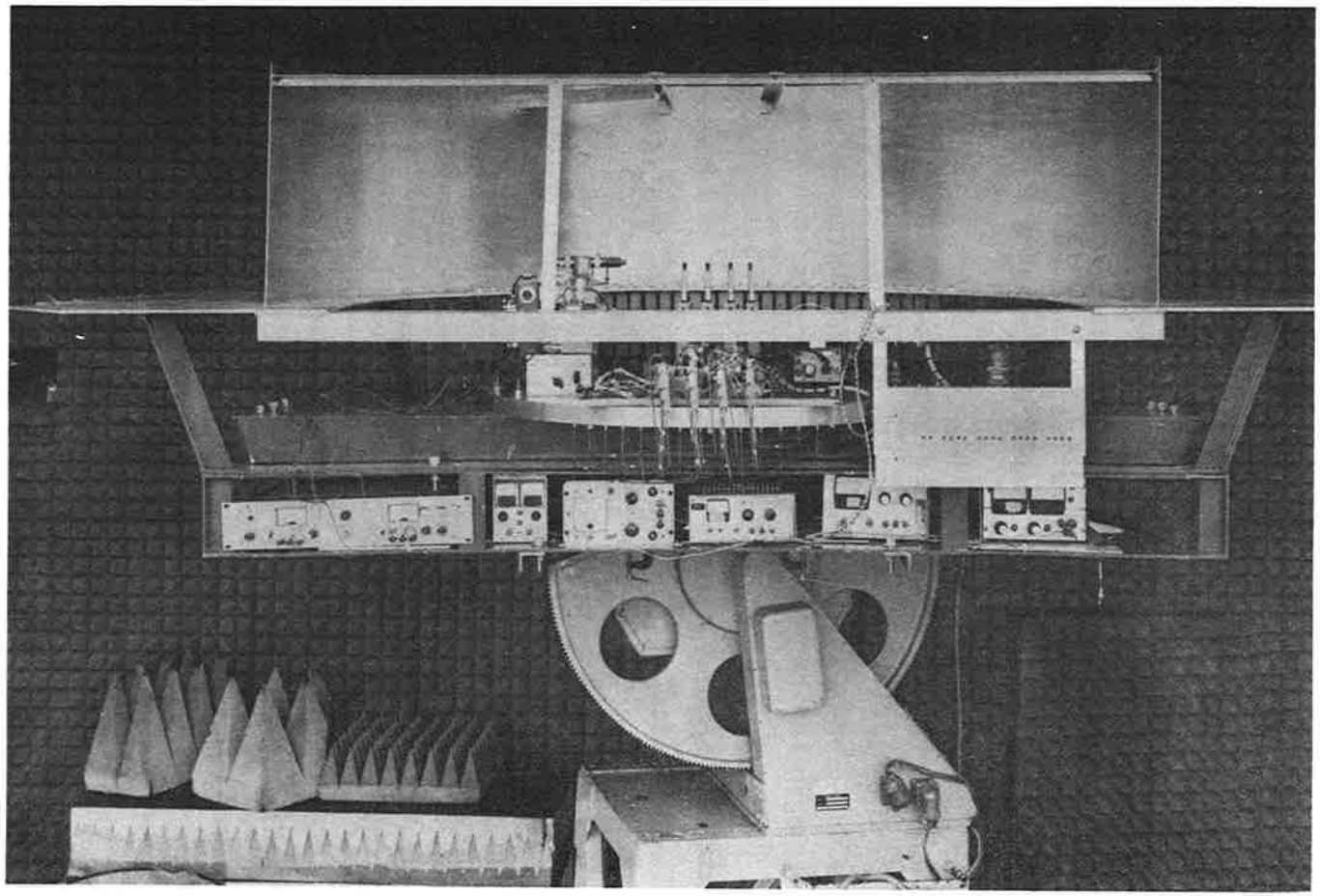

Figure 1.4.2 Rear View of Lens-Fed Azimuth Antenna

three-bit electronic attenuators, single-pole-two-throw switches, output cables, antenna elements, antenna structure, manual logic, sweep logic, control panel, control cables, monitoring lights, standard gain horn reference, optical sighting instrument, and power supplies. The logic is much more complicated than for the step-scan system, since the phase shifters and attenuators require extensive memory, plus the fact that a great deal of flexibility is included, namely, variable scan rate, variable sweep rate, variable step size, manual switching, and monitoring lights. The antenna, structure, and related equipment is the same as for the other circular array.

The work performed includes the procurement and extensive testing and retesting of components, fabrication and assembly of logic, cables, and control panel. There remains only assembly and testing of the complete antenna.

1.4.4 Linear Array

The elevation antenna was designed, and contracts awarded for phase shifters and power dividers. The elements were designed, but found to have a high unwanted cross-polarized component of radiation; the elements will have to be redesigned and fabricated. Attenuators and mechanical phase shifters necessary for setting up the aperture distribution and for near-field focusing are on hand. The only additional procurement is the logic to drive the phase shifters.

1.4.5 Receiver

A receiver for use in dynamic patterns was designed, and the components were procured. The unit is quite similar to the front end of the RTCA SC-117 design, and utilizes double conversion. The components were assembled, and the unit was debugged. Additional control circuitry was added to enable time-coding to be used. The unit was used with the lens-fed antenna

to obtain dynamic patterns (patterns in which the antenna is steered electronically--this corresponds to the amplitude of the signal seen by the aircraft).

1.4.6 Sources

Solid state C-band sources are critical items if reliable performance is to be achieved. Two narrow-band (40 MHz) varactor-multiplier chains utilizing X48 frequency multiplication were procured which yield 2 watts each and have spurious responses greater than 65dB below the signal. In addition, Standford Research Institute developed an 8-watt amplifier on a joint DOT/NASA contract (Contract DOT/TSC-158) monitored by this group. This represents state-of-the-art performance.

2. THE EFFECTS OF PHASE AND AMPLITUDE ERRORS ON PHASED ARRAY PERFORMANCE

CONTENTS

LIST OF ILLUSTRATIONS

LIST OF ILLUSTRATIONS (CONTINUED)

LIST OF TABLES

In general, phase errors at the elements of a phased array antenna cause both pointing errors and an increase in sidelobe level; amplitude perturbations do not cause pointing errors, but do contribute somewhat to a general rise in sidelobe level. Phase errors arise from random component imperfections and quantization by phase shifters. Random and quantization errors are similar in their effect on boresight shift and sidelobe level while the non-random nature of quantization causes sidelobes to appear in particular directions. Antenna designs requiring low sidelobes are more sensitive to phase errors than those not so stringent. For example, a given level of phase errors might affect an 18dB sidelobe antenna pattern very little, but would cause the sidelobes to rise from a design goal of 30dB to 24dB. The economic cost of a low sidelobe antenna is quite high since tighter tolerances are required on the components, which are then more expensive to produce.

Both random and quantization types of phase errors are considered in this section. The boresight errors depend upon the threshold used in the receiver to determine the beam center, as well as the processing used (beam center or centroid). The predictions developed here can be used to tailor each beam portion of an array and correct for quantization errors by appropriately adjusting the phase shift command memory in the control logic.

2.1 DEVELOPMENT OF EXPRESSIONS FOR THE EFFECT OF PHASE PERTURBATIONS ON THE LOCATION OF THE BEAM CENTER AND BEAM PEAK

ABSTRACT

The effects of phase perturbation depend on the process used to determine the location of the beam center; that is, the beam peak, -3 dB beam center, -10 dB beam center, and null beam center are affected differently by phase perturbations. Expressions are developed for different definitions of beam center (and for a difference beam null) for both linear and circular arrays. These expressions give the beam center motion for a small ($\leq 45°$) phase error on one phase shifter, as a function of the location on the array of the affected element.

2.1.1 Introduction

This section deals with the effect of phase errors on the beam pointing accuracy of phased arrays. These errors can be caused by unit-to-unit variations, imbalances, or by quantization in the feed components. The approach taken here is to examine the effect of a perturbation at a single array element. The results are easily extendable to calculating the effects of perturbations at any number of elements. A major point of this section is that the effects of phase perturbation depend on the process used to determine the beam pointing angle. Results are given for several definitions in common usage.

In this section, the terms "beam peak", and "beam center", have specific meanings: "beam peak" refers to the point on the antenna pattern of maximum radiation - it has more mathematical than practical meaning; "beam center" is defined as the halfway point between points on opposite sides of the main beam which are at some specified power level below maximum (threshold) [e.g. "10 dB beam center," "null beam center", etc.] - its location varies with different specified levels.

Past work has primarily been devoted to the effects of phase perturbations on the beam peak and monopulse null in linear arrays.[1, 2, 3] Hatcher[1] discussed primarily the effect of quantized phase shifts near the ends of a uniformly illuminated linear array on beam peak motion. Jones, et al.[2] derived an expression for the beam peak and difference null error caused by phase errors in linear arrays. Frank and Ruze[3] likewise discussed the sum and difference beam motions in linear arrays, and pointed out the different dependence of the sum beam peak motion and difference beam

[1] Burrell R. Hatcher, Granularity of Beam Positions in Digital Phased Arrays Proc. IEEE, Vol. 56, Nov. 1968, p. 1795.

[2] Allen Jones, Chris Hemmi and Glen Gaustad, Factors Affecting Beam Granularity and Pointing Accuracy in an Electronically Scanned Phased Array, 18th Annual Symposium on USAF Antenna R&D, Oct. 1968.

[3] J. Frank and John Ruze, Beam Steering Increments for a Phased Array, IEEE Trans. Antennas and Propagation, Nov. 1967, p. 820.

null motion on the element location. The present work deals additionally with beam center motion, which differs from the beam peak, and applies to circular arrays as well. The results can be rather trivially extended to quite arbitrary arrays, having unequally spaced elements, and not lying along a regular contour. As stated above, the treatment is believed to be more useful in that the beam center definitions are more closely related to processing schemes in actual use.

One of the chief uses of the results lies in the control commands of circular arrays, where the switched distribution allows a fairly simple logic control and one which permits precise tailoring of beam pointing. By using the results here, one or two phase shift commands can be adjusted which correct in one iteration for the pointing error due to phase quantization.

2.1.2 General Expression for the Effect of Phase Perturbations on the Location of the Beam Center and Beam Peak

It is possible to derive an expression for the motion of the beam center, as defined by leading and trailing beam edges, which applies to any array which forms a coherent beam, either a sum or difference beam. From the general formulation, the specific application to linear and circular arrays can be derived for an arbitrary beam edge definition.

The basic idea involved is the following: the unperturbed power pattern $f_o^* f_o(\phi)$ of any antenna forming a coherent beam has beam edges at ϕ_o defined by

$$f_o^* f_o(\phi_o) = K^2 \tag{2.1.1}$$

where K^2 is the power level used to define the beam edges (e.g., -3 dB point, -10 dB point, etc.). The effect of the perturbation is to shift the beam slightly. If $f^* f(\phi)$ is the perturbed field, then the problem is to find the new beam edges at ϕ such that

$$f^* f(\phi) = f_o^* f_o(\phi_o) = K^2 \tag{2.1.2}$$

This is accomplished by expanding $f^*f(\phi)$ in a Taylor series around the unperturbed beam edge ϕ_o :

$$f^*f(\phi) = f^*f(\phi_o) + (\phi - \phi_o) \frac{d}{d\phi} f^*f(\phi)\Big|_{\phi = \phi_o} \qquad (2.1.3)$$

The shift of the beam edge is then given by

$$\Delta\phi_o = \phi - \phi_o = \frac{f_o^*f_o(\phi_o) - f^*f(\phi_o)}{\frac{d}{d\phi}f^*f(\phi)\Big|_{\phi = \phi_o}} \qquad (2.1.4)$$

where ϕ_o is defined by equation (2.1.1).

A general cophasal array of N elements having omnidirectional elements and lying in the x-y plane has a far field behavior given by

$$f_o(\phi) = \sum_{n=1}^{N} A_n e^{ju_n(\phi)} \qquad (2.1.5)$$

where

$$u_n(\phi) = kx_n(\cos\phi - \cos\phi_b) + ky_n(\sin\phi - \sin\phi_b) \qquad (2.1.6)$$

Here (x_n, y_n) is the location of the phase center of the nth element, ϕ is the observation angle, ϕ_b is the pointing angle, and k is the wave number. The unperturbed power pattern is thus

$$f_o^*f_o(\phi) = \sum_n \sum_m A_nA_m\cos(u_n - u_m) \qquad (2.1.7)$$

If a phase perturbation of ϵ_p is introduced at the p-th element, the perturbed pattern is given by

$$f(\phi) = \sum_n A_n e^{ju_n(\phi)} e^{-j\epsilon_n \delta_{np}} \tag{2.1.8}$$

where $\delta_{np} = 1$ if $n = p$, but is zero otherwise. The power pattern $f^*f(\phi)$ can be written as:

$$f^*f(\phi) = \sum_n \sum_m A_n A_m \cos(u_n - u_m) + 4A_p^2 \sin^2(\epsilon_p/2) - 4A_p \sin(\epsilon_p/2) \sum_n A_n \sin(u_n - u_p + \epsilon_p/2) \tag{2.1.9}$$

The first term on the right is simply the unperturbed pattern $f_o^*f(\phi)$. By substituting into equation (2.1.4), and ignoring higher order terms in $\sin(\epsilon_p/2)$, the beam edge shift is found by

$$\Delta\phi_o = \frac{-4A_p \sin(\epsilon_p/2) \sum_n A_n \sin(u_{n_o} - u_{p_o} + \epsilon_p/2)}{\sum_n \sum_m A_n A_m (u_{n_o}' - u_{m_o}') \sin(u_{n_o} - u_{m_o})} \tag{2.1.10}$$

where $u_{n_o} = u_n(\phi_o)$ and $u_{n_o}' = \frac{d}{d\phi} u_n(\phi)\Big|_{\phi = \phi_o}$. After some manipulation:

$$\begin{aligned}
NUM &= \left\{-2A_p \sin(\epsilon_p/2)\right\} \cdot \left\{\cos(u_{p_o} - \epsilon_p/2) \textstyle\sum_n A_n \sin u_{n_o} - \sin(u_{p_o} - \epsilon_p/2) \sum_n \cos u_{n_o}\right\} \\
DENOM &= \left\{\textstyle\sum_n A_n u_{n_o}' \sin u_{n_o} \sum_m A_m \cos u_{m_o}\right\} - \left\{\sum_n A_n \sin u_{n_o} \sum_m A_m u_{m_o}' \cos u_{m_o}\right\} \\
\Delta\phi_o &= NUM/DENOM
\end{aligned} \tag{2.1.11}$$

It now becomes necessary to distinguish between left and right edges of the beam; both must satisfy equations (2.1.2), and

(2.1.11) gives the motion of each. Then by the definition of the beam center, the beam center shift is given by $\Delta\phi$, where

$$\Delta\phi = \frac{\Delta\phi_\ell + \phi_r}{2} \qquad \text{(radians)} \qquad (2.1.12)$$

where $\Delta\phi_\ell$ and $\Delta\phi_r$ are the shifts of the left and right edges of the beam, respectively.

If all phase shifters have errors, then the total beam shift is given by summing (2.1.11) over all N elements, provided that the average error is small.

The beam peak can be found by taking the limit of (2.1.12) as ϕ approaches the intended boresight angle ϕ_b. The motion of the peak and nulls can also be determined by setting the first derivative of the power pattern to zero. The results are identical to those derived here.

2.1.2.1 Expressions for Beam Motion for Linear Arrays - If a linear array is used, the u_n's are defined by

$$u_n = \left(n - \frac{N+1}{2}\right) kd\,(\sin\phi - \sin\phi_b) \qquad (2.1.13)$$

where k is the wave number, d the spacing between adjacent elements, ϕ the observation angle, and ϕ_b the intended beam direction. The elements are assumed equally spaced along the y-axis. This can be abbreviated to read

$$u_n = q_n u(\phi) \qquad (2.1.14)$$

where $q_n = n - \frac{N+1}{2}$ and $u = kd\,(\sin\phi - \sin\phi_b)$.

2.1.2.1.1 Expression for Sum Beam Center Motion in Linear Arrays - Several properties can be observed from equation (2.1.14). One is that $u_{N+1-n} = -u_n$, so that for symmetric distributions, where $A_{N+1-n} = A_n$,

$$\sum_n A_n \sin u_n = 0 \tag{2.1.15}$$

and from (2.1.11)

$$\Delta\phi_o = \frac{2A_p \sin(\epsilon_p/2) \sin(q_p u_o - \epsilon_p/2)}{u_o' \sum_n A_n q_n \sin q_n u_o} \tag{2.1.16}$$

where $u_o = u(\phi_o)$. From equation (2.1.15), the unperturbed pattern reduces to

$$f_o^* f_o(\phi) = \left(\sum_n A_n \cos q_n u\right)^2 \tag{2.1.17}$$

The pattern peaks at $u = 0$, where $\phi = \phi_b$. It can be seen from (2.1.17) that $f_o^* f_o(\phi_\ell) = K^2$ if $f_o^* f_o(\phi_r) = K^2$, and if ϕ_ℓ satisfies

$$u(\phi_\ell) = u_\ell = -u(\phi_r) = -u_r \tag{2.1.18}$$

or

$$\sin\phi_\ell = 2 \sin\phi_b - \sin\phi_r \tag{2.1.19}$$

Also, $u'(\phi) = kd \cos\phi$, so that from (2.1.12) and (2.1.14), the beam shift becomes

$$\Delta\phi = \frac{A_p \sin(\epsilon_p/2)}{kd \sum_n A_n q_n \sin q_n u_r} \left\{ \frac{\sin(q_p u_r - \epsilon_p/2)}{\cos\phi_r} + \frac{\sin(q_p u_\ell + \epsilon_p/2)}{\cos\phi_\ell} \right\} \tag{2.1.20}$$

For reasonably narrow-beam antennas, $\cos\phi_r$ and $\cos\phi_\ell$ can be approximated by $\cos\phi_b$, giving

$$\Delta\phi = \frac{A_p \sin\epsilon_p \sin(q_p u_r)}{kd \cos\phi_b \sum_n A_n q_n \sin(q_n u_r)} \qquad (2.1.21)$$

2.1.2.1.1.1 Expression for Sum Beam Peak Motion for Linear Arrays - The motion of the beam peak may be obtained by taking the limit of (2.1.21) as u_r vanishes. The beam peak motion is thus given by

$$\Delta\phi = \frac{A_p\left(p - \frac{N+1}{2}\right) \sin\epsilon_p}{kd \cos\phi_b \sum_n A_n\left(n - \frac{N+1}{2}\right)^2} \qquad (2.1.22)$$

Several properties can be noted from this: (1) for elements near the center, $\left|p - \frac{N+1}{2}\right|$ is small, and the resultant beam peak motion is small; (2) the beam peak motion is proportional to the voltage excitation coefficient of the perturbed element; (3) a perturbation of an element to the left of center causes a beam peak shift equal to one to the right of center, but opposite in direction; (4) for scan angles off broadside, the beam peak shift increases; however, the beam broadens by the same factor, so that the shift in fractions of a beamwidth is constant.

Further insight is gained by considering a uniform distribution, where $A_n = 1$, the beam peak shift is

$$\Delta\phi = \frac{6\left(\frac{p}{(N+1)/2} - 1\right)\sin\epsilon_p}{kd \cos\phi_b \, N(N-1)} \qquad (2.1.23)$$

The beam peak shift is approximately inversely proportional to the square of the number of elements. Since the beamwidth is approximately inversely proportional to the number of elements, the beam peak shift in fractions of a beamwidth is inversely proportional

to the number of elements. Thus, the narrower the beamwidth, the less the effect of a phase perturbation at one element measured in fractional beamwidths. This behavior is true of sum beams in general.

2.1.2.1.1.2 Expression for Sum Null Beam Center Motion for Linear Arrays - Another instructive case is that of a uniform linear array where the beam center is defined by the nulls ($K^2 = 0$). In this case, (2.1.17) reduces to

$$f_o^* f_o = \left(\frac{\sin \frac{Nu}{2}}{\sin \frac{u}{2}} \right)^2 \tag{2.1.24}$$

This obviously has main beam nulls at $u = \pm 2\pi/N$. After some manipulation (2.1.21) reduces to

$$\begin{aligned} \Delta\phi &= \frac{\sin\epsilon_p \sin(2q_p\pi/N)}{kd\cos\phi_b \sum_n q_n \sin(2q_n\pi/N)} \\ &= \frac{2\sin\epsilon_p \sin(\pi/N)\sin\left[\left(p - \frac{N+1}{2}\right)\frac{2\pi}{N}\right]}{Nkd\cos\phi_b} \\ &= \frac{2\pi\sin\epsilon_p \sin\left[\left(p - \frac{N+1}{2}\right)\frac{2\pi}{N}\right]}{N^2 kd\cos\phi_b} \end{aligned} \tag{2.1.25}$$

Comparison of this result with the beam peak motion in (2.1.23) shows that while the beam peak is most strongly affected by phase errors at the edge of the array, the same errors have little effect on the null beam center motion in (2.1.25). This comparison is shown in Figure 2.1.1 for $\phi_b = 0$, along with beam center motion for the beam edges defined at the -3 dB and -10 dB points.

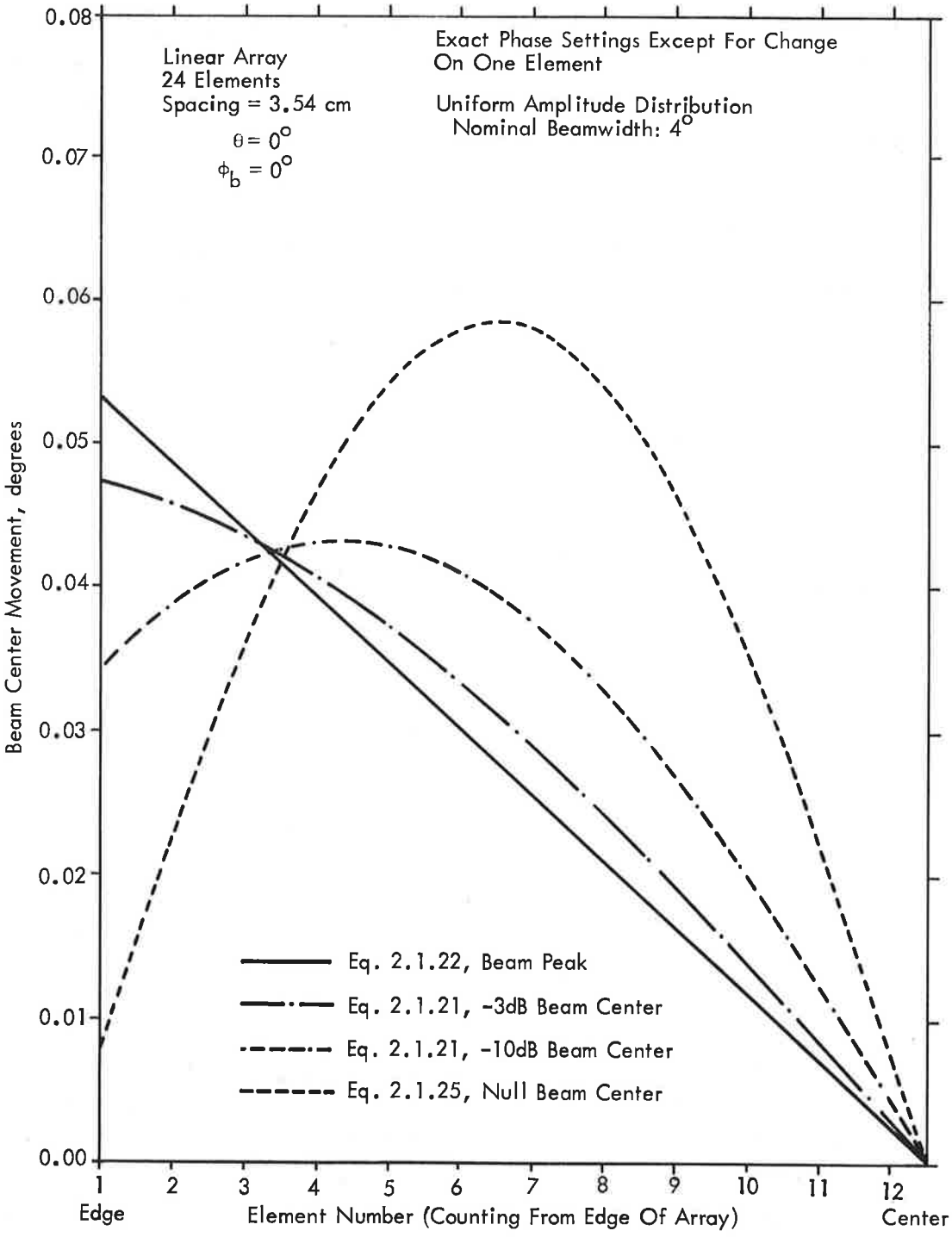

Figure 2.1.1 Calculated Effect of a 22.5° Change in One Phase Shifter on the Beam Center Position-Uniform Amplitude Distribution, Linear Array

Figure 2.1.2 shows the beam motion for the same array using a tapered amplitude distribution. The particular amplitude distribution assumed is a cosine-squared-on-a-pedestal type, given by

$$A_n = \frac{p + \cos^2\left[\left(\frac{n - \frac{N+1}{2}}{N-1}\right)\pi\right]}{1+p} \qquad (2.1.26)$$

where p is chosen here as 1/2.

Figures 2.1.3 and 2.1.4 show the effect of scanning the beam of the array used in Figure 2.1.2 out to azimuth angles 15° and 30° respectively. It can be seen that even the simpler formula, equation (2.1.21), holds very well out to 30° of scan.

2.1.2.1.2 Expression for the Difference Beam Null Motion for Linear Arrays - The difference beam motion exhibits a different behavior. It can be derived from equation (2.1.11) by assuming that $A_{N+1-n} = -A_n$. That is, the distribution is anti-symmetric, a condition which is attained if a hybrid feeds each element pair of the array. The difference signal on receive corresponds approximately with phase monopulse. Here the beam null is of most interest. The definition of the element phase $u_n(\phi)$ remains the same, so that $u_{N+1-n} = -u_n$. Then,

$$\sum_n A_n \cos u_n(\phi) = 0 \qquad (2.1.27)$$

and equation (2.1.11) becomes

$$\Delta\phi = \frac{A_p \sin\epsilon_p}{kd\cos\phi_b \sum_n A_n\left(n - \frac{N+1}{2}\right)} \qquad (2.1.28)$$

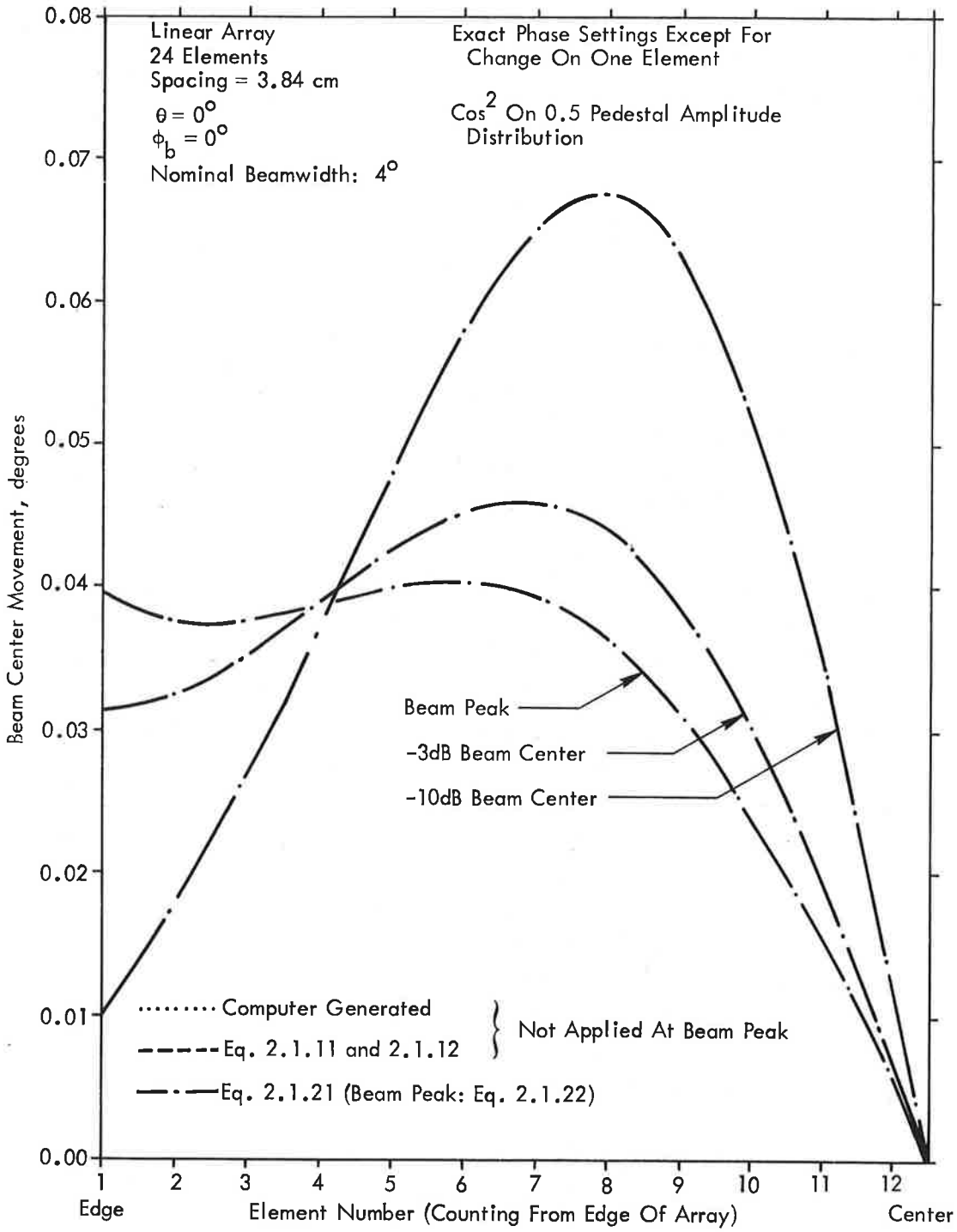

Figure 2.1.2 Calculated Effect of a 22.5° Change in One Phase Shifter on the Beam Center Position-Tapered Distribution, Linear Array

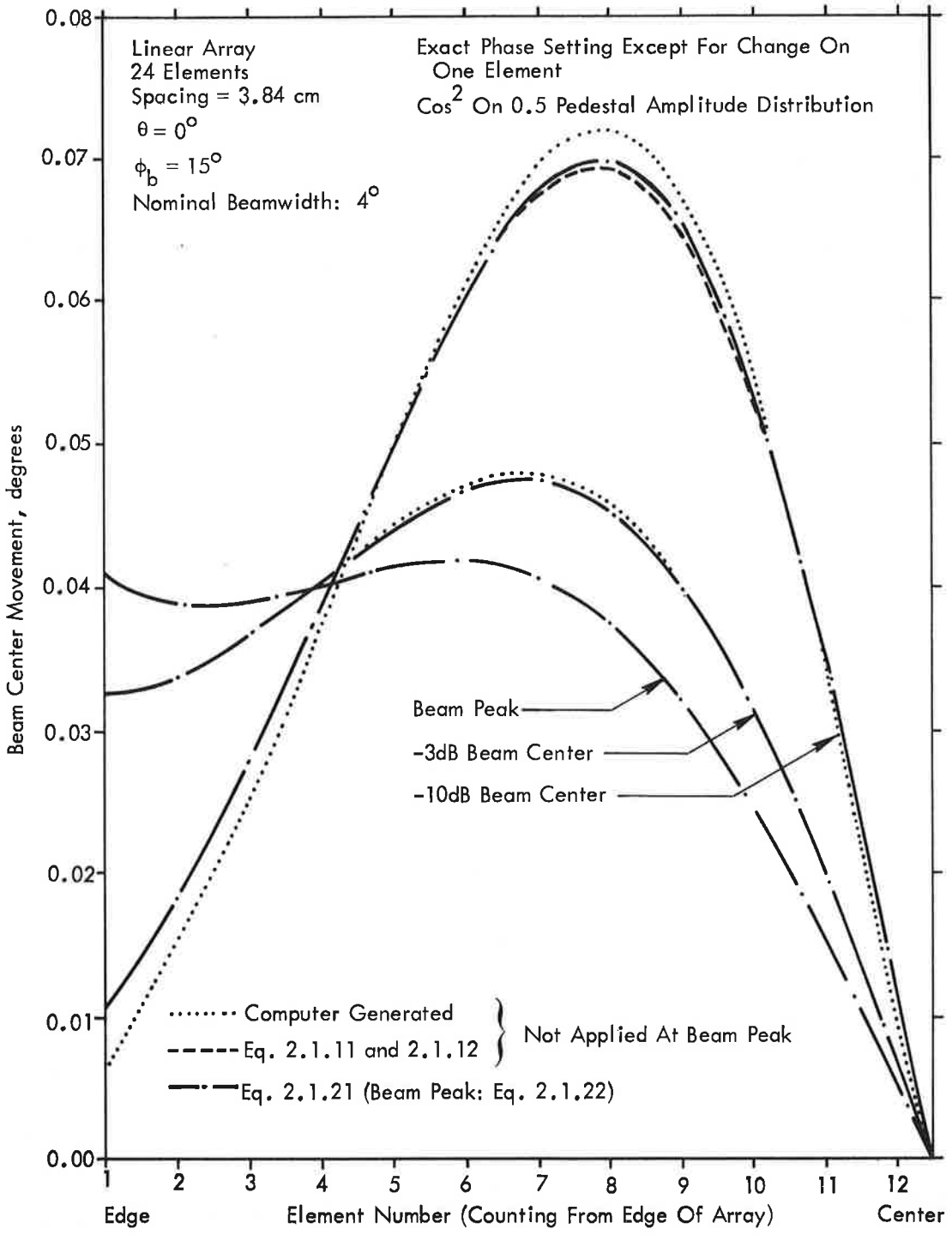

Figure 2.1.3 Calculated Effect of a 22.5° Change in One Phase Shifter on the Beam Center Position-Linear Array, Scanned to 15°

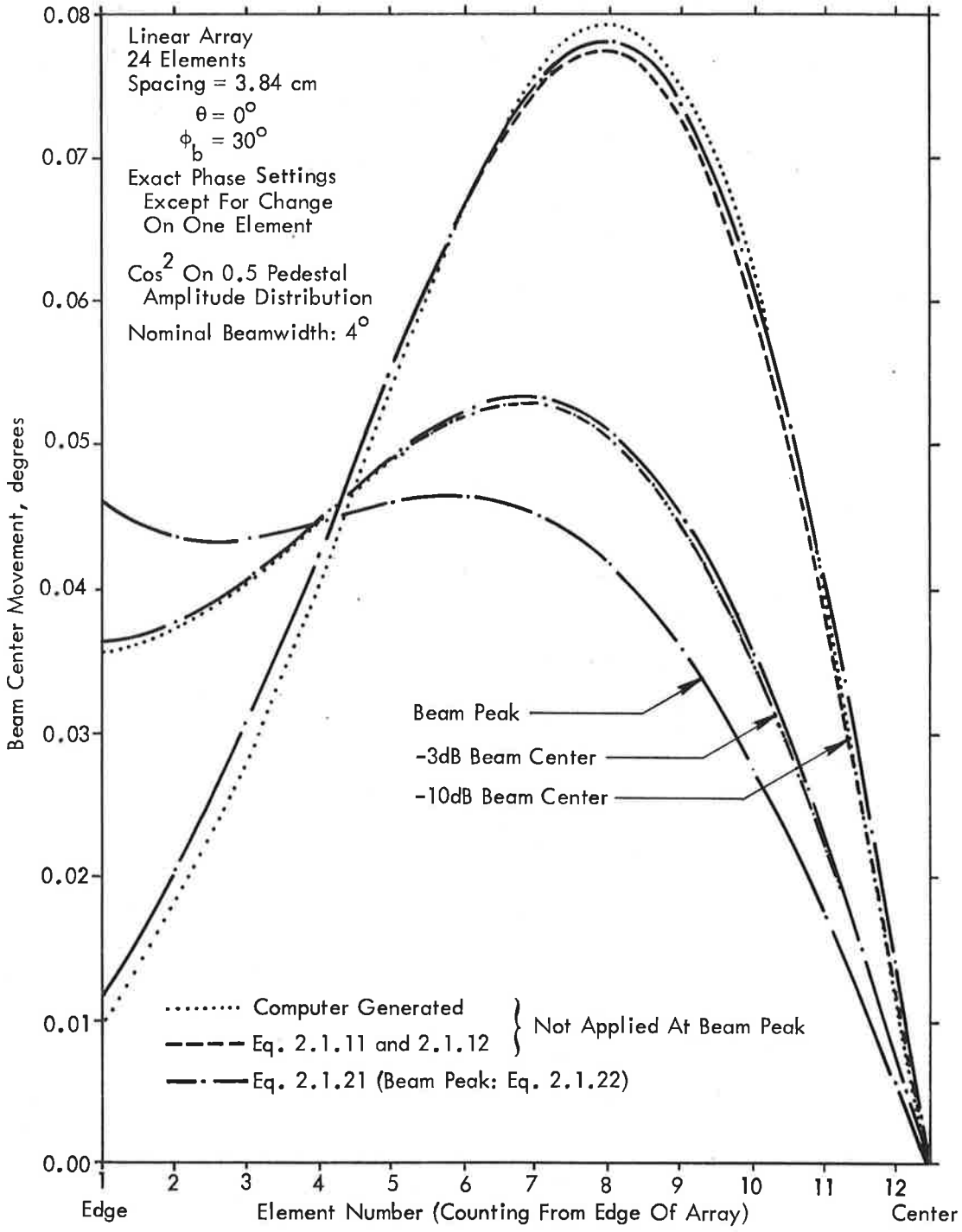

Figure 2.1.4 Calculated Effect of a 22.5° Change in One Phase Shifter on the Beam Center Position-Linear Array, Scanned to 30°

Thus for a difference beam, a given phase perturbation results in the same null shift, independently of element location. For a uniformly illuminated linear array, this reduces to

$$\Delta\phi = \frac{-4A_p \sin\epsilon_p}{N^2 kd \cos\phi_b} \tag{2.1.29}$$

where $A_p = \pm 1$, depending on which side of center the element is located. It can be seen that the same dependence on the number of elements exists for the difference beam as for the sum beam.

2.1.2.2 Expressions for Beam Motion for Circular Arrays - The formulation for circular arrays is not as general as for the linear arrays. The reason for this is that the property $u_{N+1-n} = -u_n$ holds only for scan angles near broadside. For a circular array having an active sector from $-\phi_a/2$ to $+\phi_a/2$,

$$\begin{aligned} u_n(\phi) &= kR[\cos(\phi - \phi_n) - \cos(\phi_b - \phi_n)] \\ &= kR\cos\phi_n(\cos\phi - \cos\phi_b) + kR\sin\phi_n(\sin\phi - \sin\phi_b) \end{aligned} \tag{2.1.30}$$

where R is the array radius, and ϕ_n is the angular location of the element. The elements can be arranged so that $\phi_{N+1-n} = -\phi_n$; the second term of (2.1.30) then satisfies the anti-symmetric relation, but the first does not. However, for angles near boresight ($\phi \approx \phi_b$), with ϕ_b small, the second term dominates, and the relation is approximately true.

2.1.2.2.1 Expression for Sum Beam Center and Beam Peak Motion for Circular Arrays - With the above limitation, equation (2.1.12) becomes, for the sum beam,

$$\Delta\phi = \frac{A_p \sin\epsilon_p \sin[kR\sin\phi_p(\sin\phi_r - \sin\phi_b)]}{kR\cos\phi_b \sum_n A_n \sin\phi_n \sin[kR\sin\phi_n(\sin\phi_r - \sin\phi_b)]} \tag{2.1.31}$$

The beam peak motion reduces to

$$\Delta\phi = \frac{A_p \sin\epsilon_p \sin\phi_p}{kR \cos\phi_b \sum_n A_n \sin^2\phi_n} \qquad (2.1.32)$$

The distance of the p-th element from the center along the y-axis is $R \sin\phi_p$, so that the differences between the circular array formulas and those of the linear array are merely the y-components of the element locations; i.e., if the element locations of a circular array were staggered such that the projections onto the y-axis were equally spaced, the formulas would be identical.

It is evident that the reason that the circular array formulas are limited to scan angles near broadside lies in the fact that the element locations deviate from a straight line. This can be seen by looking at the phase factor of an arbitrary symmetric array in the x-y plane:

$$u_n(\phi) = kx_n(\cos\phi - \cos\phi_b) + ky_n(\sin\phi - \sin\phi_b) \qquad (2.1.33)$$

where

$$x_{N+1-n} = x_n, \text{ and } y_{N+1-n} = -y_n.$$

The second term on the right satisfies the anti-symmetric condition, but the first does not. When the first term is constant with n, the scan angle is umlimited, but not otherwise. The motion of the beam can, of course, still be derived from equations (2.1.9) and (2.1.10).

Figures 2.1.5 and 2.1.6 show the results for circular array of radius 88.3 cm and an active sector of 60°, using the approximate formulas (2.1.31) and (2.1.32) as well as the more exact formulas (2.1.11) and (2.1.12). In this case the simpler formulas are essentially as good as the more exact formulas for scan angles

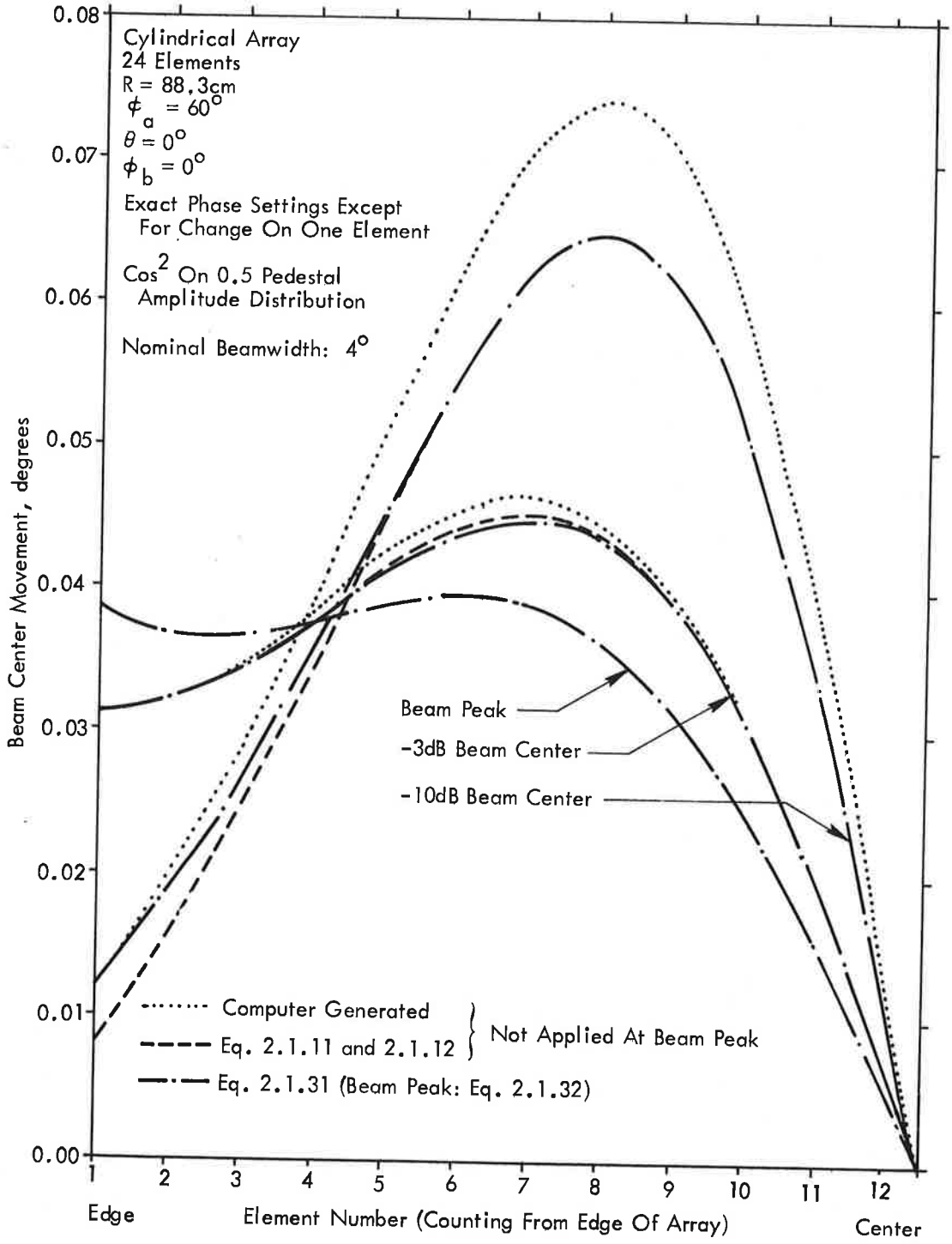

Figure 2.1.5 Calculated Effect of a 22.5° Change in One Phase Shifter on the Beam Center Position-Broadside -Circular Array

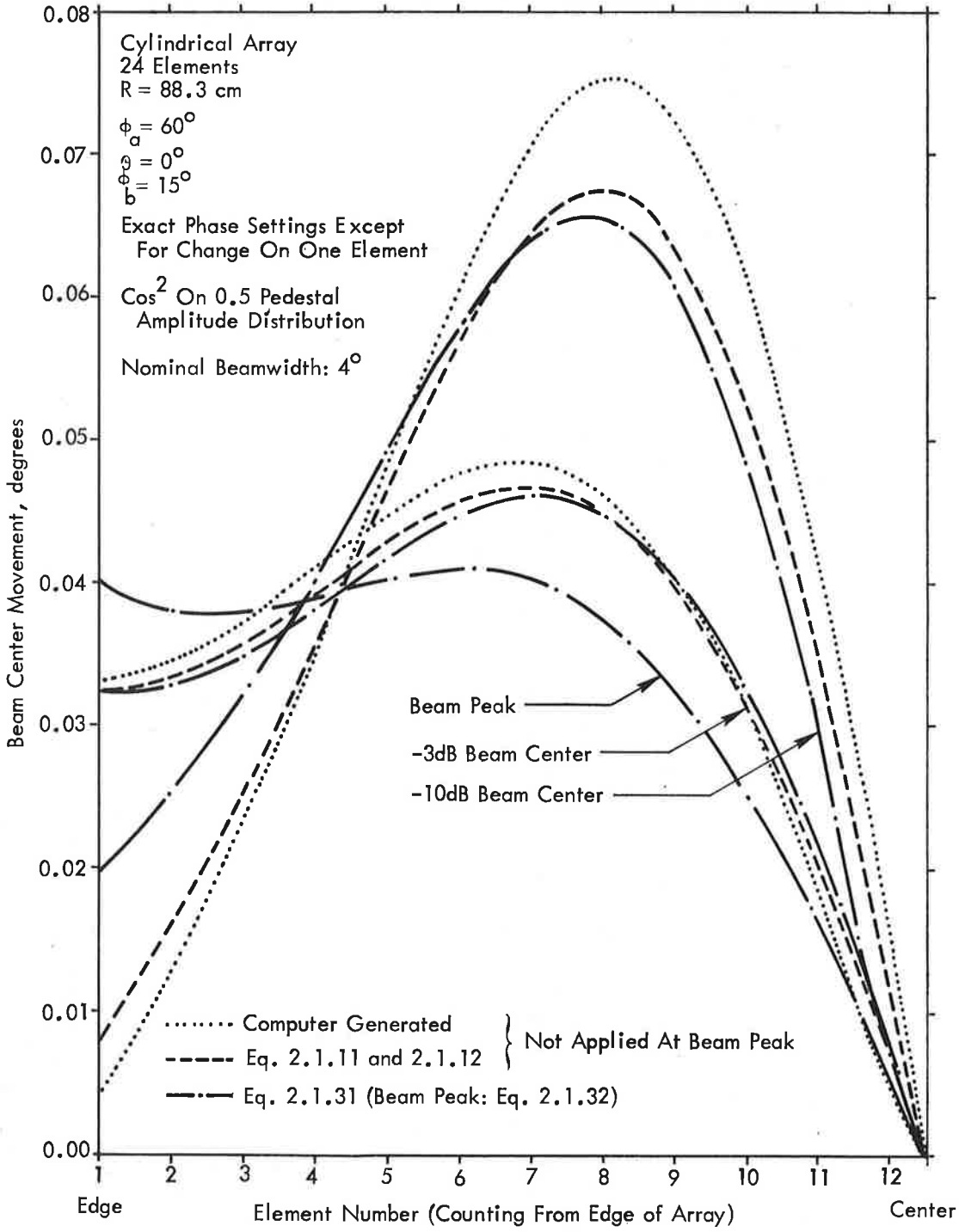

Figure 2.1.6 Calculated Effect of a 22.5° Change in One Phase Shifter on the Beam Center Position-Circular Array-Scanned to 15°

out to $\pm 5°$. Most circular array feed networks involve coarse-fine switching techniques, which means that the actual scan angles involved are quite small, and the simpler formulas hold to a high degree of accuracy.

2.1.2.2.2 Expression for Difference Beam Center Motion for Circular Arrays - The motion of the null of the difference pattern for a circular array is given by

$$\Delta\phi = \frac{A_p \sin\epsilon_p}{kR \cos\phi_b \sum_n A_n \sin\phi_n} \qquad (2.1.34)$$

The amount of beam null shift is independent of the element location, as with a linear array. Figure 2.1.7 shows the beam motion for a circular array of radius 88.3 cm, an active sector of 60°, and 24 elements. Here the phase error is assumed to be 22.5° and the amplitude distribution is given by

$$A_n = \frac{\pi}{\phi_A} \sin\left(\frac{3\pi\phi_n}{\phi_A}\right) - \frac{2p\phi_n}{\phi_A}, \quad p = 1/2 \qquad (2.1.35)$$

The -3 dB lobe widths are 3.30°.

2.2 EFFECTS OF RANDOM PHASE ERRORS ON BORESIGHT ANGLES AND SIDELOBES

ABSTRACT

To obtain an estimate of the overall effect of inherent component errors on the boresight angles and sidelobe levels, a brief study was conducted wherein the error on each element was chosen randomly between set limits. The results indicate that for the array considered, (4° beamwidth, circular), random errors ranging between ±15° on each element may produce beam pointing errors of nearly a whole fine scan position, or 0.08°.

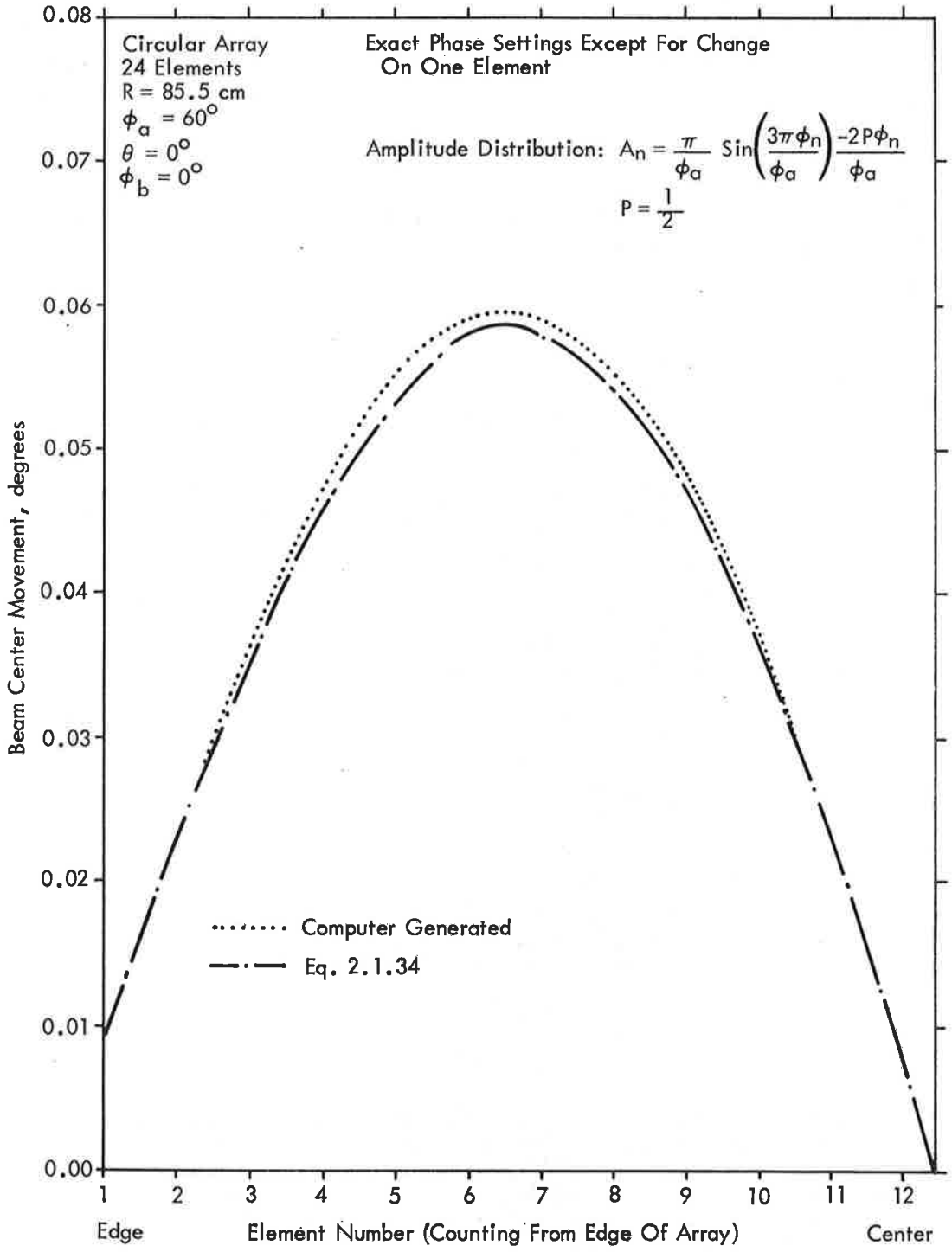

Figure 2.1.7 Calculated Effect of a 22.5° Change in One Phase Shifter on the Beam Null Position of a Difference Beam

Since the inherent errors in the components will combine to produce a different variation from the nominal (quantized) phase setting at each element, a brief study was conducted to obtain an estimate of the effect of these errors on beam direction and sidelobe level.

It should be noted that the errors at the elements caused by the inherent component errors are not random once the system is assembled and operating. In fact, from one fine scan position to the next, only two or three phase shifters will change state, thus only about three out of twenty four elements will have different errors. However, in a particular state the distribution of phase errors on the elements and the limits between which these errors range are determined by all the errors (phase, amplitude, VSWR) in all the components in the system. If the components were connected in a different arrangement, a very different distribution of phase errors on the elements would result. Therefore, exactly what error appears on a particular element is a function of how the components of the system were combined as well as a function of which portion of the scan is being examined, components are usually randomly combined.

Thus, as a first approximation for determining the effect of component errors on antenna performance the phase error on each element was chosen from a uniform random distribution with set limits such as ± 10 degrees. The resulting average effects on beam pointing and sidelobe level are shown in Figures 2.2.1 and 2.2.2. These results indicate that random errors ranging between $\pm 15°$ on all elements may produce beam pointing errors of nearly a whole fine scan position.

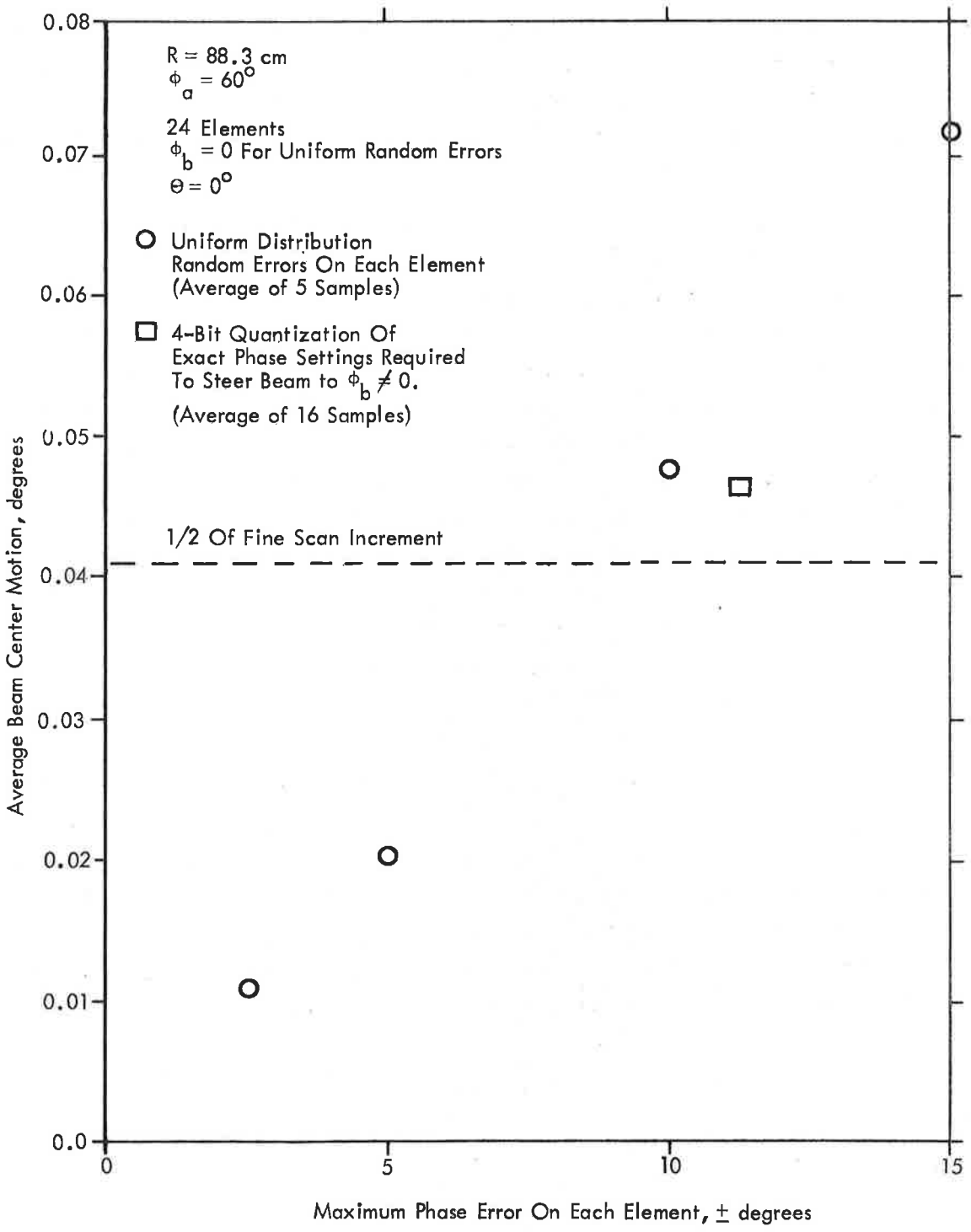

Figure 2.2.1 Calculated Average Beam Center Motion Due to Random Phase Errors Applied to All Elements

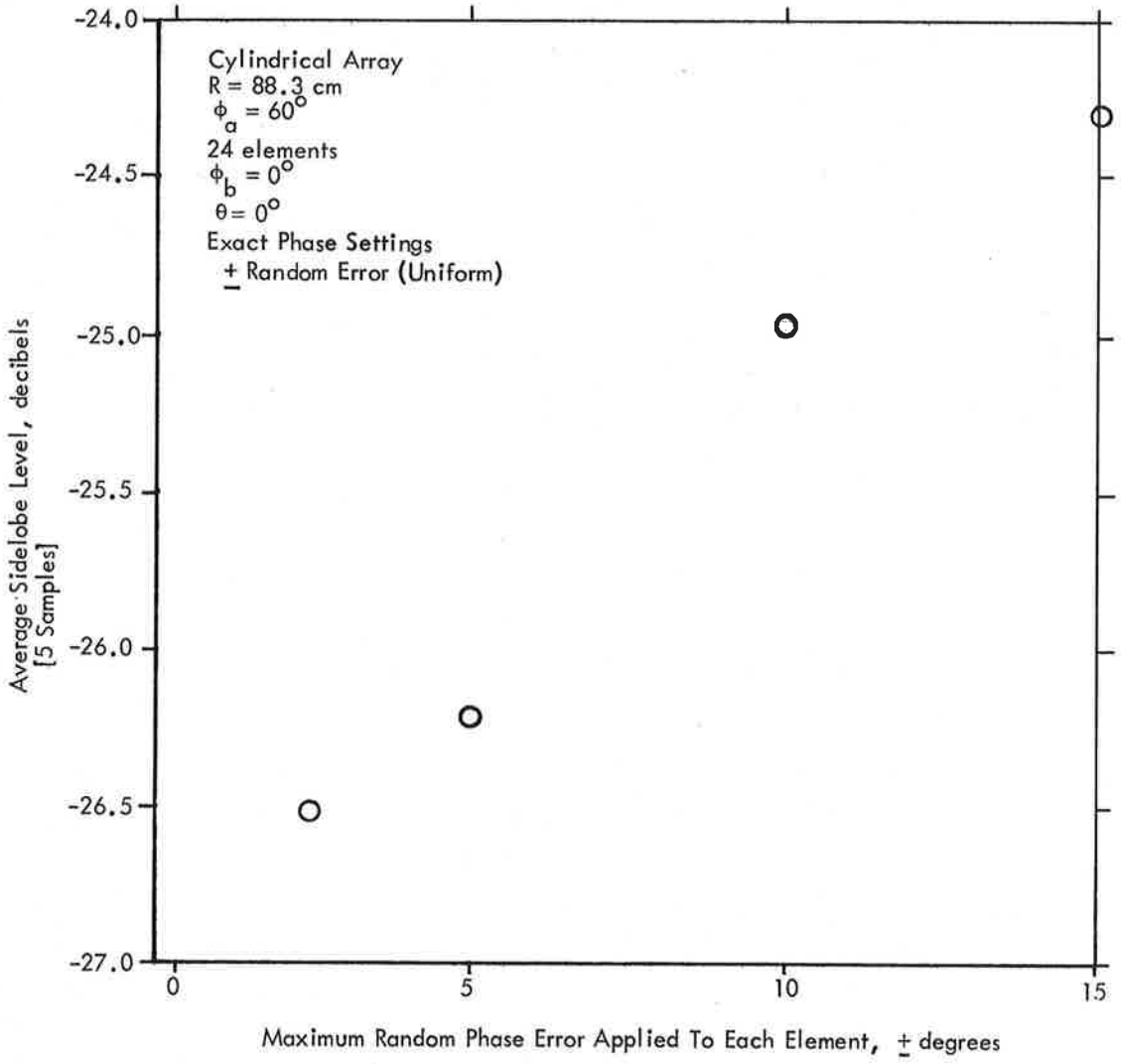

Figure 2.2.2 Calculated Average Sidelobe Level Due to Random Phase Errors Applied to All Elements

2.3 EFFECT OF AMPLITUDE AND PHASE QUANTIZATION ERRORS ON BORESIGHT ANGLES AND SIDELOBES

ABSTRACT

The effect of phase and amplitude quantization errors is to raise the sidelobes, change the beamwidth and move the beam center. The finer the quantization the smaller the effects on antenna performance. A 4 bit phase quantization can cause beam pointing errors of more than 1.5 fine scan positions or 0.13° on a 4° beamwidth circular array. The average of the beam pointing errors due to quantization corresponds to the average of the beam pointing errors caused by random phase errors of the same size.

Since each electronic phase shifter or attenuator is a digital device and since a transfer matrix would only allow a small set of amplitude levels, the phase and amplitude at each element would not be exactly at the "ideal" values even if there were no errors in the components, but rather they would be constrained to a set of "quantized" values. Generally the effect of these quantization errors in phase and amplitude is to raise the sidelobes, change the beamwidth, and move the beam center. Table 2.3.1 shows these calculated effects of different quantizations of phase and amplitude on the sidelobe level and beamwidth. The last line is approximately the case of the azimuth attenuator-fed antenna. It may be observed that the finer the quantization, the smaller its effects on antenna performance.

Table 2.3.2 shows the calculated beam center location and beamwidth for the fine scan positions in azimuth of a 4° beamwidth cylindrical array using exact (or "analog") settings on the phase shifters. The deviations from the desired azimuth angle, ϕ, which increase as the beam is steered to larger and larger ϕ are due to beam skewing resulting from the fact that the antenna is focused at an elevation angle of 10° and the beam center location is being determined at an elevation angle of 0°.

Table 2.3.3 shows results for the same antenna system as is used in Table 2.3.2 except that the phases are quantized as they would be by 4-bit phase shifters. It should be noted that the beam center deviates significantly from its position for "analog" phase settings. The average of the deviations of the beam center

from its position for "analog" phase settings is plotted in Figure 2.2.1 and corresponds closely to movements of the beam center caused by random phase errors.

TABLE 2.3.1 CALCULATED EFFECT OF PHASE AND AMPLITUDE QUANTIZATION ON SIDELOBE LEVEL AND BEAMWIDTH

Phase Settings	Amplitude Distribution	Sidelobe Level	Rise in SLL	3 dB Beamwidth
Continuous	Continuous	-25.29 dB	———	4.0131°
3 bit	Continuous	-20.33	4.96 dB	4.0154
4 bit	Continuous	-24.24	1.05	4.0196
Continuous	2 level	-19.38	5.91	3.9171
Continuous	3 level	-24.11	1.18	3.9695
Continuous	4 level	-25.05	0.24	3.9945
Continuous	6 level	-25.05	0.24	3.9975
4 bit	4 level	-24.12	1.17	4.0019
4 bit	3 bit attenuator 1.45 dB steps	-23.96	1.33	4.0246

R = 85.5 cm
f = 5.10 GHz
24 Elements

θ_f = 10
θ = 0°
ϕ_b = 0°

TABLE 2.3.2 CALCULATED FINE SCAN BEAM POSITIONS GENERATED BY ANALOG PHASE SETTINGS

Position #	Desired ϕ	θ	-10 dB Point	+10 dB Point	Actual Beam Center	%* Off	BW (10 dB)
17	0.0°	0°	-3.3527°	+3.3527°	0.0°	0.0	6.7054°
16	0.08152	0	-3.2723	+3.4331	0.0804	-1.4	6.7054
15	0.16304	0	-3.1919	+3.5135	0.1608	-2.8	6.7054
14	0.24457	0	-3.1116	+3.5939	0.2412	-4.2	6.7055
13	0.32609	0	-3.0312	+3.6743	0.3216	-5.6	6.7055
12	0.40761	0	-2.9509	+3.7547	0.4019	-7.0	6.7056
11	0.48913	0	-2.8706	+3.8351	0.4823	-8.4	6.7057
10	0.57065	0	-2.7902	+3.9156	0.5627	-9.8	6.7058
9	0.65217	0	-2.7099	+3.9960	0.6431	-11.2	6.7059
8	0.73370	0	-2.6296	+4.0765	0.7235	-12.6	6.7061
7	0.81522	0	-2.5493	+4.1569	0.8038	-14.0	6.7062
6	0.89674	0	-2.4690	+4.2374	0.8842	-15.4	6.7064
5	0.97826	0	-2.3887	+4.3179	0.9646	-16.8	6.7066
4	1.05978	0	-2.3084	+4.3984	1.0450	-18.1	6.7068
3	1.14130	0	-2.2282	+4.4789	1.1254	-19.6	6.7070
2	1.22283	0	-2.1479	+4.5594	1.2058	-20.9	6.7073
1	1.30435	0	-2.0677	+4.6399	1.2861	-22.4	6.7076

*% of one fine scan position or 0.082°

R = 88.3 cm

ϕ_A = 60°

ϕ_f = 10°

Analog Phases

TABLE 2.3.3 CALCULATED FINE SCAN BEAM POSITIONS GENERATED BY 4-BIT QUANTIZED PHASE SETTINGS

Position #	Desired ϕ	θ	-10 dB Point	+10 dB Point	Actual Beam Center	%* Off	BW (10 dB)
17	0.0°	0°	-3.3348°	3.3448°	0.0°	0.0	6.6896°
16	0.08152	0	-3.2896	3.4029	0.0567	-30.5	6.6925
15	0.16304	0	-3.2149	3.4933	0.1392	-29.2	6.7081
14	0.24457	0	-3.1810	3.5539	0.1865	-71.3	6.7349
13	0.32607	0	-3.0627	3.6583	0.2978	-34.7	6.7210
12	0.40761	0	-2.9113	3.8068	0.4478	+49.2	6.7181
11	0.48913	0	-2.8182	3.8786	0.5302	+50.4	6.6968
10	0.57065	0	-2.8181	3.8785	0.5302	-49.6	6.6966
9	0.65217	0	-2.7628	3.9265	0.5819	-86.3	6.6893
8	0.73370	0	-2.7532	3.9741	0.6105	-151.2	6.7273
7	0.81522	0	-2.6774	4.0366	0.6796	-166.4	6.7140
6	0.89674	0	-2.3968	4.2963	0.9498	+65.0	6.6932
5	0.97826	0	-2.3723	4.3242	0.9760	-2.8	6.6964
4	1.05978	0	-2.3270	4.3724	1.0227	-45.5	6.6994
3	1.14130	0	-2.2395	4.4525	1.1065	-42.7	6.6920
2	1.22283	0	-2.0879	4.6027	1.2574	+42.4	6.6906
1	1.30435	0	-2.0408	4.6599	1.3096	6.4	6.7006

*% of one fine scan position or 0.082°

24 Elements
R = 88.3 cm
ϕ_a = 60°
θ_f = 10°
4-Bit Quantization of Analog Phases

2.4 USE OF CALCULATED EFFECT OF A ONE BIT CHANGE IN ONE PHASE SHIFTER TO MINIMIZE THE EFFECT OF QUANTIZATION ERRORS ON BEAM CENTER POSITION

ABSTRACT

Using the calculated effect of a one bit change in one phase shifter on the beam center position it is possible to reduce beam pointing errors due to quantization by changing the settings of one or more phase shifters by one bit.

Although the quantization errors caused by digital phase shifters move the beam center these errors can be compensated for, if desired, by changing the settings of one or two of the phase shifters. It is only necessary to know the approximate amount of beam motion caused by a one bit change in one phase shifter as a function of where the element affected by that phase shifter is located on the array, (see Figure 2.1.5). It is then possible to select one phase shifter or a group of phase shifters which will produce the desired beam center correction with a one bit change on each. It is desirable to select those phase shifters which already have a maximum phase error so that when the setting is changed by one bit the new error will not be significantly larger than the other errors in the array. For example, a shifter with an initial quantization error of -10.0° would, after a one bit change, have an error of +12.5°, whereas a shifter with an initial error of -3° would have an error of +19.5°.

Table 2.4.1 shows results for the same antenna system with 4-bit phase shifters as is used in Table 2.3.2 except that perturbations have been made in some of the phase settings to improve the beam pointing.

TABLE 2.4.1 CALCULATED FINE SCAN BEAM POSITIONS GENERATED BY PERTURBED 4-BIT QUANTIZED PHASE SETTINGS

Position #	Desired ϕ	θ	-10 dB Point	+10 dB Point	Actual Beam Center	%* Off	BW (10 dB)
17	0.0°	0	-3.3448°	+3.3448	0.0°	0.0	6.6896°
16	0.08152	0	-3.2798	+3.4290	0.0746	-8.5	6.7088
15	0.16304	0	-3.1974	+3.5213	0.1619	-1.3	6.7187
14	0.24457	0	-3.1307	+3.6084	0.2389	-7.0	6.7391
13	0.32609	0	-3.0459	+3.6919	0.3230	-3.8	6.7378
12	0.40761	0	-2.9577	+3.7586	0.4004	-8.8	6.7163
11	0.48913	0	-2.8599	+3.8486	0.4944	+6.4	6.7085
10	0.57065	0	-2.7763	+3.9267	0.5752	+5.6	6.7030
9	0.65217	0	-2.7202	+4.0131	0.6465	-7.0	6.7333
8	0.73370	0	-2.6223	+4.0858	0.7317	-2.4	6.7081
7	0.81522	0	-2.5426	+4.1653	0.8113	-4.7	6.7079
6	0.89674	0	-2.5334	+4.3265	0.8965	-0.3	6.8599
5	0.97826	0	-2.3723	+4.3242	0.9759	-2.8	6.6964
4	1.05978	0	-2.2880	+4.4068	1.0594	-0.5	6.6948
3	1.14130	0	-2.2039	+4.4931	1.1446	+4.0	6.6969
2	1.22283	0	-2.1280	+4.5704	1.2212	-2.0	6.6985
1	1.30435	0	-2.0408	+4.6599	1.3095	+6.4	6.7006

*% of one fine scan position or 0.082°

24 Elements

R = 88.3 cm

ϕ_a = 60°

θ_f = 10°

4-Bit Quantization of Phases and Beam Steering Perturbations

3. NEAR-FIELD EFFECTS STUDY

CONTENTS

ILLUSTRATIONS

TABLES

When an aircraft enters the near field of a scanning beam antenna, the antenna pattern it sees begins to broaden, and sidelobes fill in and increase in level. This results in reduced accuracy. In section 3.1 below, beam shapes are presented as a function of beamwidth and range, and a criterion derived for the closest allowable range between antenna and aircraft. This minimum range can be reduced by near-field focusing, which results in somewhat reduced performance at larger distances. Recommendations on the limits of this technique are included. It is concluded that there is no problem with any except the fine elevation antenna. The problem with EL #2 is discussed in section 3.2. It turns out that the near-field problem and the multipath problem are inextricably related. This is discussed in some detail in section 4.2.2. There it is concluded that the recommended lower coverage limit of the RTCA report is out of line with achievable performance at C-band or Ku-band.

3.1 EFFECTS OF THE NEAR-FIELD ON ANTENNA PATTERNS AND BEAMWIDTHS

ABSTRACT

A reasonably designed antenna will exhibit fairly deep nulls in the far-field, if it is focused at infinity (collimated rays). However, at close ranges, the beam broadens, and nulls fill in and increase in amplitude. These cause a deterioration in the accuracy of the system. It is concluded here that the aircraft receiver can come to within .25 of the distance to the near-far-field boundary, given by the familiar $2D^2/\lambda$.

It is not necessary to calculate the antenna patterns for every different beamwidth encountered, since the effects are quite similar. Consider a linear array or linear aperture focused at infinity, as in Figure 3.1.1.

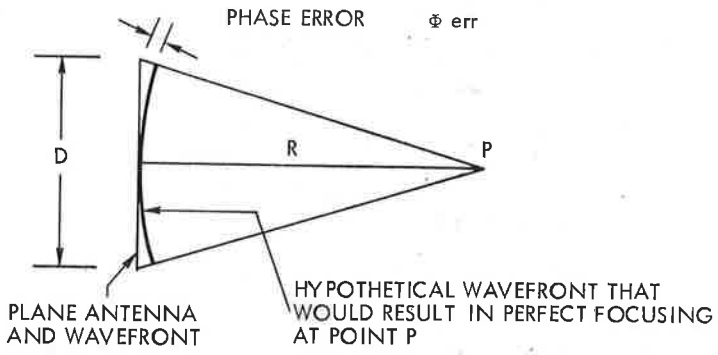

Figure 3.1.1 Geometry for Near-Field Analysis

At a point a distance R away, the rays arrive in different phases, unless R is very large. Thus, given a defocusing error Φ_{err}, the distance R can be found to be

$$R = \frac{2D^2}{\lambda}\left(\frac{\pi}{16\Phi_{err}}\right) \qquad (3.1.1)$$

where Φ_{err} is in radians.

The quantity Φ_{err} determines the sidelobe level and beam broadening; by specifying a worstcase phase error of 90°, for example, the closest distance allowable is given by 1/4 of $2D^2/\lambda$, regardless of the beamwidth. Thus by using an array having a modest beamwidth of 4°, the results can be scaled to other beamwidths for antennas having similar aperture distributions. To show this, a 4° beamwidth pattern at $D^2/2\lambda$ is compared with an 8° beamwidth pattern at $D^2/2\lambda$ in Figure 3.1.2. It can be seen that there is little difference, except for the scale factor.

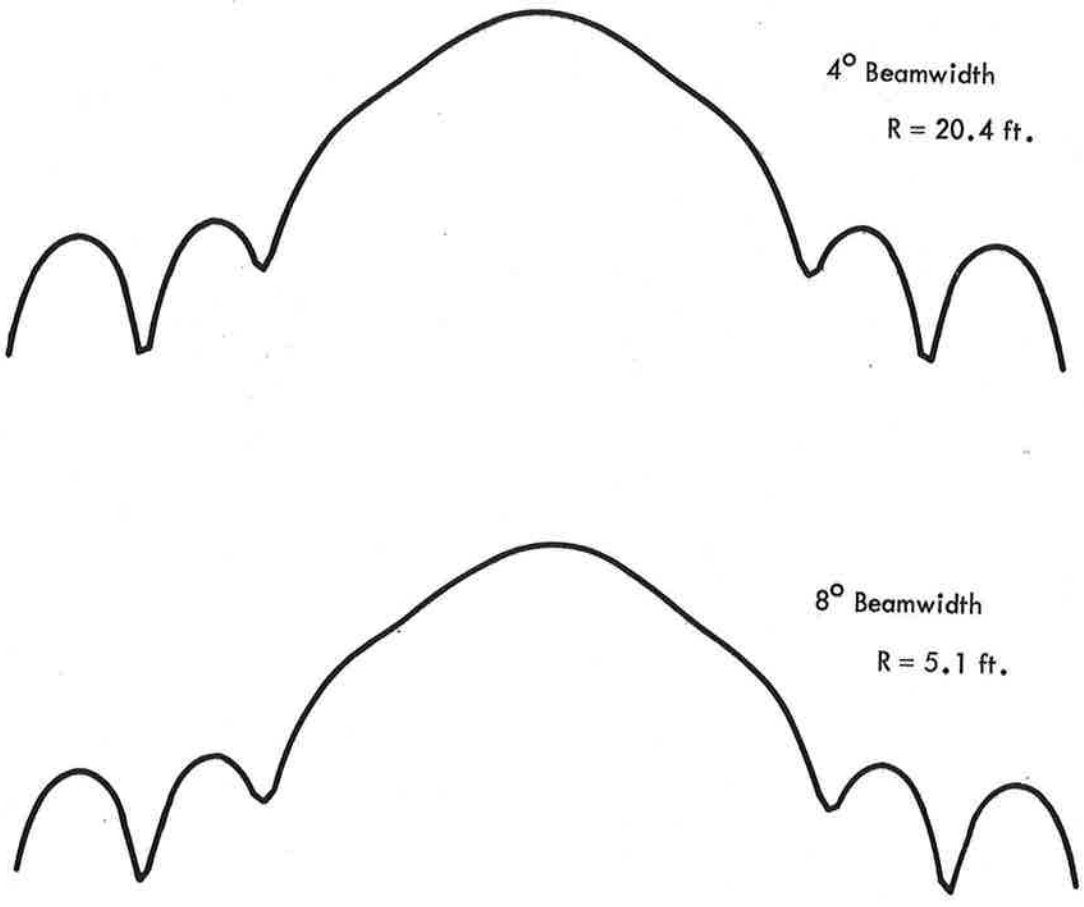

Figure 3.1.2 Near-Field Patterns of 4° and 8° Antennas, Receiver at α=.25

Another consideration is that it is more accurate to say that the beamwidth, rather than aperture, defines the near-far-field boundary given by $2D^2/\lambda$; another way of saying this is that the quantity D should be the effective, rather than physical, linear dimension. The far-field criterion can be written in beamwidths as follows:

$$\frac{2D_{eff}^2}{\lambda} = 2\lambda\left(\frac{D_{eff}^{\ 2}}{\lambda}\right) = \frac{2\lambda}{(\Delta\theta)^2} \qquad (3.1.2)$$

Equation (3.1.1) can be re-written as

$$R = \frac{\lambda\pi}{8\Phi_{err}(\Delta\theta)^2} \qquad (3.1.3)$$

Figures 3.1.3 through 3.1.8 show the beam shapes encountered in the near field of an antenna focused at infinity. The beam broadening is shown in Figure 3.1.9 as a function of α, where α is defined as the ratio between the distance receiver and the near-far-field boundary:

$$\alpha = \frac{R(\Delta\theta)^2}{2\lambda} \qquad (3.1.4)$$

There is an abrupt widening of the beam below about $\alpha = .2$. In addition, at $\alpha = .2$ the sidelobes are more than 6db above the design.

It is concluded that $\alpha = .25$ represents the closest allowable distance of the aircraft to the antenna for good performance. Table 3.1 shows the recommended minimum distances for the various antennas.

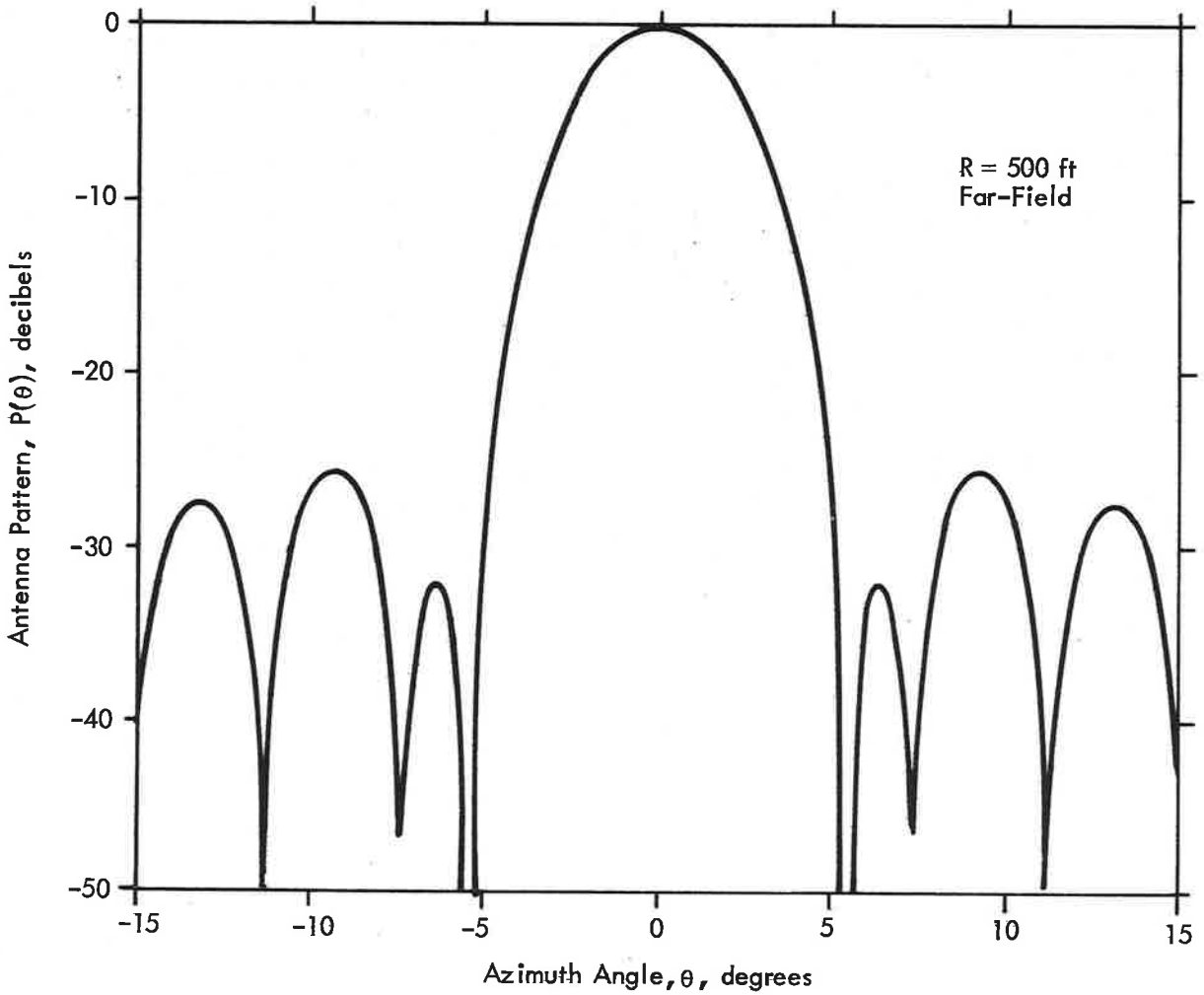

Figure 3.1.3 Patterns of a 4° Antenna, $\alpha=\infty$ (Far-Field)

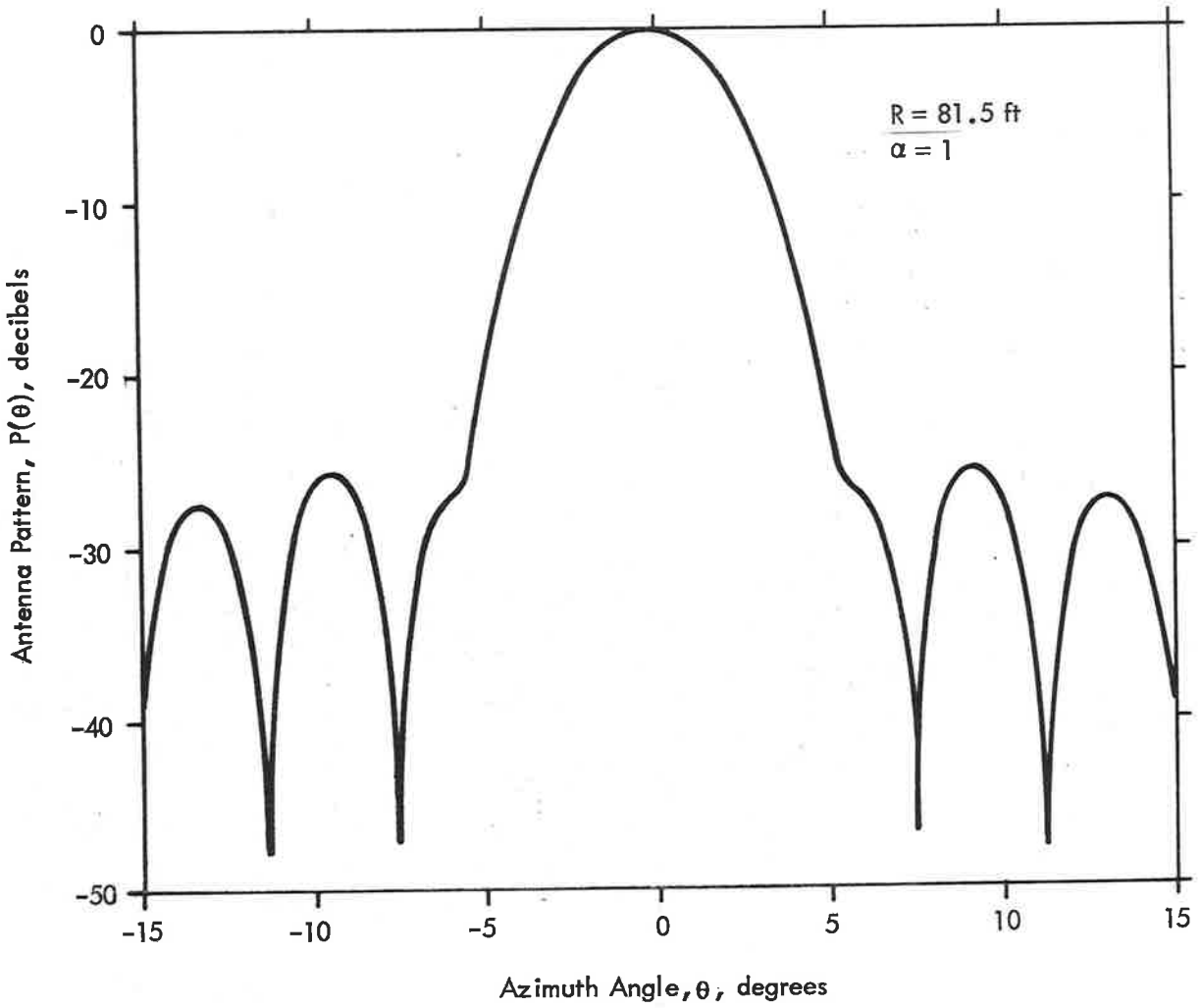

Figure 3.1.4 Patterns of a 4° Antenna, $\alpha = 1$ (at $2D^2/\lambda$)

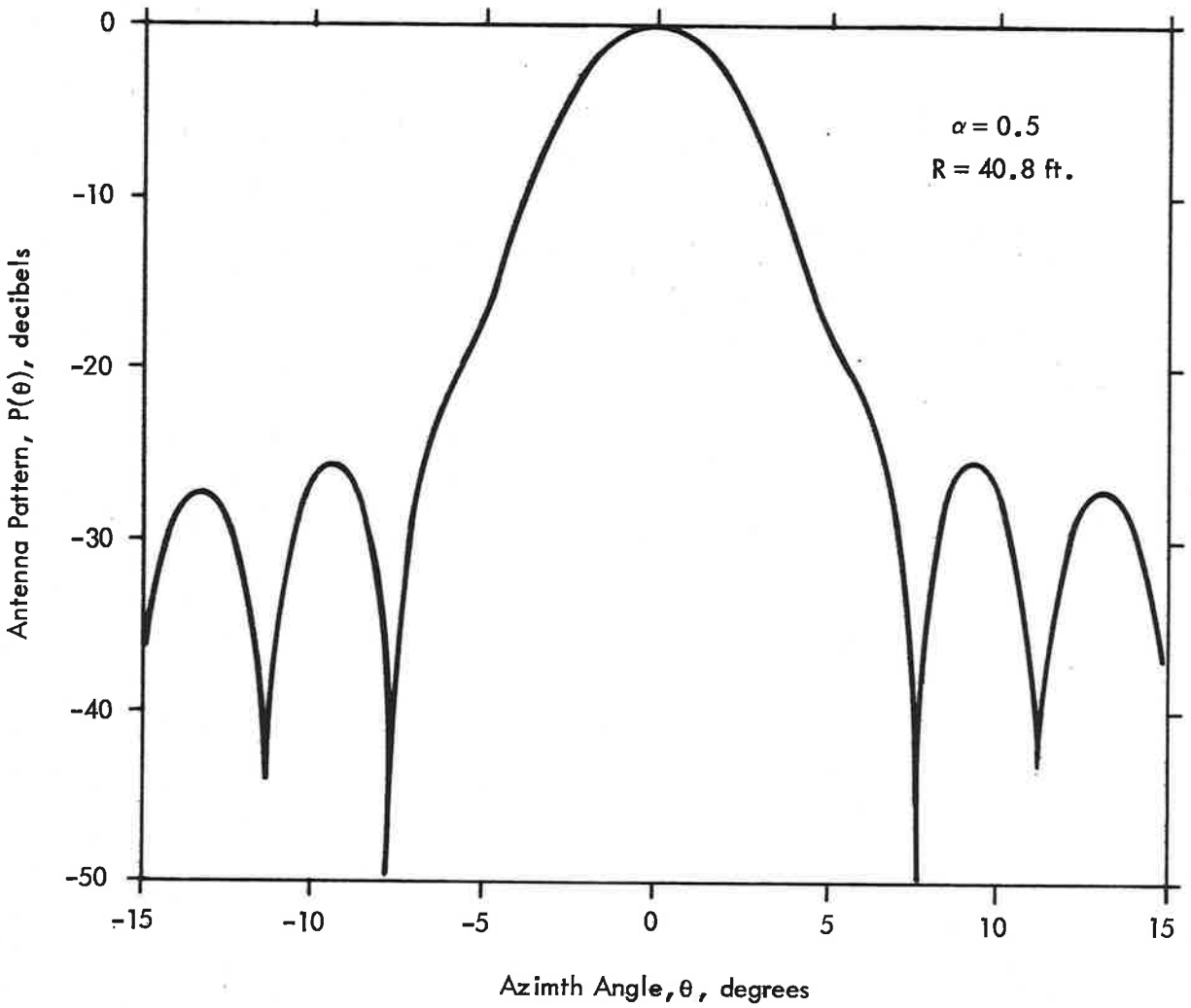

Figure 3.1.5 Patterns of a 4° Antenna, $\alpha = .5$

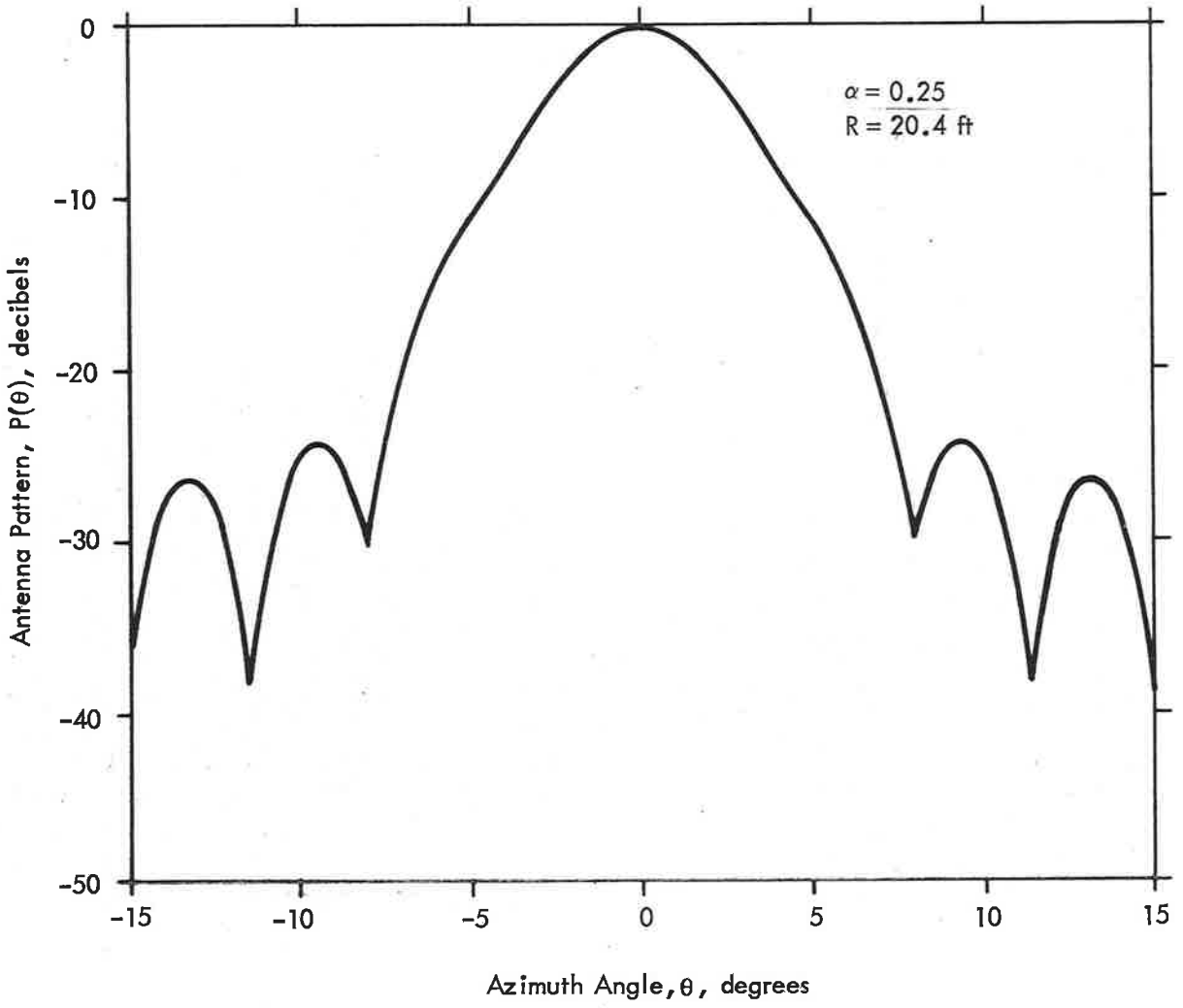

Figure 3.1.6 Patterns of a 4° Antenna, $\alpha = .25$

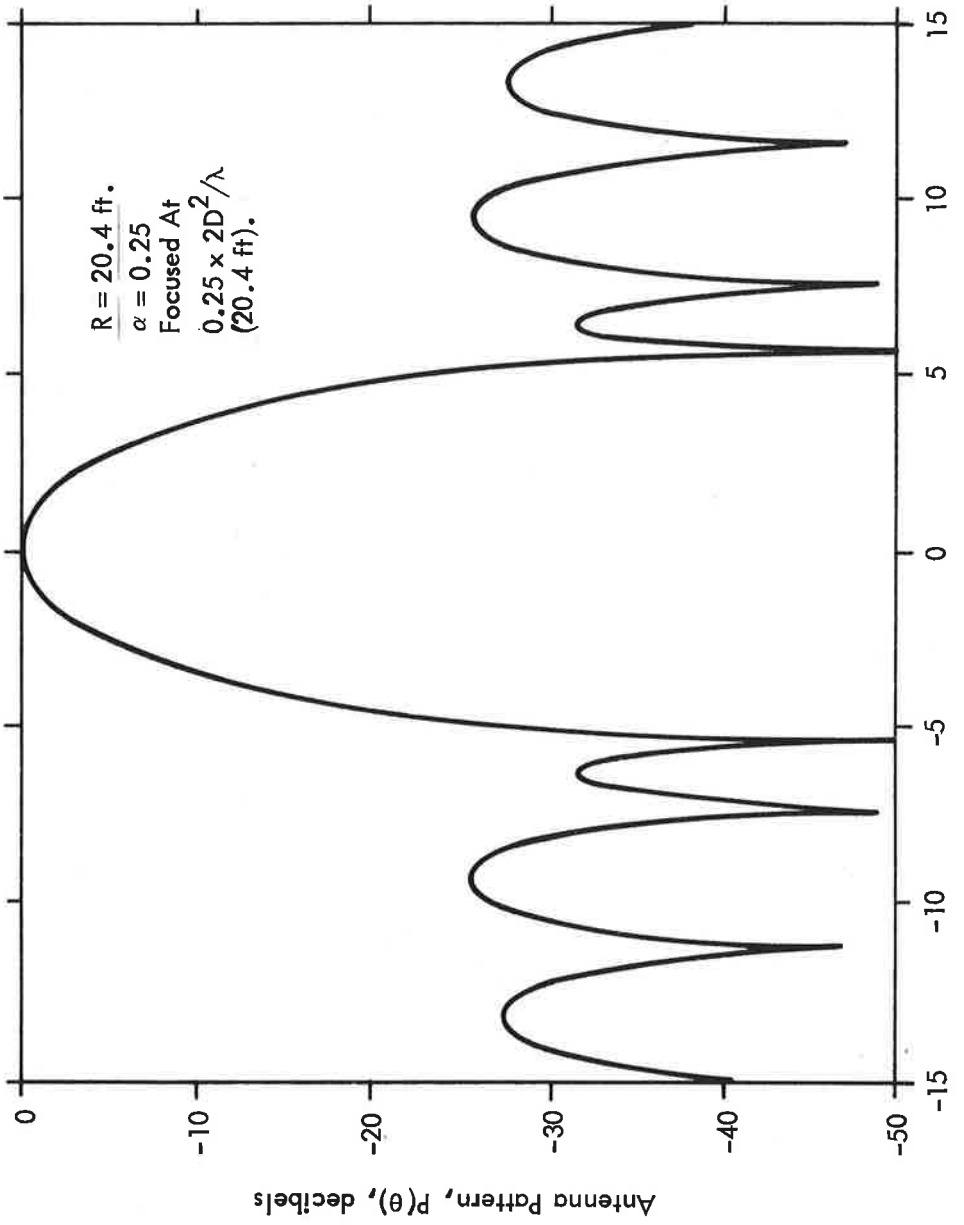

Figure 3.2.1 Patterns of a 4° Antenna Focused in the Near-Field, $\alpha = .25$

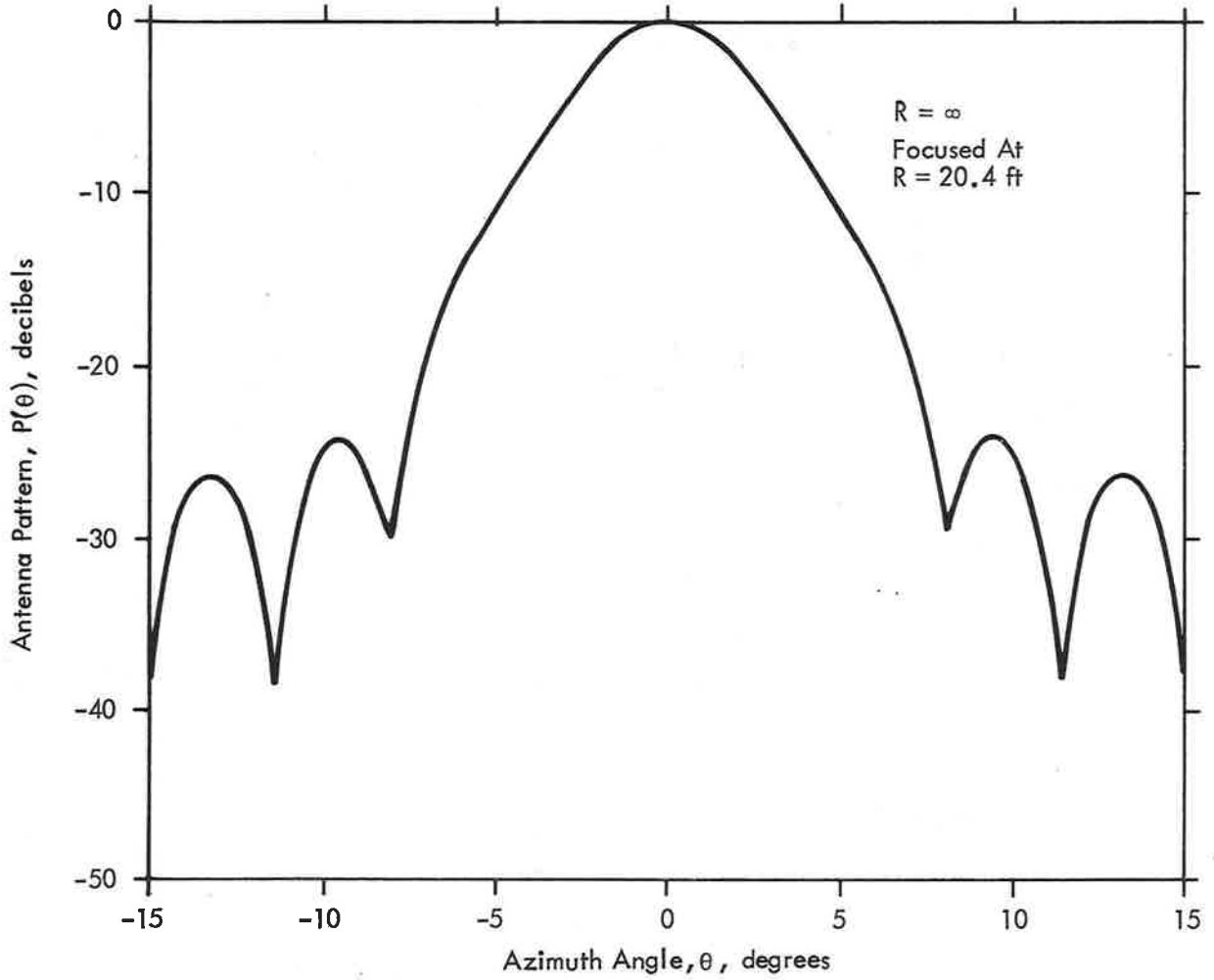

Figure 3.2.2 Patterns of a 4° Antenna Focused in the Near-Field, $\alpha = \infty$

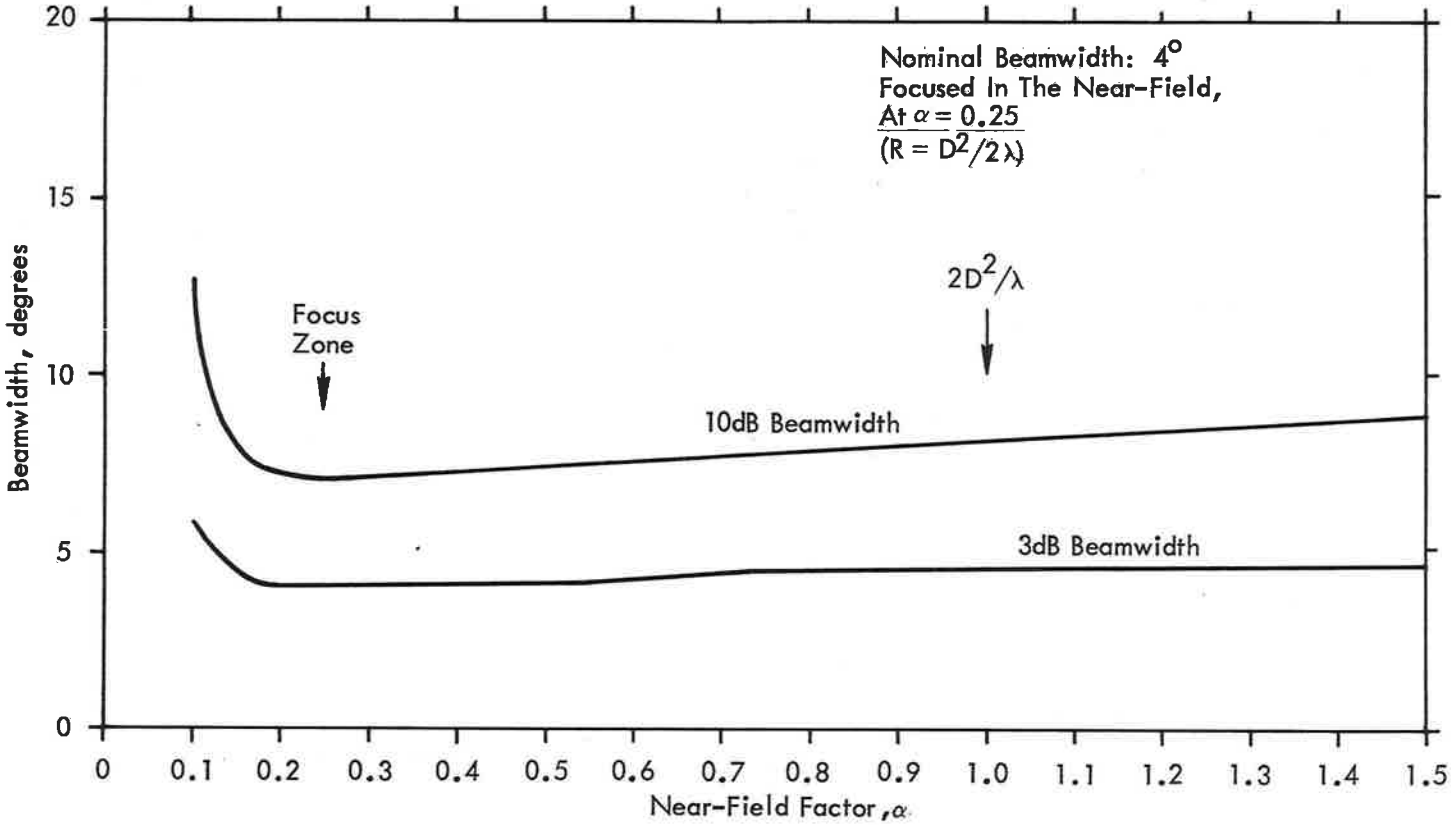

Figure 3.2.3 Beam Broadening in the Near-Field of a 4° Antenna Focused at .25 x $2D^2/\lambda$

However, for EL #2 the lower coverage limit is crucial. The sidelobe radiation level is higher, and it appears that any advantage to be gained by moving the antenna down to the coverage zone would be offset by the degraded performance at larger distances. While this conclusion should be subjected to experimental verification, near-field focusing does not appear to be a means of improving performance of EL #2.

4. EFFECTS OF GROUND REFLECTIONS ON ANTENNA PATTERNS

CONTENTS

ILLUSTRATIONS

ILLUSTRATIONS (CONT.)

ILLUSTRATIONS (CONT.)

Ground reflections constitute the chief source of multipath in the ground equipment. They play a dominant role in the low angle coverage capability in both azimuth and elevation. The following sections are concerned with ground reflections rather than reflections from buildings, aircraft, etc. Recommendations on siting and beamwidths are primarily based on the results of ground reflections. It is recognized that particular sites may have severe problems from other sources. This is particularly true of elevation guidance requiring wide azimuth coverage - it is doubtful if one universal coverage volume requirement is feasible.

4.1 EFFECTS OF GROUND REFLECTIONS ON THE DESIGN OF THE AZIMUTH ANTENNAS

ABSTRACT

Ground reflections play an important role in the design of the vertical aperture of the azimuth antennas. The reflected ray moves in and out of phase with the direct ray at different elevation angles, causing ripples in the patterns, called scalloping. The scalloping depends on the frequency, the surface material (concrete or grass, sand, etc.), the height of the antenna and the antenna elevation pattern. The elevation pattern can be shaped to reduce radiation toward the ground, but at a cost: the sharper the cutoff of the below-the-horizon radiation, the larger the aperture and hence the cost. A discussion is given of the problem with recommendation on the design and height of the azimuth antennas.

In order to specify the requirements on the elevation pattern characteristics and height of the azimuth antennas, three considerations must be taken into account:

1. Coverage (range and elevation). This affects the acquisition properties of the system in the initial approach region. Ripples in the pattern can cause loss of range for some elevation angles.
2. Signal variations on the approach glide path. This is especially relevant to AZ#2, since an aircraft in the final approach region moves down through the lobing pattern. The AGC must respond quickly enough and the

dynamic range of the receiver must be wide enough to accommodate the signal variations.

3. Signal strengths during rollout. During rollout, the aircraft needs azimuth guidance. Since the antenna may be as low as 3-5 feet above the ground, the reflected ray strongly reduces the signal strength; the signal must be strong enough to be above the receiver threshold.

These are treated in the forthcoming sections. First, a discussion is presented of the effect of ground reflections on the antenna patterns. Then the above considerations are addressed, and in the final section some tentative recommendations are made. These recommendations are made with the understanding that certain critical experiments need to be performed in order to verify and refine the numbers presented here.

4.1.1 Effect of Antenna Height and Aperture on Azimuth Vertical Antenna Patterns

In this section theoretical predictions are developed based on a flat-surface assumption. In practice, runways and grassy airport surfaces may deviate significantly from a flat surface. In particular, convex runways can cause significant reductions of signal level near the runway and at low coverage angles. The result of such a situation is that antenna heights should be increased, even though lobing null depths may also increase. However, most airports are nearly flat, and for low grazing angles, the specular reflection assumption is quite forgiving of small-scale surface deviations. There the flat-surface assumption gives ball-park figures, and are indicative of the numbers to be encountered in actual airport installations.

First, suppose an antenna is placed at a height h above the ground, having a pattern given by $g(\theta)$ when no reflections are present. Assume, also, that the aircraft is far enough away that the following criterion is reached:

$$d > \frac{2(2h + L)^2}{\lambda} \qquad (4.1.1)$$

where d is the distance along the ground from antenna to aircraft, h is the antenna height, L is the antenna vertical aperture dimension, and λ is the wavelength of the Signal. This situation is shown in Fig. 4.1.1. The composite pattern in elevation is given

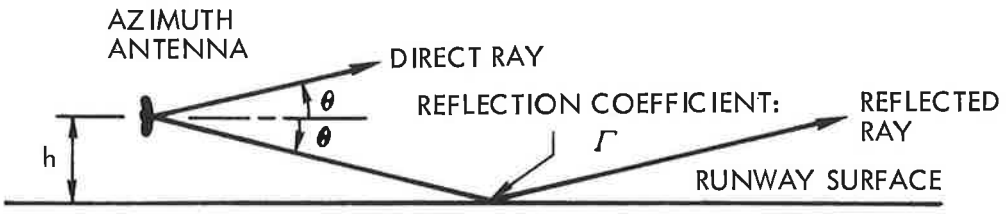

Figure 4.1.1 Geometry for Analyzing Ground Reflections-Azimuth Antenna Pattern in Elevation

by $f(\theta)$, where

$$f(\theta) = g(\theta) + \Gamma e^{-j2kh \sin \theta} g(-\theta) \qquad (4.1.2)$$

and Γ is the reflection coefficient of the surface material. This is the (complex) amplitude pattern. Since the receiver measures power, we are interested in the power pattern $f^*f(\theta)$, which, from equation (4.1.2), can be written

$$f^*f(\theta) = g^2(\theta) + \Gamma^2 g^2(-\theta) + 2\Gamma g(\theta)g(-\theta) \cos(2kh \sin \theta) \qquad (4.1.3)$$

We are primarily interested in the angles where the signal is reduced, i.e., where $f^*f(\theta)$ is minimized. Since the first two terms are positive, the third term determines the region of minimum radiation. When the third term reaches a minimum, it is negative, and

thus results in decreased radiation. Thus we are concerned with the term

$$-\Gamma\, g(\theta)g(-\theta)\cos(2kh\sin\theta)$$

where it is maximum, and what its amplitude is.

For low grazing angles Γ is close to -1. A typical plot is shown in Figure 4.1.2, using the uniform dielectric model of Kerr.[1] Based on what little is available on the reflection properties of earth, concrete, etc. it appears reasonable to assume that the phase of Γ is close to 180° for grazing angles up to about 5°. The pattern $g(\theta)$ is assumed to be derived from the Woodward-Lawson synthesis technique.[2] It was shown in the first annual report that the pattern which matches the coverage recommended by RTCA is given by

$$g(\theta) = \frac{\sin \pi u}{\pi}\left[\frac{\chi}{u} + \sum_{m=1}^{M_1}\frac{(-1)^m}{(u-m)} + \sum_{m=M_1+1}^{M}\frac{u_1(-1)^m}{m(u-m)}\right] \qquad (4.1.4)$$

where $u = \frac{L}{\lambda}(\sin\theta - \sin\theta_o)$, M_1 is the largest integer smaller than u_1, $u_1 = \frac{L}{\lambda}(\sin\theta_1 - \sin\theta_o)$, L is the vertical aperture dimension, M is the number of beams, and θ_o, θ_1, and χ are parameters that can be varied. Typically, $\theta_o = 0$, $\theta_1 = 7.5°$, and χ varies between .3 and .7. The parameter χ is then the value of the pattern at the horizon. The number of beams M is usually the largest integer less than L/λ.

A plot of $g(\theta)$ for $L/\lambda = 19.11$ and $\chi = .7$ is given in Figure 4.1.4. Since the function is real, $g(\theta)$ is positive for positive θ; for negative angles, it oscillates between positive and negative values.

---

[1] Kerr, D.E., "Propagation of Short Radio Waves" Dover Publications, 1951, pp. 396-403.

[2] First Annual Report, 1971, pp. 69-84.

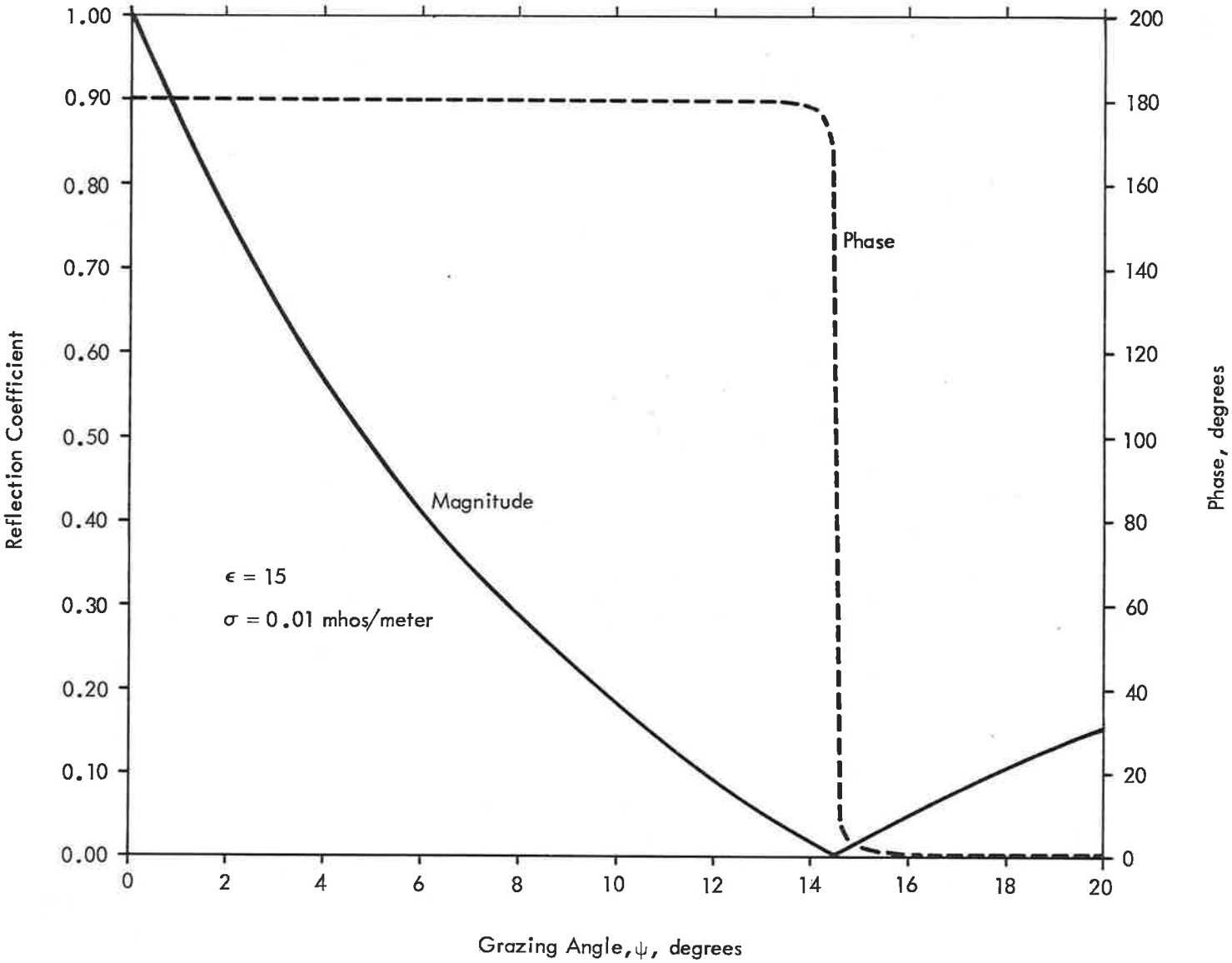

Figure 4.1.2 Typical Reflection Coefficient for Vertical Polarization

Thus we are interested in the term

$$T(\theta) = |\Gamma|\, g(-\theta) \cos(2kh \sin\theta) \qquad (4.1.5)$$

The term $g(-\theta)$ has nulls at θ_n, where

$$\sin\theta_n = n\,\lambda/L \qquad (4.1.6)$$

and is positive up to the first null at λ/L. The term $\cos(2kh \sin\theta)$ has maxima given by θ_m, where

$$\sin\theta_m = \frac{m\lambda}{2h} \qquad (4.1.7)$$

It is evident that if the vertical dimension of the antenna is L, the height must be greater than L/2 in order to clear the ground. This means that the cosine term reaches a maximum (and thus the composite pattern $f(\theta)$ has a minimum) while $g(-\theta)$ is positive. Except for this first lobing minimum, the optimum height-to-aperture relation appears to be at h = L; this is a judgment which is based on the diagram of Figure 4.1.3.

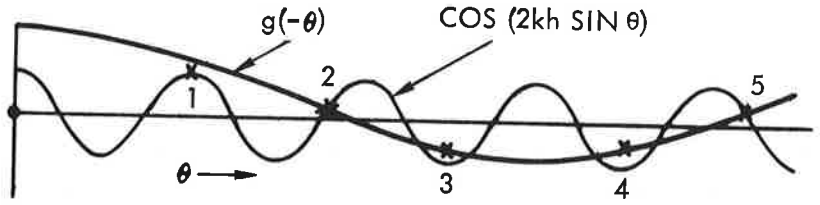

Figure 4.1.3 Oscillating Functions in Cross-Product of Reflection Term

The cross-marks indicate where the minima of the composite pattern exist. The parameters are chosen so that the second peak of the cosine term after zero coincides with the null of $g(-\theta)$. Not until null number 6 is reached do the two terms peak at the same point;

by this time the amplitude of $g(-\theta)$ is small, and the reflection coefficient, too. The first null is the worst; it may well turn out that it would be more desirable to reduce the first null by reducing the height. On the other hand, siting restrictions may preclude placing the antenna near the ground. If the antenna is raised to 20 feet, for example, several minima will occur, and may be quite deep.

It may also turn out that the runway topography may dictate the height, or in any case will change the lobing structure. These must be borne in mind while interpreting the data presented here.

The effect of aperture height on the composite pattern can be seen by comparing a 1-foot vertical aperture with an 8-foot aperture, where a 4-foot snow clearance is provided. This puts the center of the 1-foot antenna at 4.5 feet, and that of the 8-foot aperture at 8 feet. Figure 4.1.5a shows the free-space pattern of the 1-foot aperture, and 4.1.5b shows the composite pattern. It can be seen that there are angles for which the signal is reduced by 13 dB from its free-space value. The corresponding patterns for the 8-foot aperture show less scalloping and better low-angle performance (Figure 4.1.6). The reflecting surface is assumed to be a dielectric having parameters $\epsilon = 15$, $\sigma = 0.01$ mhos/meter. The antenna is assumed to have its horizon radiation intensity 3 dB below the maximum.

Variations of the pattern with antenna height are shown in Figures 4.1.7a-h for an aperture of 3.76 feet. It can be seen that the pattern variations near optimum ($h = 4$ feet) are not strikingly different from others. This suggests that the optimum configuration does not offer significantly better performance.

Variations of the pattern with the dielectric constant of the reflecting surface are shown in Figure 4.1.8a and 4.1.8b for dielectric constants of 3 and 30. The differences are not significant. A dielectric constant of 3 is typical of dry sand and concrete, while 30 is representative of marsh land.

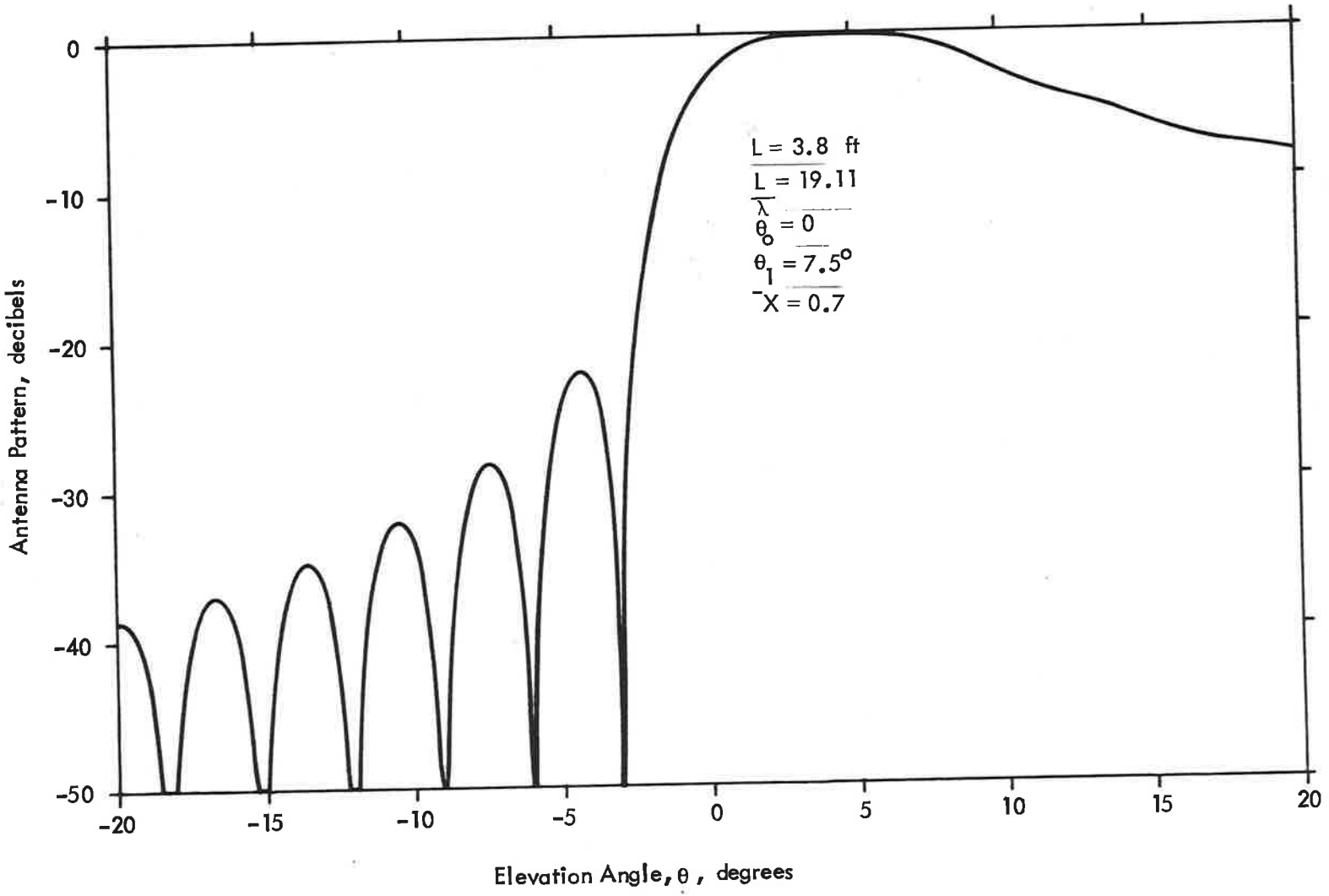

Figure 4.1.4 Free-Space Vertical Antenna Pattern-Typical Design

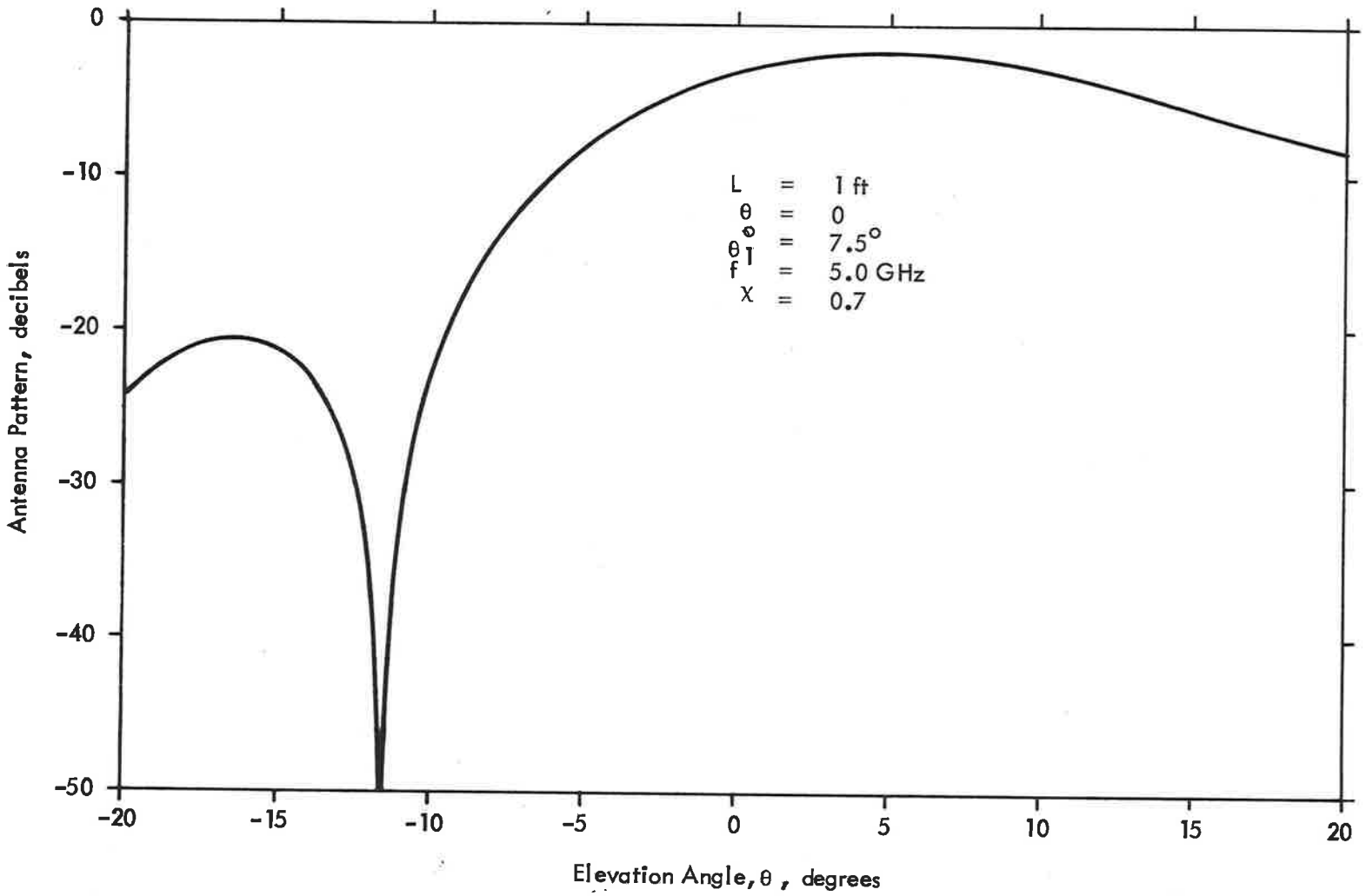

Figure 4.1.5a Free-Space Vertical Antenna Pattern-1 Foot Aperture

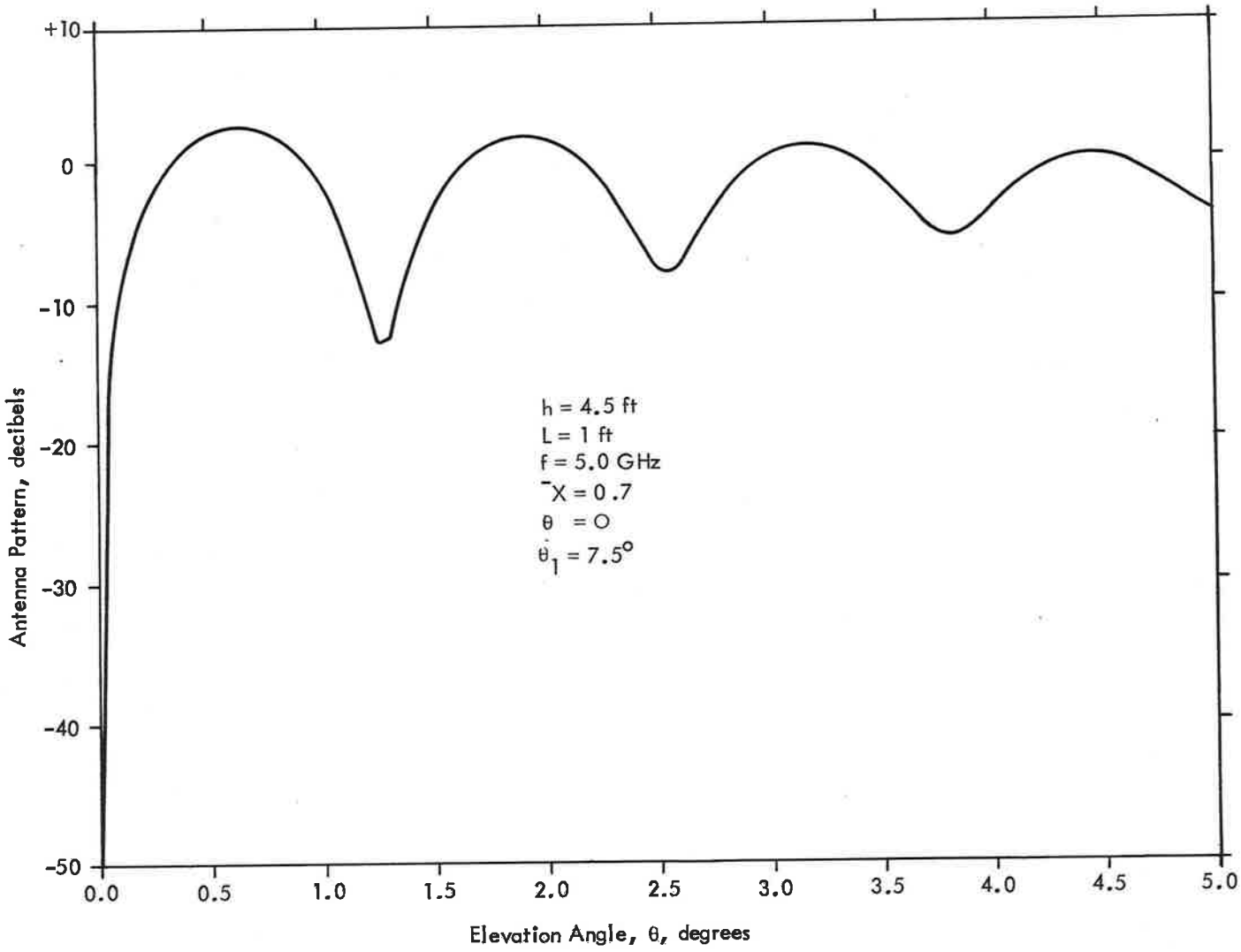

Figure 4.1.5b Composite Vertical Antenna Pattern-1 Foot Aperture, 4.5 Foot Height

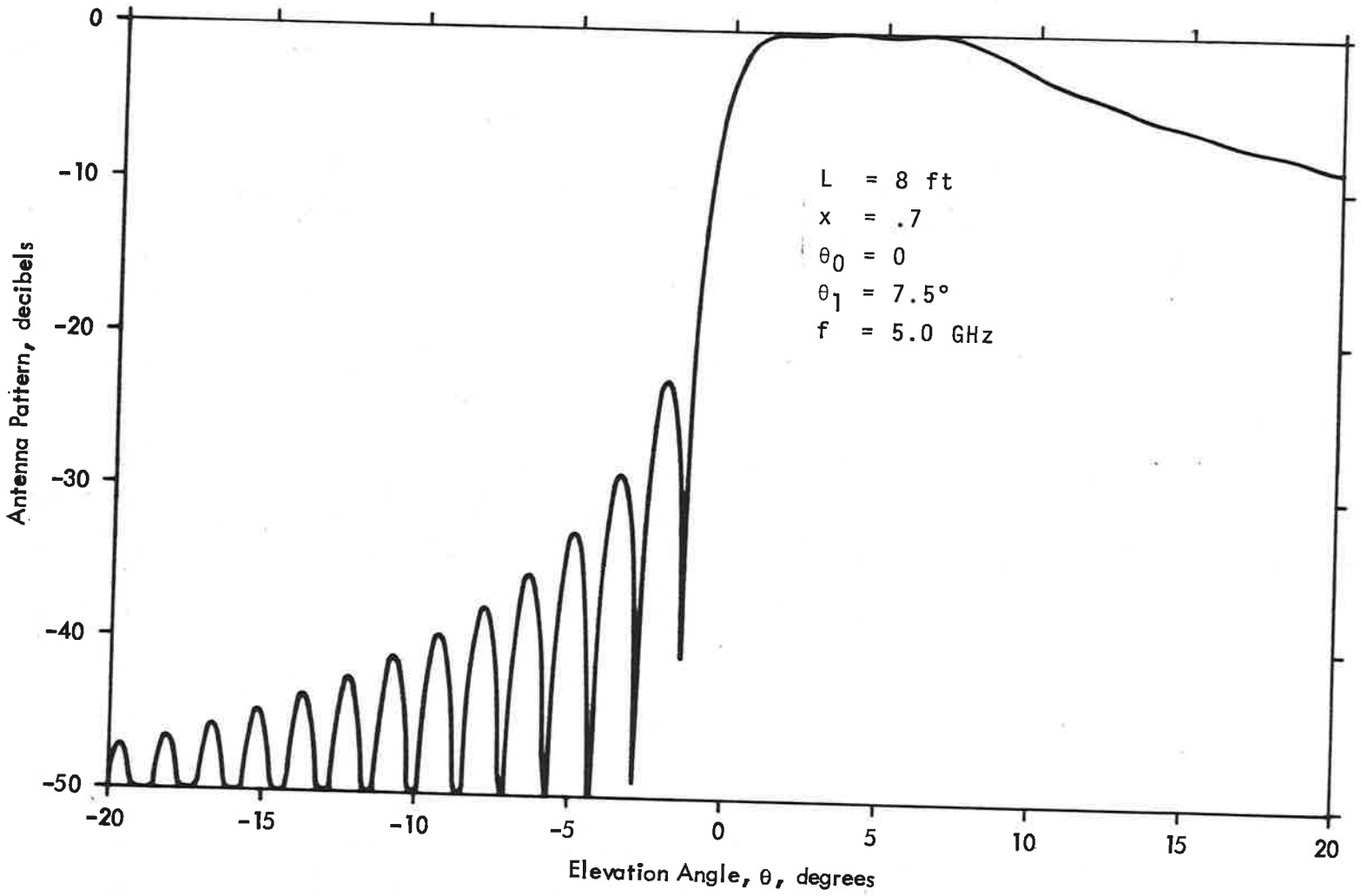

Figure 4.1.6a Free-Space Vertical Antenna Pattern-8 Foot Aperture

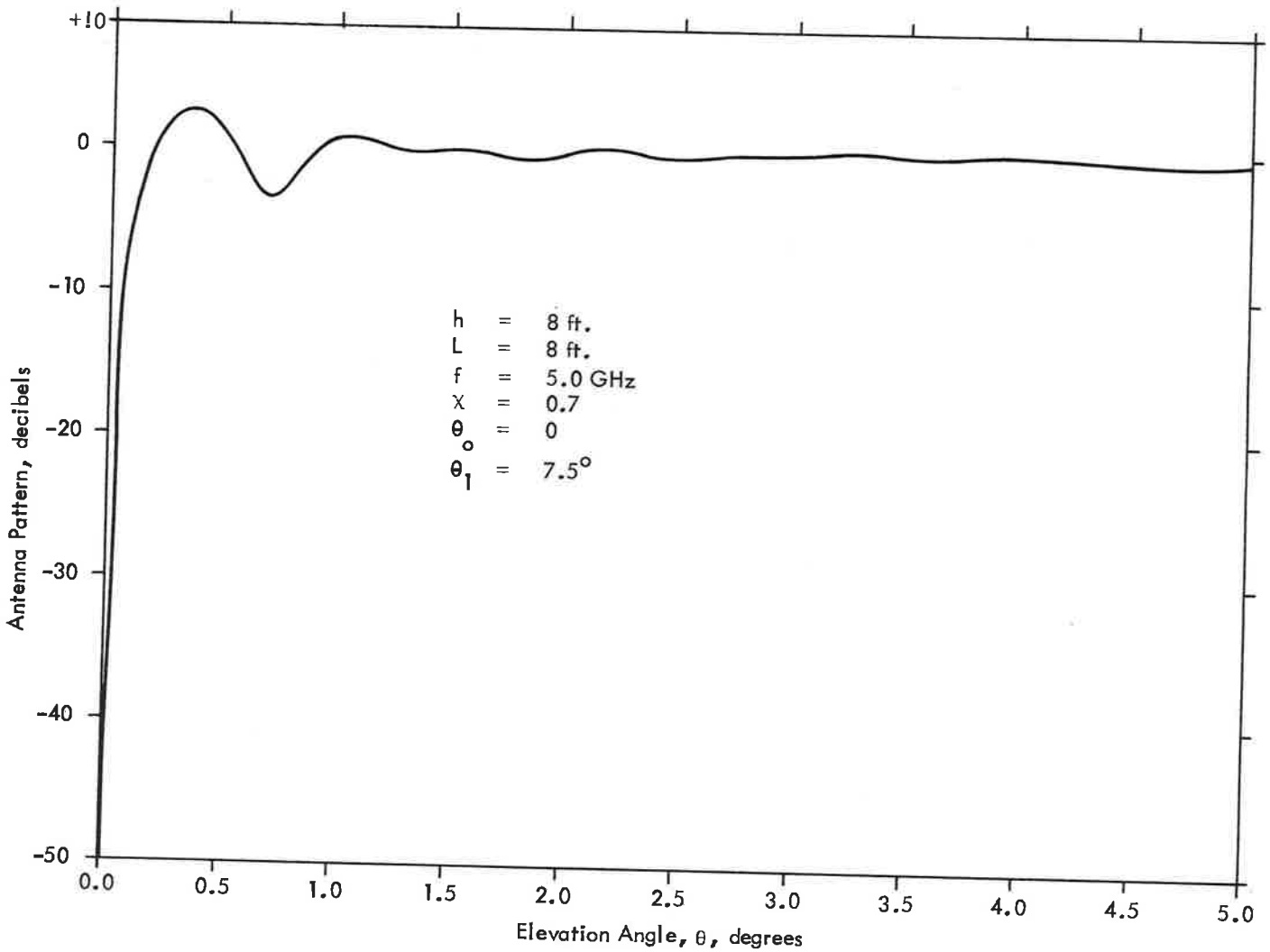

Figure 4.1.6b Composite Vertical Antenna Pattern-8 Foot Aperture, 8 Foot Height

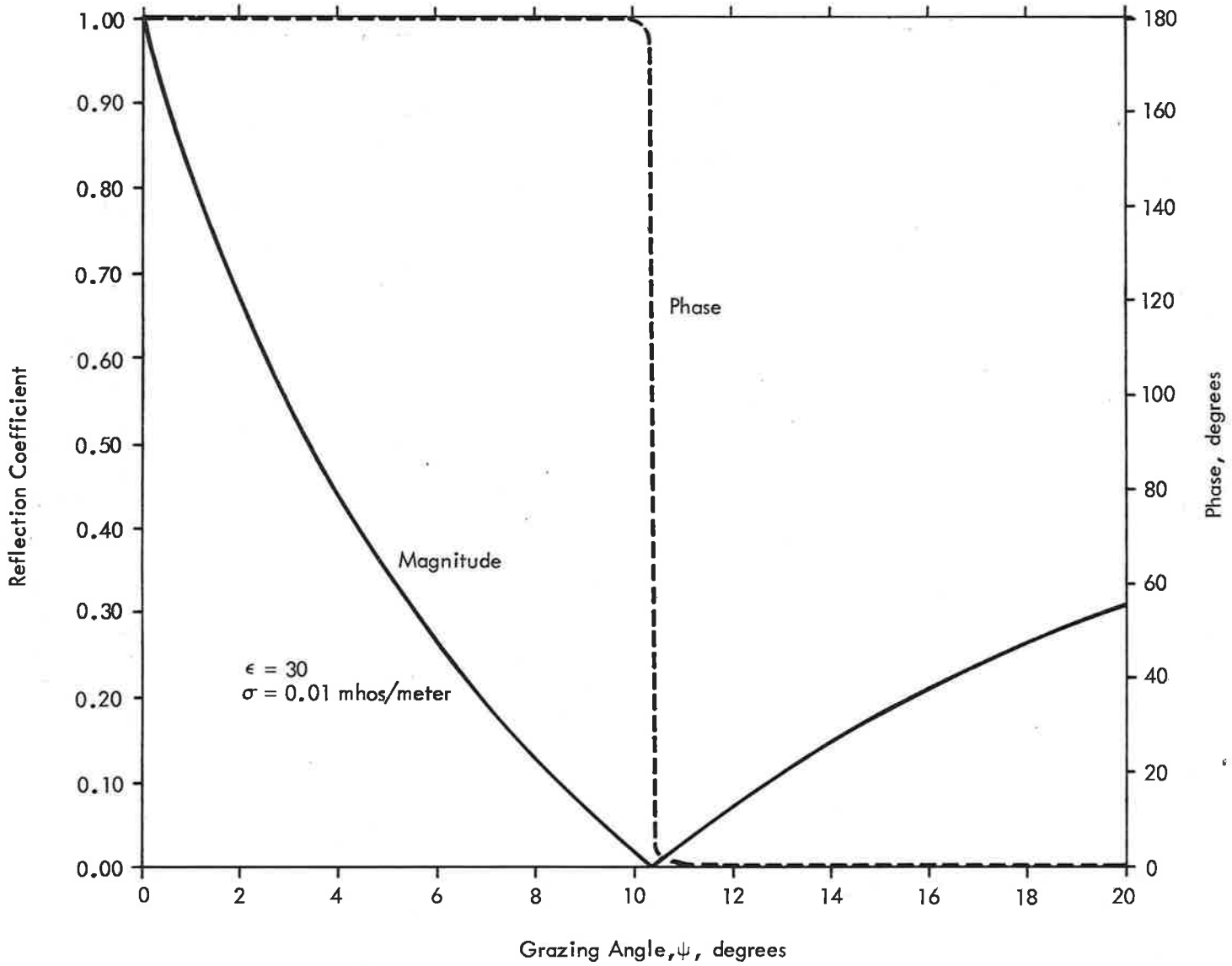

Figure 4.1.7a Reflection Coefficient, Vertical Polarization, $\epsilon = 30$

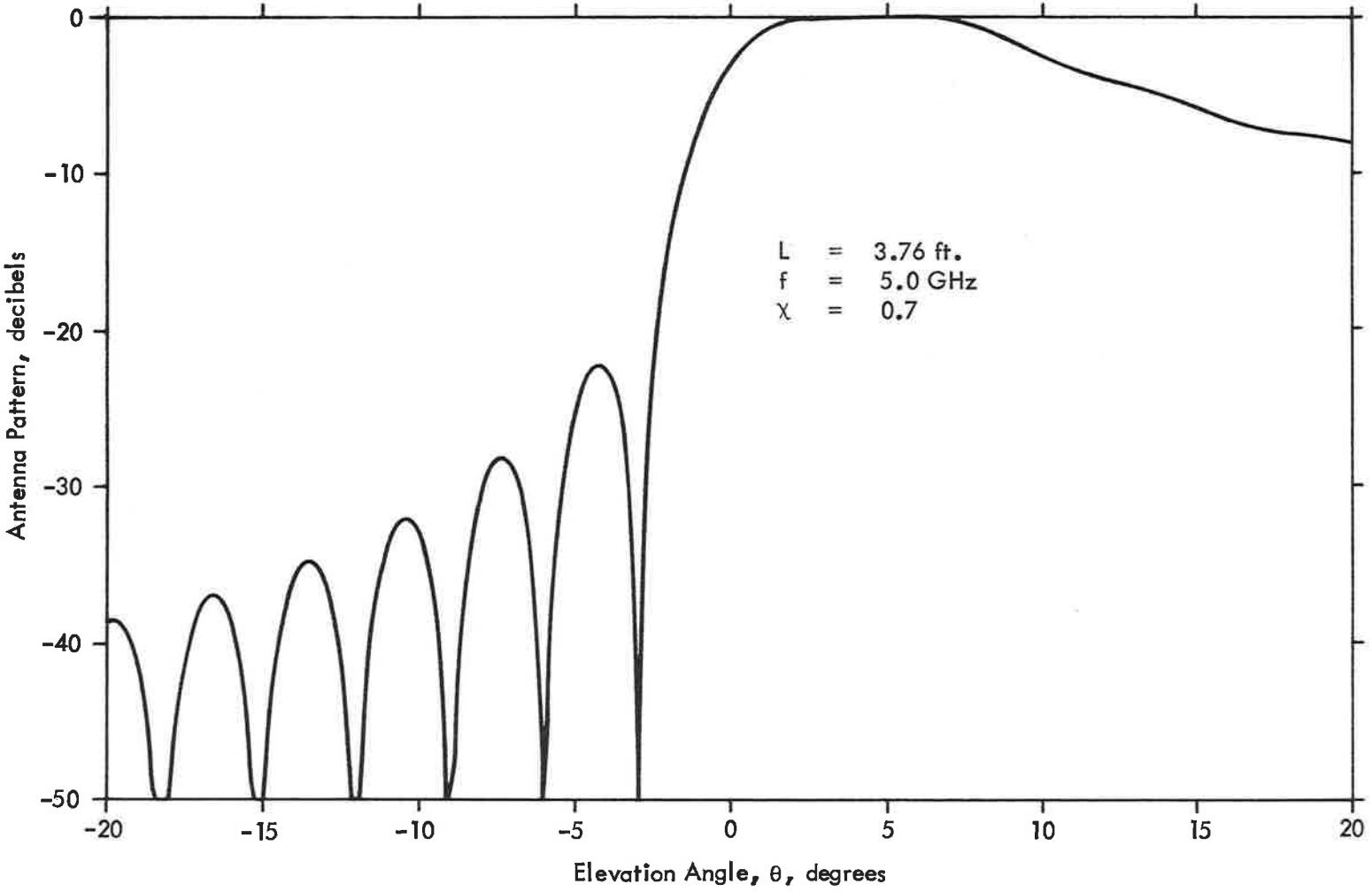

Figure 4.1.7b Free-Space Vertical Antenna Pattern-3.76 Foot Aperture

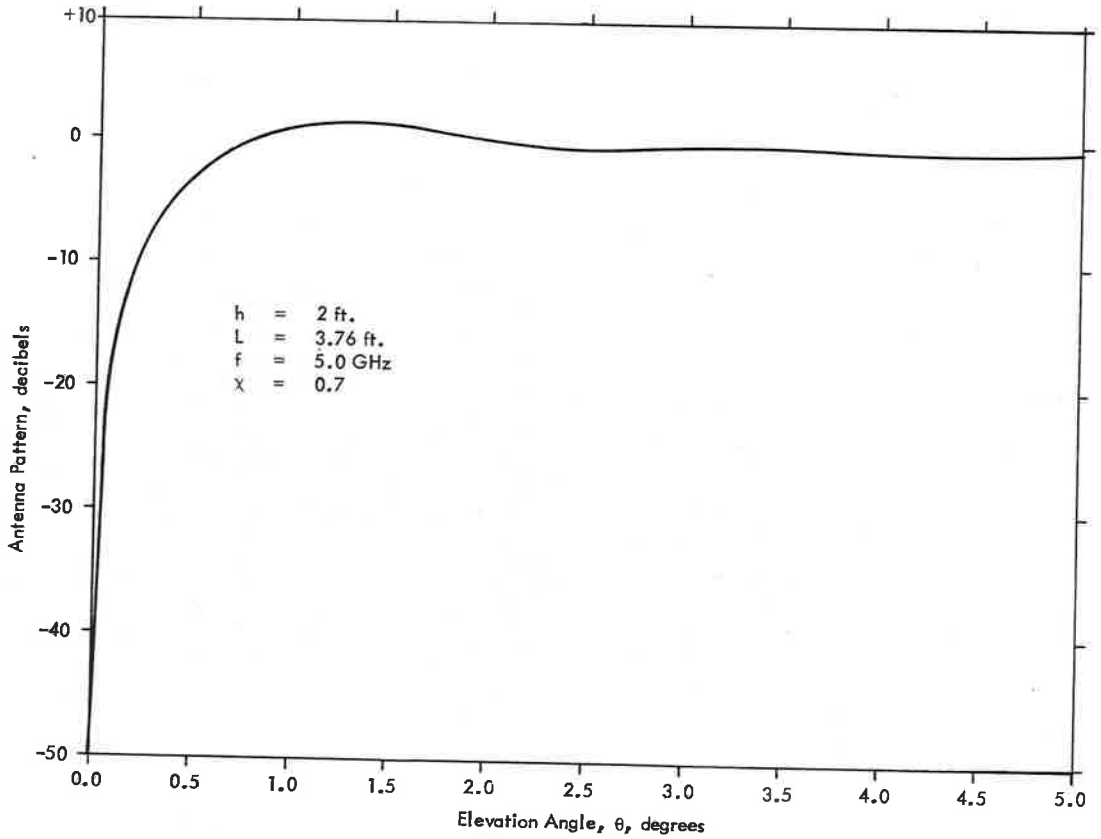

Figure 4.1.7c Composite Vertical Antenna Pattern-2 Foot Height

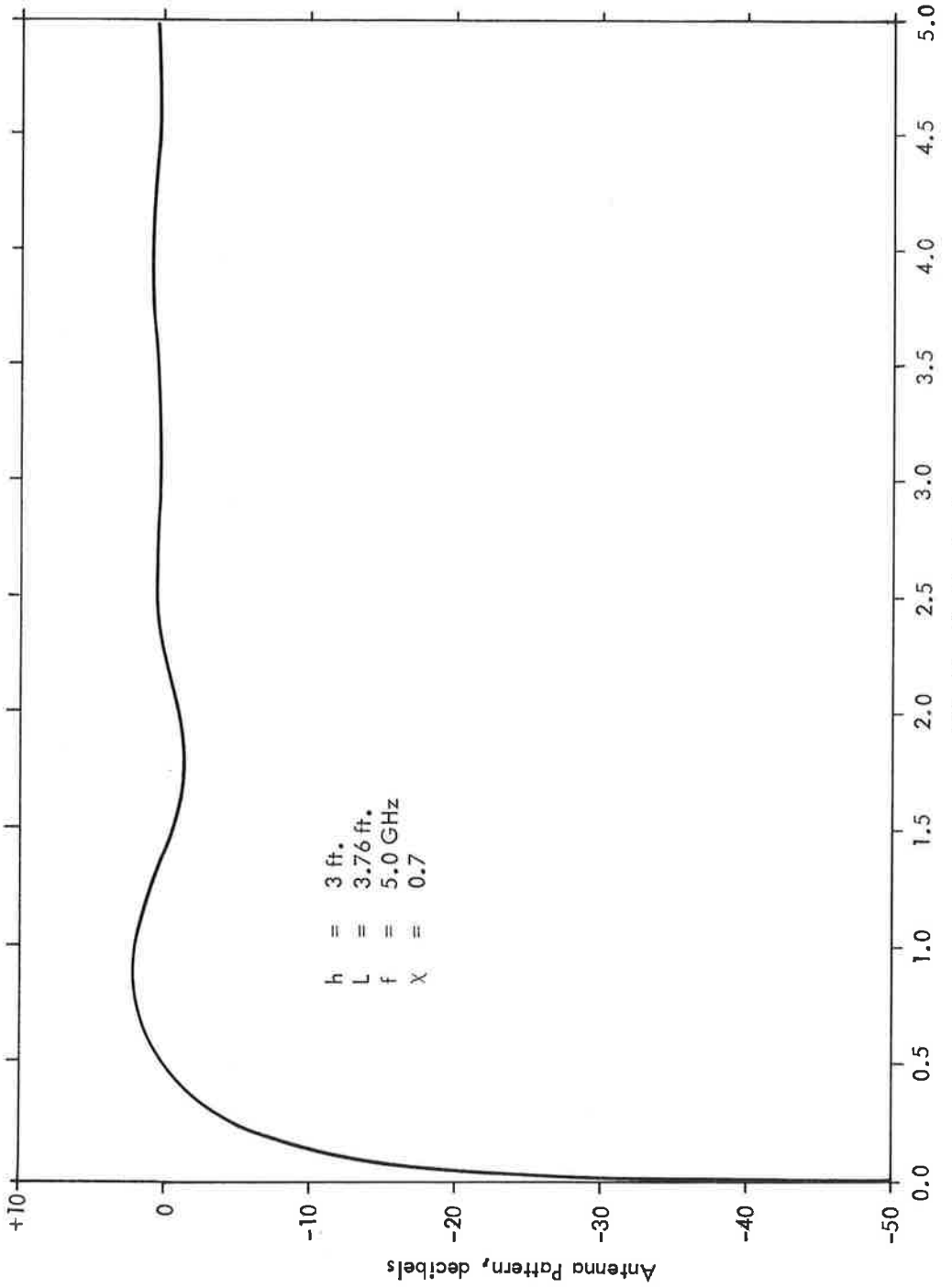

Figure 4.1.7d Composite Vertical Antenna Pattern-3 Foot Height

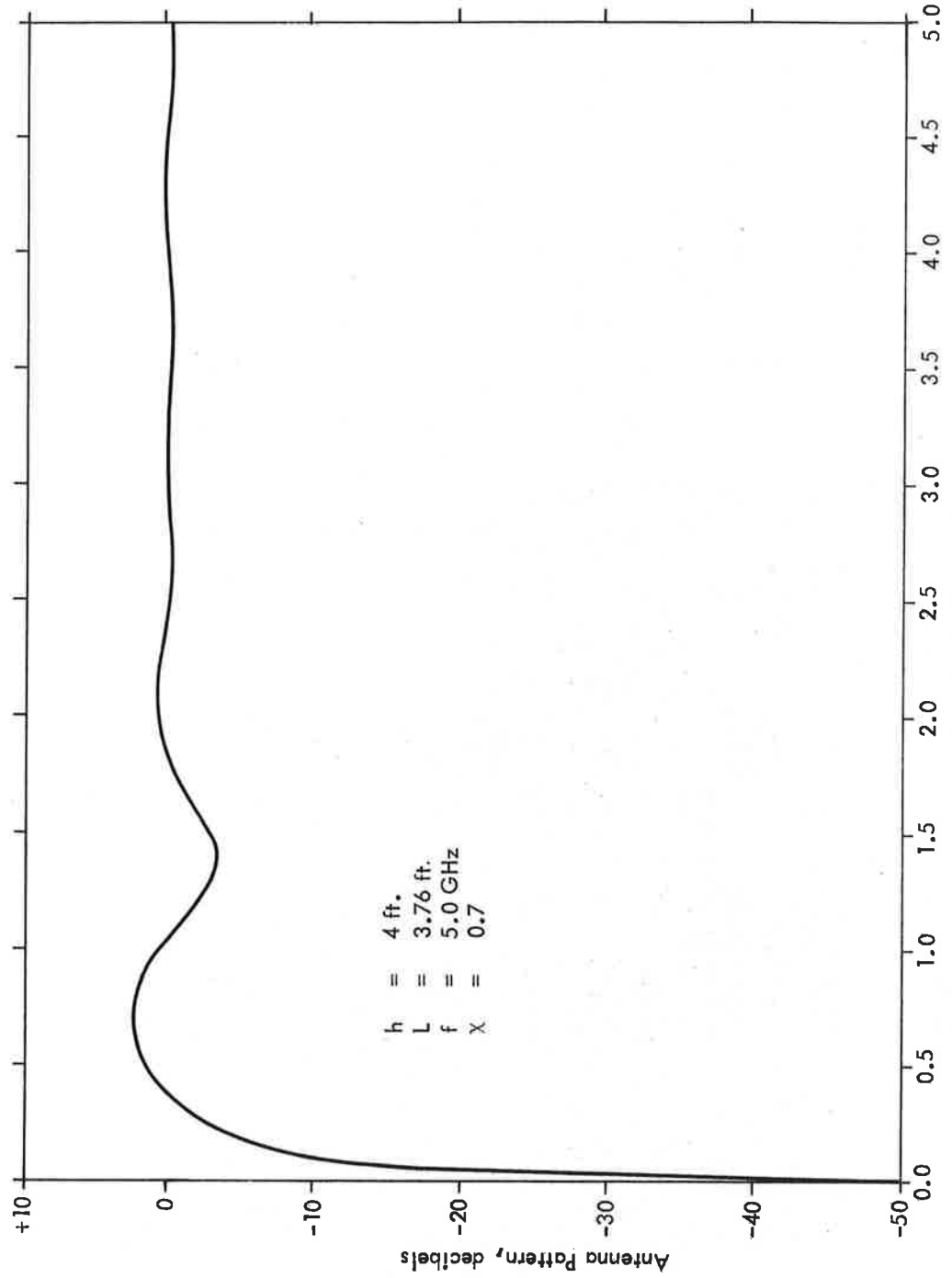

Figure 4.1.7e Composite Vertical Antenna Pattern-4 Foot Height

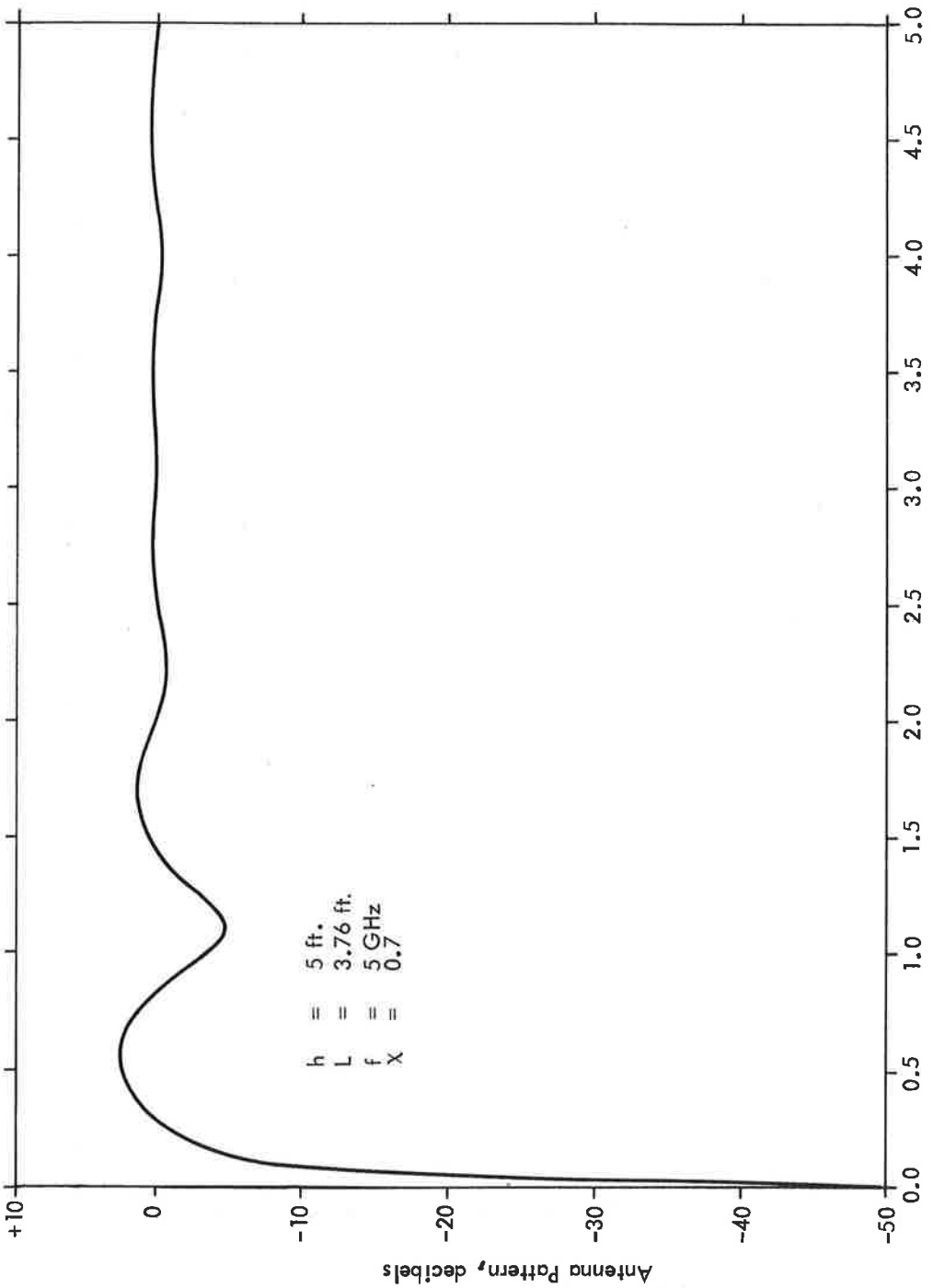

Figure 4.1.7f Composite Vertical Antenna Pattern-5 Foot Height

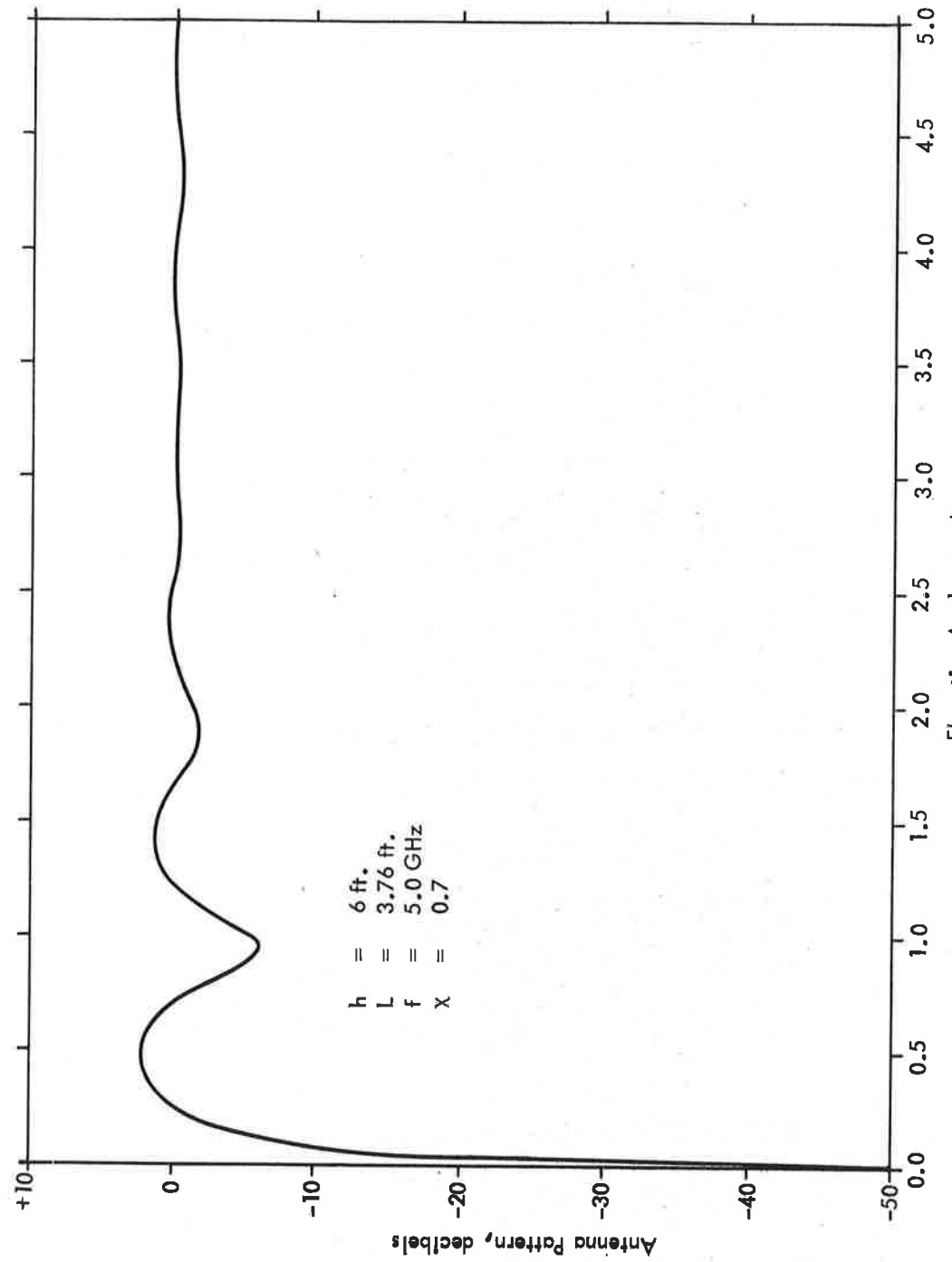

Figure 4.1.7g Composite Vertical Antenna Pattern-6 Foot Height

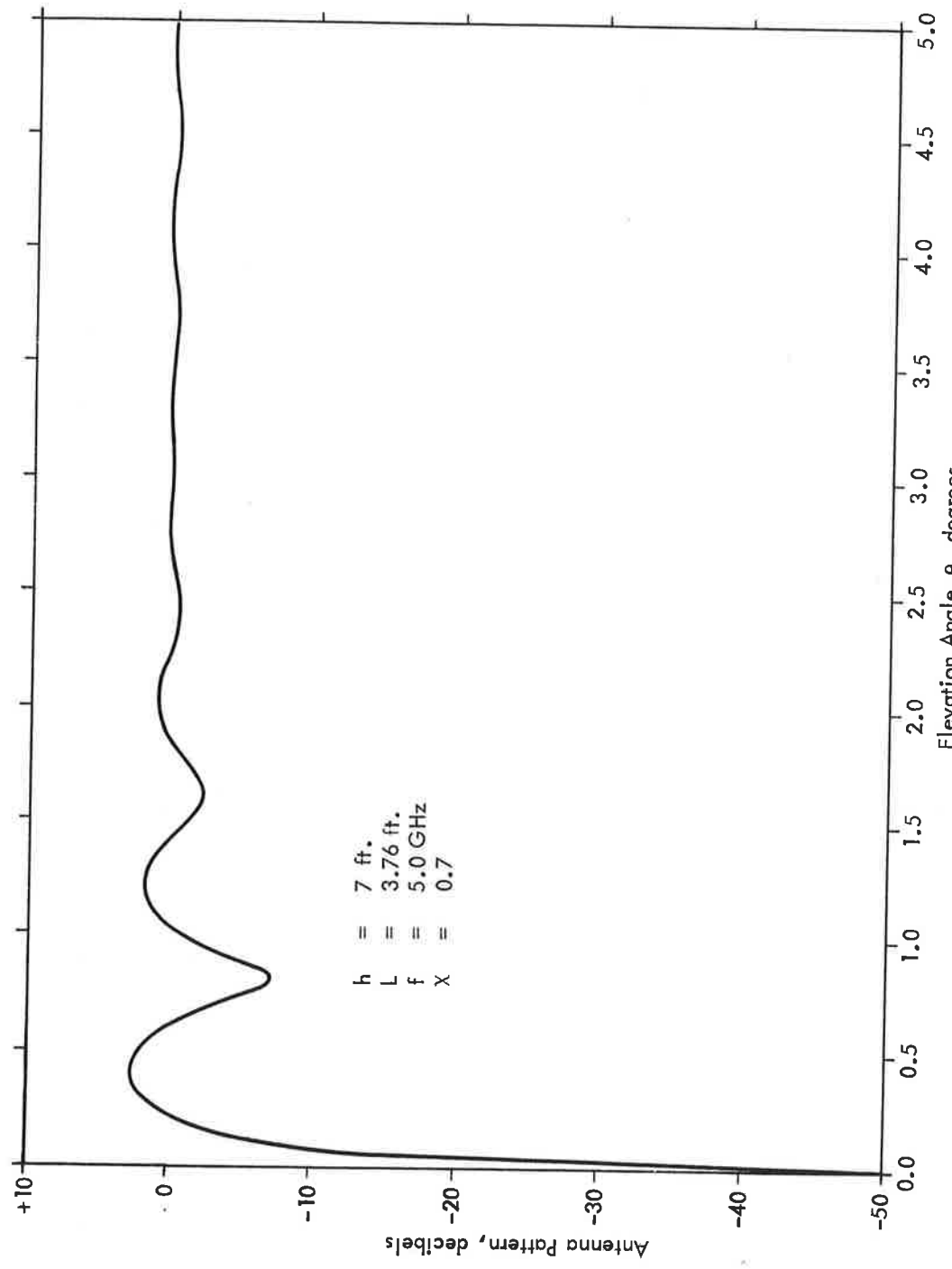

Figure 4.1.7h Composite Vertical Antenna Pattern-7 Foot Height

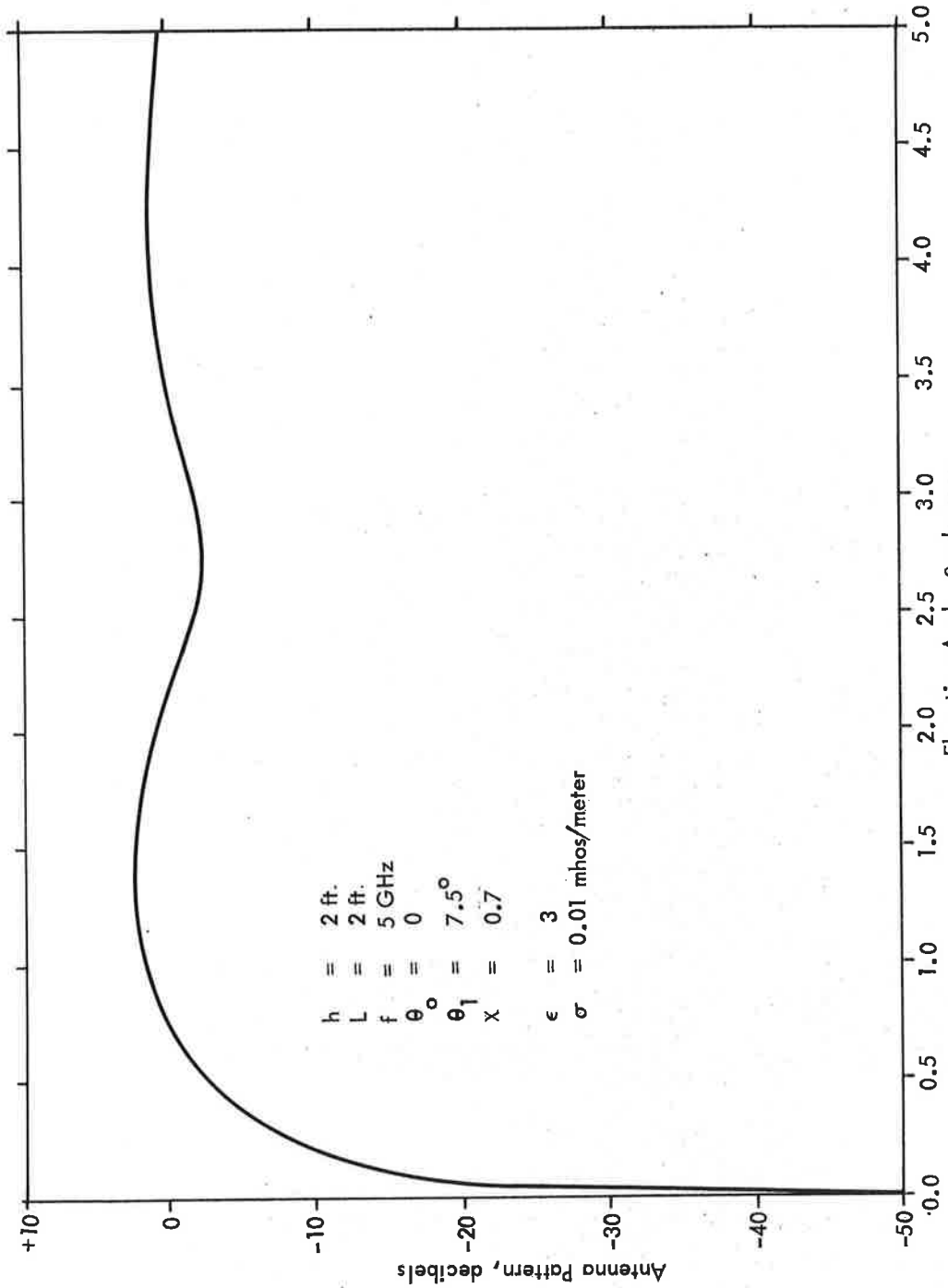

Figure 4.1.8a Composite Vertical Antenna Pattern Above a Dielectric of ϵ=3

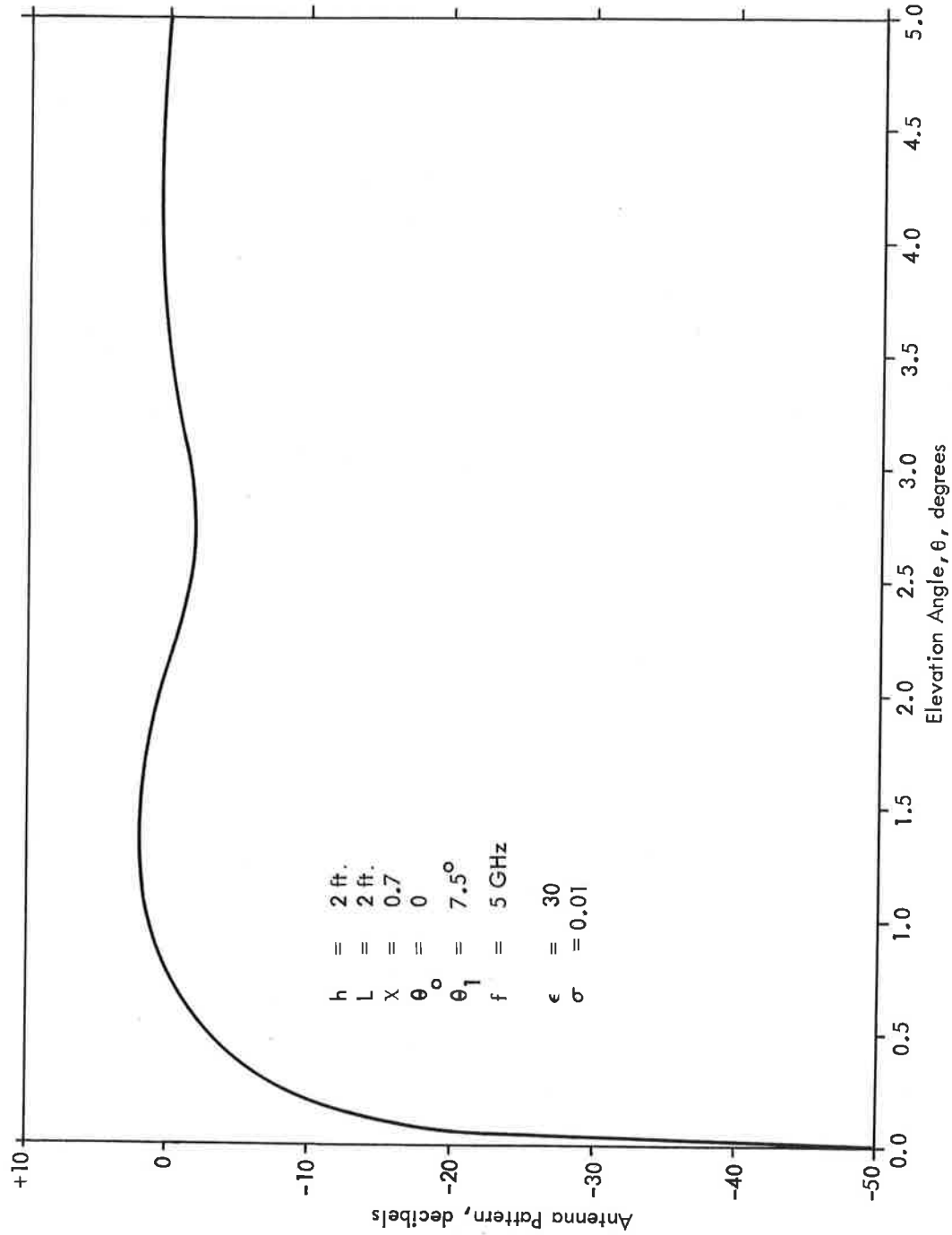

Figure 4.1.8b Composite Vertical Antenna Pattern Above a Dielectric of ϵ=30

4.1.2 Range and Elevation Coverage

Coverage to 20,000 feet in altitude and 25 nautical miles in range is achieved in principle by a shaped-beam pattern in the vertical which is essentially flat from 1° to 7.5° in elevation, and follows the cosecant behavior beyond that. This is discussed in the first annual report.[1] However, the effect of the reflections from the ground is to reduce the range of the antenna at elevations near the minima of the composite patterns. A 6dB reduction in signal results in a range reduction of 2:1. It is important to have enough vertical aperture to reduce these minima. The height determines the location of the minima, and should be adjusted to provide maximum range at highly utilized glide slope angles.

Figure 4.1.9 shows the range variations obtained by use of a 1-foot aperture and an 8-foot aperture. It is apparent then that there must be a tradeoff between three quantities: (1) range requirements at different elevation angles, (2) transmitter power, and (3) azimuth antenna vertical aperture. Since 30 nautical miles is the desired range, and 20 the minimum, a reasonable figure would be 3 dB for the reduction in signal below the full-range value. Also, if between 1° and 2°, this were allowed to relax to 6 dB (a range of 15 nm), an aperture of 4 feet would be more than adequate. In fact, a 2-foot aperture mounted with its center about 6 feet above the ground would satisfy the 20 nm requirement at 2.5°. Allowing for snow clearance, and accounting for the fact that the power requirement is not serious, the vertical aperture requirement appears to be met by an aperture of 4-6 feet at a height of 5-7 feet at the antenna center. However, this does not account for touchdown coverage, nor for the collocation problem with the present ILS. This is discussed further in sections 4.1.3 and 4.1.4

[1] First Annual Report, p.80.

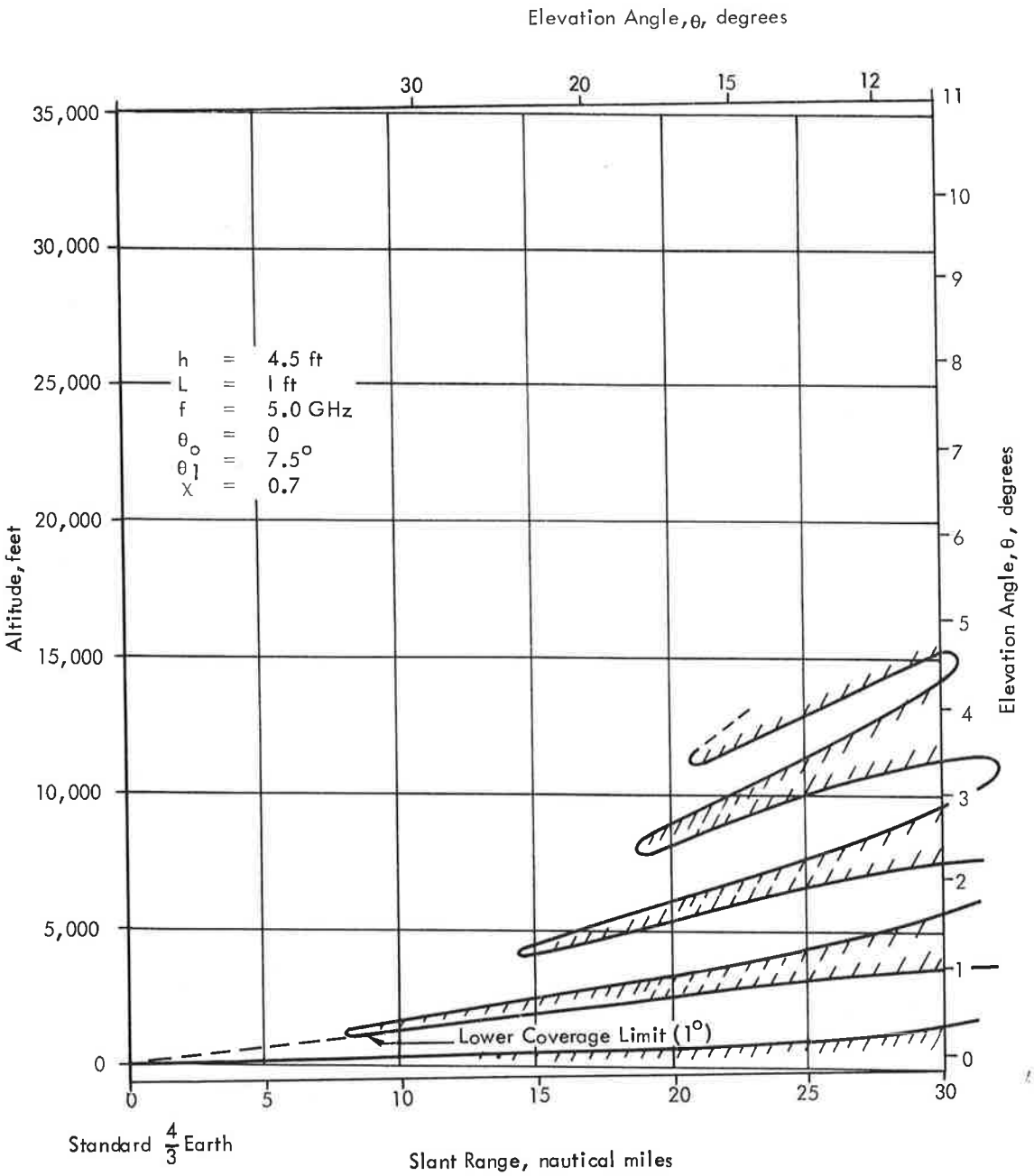

Figure 4.1.9a Range Map for a One-Foot Aperture Mounted 4.5 Feet High

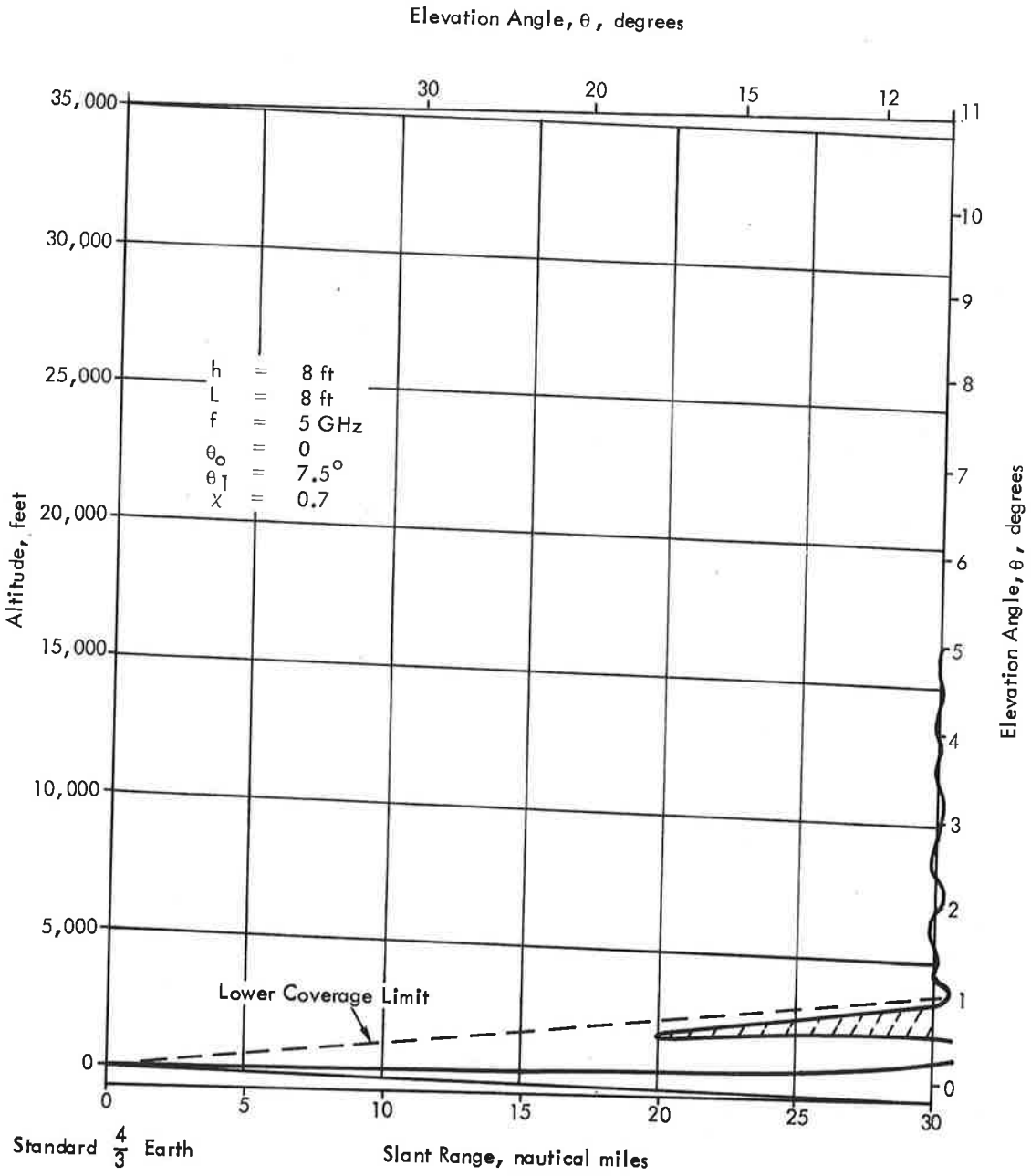

Figure 4.1.9b Range Map for an Eight-Foot Aperture Mounted 8 Feet High

4.1.3 Azimuth Signal Variations in Elevation Plane

As an aircraft comes down the glideslope, it will pass through the minima of the vertical pattern of the AZ antenna. This is demonstrated in Figure 4.1.10.

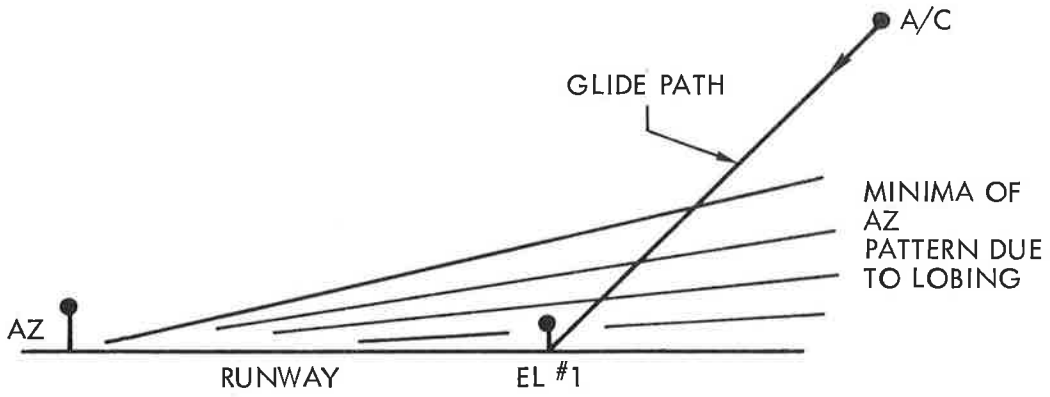

Figure 4.1.10 Geometry Illustrating Why Signal Variations Occur from the AZ Antenna

The signal variations down to the last 2000 feet are not severe for antenna heights which are low to the ground, i.e., having heights comparable to the vertical aperture dimension. This is shown in Figures 4.1.11 and 4.1.12 for an aperture of 4 feet located 3 and 6 feet above the ground. Here the zero dB level indicates the signal level that would be encountered at 30 nautical miles (no attenuation by rain, etc.) and can be taken as -111 dBw.

During the last 2000 feet the signal fades severely. The curves cut off at 250 feet of range, corresponding to a height of about 13 feet (3° glide slope angle). At touchdown the signal can be 8-12 dB below that at 250 feet of range. This suggests that the receiver must be able to follow a signal level that fades by as much as 25 dB in 10 seconds. Additionally if the antenna height is low, the signal at touchdown may be less than that at 30 nautical miles, a topic discussed in the next section.

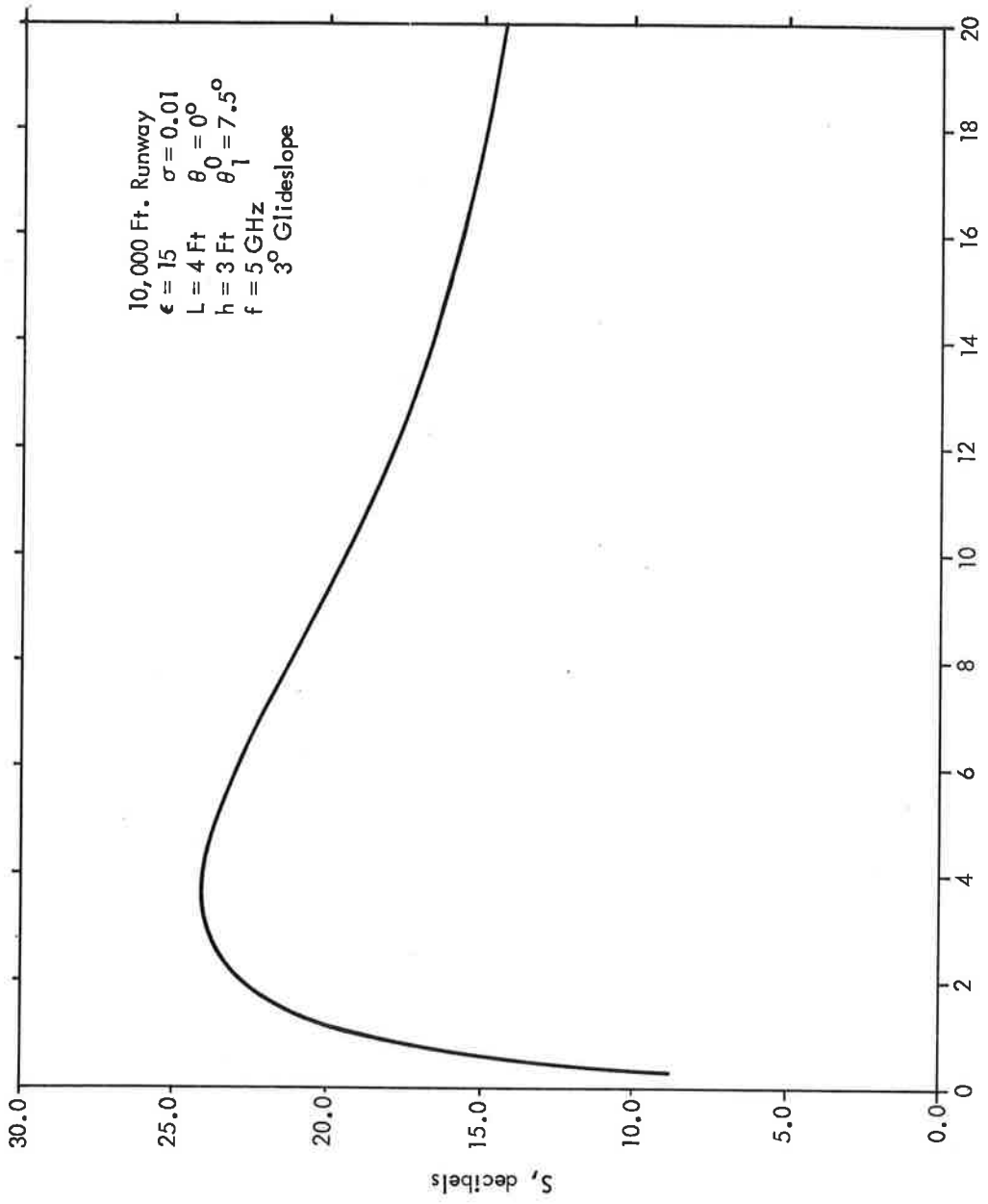

Figure 4.1.11 Signal Variations Encountered on a 3° Glideslope; Antenna Height-3 Feet

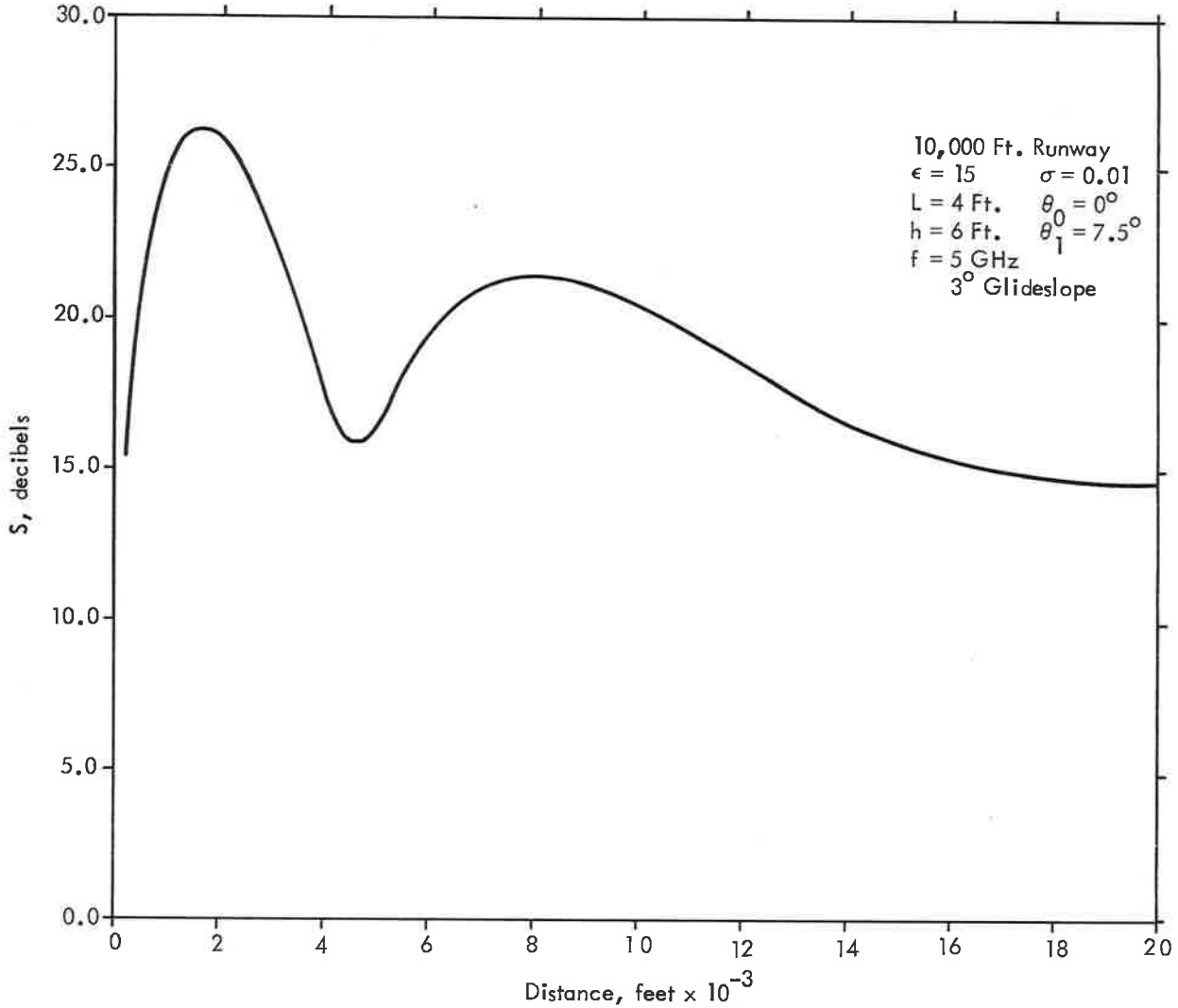

Figure 4.1.12 Signal Variations Encountered on a 3° Glideslope; Antenna Height-6 Feet

The previous discussion relates to the situation where there are no restrictions on antenna height. However, the problem of collocation with the present ILS localizer may require an elevated AZ antenna. The vertical aperture requirement will have to meet two criteria: (1) large enough to reduce signal fluctuations, and (2) large enough to "see over" the localizer, i.e., to reduce the energy reflected off the localizer. A typical situation is indicated in Figure 4.1.13 for a runway length of 14,000 feet, a glideslope angle of 3°, a height of 20 feet, and a 4-foot aperture. The fluctuations are as much as 17 dB, and can occur in 3 seconds. The receiver AGC must be able to follow the most rapid fluctuations likely to be encountered, which means for the case of the greatest antenna height to be encountered. Twenty feet appears to be a good working figure. The fact that the nulls are narrow means that a slower AGC response may be adequate, since 1-3 data samples may be lost without affecting the system performance.

It should be borne in mind that these are calculated figures, and that a measurement may determine that the fading is not as great as predicted here.

4.1.4 The Effect of Antenna Height on the Signal Level During Rollout

As an aircraft approaches the runway, the signal level from the azimuth antenna increases in level since the aircraft is closer to the transmitter. Near touchdown the signal fluctuates due to the lobing. At touchdown the reflected ray and direct ray are almost out of phase, so that the signal level becomes very small, and can fall below the signal level at 30 nm if the transmitter height is too low. The solution in the case of too small a signal during some phase of rollout is simply to raise the transmitting antenna; a larger aperture buys very little. In practice, convex runways may require a further increase in antenna height. A good working figure appears to be a height of about 9 feet for a 10,000 foot runway.

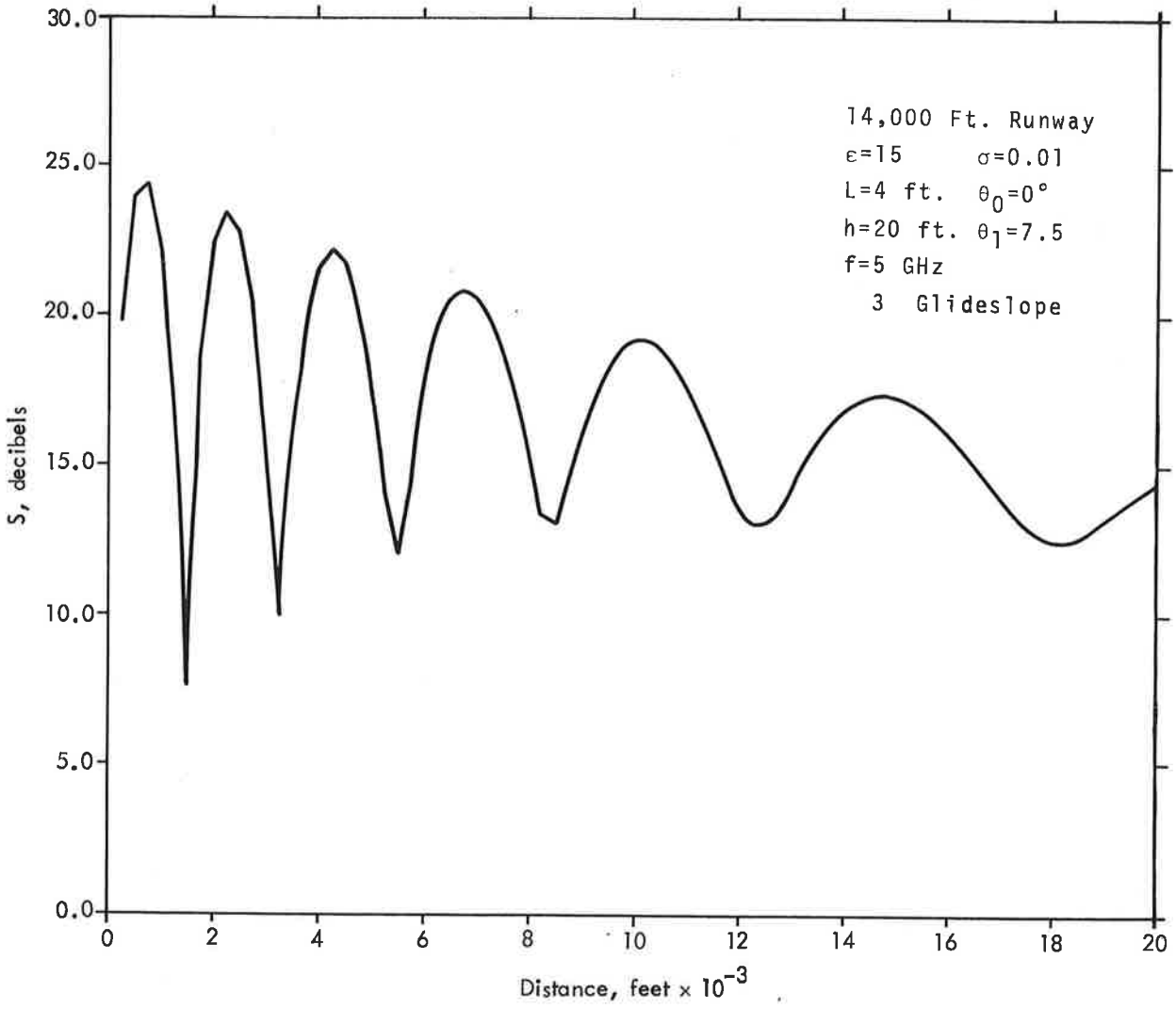

Figure 4.1.13 Signal Variations Encountered on a 3° Glideslope; Antenna Height-20 Feet

The analysis is straightforward: the angular variation of the signal is found from equation (4.1.2). It is assumed that $\theta \approx 0$, and $\Gamma \approx -1$; then

$$f(z) \approx g(o)\left[1 - e^{-jkhz/x} \right] \qquad (4.1.8)$$

where z is the aircraft antenna height, and x is the distance along the ground between transmitting and receiving antennas. The signal power falls off as $1/x^2$, so that

$$S(z,x) \sim \left| f(z,x) \right|^2 / x^2 \qquad (4.1.9)$$

For purposes of comparison, assume that the range of the antenna is 30 nm at an elevation angle of 3°, and use the free-space antenna pattern there; the signal there is

$$S(3°,\ 30\ nm) = S_o \sim \left| g(3°) \right|^2 / (180{,}000)^2 \qquad (4.1.10)$$

Then the relative signal s(z,x) is given by

$$s(z,x) \triangleq \frac{S(z,x)}{S_o} = \left[\frac{f(z,x)}{g(3°)} \cdot \frac{180{,}000}{x} \right]^2 \qquad (4.1.11)$$

The smallest signal occurs at touchdown, where x is the maximum distance away; let z be 3 feet, as a reasonable lower limit on aircraft antenna heights to be encountered, and let x = 10,000 feet. Then the problem is to find the height for which s(z,x) = 1, i.e. that height which results in a signal level at touchdown that is equal to the signal level at 30 nm and 3° elevation. Since the exponential is small,

$$e^{-jkhz/x} \approx 1 - jkhz/x \qquad (4.1.12)$$

and we get, solving for h:

and we get, solving for h:

$$h = \frac{g(3°)}{g(o)} \cdot \frac{10,000}{180,000} \cdot \frac{10,000\lambda}{2\pi \cdot 3} = \frac{5.9}{\chi} ft \qquad (4.1.13)$$

If the antenna pattern at the horizon is down by 3 dB from that at 3°, h = 8.5 feet at C-band and 2.8 feet at Ku-band. If aircraft antenna heights are 6 feet above the ground or more, the heights listed above can be halved.

This is premised on the assumption of a flat runway. Clearly, if the runway is convex, the antenna will have to be raised. Another solution is to increase the power, although this is probably less desirable.

As the antenna is raised, the signal amplitude variations encountered by an approaching aircraft can be quite severe, as noted in the previous section. On the other hand, the transmitter power needed to attain 30 nautical miles includes 3-6 dB of margin to account for rainfall attenuation. Since the attenuation over the much shorter distance on the runway is quite small, the need for the margin is reduced. Thus if a 6 dB margin were used to determine transmitter power, the heights listed above could be halved.

It is believed, then, that a 4-foot aperture at C-band mounted 6 feet above the ground will probably suffice for most cases. This is a critical judgement that requires experimental verification before these numbers are to be treated as final recommendation.

The problem of collocation of the MLS equipment with the present ILS equipment is a very difficult issue. The treatment above assumes that there are no restrictions. However, if the MLS AZ antenna is placed in front of the localizer, it may be necessary to use low-profile antennas. If behind, it may be necessary to raise it to 20 feet or more in height, which causes severe lobing, and requires a large structure.

4.2 ELEVATION ANTENNA - THE EFFECT OF LOWER COVERAGE LIMIT REQUIREMENTS ON BEAMWIDTH AND ANTENNA HEIGHT

ABSTRACT

As an elevation beam is scanned downward, energy from sidelobes pointed at the ground are reflected up and received by the aircraft receiver; they cause pointing errors. As the beam is scanned further downward, part of the main beam is reflected up (in-beam multipath). An aircraft too low will see both the direct and the reflected beam above the threshold, which can result in a severe error (up to half a beamwidth). The first section below deals with the pointing error due to a sidelobe reflection, and results in a recommendation on sidelobe level requirements and heights for the elevation antennas. The second deals with low angle coverage and the near-field problem associated with EL #2.

4.2.1 Beam Pointing Errors Due to Ground Reflections: Optimum Height Considerations

The method used to calculate the maximum angular error encountered by an aircraft due to ground reflections is a conservative one: the aircraft is assumed to be located on the beam threshold (e.g., the 10 dB point on the free-space pattern). The reflection causes a beam shift which depends on the relative path

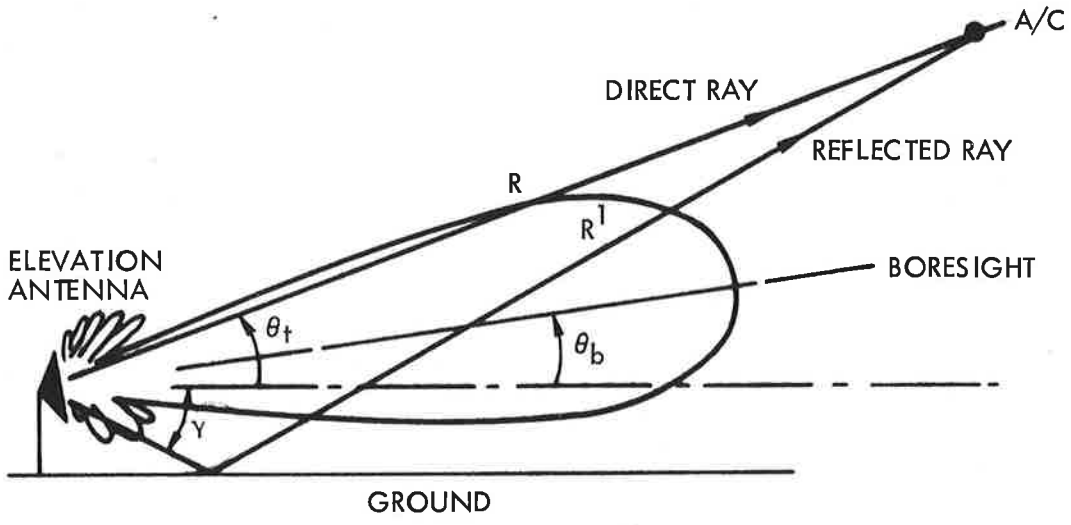

Figure 4.2.1 Reflections from Sidelobes - Geometry

lengths of direct and reflected rays. The worst possible relation is assumed, and the beam edge shift is calculated. The total beam center shift must be less than this.

Assume that the antenna has a free-space elevation field pattern given by $g(\psi)$, where $\psi = 0$ defines the boresight angle and $g(0) = 1$. The free-space power pattern $f_o^* f_o$ is given by $g^*(\psi)g(\psi)$, where the asterisk denotes the complex conjugate. The composite field pattern, taking into account reflections, is given by

$$f(\theta_t, \theta_b) = g(\theta_t - \theta_b) + \epsilon(\theta_t, \theta_b) \qquad (4.2.1)$$

where θ_t is the target angle of the aircraft, θ_b is the boresight angle, and

$$\epsilon = \Gamma e^{-jk(R' - R)} g(-\gamma) \qquad (4.2.2)$$

where Γ is the (complex) reflection coefficient of the earth, and the other parameters are shown in Figure 4.2.1.

With no reflections, the beam edge θ_{bo} is defined as the angle at which the power pattern is equal to some prescribed level:

$$f_o^* f_o(\theta_t, \theta_{bo}) = \left| g(\theta_t - \theta_{bo}) \right|^2 = K^2 \qquad (4.2.3)$$

(For example, if the 0.1-power point defines the beam edge, $K^2 = .1$).

Accounting for reflections, the beam edge is at θ_{b1}, where θ_{b1} is found from the relation

$$\begin{aligned} f^* f(\theta_t, \theta_{b1}) &= K^2 \\ &= \left| g(\theta_t - \theta_{b1}) \right|^2 + \left| \epsilon(\theta_t, \theta_{b1}) \right|^2 \\ &\quad + 2\mathrm{Re}\left\{ g(\theta_t - \theta_{b1})\, \epsilon(\theta_t, \theta_{b1}) \right\} \end{aligned} \qquad (4.2.4)$$

Assuming the shift in the beam edge is small, the following relations hold:

$$g^*(\theta_t - \theta_{b1})g(\theta_t - \theta_{b1}) \doteq g^*(\theta_t - \theta_{bo})g(\theta_t - \theta_{bo}) + \delta\theta_b \frac{d}{d\theta_b}\left(g^*g(\theta_t - \theta_b)\right)\Big|_{\theta_b = \theta_{bo}} \quad (4.2.5)$$

where $\delta\theta_b = \theta_{b1} - \theta_{bo}$, and

$$\epsilon(\theta_t, \theta_{b1}) \doteq \epsilon(\theta_t, \theta_{bo}) \quad (4.2.6)$$

From relations (4.2.3) to (4.2.6), the boresight shift is

$$\delta\theta_b = \frac{2\mathrm{Re}\left\{ g(\theta_t - \theta_{bo})\, \epsilon(\theta_t, \theta_{bo}) \right\}}{\frac{d}{d\theta_b}\left(g^*(\theta_t - \theta_b)g(\theta_t - \theta_b)\right)\Big|_{\theta_b = \theta_{bo}}} \quad (4.2.7)$$

This expression looks more complicated than it is. Basically it says that the boresight shift due to reflections is proportional to the strength of the reflected field, and inversely proportional to the slope of the antenna pattern at the beam edge.

The <u>maximum</u> beam edge shift occurs when $g(\theta_t - \theta_{bo})$ and $\epsilon(\theta_t, \theta_{bo})$ are exactly in or out of phase; thus

$$\left|\delta\theta_b\right| \le \frac{2\left| g(\theta_t - \theta_{bo})\epsilon(\theta_t, \theta_{bo})\right|}{\left|(g^*g)'\right|} \quad (4.2.8)$$

where the denominator term of (4.2.8) is merely a short-hand way of expressing the denominator of (4.2.7). This can be re-written as

$$\left|\delta\theta_b\right| \le \frac{\left|\epsilon(\theta_t, \theta_{bo})\right|}{\left|\frac{d}{d\theta_{bo}} g(\theta_t - \theta_{bo})\right|} \quad (4.2.9)$$

To get some useful results, let us consider a typical beam shape of the form sin x/x:

$$g(\psi) \doteq \frac{\sin(\pi\psi/\Delta\theta)}{\pi\psi/\Delta\theta} \tag{4.2.10}$$

where $\Delta\theta$ is the 3 dB beamwidth, approximately. The derivative is given by

$$\frac{dg}{d\psi} = \frac{\cos(\pi\psi/\Delta\theta)}{\psi} - \frac{\sin(\pi\psi/\Delta\theta)}{\pi\psi^2/\Delta\theta} \tag{4.2.11}$$

At the 3 dB points $\left| \psi \right| = \Delta\theta/2$, and

$$\left|\frac{dg}{d\psi}\right| = \frac{4}{\pi\Delta\theta} \tag{4.2.12}$$

The maximum beam edge shift is, in fractional beamwidths,

$$\frac{\delta\theta_{b,max}}{\Delta\theta} = \frac{\pi}{4}\left| \epsilon(\theta_t, \theta_{bo}) \right| \tag{4.2.13}$$

From equation (4.2.2), if the reflection coefficient is -1, $\epsilon(\theta_t, \theta_{bo})$ is merely the sidelobe level of the reflected wave. (For angles of arrival near grazing incidence, the reflection coefficient is near -1.) Then (4.2.13) can be written in the convenient form

$$\frac{\delta\theta_{b,max}}{\Delta\theta} = \frac{\pi}{4} \cdot \text{SLL} \tag{4.2.14}$$

This is plotted in Figure 4.2.2. It can be seen that to keep the beam edge shift less than 1/50-th of a beamwidth the sidelobe level requirement on the antenna would be 32 dB, which is quite a severe requirement. If the other beam edge is undisturbed, the beam shift is half that value.

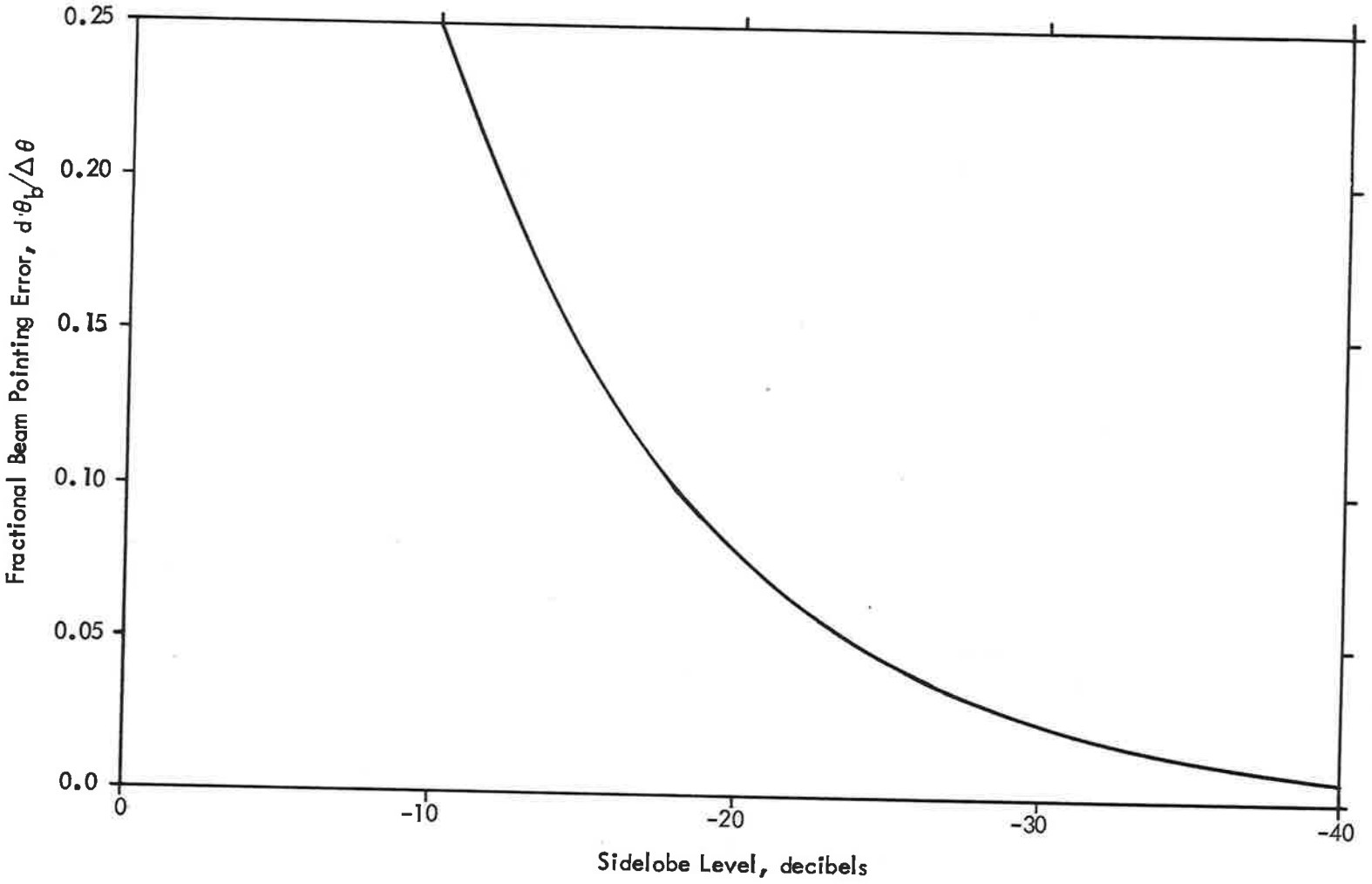

Figure 4.2.2 Maximum Beam Pointing Error Due to Reflections from Sidelobes

The analysis thus far is a worst-case study in two respects: one is that the phase of the reflected ray is such as to cause the largest beam edge shift; the other is that the reflection coefficient is conservatively assumed to be -1. The actual reflection coefficient Γ as a function of grazing angle can only be determined by experiment.

The phase of the reflected ray depends on the height of the antenna as well as the phase of the reflection coefficient. Thus the possibility of choosing a height which minimizes the effect of a chosen sidelobe (the nearest one) presents itself. In order to study this, a cosine-square-on-a-pedestal distribution was used to vary the sidelobes of a linear aperture. Thus in equation (4.2.1),

$$g(\theta_t, \theta_b) = \frac{\sin \pi u}{\pi u}\left(1 - \frac{u^2}{(2p + 1)\ (u^2 - 1)}\right) \qquad (4.2.15)$$

where $u = \frac{L}{\lambda}(\sin \theta_t - \sin \theta_b)$, p is the aperture edge amplitude, and L is the aperture height.

In order to bracket the errors, the reflection coefficient T is assumed to be -1, and the exponential term of equation (4.2.2) is assumed to be unity (this corresponds to an antenna height of zero, physically impossible). In Figure 4.2.3, the resulting boresight angles are plotted against the actual target angles for two different receiver thresholds, and for two different sidelobe levels in the free-space pattern.

It is evident that lower sidelobe levels result in better accuracy and that a lower receiver threshold gives better discrimination against the sidelobe multipath. The latter result comes about primarily because the slope of the antenna pattern at the 10 dB points is steeper than at the 3 dB points. (The difference in slopes does not appear to account for all the variation observed, however.)

Taken to the limit, it would appear that for actual elevation angles below about .8 beamwidths that the indicated angle is about .7 beamwidths. However, this is an artificial result which comes

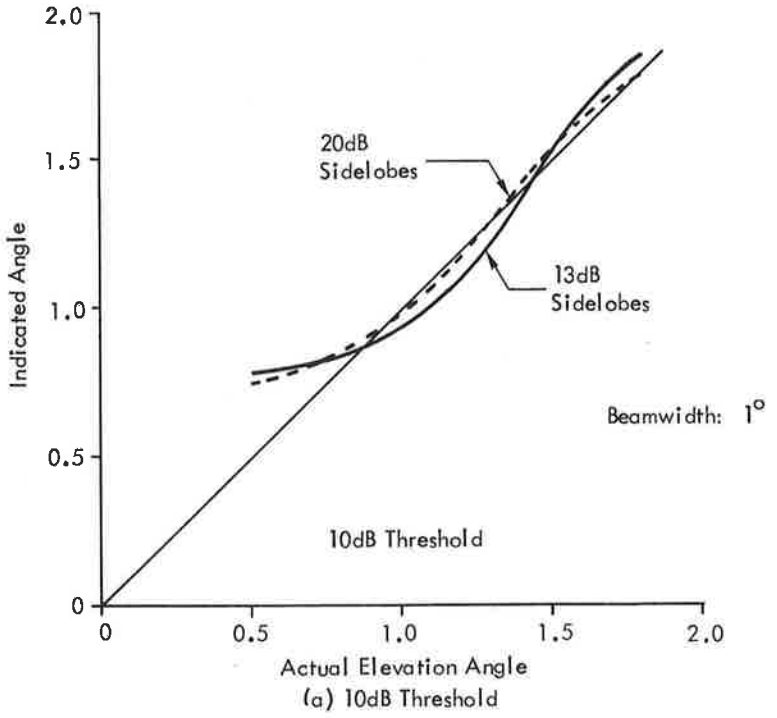

(a) 10dB Threshold

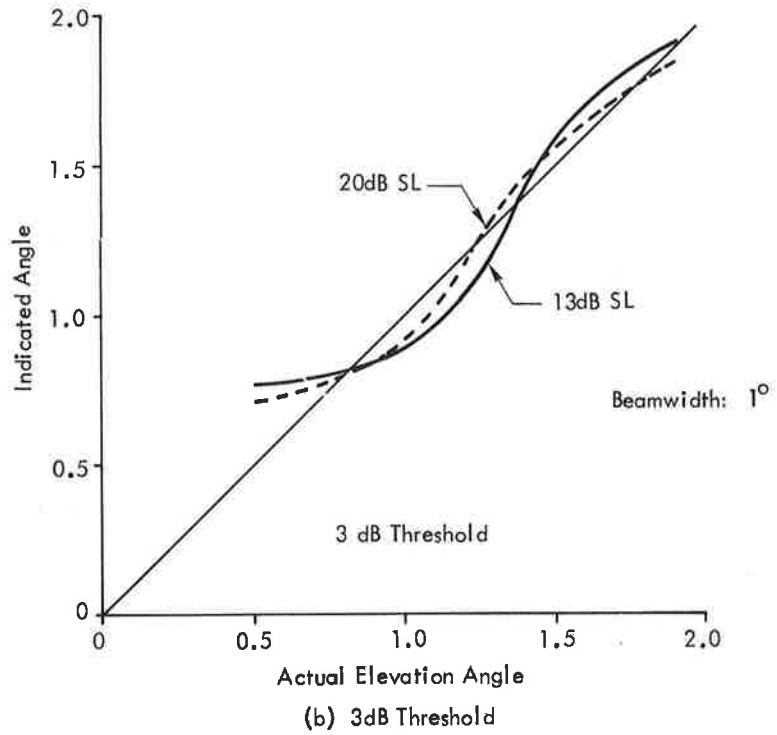

(b) 3dB Threshold

Figure 4.2.3 Measured Elevation Angle vs Actual Elevation Angle for Various Sidelobe Levels-Worst Case

about from the zero height assumption (for zero height, there is a pattern null when the beam points at the horizon). For practical antenna heights this does not occur. Thus the figures should not be interpreted below about .8 beamwidths.

The error in measurement which would occur at the receiver is shown in Figure 4.2.4 for sidelobe levels of 13 dB, 20 dB, and 30 dB, for which $p = \infty$, 1.17, and 0.48, respectively. The shape of the curves for aperture distributions other than cosine^2-on-a-pedestal would be different in shape, but similar in magnitude to those presented here. In these figures, the beamwidth was maintained by increasing the aperture dimension.

The next step of varying the transmitter height was taken by using a variety of heights from 7 feet to 16 feet for a 1° beamwidth antenna, and looking at the results.

It turns out that the optimum height appears to be slightly larger than the aperture height; this holds for different sidelobe levels as well. For the optimum height, the error above .8° is reduced to 50-60% of the worst-case value. Thus a 52 λ aperture with its center 13 feet above the ground with 20 dB sidelobes ideally can give a maximum error of .050°. The use of a larger aperture, namely 61λ high, yields 20 dB sidelobes and has a 1° beamwidth, which is a better comparison (a 52 λ aperture with 20 dB sidelobes has a beamwidth of 1.15°). For this antenna, the error is .045°. Below .8° the in-beam multipath causes the reflected beam to merge with the main beam, resulting in a sudden large error, giving essentially a zero-angle indication. (This assumes that the transmitter is not turned off for boresight angles below the horizon).

The RTCA accuracy requirement is that the error in height not exceed 1.2 feet, at the minimum guidance height of 50 feet for CAT II and at the threshold for CAT III. For EL#1, this results in an error limit of .024° at an elevation angle of 1°. For higher angles the allowable angular error is less severe. This puts the allowable sidelobe level at about 30 dB, which is unrealistic.

The region between 1° and 2° needed primarily for coverage; glide slopes are usually above 2°. It does not appear that the

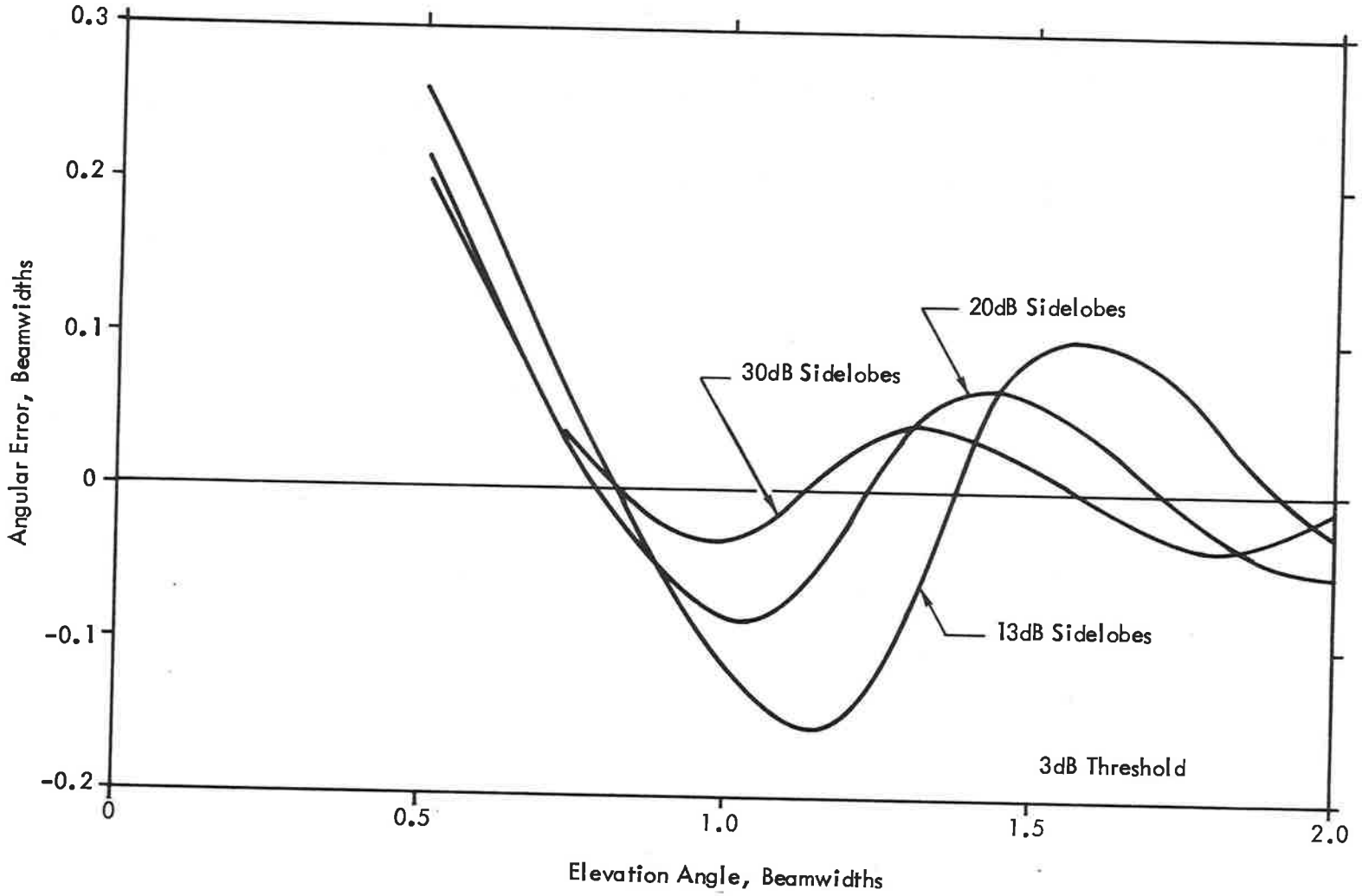

Figure 4.2.4 Measurement Error in Elevation Angle for Various Sidelobe Levels-Worst Case

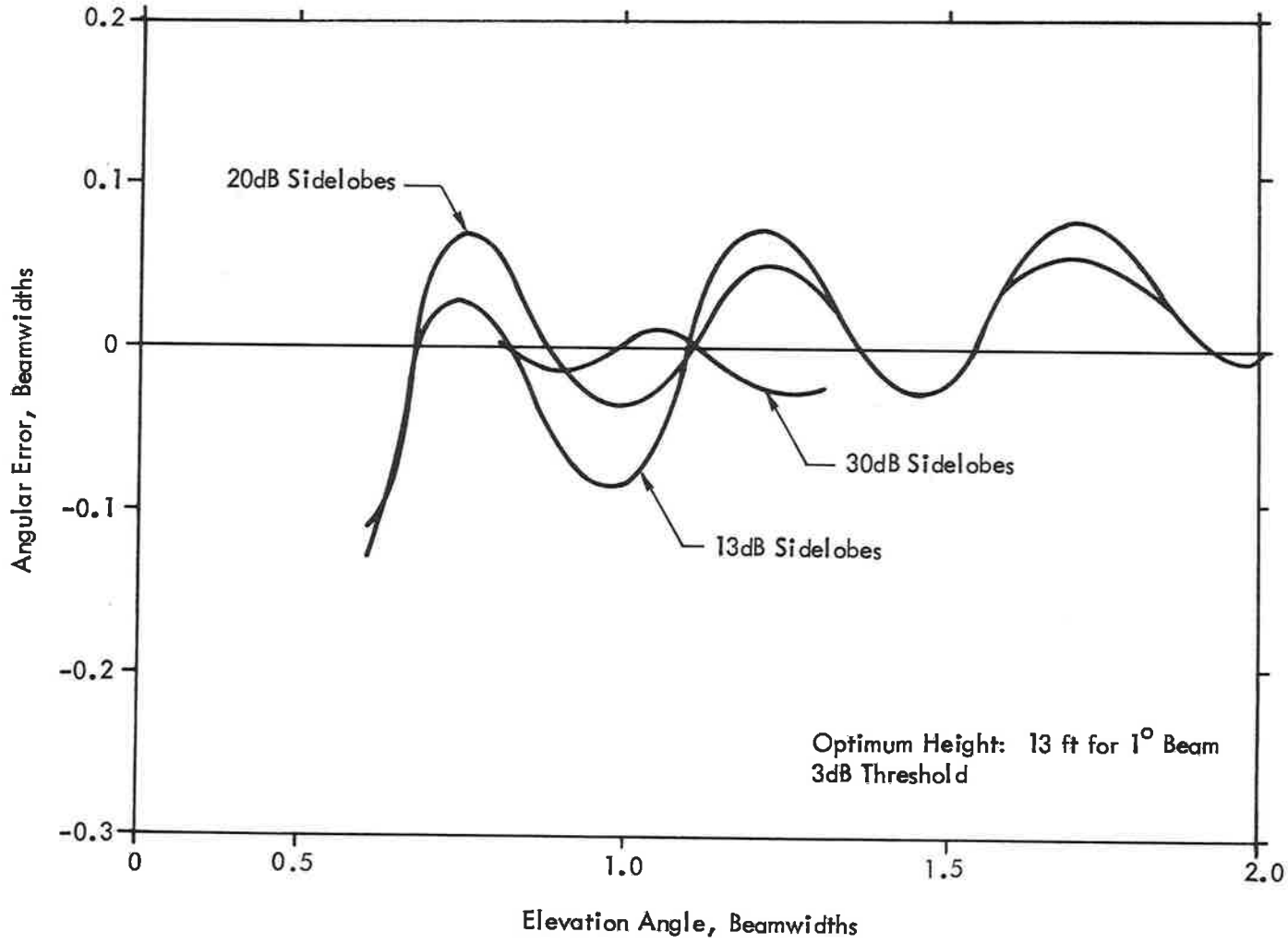

Figure 4.2.5 Calculated Measurement Error in Elevation Angle for Various Sidelobe Levels-Optimized Height

error incurred with 20 dB sidelobes is excessive (namely, 2.3 feet at a distance of 3000 feet). Additionally, the reflection coefficient magnitude may be reduced somewhat in practice below the unity figure assumed here. This is an important measurement which needs to be made before final specifications are frozen. At this point, a design goal of 25 dB sidelobes and a minimum of 22 dB appears to be a reasonable choice for EL#1.

In practice the phase of the reflection coefficient may deviate from 180°, and the antenna pattern itself may have far-field phase deviations which qualify the choice of heights for the antenna. This is another important matter which needs experimental verification. Subject to the qualifications above, the criterion for optimum height is given by

$$h_{opt} = \frac{5L}{4} \tag{4.2.16}$$

where L is the aperture in feet. Expressed in terms of frequency, this becomes, approximately,

$$h_{opt} = \frac{65}{f\Delta\theta} \quad \text{(feet)} \tag{4.2.17}$$

where f is in GHz. For a 1° beamwidth, as in EL#1, the optimum height is about 13 feet. For 25 dB sidelobes, an aperture of about 12.3 feet is necessary, which puts the lower edge of the antenna about 7 feet above the ground. For EL#2, the optimum height is about 8.7 feet.

For EL#2 the error must be less than 1.4 feet at the threshold, about 3000 feet away. This corresponds to an error of 0.027°, which is .054 beamwidths. This is achievable with 20 dB sidelobes, using the discussion above and scaling to the EL#2 beamwidth of 0.5°. Since guidance information is crucial in the flareout region, it is recommended that a design goal of 26 dB be used on EL#2. Since the frequency here is 15 GHz, the technological problem of achieving 26 dB sidelobes is difficult, and may prove unfeasible. The

random error corresponding to 26 dB sidelobes is about 6° rms, which is very tight.

The conclusions of this section can be summed up in the following recommendations:

1. If operationally permissible the requirements for CAT II guidance should be relaxed to read as follows: 2.5 foot accuracy from 1° to 2°, at the minimum guidance height. This is subject to experimental verification; it may well prove that due to undulations in airport surfaces, even more relaxation of the specification to 4 feet of accuracy may be necessary.
2. The requirements for CAT I guidance may require similar alleviation near the lower coverage limit, if permissible operationally.
3. The sidelobe specifications for EL#1 and EL#2 are as follows: 25-26 dB design goal, 22-23 dB minimum for sidelobes out to 4 beamwidths from the beam center; 30 dB sidelobes beyond that.
4. The optimum height for EL#1 is about 13 feet; for EL#2, about 8.7 feet.
5. All of the above recommendations are tentative, and subject to experimental verification with an elevation antenna.

4.2.2 The Effect of Lower Coverage Limit Requirements on Beamwidth, Height, and Location of EL#2 Antenna

In the previous section sidelobe reflections were discussed. It can be seen that if the beam is scanned further down, eventually the main beam itself would be reflecting from the ground. The signals seen by the aircraft well above a critical height, and below a critical height are shown in Figure 4.2.6. It is assumed that the antenna is scanning downward (i.e., from high elevation angles to low).

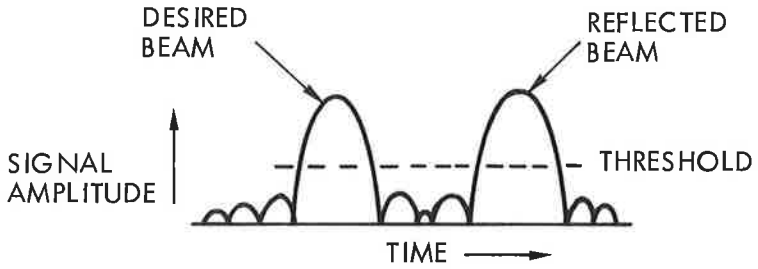

Figure 4.2.6a Signal Seen by an Aircraft above the Critical Height

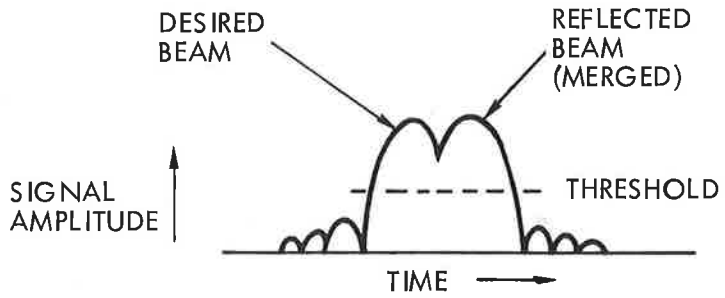

Figure 4.2.6b Signal Seen by an Aircraft below the Critical Height

Since the desired beam appears first, the reflected beam is easily ignored above the critical height. (Also, the antenna may be switched off before it points toward the ground.) Below the critical height, however, the lagging beam edge of the desired beam is not detected, but rather that of the reflected beam, resulting in as much as a half-beamwidth error. In order to avoid this, coverage cannot be maintained below some critical height, which will now be determined.

A typical antenna beam pattern is shown in Figure 4.2.7. The locations of aircraft, boresight, and reflections are given at the scan angle at the time when the aircraft is at the threshold point on the beam, and the reflection angle is at the upper null of the beam.

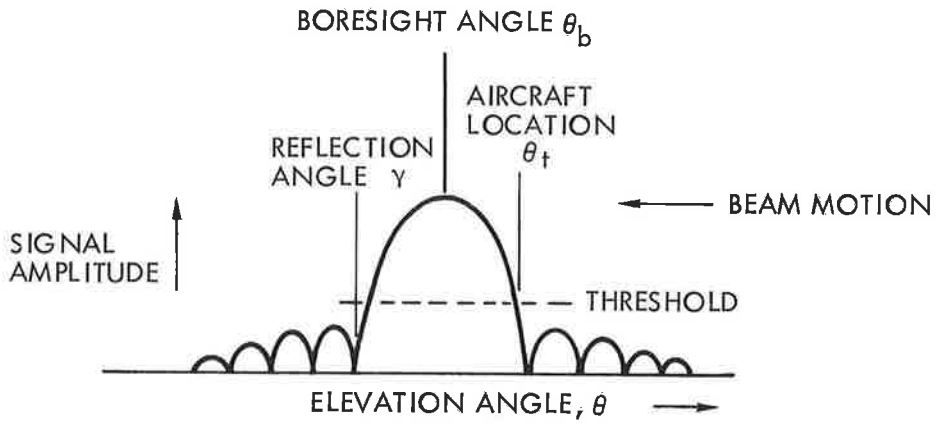

Figure 4.2.7 Angular Locations of Aircraft and Reflections on Beam for Critical Height

This is the condition for the critical height. At this height the received signal appears as in Figure 4.2.8. At any height lower than this the beams will merge, as in Figure 4.2.6b and an unacceptably high error results. The geometry of the situation at

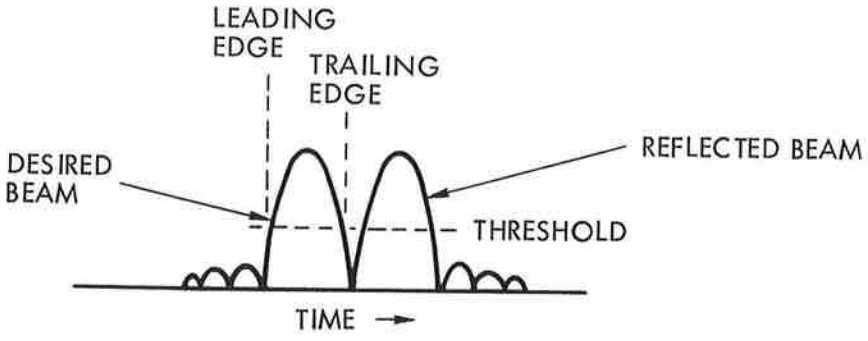

Figure 4.2.8 Signal Seen by an Aircraft at Critical Height

this scan angle is shown in Figure 4.2.9. In other words, the beam is scanning downwards, and passes by the aircraft until it is on the trailing edge of the beam. At this time the reflected ray is on a null of the pattern. A receiver at a height lower than

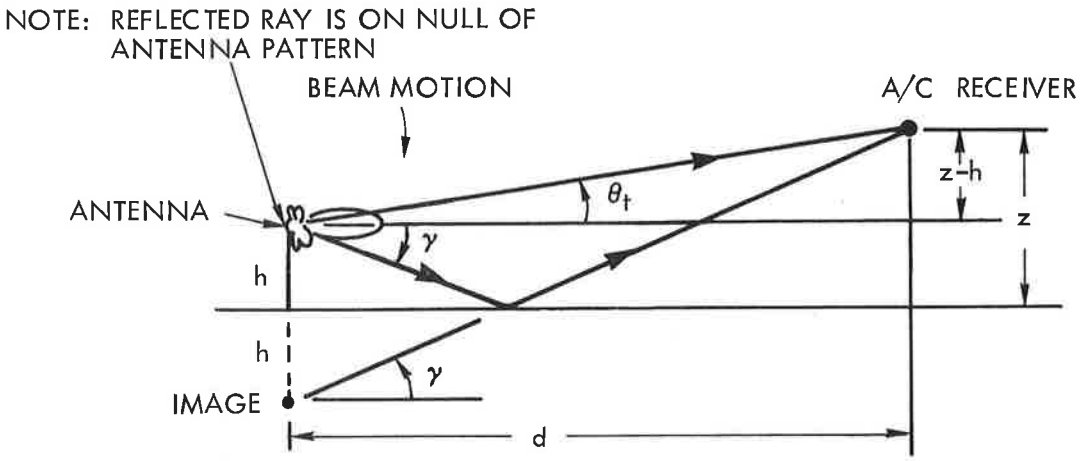

Figure 4.2.9 Geometry with Aircraft Receiver at Critical Height

this would not see the trailing edge of the direct beam until the beam had scanned further down; the reflected ray would then take place through the main beam, which results in a large error.

A typical antenna beam is shown in Figure 4.2.10. The beamwidth $\Delta\theta$ is the common 3 dB beamwidth; $K_T\Delta\theta$ is the beamwidth at

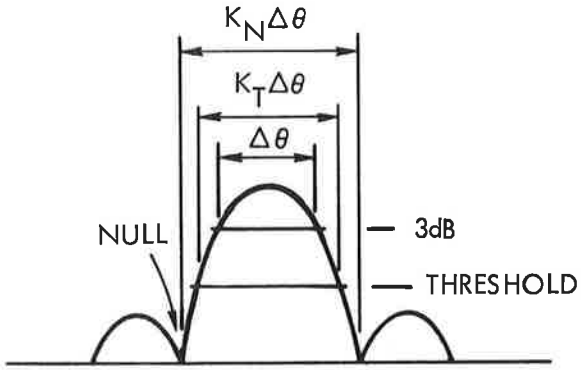

Figure 4.2.10 Antenna Beamwidth Relations

the threshold level, and $K_N\Delta\theta$ is the null beamwidth. A comparison of Figures 4.2.7 and 4.2.10 yields the following relations:

$$\theta_t - \theta_b = K_T\Delta\theta/2 \tag{4.2.18}$$

$$\theta_b + \gamma = K_N\Delta\theta/2 \tag{4.2.19}$$

If the antenna height and receiver height are small compared with the distance d in Figure 4.2.19, small angle approximations can be used for the trigonometric functions. From this figure the following relations can be derived,

$$\theta_t \triangleq \frac{z - h}{d} \text{ radians} \tag{4.2.20}$$

$$\gamma \triangleq \frac{z + h}{d} \text{ radians} \tag{4.2.21}$$

These four relations can be used to obtain a great deal of information: (1) the beamwidth necessary to achieve guidance down to a specified height, (2) the lowest pointing angle necessary before the transmitters can be turned off, and (3) the fact that the beamwidth is independent of the height of the antenna.

The beamwidth is found by eliminating the boresight angle θ_b and γ from equations (4.2.18) to (4.2.21). The antenna height drops out as well (hence (3) above), and one obtains

$$\Delta\theta = \left(\frac{4}{K_N + K_T}\right)\frac{z}{d} \tag{4.2.22}$$

The boresight angle for this condition is

$$\theta_b = \left(\frac{K_N - K_T}{K_N + K_T}\right)\frac{z}{d} - \frac{h}{d} \tag{4.2.23}$$

If the aircraft were far enough away that the height h in those relations is small compared to other terms, then $z/d \doteq \theta_t$, and (4.2.22) can be re-written as

$$\frac{\theta_t}{\Delta\theta} = \frac{K_N + K_T}{4} \qquad (4.2.24)$$

This states that, in fractional beamwidths, the lowest coverage is given by the right-hand side of the equation, which involves the choice of receiver thresholds. For a sin x/x main beam shape, $K_N = 2.25$, $K_3 = 1.0$, and $K_{10} = 1.67$ (the numbered subscripts refer to K_T). For a 3 dB threshold, $\theta_t/\Delta\theta$ is .8, and for a 10 dB threshold, it is approximately 1.0. Looking back at Figure 4.2.3 it is apparent that the value of .8, rather than 1.0, is consistent with the results presented there for thresholds of 3 dB and 10 dB. Furthermore, this holds well for different shapes of beams. Thus in the results to follow, K_T is set to unity, and K_N to 2.25. Then for these values,

$$\Delta\theta = .8z/d \qquad (4.2.25a)$$

and

$$\theta_b = (.39z - h) \qquad (4.2.25b)$$

For example, this states that in order to obtain coverage down to 8 feet at 2000 feet (RTCA requirement for EL#2), a beamwidth of .18° would be necessary.

The near field conditions play an important role in the location and beamwidth of EL#2. It was shown in section 3.1 that the far field limit is given by

$$L = \frac{2\lambda}{(\Delta\theta)^2} \qquad (4.2.26)$$

($\Delta\theta$ is in radians) and that in order to maintain beam integrity, the minimum antenna-to-aircraft spacing, d_m, should be more than some fraction of this, i.e.

$$d_m \geq \alpha L = \frac{2\alpha\lambda}{(\Delta\theta)^2} \tag{4.2.27}$$

Looking back on the discussion just given, it can be seen that a beamwidth narrower than that given by equation (4.2.22) will also give guidance down to the critical height; this establishes that beamwidth as an upper limit:

$$\Delta\theta \leq \frac{4z/d_o}{K_T + K_N} \tag{4.2.28}$$

where d_o is the distance from the antenna to the farthest point for which coverage down to a fixed height z is required. By re-arranging equation (4.2.27) the following condition results:

$$\sqrt{\frac{2\alpha\lambda}{d_m}} \leq \Delta\theta \leq \frac{4z}{d_o\,(K_T + K_N)} \tag{4.2.29}$$

A landing system is required to provide guidance down to some required height over a prescribed length of the runway (c). In the RTCA report c is 1500 feet. This means that d_m and d_o are related by

$$d_o = d_m + c \tag{4.2.30}$$

Ignoring the beamwidth for a moment, the inequality of equation (4.2.29) can be put in terms of z:

$$z \geq \frac{(K_T + K_N)(d_m + c)}{2}\sqrt{\frac{\alpha\lambda}{2d_m}} \tag{4.2.31}$$

The term on the right becomes indefinitely large if $d_m = 0$ or infinity. This means that there is some d_m that minimizes the right hand term; it turns out to be, simply:

$$d_m = c \tag{4.2.32}$$

Stated another way, we have derived a siting criterion for EL#2 that optimizes the height coverage minimum: the closest antenna-to-aircraft spacing should be equal to the length of the portion of the runway over which a prescribed coverage minimum height is required.

Furthermore by setting $d_m = c$ in the right hand term of equation (4.2.31) we have derived the minimum possible coverage height:

$$z_{min} = (K_T + K_N)\sqrt{\frac{\alpha\lambda c}{2}} \tag{4.2.33}$$

Assuming a sin x/x beam shape, and using $\alpha = .25$ as chosen in section 3.1, c = 1500 feet, and $\lambda = 1/15$ at Ku-band, we get z_{min} = 11.4 ft, and a beamwidth of 0.27°.

The RTCA report calls for coverage down to 8 feet; the ICAO requirement is 5 feet. The results obtained here strongly suggest that these are unrealistic at Ku-band and even more unrealistic at C-band, unless some schemes are devised which circumvent this problem.

It should be noted that the Doppler scheme is plagued with the same problem. In fact, the Doppler scheme presented in the RTCA report will always have a large reflected signal in the pass-band. In the conventional scan this is eliminated by turning the transmitter off for target angles below the lower coverage minimum; the doppler scheme must use filters. These only help above the critical height, however.

Another way of approaching the problem is to choose a beamwidth, locate it according to the near-far field criterion, and ask about its low-angle guidance capability. Thus from equation (4.2.29), once $\Delta\theta$ is fixed,

$$d_m = \frac{2\alpha\lambda}{(\Delta\theta)^2} \qquad (4.2.34)$$

and the minimum height is given by

$$z_{min} = \frac{(K_T + K_N)(d_m + c)\Delta\theta}{4} \qquad (4.2.35)$$

At Ku-band λ = 1/15 foot; for a beamwidth of 0.5°, we get d_m = 440 ft. This is below the 500 feet chosen by RTCA, which should be considered a minimum distance; therefore set d_m = 500 feet. Then z_{min} = 14.1 feet at 2000 feet from the antenna and 21.2 feet at the threshold of the runway. This is shown in Figure 4.2.11 along with similar results for the previously derived 0.27° beamwidth.

Regarding the possibility of an all C-band system, it is of interest to apply these formulas using λ = 1/5 feet. The optimum beamwidth becomes .47° and gives a minimum guidance of 19.7 feet or better throughout the coverage zone. Choosing beamwidths of 0.47° and 1°, the guidance minimum heights are shown in Figure 4.2.12 for receiver thresholds of 3 dB and 10 dB.

From Figures 4.2.11 and 4.2.12 it is evident that beamwidths larger than optimum result in better low-angle coverage closer in, and worse farther out. It is not shown in the figures, but it turns out that smaller beamwidths result in worse coverages everywhere.

It is unlikely that the coverages available at C-band would be operationally acceptable; however, they are presented here in order that the consequences of a decision having an all C-band system be well understood.

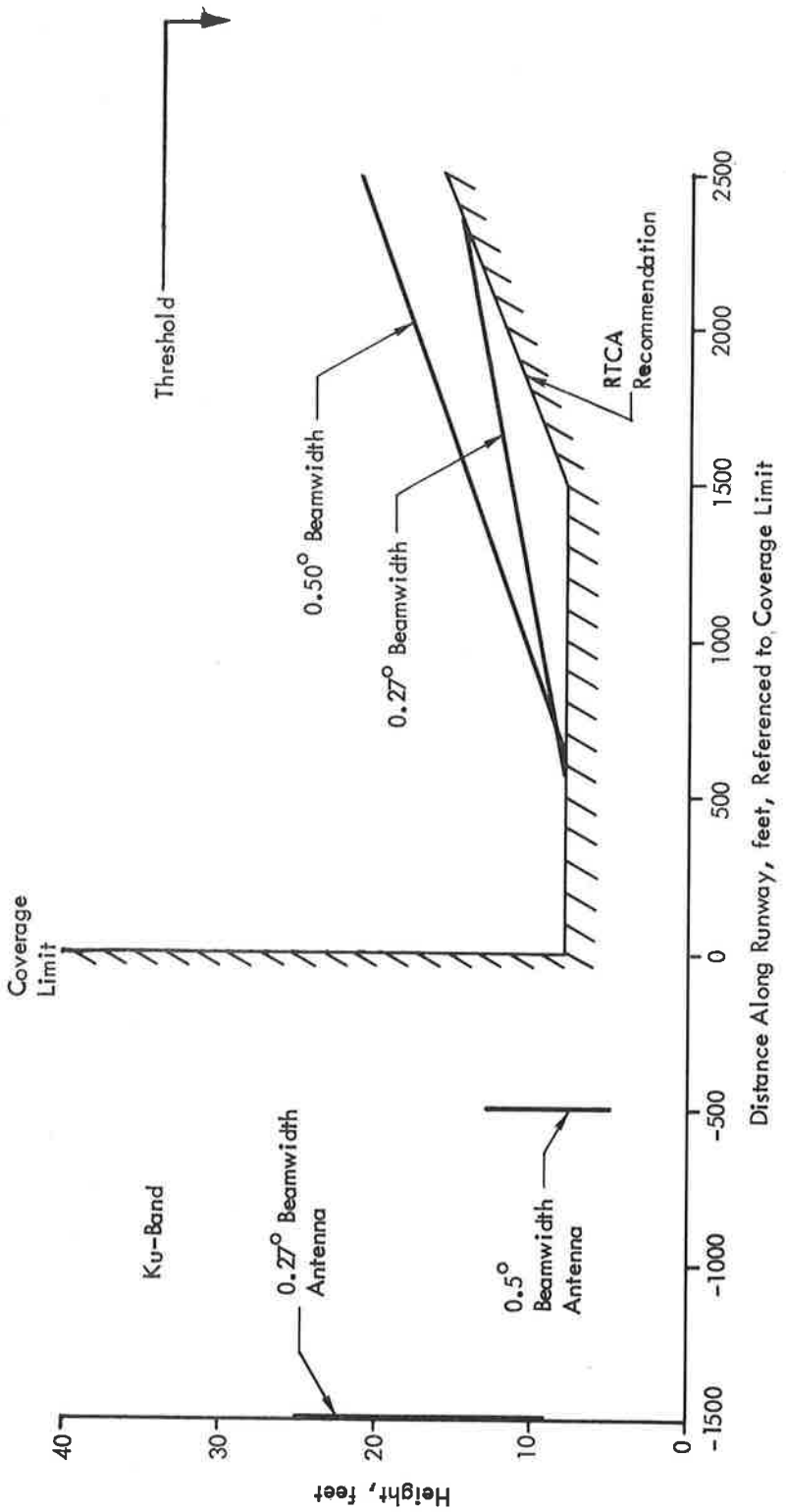

Figure 4.2.11 Coverage Capabilities of EL#2--Ku-Band

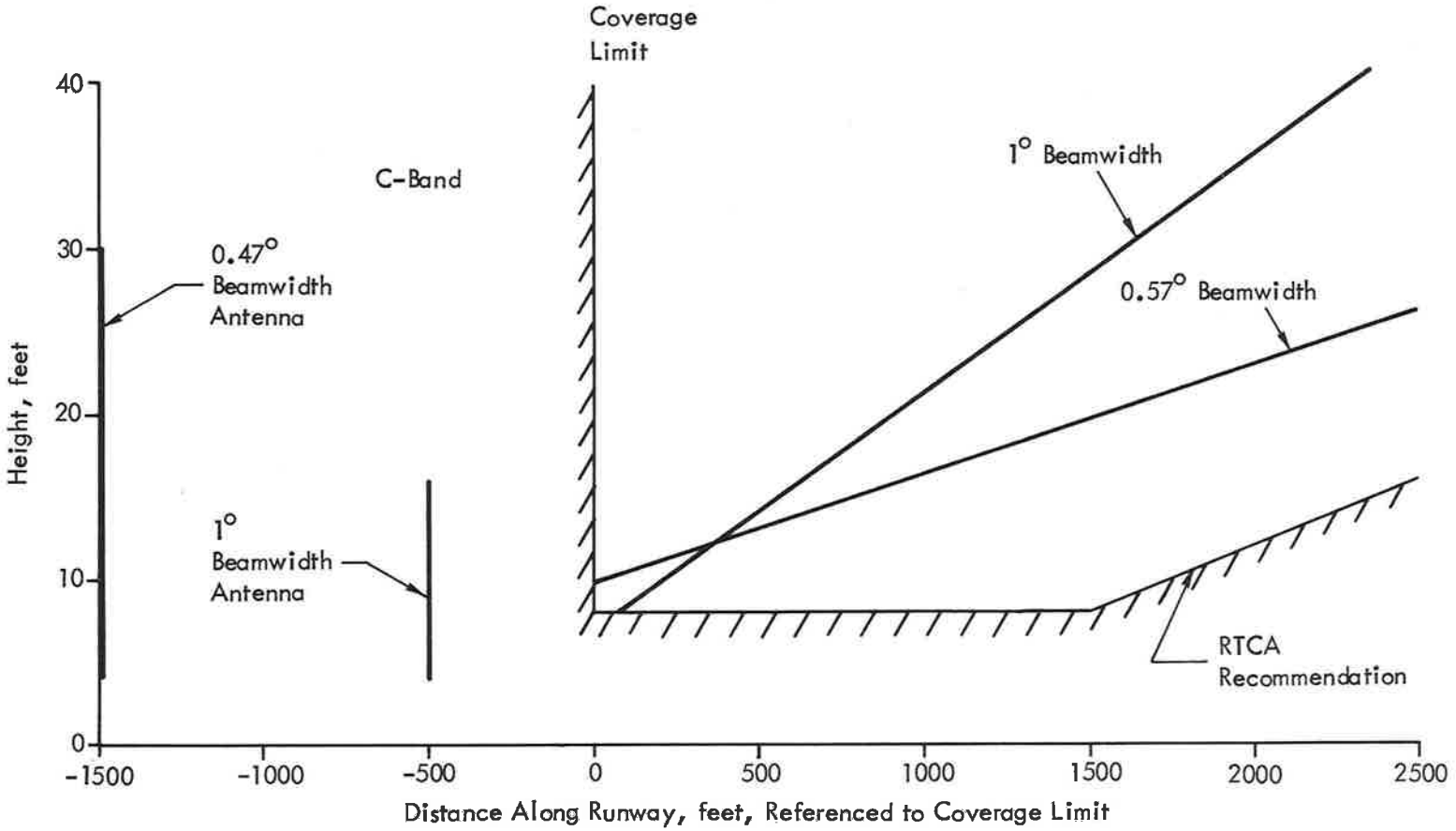

Figure 4.2.12 Coverage Capabilities of EL#2--C-Band

It should be pointed out that this analysis is based on the assumption of a flat runway and airport surface, and that the scattering is specular. While the latter is a good assumption, a proper approach to the surface effects would involve a Fresnel-zone analysis. A Fresnel-zone analysis accounts, to some extent, for gradual topographical deviations from the flat-surface assumption. Such analysis should be carried out wherever variations of more than a foot are encountered between EL#2 and the threshold.

Also, the work above should be subjected to experimental verification in environments where the reflecting surface is representative of airport runways and surfaces.

In summary, the chief conclusions of this section are:

1. The RTCA requirement of coverage down to 8 feet above the runway for a 1500 foot touchdown region (and the corresponding ICAO requirement of 5-foot coverage) is impossible to achieve, with either Doppler or Conventional Scan, unless some unconventional techniques are used to circumvent this problem.

2. There is an optimum beamwidth and antenna location for achieving the lowest possible coverage over a specified length of runway.

3. The beamwidth recommended by RTCA (0.50°) results in coverage down to 14.1 feet, while the optimized beamwidth (0.27°) gives coverage down to 11.5 feet. The cost of the last three feet of coverage is high.

4. Attempts to use C-band for EL#2 will result in significantly worse low-altitude coverage capability, even if below-the-horizon scan did not introduce additional multipath problems.

5. MONITORING CONSIDERATIONS

CONTENTS

ILLUSTRATIONS

TABLES

A reliable landing system must have a set of sensors which indicate when the ground equipment is not functioning properly. The outputs of these sensors should be utilized in such a way that aircraft are alerted that certain functions are not available, or are operating in a "casualty mode". Preferably the monitoring system should perform some interpretation so that optimum use is made of the information which is valid. For example, the loss of a signal in one arm of a phased array might cause errors so small that no operational change is necessary; loss of signal in two might rule out CAT-III guidance, but maintain safe CAT-II operation. Other errors could require shutdown of the function entirely. In such a complex system, shutdown on every alarm could render the system useless.

Furthermore, the sensors themselves can sound alarms even when the system is operating perfectly. This is common on the present ILS and the family automobile. This can be caused either by malfunction of the sensors or by reflections from taxiing aircraft.

A thorough analysis of the monitoring system must of necessity be specifically oriented toward a particular set of equipment. This is particularly true of the internal monitoring. Hence in the discussion to follow, the electronic attenuator-fed azimuth antenna is used as the basis for the internal monitoring. General statements are made where possible.

5.1 GENERAL

ABSTRACT

An introduction and a tabulation of general effects of malfunctions are presented.

There are several areas in an electronically scanned antenna where malfunctions can occur which will degrade the antenna performance. It is necessary to monitor as many of these areas as possible in order to pinpoint the location of the problem and facilitate repairs. It is also desirable to detect a failure that

does not degrade performance sufficiently to register on an external monitor because such a failure would render the system even more vulnerable to a second failure.

The effects of malfunctions that could occur in several areas can be described in a general sense. Table 5.1.1 lists the type of effects that probably would be seen for several different malfunctions. Some of these areas can be most effectively monitored internally, while others are best handled with external monitors.

TABLE 5.1.1 ANTENNA SYSTEM MALFUNCTIONS AND SOME OF THEIR PROBABLE EFFECTS ON PERFORMANCE

Malfunction	Probable Effects of Malfunction			Likelihood of Catastrophic Failure	
	Beam Moves	Sidelobe Levels Rise	Range Dec.	High	Low
Control Logic Failure	X	X	X	X	
Component Driver Failure	X	X			X
RF Diode Failure in Component	X	X			X
RF Mechanical Failure	X	X			X
Source Power Drops			X	X	
Source Frequency Changes	X	X		X	
Wind Deformation of Antenna	X	X			X
Thermal Deformation of Antenna	X	X			X
Objects in the Near Field	X	X	X	X	

5.2 INTERNAL MONITORING CONSIDERATIONS

ABSTRACT

Internal monitors are required in order to be able to pinpoint failures. The effects of several types of malfunction on the antenna performance are discussed and the results of some computer studies on this subject are tabulated. Internal monitoring techniques are presented for failures in the control logic, component drivers, RF diodes, RF circuit paths (mechanical failures), source power, and source frequency, as well as wind or thermal deformation of the antenna.

5.2.1 Control Logic

A malfunction in the control logic could very easily result in catastrophic degradation of antenna performance. For example, a single incorrect bit could appear in eight places in the system if the error occurred on the reading of the 24-bit words from memory, since eight of these reads are executed to fill the 192-bit buffer before the next fine scan position is commanded (see section 6.3.2).

Control logic cannot be completely monitored internally except by having a duplicate logic system and comparing the commands. Although this approach should detect any failures in the logic, pin-pointing the failures would be very difficult and time consuming.

A parity check system could cover many of the possible failures in the logic; however, some problems, such as a malfunction in the timing clock, could not be detected in this way. Parity checking would require only an extra bit on each word; thus a larger memory and more wiring would be required. In addition several circuits would be required to check parity in each buffer. But parity checking would cost far less than a duplicate logic system and would provide much of the same protection as well as better information on the location of the faults.

Since a fault in the logic is likely to have a catastrophic effect on antenna performance, since locating the fault (even with a parity check system) is apt to be time consuming and since repairing the fault would be more time consuming than other types of

faults where a component could be completely replaced, it would be desirable to build the control logic with the maximum possible reliability. MIL-SPEC diodes and NASA-qualified solderers and inspectors should be required.

5.2.2 Component Drivers

A failute in a component driver would probably cause that component to be incorrectly set during part or all of the scan. The seriousness of the degradation would vary with the particular bit of the component affected, and the type of component affected. The effects of this sort of failure would be similar to the effects of failures of the RF diodes.

Computer studies have been performed at TSC wherein the calculated effects of different component failures were examined. These failures were located one type at a time on only one element of the array. The location of the faulted element on the array was varied to determine how this would affect pattern degradation. Three types of failure were studied in terms of their effect on beam pointing for the azimuth attenuator-fed antenna. These failures were: (1) phase error on one element, (22.5°; 45.0°; 90.0°; 135.0°; or 180.0°); (2) all power shut off from one element; (3) one sector switch incorrectly set so power is fed to one element outside the intended active sector and one element in the active sector is dead. The results of these studies are shown in Table 5.2.1. These results show that pointing errors of more than two fine scan increments can be caused by some of these failures. The complete removal of power from one element had comparatively little effect on beam pointing, but did cause a 3 to 4dB rise in the sidelobes.

These results give an indication of the magnitude of the performance degradation that can be expected from malfunctions in the system components. The effect of two or more of these malfunctions acting simultaneously, (a more realistic situation) was not studied. However, simultaneous malfunctions would not necessarily produce the sum of the beam pointing errors that each

TABLE 5.2.1 CALCULATED -10 dB BEAM CENTER MOTION DUE TO DIFFERENT TYPES OF FAILURES

Element Number	Phase Error 22.5°	Phase Error 45.0°	Phase Error 90.0°	Phase Error 135.0°	Phase Error 180.0°	Power Shut Off At Element	Sector Switch Incorrectly Set
1	0.0117°	0.0216°	0.0283°	0.0192°	0.0059°	0.0045°	0.0053°
2	0.0185°	0.0348°	0.0464°	0.0385°	0.0136°	0.0078°	0.0069°
3	0.0267°	0.0503°	0.0747°	0.0607°	0.0212°	0.0110°	0.0344°
4	0.0364°	0.0689°	0.1051°	0.0876°	0.0292°	0.0140°	0.0156°
5	0.0471°	0.0895°	0.1394°	0.1184°	0.0369°	0.0165°	-0.0503°
6	0.0572°	0.1091°	0.1732°	0.1503°	0.0425°	0.0179°	0.0813°
7	0.0646°	0.1239°	0.1996°	0.1756°	0.0431°	0.0177°	0.0677°
8	0.0673°	0.1295°	0.2107°	0.1846°	0.0376°	0.0155°	-0.1245°
9	0.0635°	0.1224°	0.1995°	0.1710°	0.0264°	0.0118°	0.1147°
10	0.0525°	0.1011°	0.1638°	0.1355°	0.0157°	0.0078°	0.0520°
11	0.0347°	0.0671°	0.1072°	0.0856°	0.0074°	0.0043°	-0.1523°
12	0.0122°	0.0235°	0.0369°	0.0292°	0.0021°	0.0014°	0.1613°

separate malfunction produced. For example, malfunctions in phase are usually accompanied by attenuation which should reduce the effect of the phase errors.

This study indicates that the performance degradation caused by the component malfunctions considered would probably not be catastrophic since only one element at a time should be involved.

The component drivers could be monitored by the RF diode monitors. It would be necessary to have a voltage level comparator actuated by the control logic command to the driver.

5.2.3 RF Diodes

Failures in the RF diodes should produce performance degradation similar to that produced by driver failures, (see discussion above).

The RF diodes can usually be individually monitored by means of the bias voltage or current so a "shorted" or "opened" diode could be detected.

In some instances, however, individual diodes cannot be monitored. Such is the case for the phase shifters for the elevation array. It is possible to have monitors on each diode of the 180° and 90° bits because they are hybrid bits. But the 22.5° and 45° bits are loaded-line bits and individual monitors could not detect a diode that had opened up because the diodes are in parallel as far as the bias is concerned. If a diode on one of these bits were to short out the failure would be detectable from the increased current flow on the bias lead. If a diode were to open, since the diode is about one quarter wavelength from the line it would appear as an RF short on the line and cause a large increase in input VSWR. This could be detected with a directional coupler and a detector installed at the input to the phase shifter.

5.2.4 RF Mechanical Failures

RF mechanical failures such as opening of a solder joint, thermal cracking of a stripline, (both observed in early temperature tests of some components), improperly torqued connections, etc., can cause power reflections and a resulting attenuation in power to an antenna element. The calculated effects of the total shutdown of one element have been discussed above. Comparatively little effect on beam pointing was noted; however, the sidelobe level was raised considerably. A serious mechanical failure should have a similar effect. A problem could arise due to the fact that some of the reflected power would be re-reflected at the power divider and appear on elements where it is not intended. The magnitude of this problem would depend on the isolation of the power dividers. A computer analysis of this type of malfunction would be very time-consuming, and it is felt that experimental data from the azimuth attenuator-fed antenna would be more informative.

RF mechanical failures can be monitored in the same manner as mentioned above for some RF diodes, namely by placing directional couplers and detectors in each RF path. For the attenuator-fed antenna the placement of these detectors just after the power divider would pinpoint the RF path that contained a failure. A

similar placement of the detectors in a transfer matrix-fed antenna could only pinpoint the faulted RF path if the scan position were recorded at the time of the failure.

5.2.5 Source Power

A decrease in source power would cause a decrease in range and this power loss could be sudden or great enough that the degradation of performance would be catastrophic. The source power could be monitored internally using a directional coupler and a detector. If there were several parallel amplifiers between the power dividers a detector after each amplifier would be advisable. If there is only one amplifier unit it would be better to monitor it externally, since this would reduce the complexity of the antenna feed system.

5.2.6 Source Frequency

It is likely that a frequency malfunction, if one should occur, would cause the frequency to shift far outside the band, resulting in a catastrophic situation. This catastrophic situation would require no special frequency monitor as the external monitor would no longer be detecting the signal at all.

Drift which is less than the channel bandwidth would result in measurement errors, since the modulation sidebands would be affected. Thus the receiver-monitor should have a carrier-monitor which would output a reduced signal in this case.

Internal monitoring does not appear desirable for this failure type.

5.3 EXTERNAL MONITORING CONSIDERATIONS

ABSTRACT

External monitors are necessary to detect malfunction that internal monitors cannot detect, to provide redundancy, and to determine whether a particular failure has catastrophic effects on performance. External monitors cannot pinpoint failures. External monitoring techniques for some specific malfunctions are discussed. For the proposed azimuth antenna configuration it will be possible to locate the monitors so that reflections from aircraft on runways and taxiways should not be a problem.

5.3.1 Considerations of External Monitoring

External, far-field monitors would be required to detect malfunctions that could not be detected by the internal monitors, and to provide redundancy in the event of failure of the internal monitors. Far-field monitors can also provide an indication of the extent of the performance degradation caused by a particular malfunction. Without far field monitors there would be no direct information at all on whether a particular malfunction has caused a small degradation of performance or a catastrophic degradation.

Far-field monitors, because they are monitoring the actual performance of the antenna system as a whole, can only detect the existence of a malfunction that degrades the performance beyond a certain amount. Far-field monitors can provide no information on the location of the malfunction within the antenna system nor can they detect malfunctions which cause very minor performance degradations that would fall within the normal tolerances set on performance by the intrinsic errors in the components. Internal monitors are required to pinpoint malfunctions and to detect malfunctions that have a minor effect on performance.

5.3.2 Specific Malfunctions

The parity monitors could detect most failures in control logic, (see section 5.2.1.). However, they could give no information on the performance degradation caused by these failures. External monitoring is essential in this case to determine whether or not the degradation is catastrophic. If a control logic malfunction should happen to only affect a small portion of the scan, or only one element, it might only produce measurable performance degradation in regions where external monitors are not located. But if external monitors are located in the most critical regions of the angular scan no catastrophic error would go undetected.

Source power and frequency could be monitored more simply and easily using a far-field monitor than by using an internal coupler-detector-discriminator arrangement. The same monitoring

equipment could be used in an external monitor and would have the advantage of not putting additional reflections and complexity into the antenna feed system.

Wind or thermal deformation of the antenna would probably be difficult to monitor internally but any significant performance degradation resulting from such deformation should be detectable on a far-field monitor.

Objects in the near field such as an aircraft parked near the antenna would only be detectable by means of noting their effects on antenna performance as measured by an external monitor.

5.3.3 Type and Location of External Monitors

The basic far-field monitor could be similar to the receiver system installed in an aircraft. There would have to be additional ground equipment that would store the actual angular location of the monitor relative to the antenna and would compare this to the angular location as determined by the receiver and processor.

Since there will be intrinsic errors in the components and mechanical structure of the antenna system there will be intrinsic errors in beam pointing. Thus pointing error thresholds as well as power level thresholds will have to be established for the far-field monitors so the malfunctions can be differentiated from the intrinsic system errors. It is probable that not all malfunctions will cause beam pointing errors severe enough to be detected. It has been noted, for example, in computer studies that removing all power from one element of the 4° azimuth attenuator-fed antenna has little effect on beam position but does raise the sidelobes considerably and broaden the beam slightly, (see section 5.2.2.).

It might be possible to detect smaller beam pointing errors by setting the beam edge threshold points at a lower level than is used for aircraft receivers. However, the magnitude of the intrinsic phase errors in the active components already procured

by TSC and the TSC computer studies of the amount of beam motion produced by such phase errors suggest that the intrinsic pointing errors in the system should be of the same magnitude as the smaller of the errors that could be caused by malfunctions. This implies that lowering the beam edge threshold points would serve no purpose. The actual size of the intrinsic pointing errors and of errors caused by malfunctions can be determined experimentally during range tests of the azimuth attenuator-fed antenna.

Ideally a far-field monitor should be located at the same azimuth angle with respect to the antenna as the aircraft. This is possible in the case of the azimuth antenna since it is located about 1000 feet beyond the end of the runway. A monitor placed at the end of the runway on the centerline would not be in the far field of the antenna, but since it would be located at broadside there should be no pointing errors resulting from being in the near field. One monitor set should be sufficient since this is to be a linear array and thus no sector switch will be used.

5.4 DISPLAY CONSIDERATIONS

ABSTRACT

Some monitors require threshold logic for both failure and catastrophic failure conditions. Conditions of all monitors should be displayed in one place. A possible layout for this display is presented for the azimuth antenna.

There should be one central display panel for each function where the condition of all the monitors can be observed. There should be a light for each monitor which is only lit when a fault is detected. To detect a failure each monitor must have threshold logic which will differentiate as far as possible between failures and intrinsic system errors. The far-field monitors and the source power and frequency monitors will need another threshold logic setting to detect catastrophic errors. Thus each of these

monitors must have a second display light to indicate catastrophic errors.

The display should also contain a readout of the memory address being used when the failure occurred. This allows an immediate manual re-set of the control logic to recreate the error situation.

A possible layout for the display for the azimuth attenuator-fed antenna is shown in Figure 5.4.1.

MEMORY ADDRESS	0	0	0	0	0	0	0	0	0	0

		LH	PATH NUMBER																					RH
COMPONENT		1	2	3	4	5	6	7	8	9	10	11	12	13	14	15	16	17	18	19	20	21	22	23	24
PHASE SHIFTER	DIODE	0	0	0	0	0	0	0	0	0	0	0	0	0	0	0	0	0	0	0	0	0	0	0	0
	DRIVER	0	0	0	0	0	0	0	0	0	0	0	0	0	0	0	0	0	0	0	0	0	0	0	0
	VSWR	0	0	0	0	0	0	0	0	0	0	0	0	0	0	0	0	0	0	0	0	0	0	0	0
ATTENUATOR	DIODE	0	0	0	0	0	0	0	0	0	0	0	0	0	0	0	0	0	0	0	0	0	0	0	0
	DRIVER	0	0	0	0	0	0	0	0	0	0	0	0	0	0	0	0	0	0	0	0	0	0	0	0
SECTOR SWITCH	DIODE	0	0	0	0	0	0	0	0	0	0	0	0	0	0	0	0	0	0	0	0	0	0	0	0
	DRIVER	0	0	0	0	0	0	0	0	0	0	0	0	0	0	0	0	0	0	0	0	0	0	0	0
RF MECHANICAL	(VSWR)	0	0	0	0	0	0	0	0	0	0	0	0	0	0	0	0	0	0	0	0	0	0	0	0

SOURCE MONITORS	FAILURE	CATASTROPHIC
FREQUENCY	0	0
POWER	0	0

FAR FIELD BEAM POINTING MONITORS	FAILURE	CATASTROPHIC
1 AWAY FROM RUNWAY	0	0
BROADSIDE	0	0
1 TOWARD RUNWAY	0	0
2 TOWARD RUNWAY	0	0

	BUFFER NUMBER							
	1	2	3	4	5	6	7	8
LOGIC PARITY CHECK	0	0	0	0	0	0	0	0

Figure 5.4.1 Possible Layout for Monitor Display for Azimuth Attenuator-Fed Antenna

MEMORY ADDRESS	0	0	0	0	0	0	0	0	0	0

		LH	PATH NUMBER																					RH
COMPONENT		1	2	3	4	5	6	7	8	9	10	11	12	13	14	15	16	17	18	19	20	21	22	23	24
PHASE SHIFTER	DIODE	0	0	0	0	0	0	0	0	0	0	0	0	0	0	0	0	0	0	0	0	0	0	0	0
	DRIVER	0	0	0	0	0	0	0	0	0	0	0	0	0	0	0	0	0	0	0	0	0	0	0	0
	VSWR	0	0	0	0	0	0	0	0	0	0	0	0	0	0	0	0	0	0	0	0	0	0	0	0
ATTENUATOR	DIODE	0	0	0	0	0	0	0	0	0	0	0	0	0	0	0	0	0	0	0	0	0	0	0	0
	DRIVER	0	0	0	0	0	0	0	0	0	0	0	0	0	0	0	0	0	0	0	0	0	0	0	0
SECTOR SWITCH	DIODE	0	0	0	0	0	0	0	0	0	0	0	0	0	0	0	0	0	0	0	0	0	0	0	0
	DRIVER	0	0	0	0	0	0	0	0	0	0	0	0	0	0	0	0	0	0	0	0	0	0	0	0
RF MECHANICAL	(VSWR)	0	0	0	0	0	0	0	0	0	0	0	0	0	0	0	0	0	0	0	0	0	0	0	0

SOURCE MONITORS	FAILURE		CATASTROPHIC
FREQUENCY	0		0
POWER	0		0

FAR FIELD BEAM POINTING MONITORS	FAILURE		CATASTROPHIC
1 AWAY FROM RUNWAY	0		0
BROADSIDE	0		0
1 TOWARD RUNWAY	0		0
2 TOWARD RUNWAY	0		0

	BUFFER NUMBER							
	1	2	3	4	5	6	7	8
LOGIC PARITY CHECK	0	0	0	0	0	0	0	0

Figure 5.4.1 Possible Layout for Monitor Display for Azimuth Attenuator-Fed Antenna

6. EXPERIMENTAL ANTENNA DESIGNS

CONTENTS

ILLUSTRATIONS

ILLUSTRATIONS (CONTINUED)

ILLUSTRATIONS (CONTINUED)

TABLES

The designs to be used in the experimental phase of the program are presented in this chapter. Two feed systems have been designed and fabricated for the azimuth function. One is a step-scan antenna which uses a step size of 0.65 beam widths. The other is a fine-scan design which closely approximates continuous scan. A linear array has been designed for the elevation function which allows a wide range of sidelobe levels to be generated.

6.1 GENERAL CONSIDERATIONS

ABSTRACT

The reasons for choosing the particular antennas and feed networks used here are discussed.

The purpose of the work on this program is to assess the feasibility of phased arrays for the MLS and to address certain critical issues. The circular array for azimuth guidance is more complex than a linear array and thus presents more of a challenge in feasibility. For this reason it was determined to design, construct, and test a circular array first.

The preferred design for the circular array is the electronic attenuator technique based on studies reported in the first annual report[1]. While the insertion loss is higher (by 1.5 dB) than for some other schemes, it has the advantage of extreme flexibility. The lens-fed array was originally a back-up design which was to be carried to the component stage only, but procurement difficulties with the components of the attenuator-fed antenna dictated that it be carried through to completion in a step-scan mode.

The feasibility items to be established are the following:

1. Planar beam generation
2. Accuracy of individual beams (static)
3. Sidelobe level, measured vs predicted

---

1 First Annual Report, Chapter IV.

4. Insertion loss

The issues to be addressed, in addition to the above, are:

5. Accuracy of beam center vs step size

6. Sum vs difference

The lens-fed antenna addresses only the first four items above, while the attenuator fed array covers all of them. The attenuator-fed antenna has the capability of being used as a test-bed for various modulation-receiver schemes since it provides for variable sweep rate, variable data rate, variable step size, and variable scan limits.

The linear elevation antenna design is a standard one which is intended to have the capability of variable step size, etc. It uses attenuators which allow control of sidelobe level, beam-width, and which allow arbitrary shaping of a beam; it can then be used to establish the azimuth vertical aperture requirements.

6.2 R-2R LENS STEP-SCAN AZIMUTH ANTENNA

ABSTRACT

The design parameters and detailed considerations of the RF and logic are presented for the step-scan azimuth antenna fed by an R-2R lens.

The lens-fed network for the azimuth antenna was carried through to the final stages when procurement difficulties endangered the more flexible fine-scan feed network. The system is an inexpensive method of obtaining up to $\pm 30°$ of scan with a 4° beamwidth. It is not recommended for wider scan requirements or narrow beamwidths.[1] It is described in detail in the first annual report[1] and in Appendix A. Range tests were run on this antenna; the results are presented in Section 7. The sections below deal with the design considerations and the control logic used for both automatic and manual scan.

---

1. First Annual Report, pp. 133-163

6.2.1 Design Approach for the Lens Step-Scan Azimuth Antenna

The lens feed system was designed last year[1] and was completed and tested this year. The test results on the lens itself as a component appear in Appendix A, the other components' tests appear in Appendix B, and the subsystem test results are presented in section 7.1. The parameters of the scan antenna are as follows:

Antenna radius: 33.661"

Active Sector: 60° (33.661" aperture = 15 λ)

Probes in Active Sector: 24 (others excited also due to nature of lens)

Total Number of Output Probes: 32

Scan Limits: $\pm$10°

Coarse Scan Interval: 2.62°

Coarse Beam Positions: $\pm$4 on either side of 0°

Half-Power Beamwidth: 4.0°-5.0° depending on radiating aperture distribution and frequency

The model of the lens antenna system that was built for testing was step-scanned; that is, it had no electronic phase shifters or electronic attenuators for fine scanning. If this type of scanning were to be used in a landing system the beam center would have to be located by using a "center of gravity" technique.

Figure 6.2.1 shows a diagram of the setup tested on the range. A 2-level input amplitude distribution is set up by the power dividers and attenuators. The transfer switches and the SP2T switches allow the 4 probe, 2-level distribution to be switched sequentially to all 13 lens input positions. A SP2T was added at the input for oscilloscope blanking. This switch would not be included in a final system.

---

1. First Annual Report, p. 200

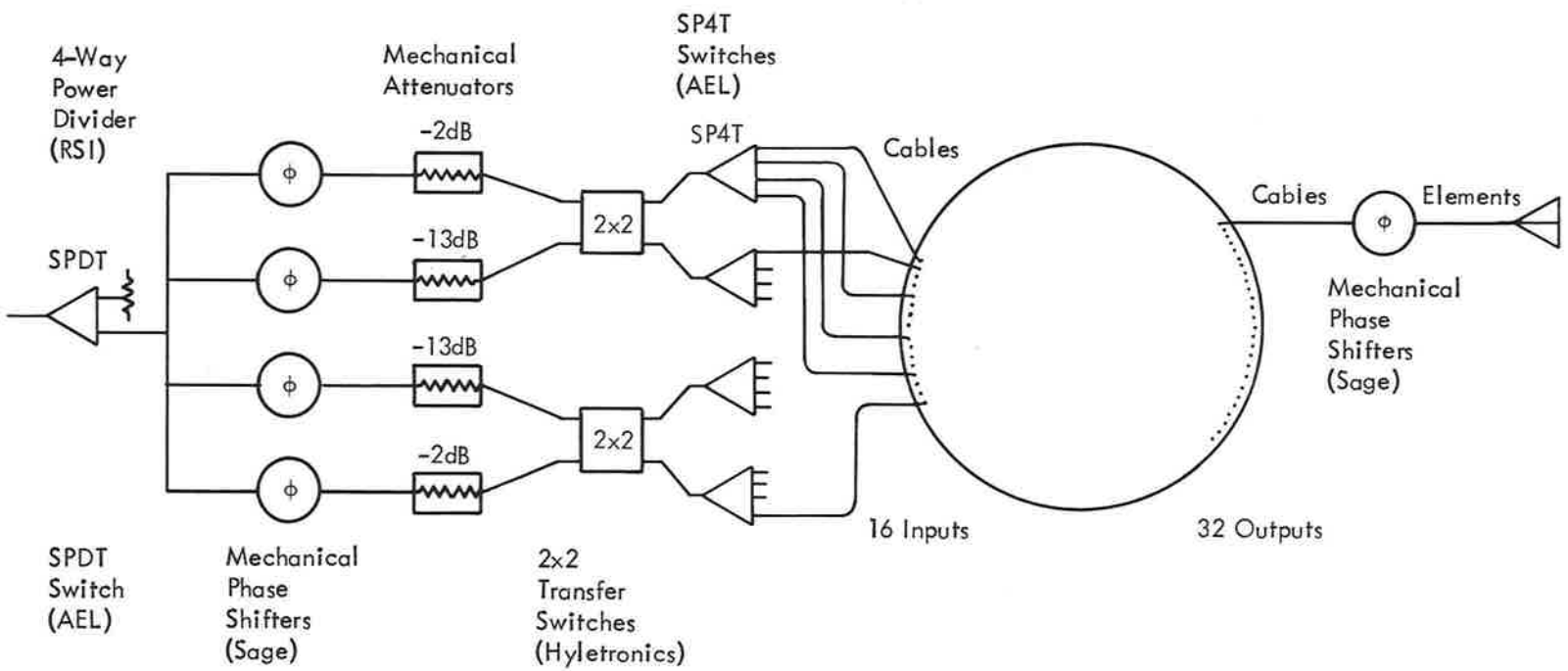

Figure 6.2.1 Range Test Setup of Step-Scan Lens-Fed Azimuth Antenna

It was assumed (Appendix A, pages A-9 and A-24) that the phase center of the lens probes were at the reflective surface of the lens. It was observed during the component tests that the phase centers were, in fact, nearly at the probes themselves. This should have resulted in the antenna being focused at about 15° elevation instead of 0° elevation. However, during the range tests the antenna was observed to be focused at about 19° elevation. This suggests that a similar effect to that observed in the lens was occurring at the elements of the antenna itself, causing their phase centers to be at or near the elements instead of at the reflective surface of the antenna. This effect is equivalent to an increase in the radius of the antenna, which would raise the focus point in elevation.

The sidelobe levels in the antenna pattern rise by several dB if the non-active input probes of the lens remain unterminated. Terminating these probes requires circulators or extra SPDT switches at the input probes, the addition of which would increase the insertion loss. In the test system these components were not added. As a result the insertion loss was lower but on the dynamic tests, where the 9 nonactive input probes had to remain unterminated, the sidelobes were 7 to 8 dB higher. Static tests taken with the probes terminated and unterminated verified that the rise in the sidelobes was due to the lack of terminations.

A component by component insertion loss budget for the lens-fed antenna is presented in Table 6.2.1. If this antenna feed system were to be built on a production basis the mechanical phase shifters and attenuators following the power divider would be eliminated and a 4-way unequal power divider used to achieve the same effect, with the result of lowering the insertion loss. The phase shifters were nominally used to eliminate phase errors introduced by the mechanical attenuators. In production, the SPDT switch at the input would not be used but SPDT's (or circulators) would be required at the lens input and they would have the same effect on loss. Also, in a production system the SP4T switches and the transfer switches could be combined in one unit, eliminating at

least one RF connection. If the antenna were to be fine scanned, 1.8 dB loss from electronic phase shifters would have to be added to the loss budget. A production unit of this type would have a corresponding insertion loss of 6.3 dB (but with only ±15° of scan).

TABLE 6.2.1 INSERTION LOSS BUDGET FOR STEP-SCAN LENS-FED AZIMUTH ANTENNA

SPDT Switch	1.1 dB
1:4 Power Divider	0.8 dB
Mechanical Phase Shifter	0.5 dB
Mechanical Attenuators	5.0 dB
2 x 2 Transfer Switch	1.1 dB
SP4T Switch	1.6 dB
Lens	1.0 dB
Mechanical Phase Shifters	0.5 dB
Cables	0.5 dB
Element VSWR	0.2 dB
Total Loss	12.3 dB

6.2.2 MLS Lens-Fed Circular Array Logic

The Azimuth Control logic for coarse scanning of the lens-fed phased array antenna in the step scan mode has been designed and fabricated in-house. The unit generates logic codes corresponding to 13 states which appear on 2 transfer switches and 4 SP4T switches in the form of sequential pulses. Figure 6.2.2 shows a table corresponding to the digital codes present on the switches for the 13 states.

The Azimuth No. 1 Logic Control Unit consists of an oscillator, power supply, a 4-bit counter, a 4 line-to-16 line decoder and several 8-Input and Dual 4-Input NAND Gates. The unit generates sequential pulses which are directed to switches for use in steering the phased-array antenna. A block diagram of the unit is

STATE	XFR SW 1	XFR SW 2	SP4T SW 1	SP4T SW 2	SP4T SW 3	SP4T SW 4
1	1	1	1000	1000	1000	1000
2	0	1	0100	1000	1000	1000
3	0	0	0100	0100	1000	1000
4	1	0	0100	0100	0100	1000
5	1	1	0100	0100	0100	0100
6	0	1	0010	0100	0100	0100
7	0	0	0010	0010	0100	0100
8	1	0	0010	0010	0010	0100
9	1	1	0010	0010	0010	0010
10	0	1	0001	0010	0010	0010
11	0	0	0001	0001	0010	0010
12	1	0	0001	0001	0001	0010
13	1	1	0001	0001	0001	0001

Figure 6.2.2 Logic Table for XFR SW, SP4T SW Outputs

shown in Figure 6.2.3. Figures 6.2.4 and 6.2.5 show more detailed schematics of logic circuits used in the unit.

The unit functions electrically in the following manner. The frequency output of the oscillator (see Figure 6.2.6) can be varied over a range between 1.19 kHz and 11.9 kHz. This frequency output controls the rate of a 4-bit counter (SN7493) whose output in turn is converted to a 16-bit counting sequence by a 4 line-to-16 line decoder (SN74154).

The 16-line output of the decoder forms a "look-up" table matrix (Figure 6.2.5) which uses 13 (1-13) of the 16 available output lines corresponding to the required 13 states for the switching. The 13 output lines from the decoder are sequentially pulsed (according to the decimal value of the 4-bit counter output) also sequentially pulsing the Single-Pole-4-Throw switches according to the logic table shown in Figure 6.2.2.

A "synch out" signal is provided, along with the Transfer Switch and SP4T, to be used for scope triggering. This signal corresponds to the SN 74154-decoder 0000 state of the 4-bit Counter, i.e., whenever the output of the 4-Bit Counter is at the 0000 state, the synch output signal goes to a logic "0".

To perform the logic computations required for the steering of the beam it was necessary to fabricate a module containing six (6) TTL integrated circuits, a clock, and an internal power supply which operates from a 115V source. The entire assembly is mounted inside a 10" D x 17" W x 3" H chassis which consumes very little space on the antenna assembly.

6.3 ELECTRONIC ATTENUATOR FINE-SCAN AZIMUTH ANTENNA

ABSTRACT

The design considerations and a detailed description of the RF and control logic are presented for the fine-scan azimuth antenna fed by electronically controlled digital attenuators.

The electronic attenuator feed network was chosen as the preferred feed network for a cylindrical array because of its

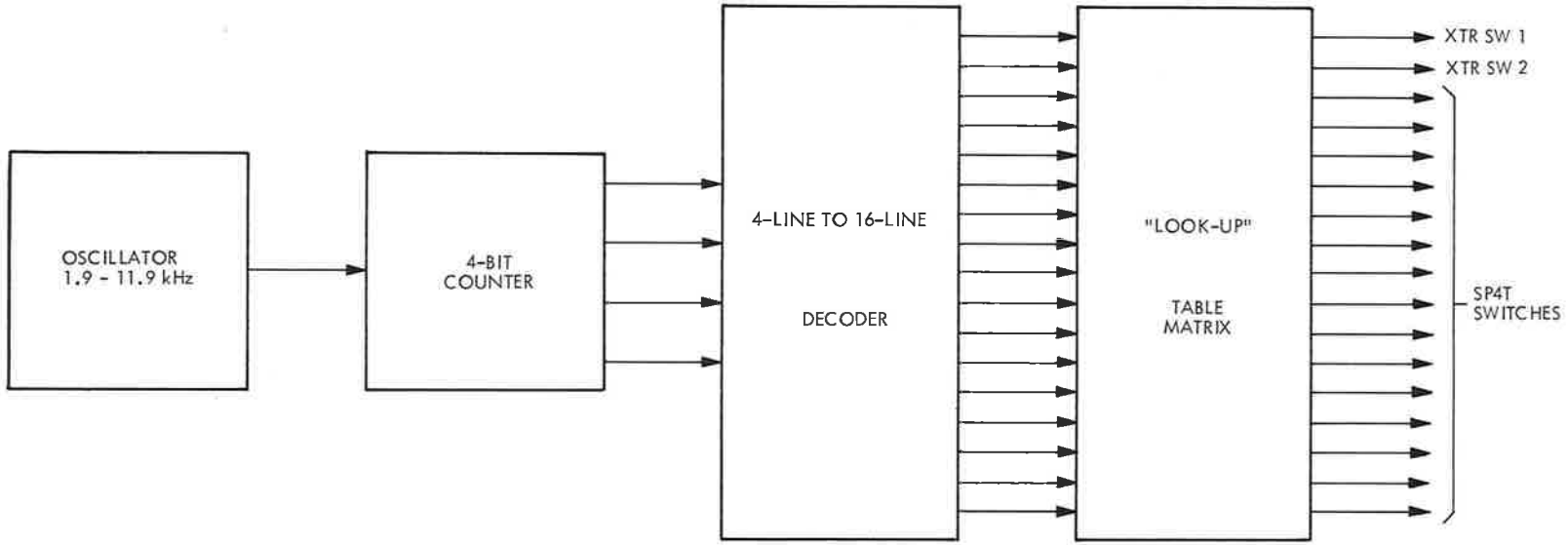

Figure 6.2.3 Azimuth Antenna Beam Steering Logic (Block Diagram) For Lens-Fed Antenna

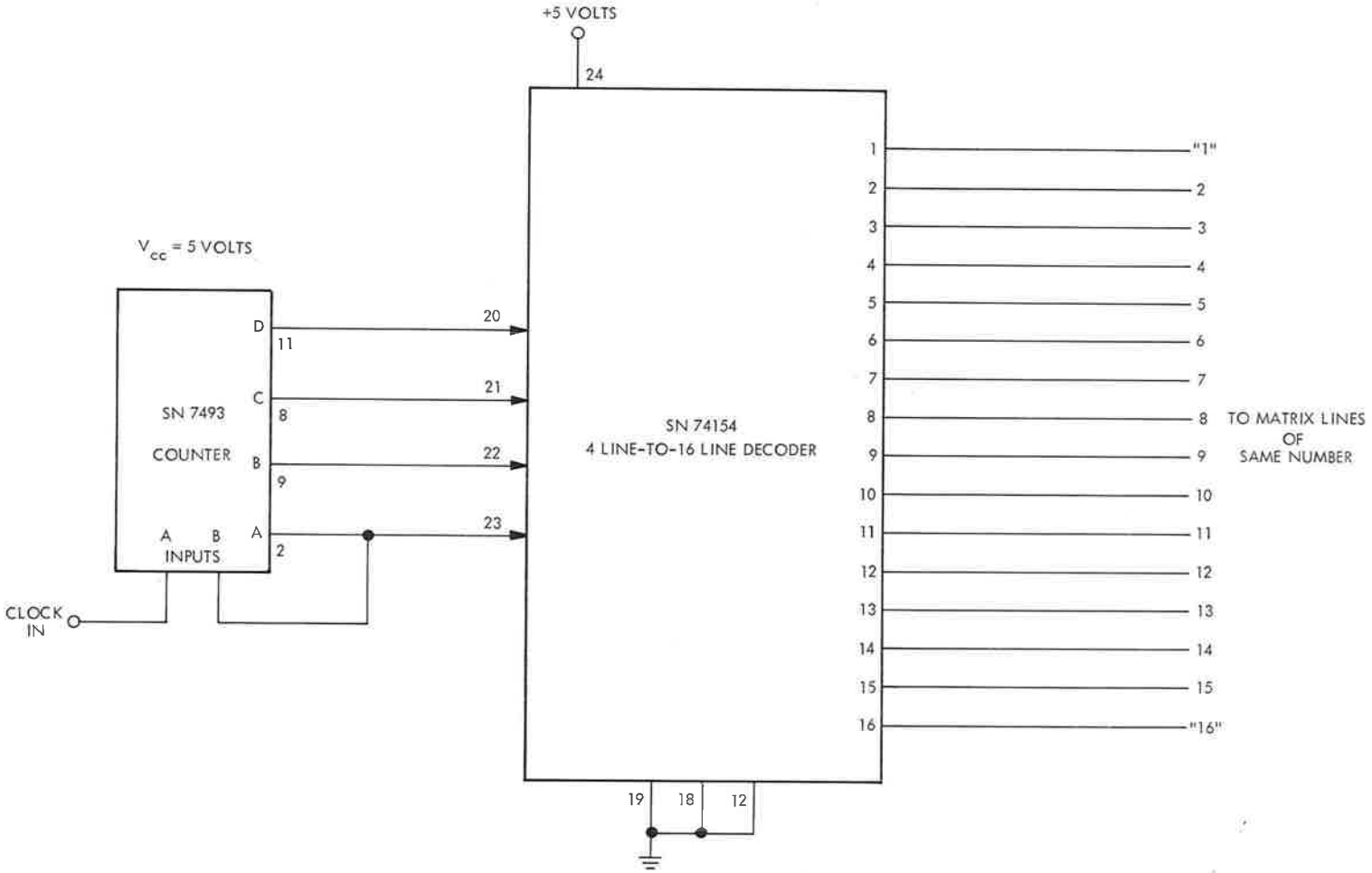

Figure 6.2.4 Coarse Azimuth Control Logic For Lens-Fed Antenna

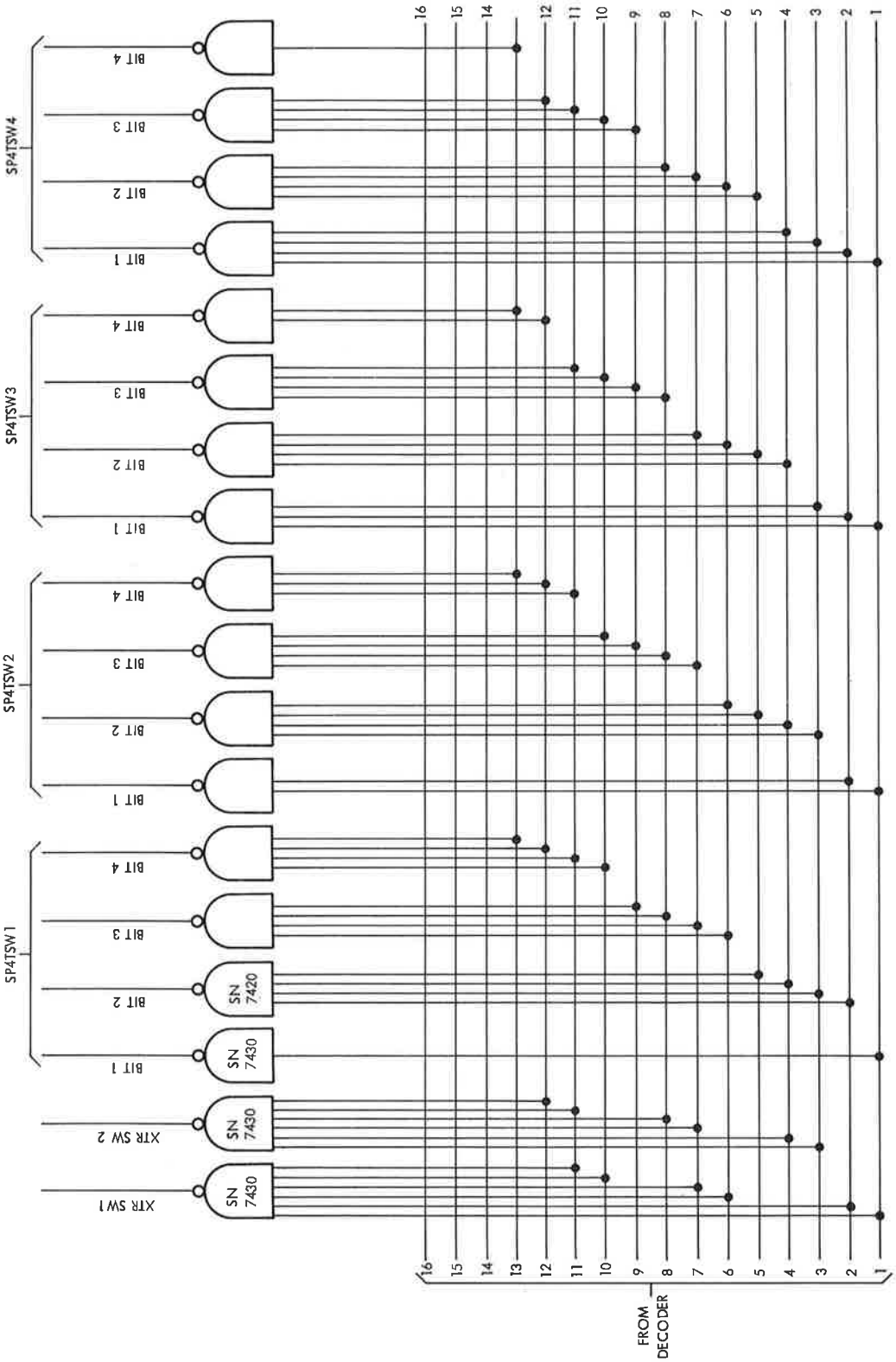

Figure 6.2.5 Azimuth "Look Up" Matrix for Lens-Fed Antenna

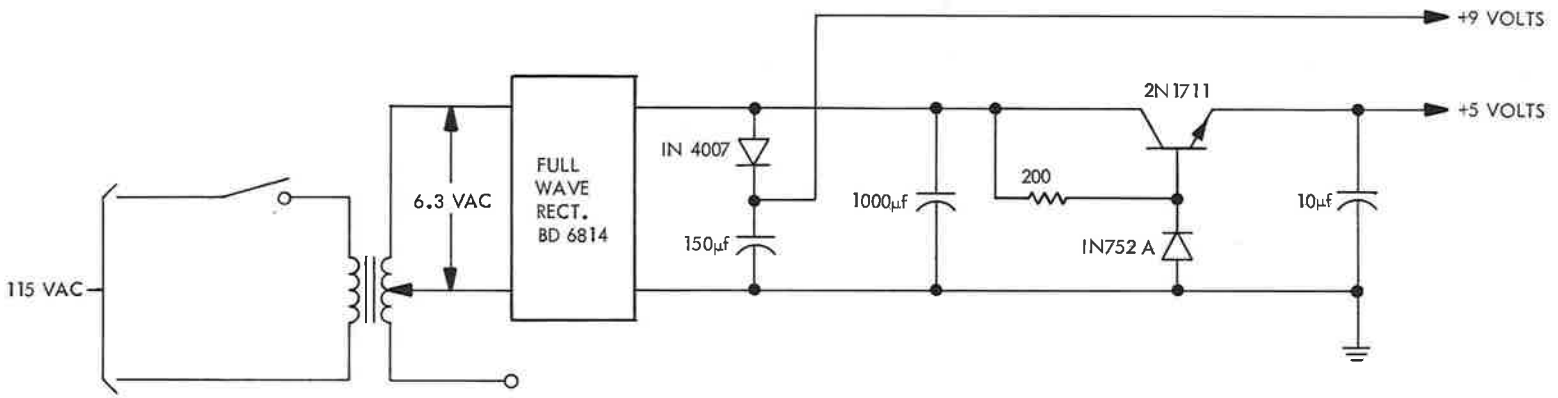

OSCILLATOR SCHEMATIC - LENS FED AZIMUTH ANTENNA

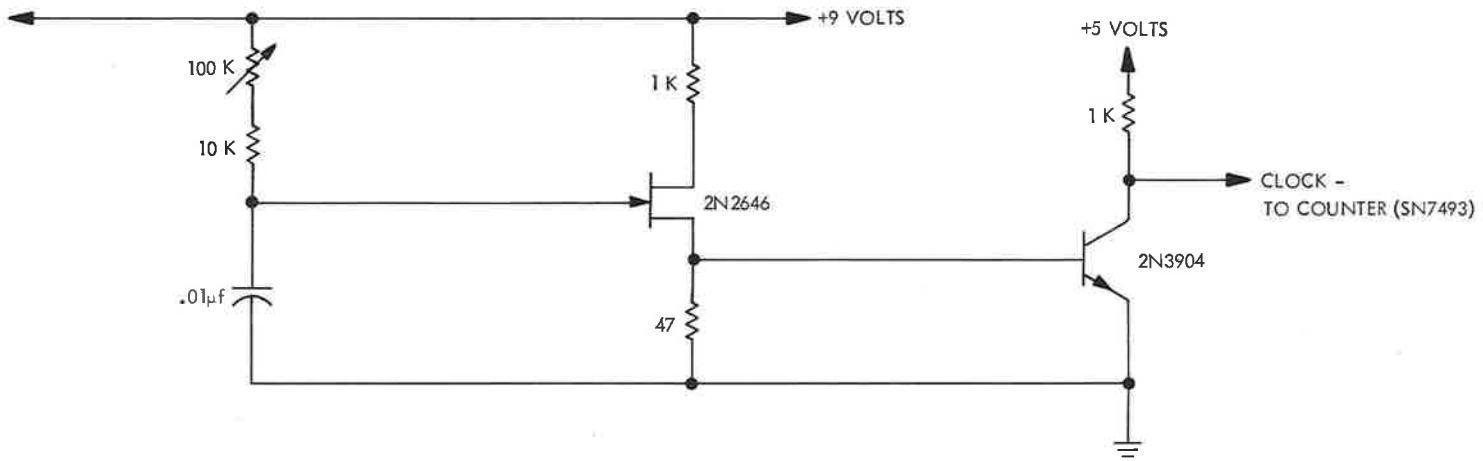

Figure 6.2.6 Power Supply Schematic, Lens-Fed Azimuth Antenna

extreme flexibility. The control logic used allows for a variety of sweep rates and data rates; step sizes can be varied; manual selection of any beam positions is possible; scan limits are adjustable; scan can either be in one direction or "back-and-forth". The control panel allows an instant display of all RF diode states. The use of a capacitive read-only-memory (ROM) allows different aperture distributions to be inserted easily, and allows minor changes to be made in the field.

The sections below describe the RF design and a detailed description of the control logic. The antenna is expected to undergo range tests early in the next fiscal year.

6.3.1 Design Approach for the Electronic Attenuator Fine-Scan Azimuth Antenna

The feed system for this antenna was designed last year.[1] The aperture distribution is set by electronically controlled attenuators. Coarse steering is accomplished by shifting the commands to the attenuators, shift register style, and resetting one sector switch. Fine steering is accomplished by the electronic phase shifters. The components for this feed system were procured and tested this year. The component test results are presented in Appendix B. The subsystem and range tests are scheduled for next year.

The parameters of the attenuator-fed fine-scan antenna are as follows:

Antenna Radius: 33.661"

Active Sector: 60° (33.661" aperture = 15λ)

Elements in Active Sector: 24

Total Number of Antenna Elements: 48

Scan Limits: $\pm 30°$

Coarse Scan Interval: 2.62°

---

1. First Annual Report, p. 138

Fine Scan Interval: 0.082°-0.64°

Coarse Beam Positions: ±12 on either side of 0°

Half-Power Sum Beamwidth: 4.0°-5.0° depending on radiating aperture distribution and Frequency.

Scanning Clock Pulse Rate: 0.6 Hz-60 kHz

Scan Rate (768 Beam Positions): 7.81×10^{-4} Hz-71.8 Hz

Repetition Rate: 0.1-100 Hz

Figure 6.3.1 shows a diagram of the setup that will be tested on the range. A component-by-component insertion loss budget for this fine-scan antenna is presented in Table 6.3.1 The total insertion loss for this antenna seems much smaller than the total insertion loss for the step-scan lens-fed antenna as presented in Table 6.2.1. However, as noted in section 6.2.1, if the step-scan antenna system were manufactured on a production basis, the insertion loss would be 5.8 dB for ±15° of scan. In order for the lens scheme to achieve ±30° of scan, additional SPDT switches would be added on the input, bringing the total to 6.9 dB. Additionally, if step scan were used in the attenuator scheme, and the same size steps were feasible, the phase shifters could be eliminated, bringing the total down to 7.4 dB as a comparison.

The model of the fine-scan antenna that is being assembled for range tests will be very flexible. The speed of scanning and the frequency of repetition of the scanning will be variable within wide limits. The granularity of the scan will be variable, that is, there can be as many as 32 or as few as 4 fine beam positions. Three capacitive read-only-memories have been obtained, each programmed to generate a different antenna pattern. These memories are field-alterable should minor changes in their data need to be made.

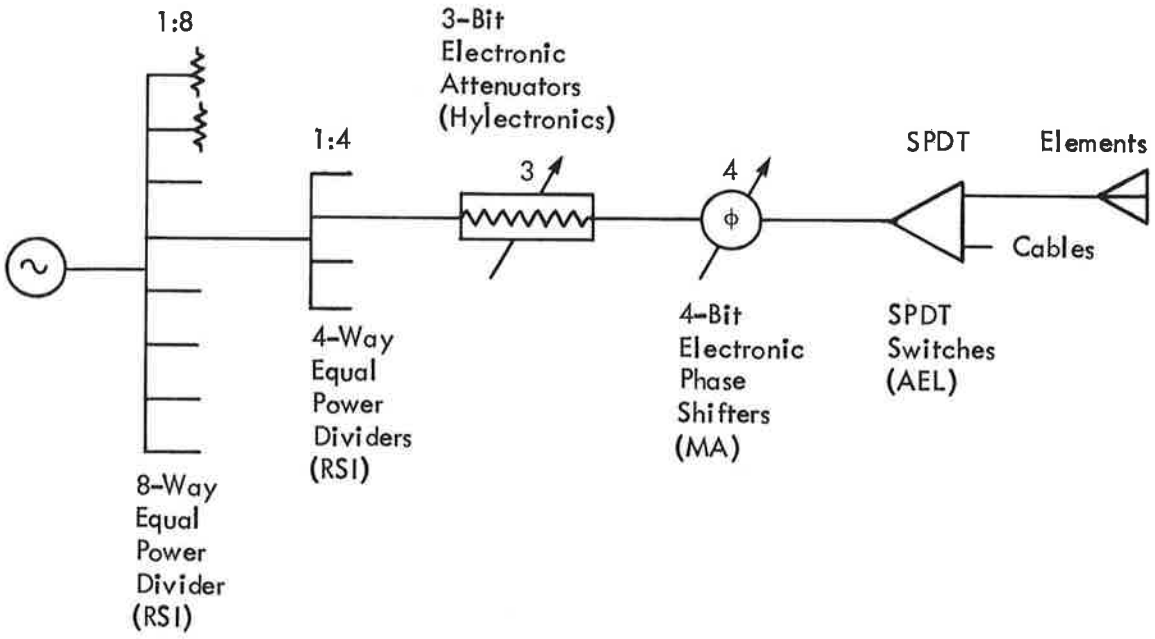

Figure 6.3.1 Range Test Setup of Fine-Scan Attenuator-Fed Azimuth Antenna

TABLE 6.3.1 INSERTION LOSS BUDGET FOR FINE-SCAN ATTENUATOR-FED AZIMUTH ANTENNA

1:8 Power Divider	1.3 dB*
1:4 Power Divider	0.8
Electronic Attenuator	1.0
Attenuation Loss	3.0
Electronic Phase Shifter	1.8
SPDT Switch	1.1
Cables	1.0
Element VSWR	0.2
Total Loss	10.2 dB

* In range test setup this loss will be 2.0 dB because only 6 of the 8 arms are used.

The first memory is programmed to have the electronic attenuators approximate, as nearly as possible, a cosine-squared on a 0.5 pedestal amplitude distribution for generating a sum beam. Data is also stored in this memory to have the electronic phase shifters steer the sum beam to 32 fine positions.

The second memory has a 180° phase shift added to all of the data for the electronic phase shifters on one half of the active sector, and the memory has data for generating a different amplitude distribution (see Figure 6.3.1) with the electronic attenuators. These settings combine to generate a difference beam, (see Figure 6.3.2 for the calculated antenna pattern).

The third memory is programmed to generate a sum beam as is the first memory; in fact, the data for the electronic phase shifters are identical. But, instead of having the electronic attenuators approximate a cosine-squared on a pedestal distribution

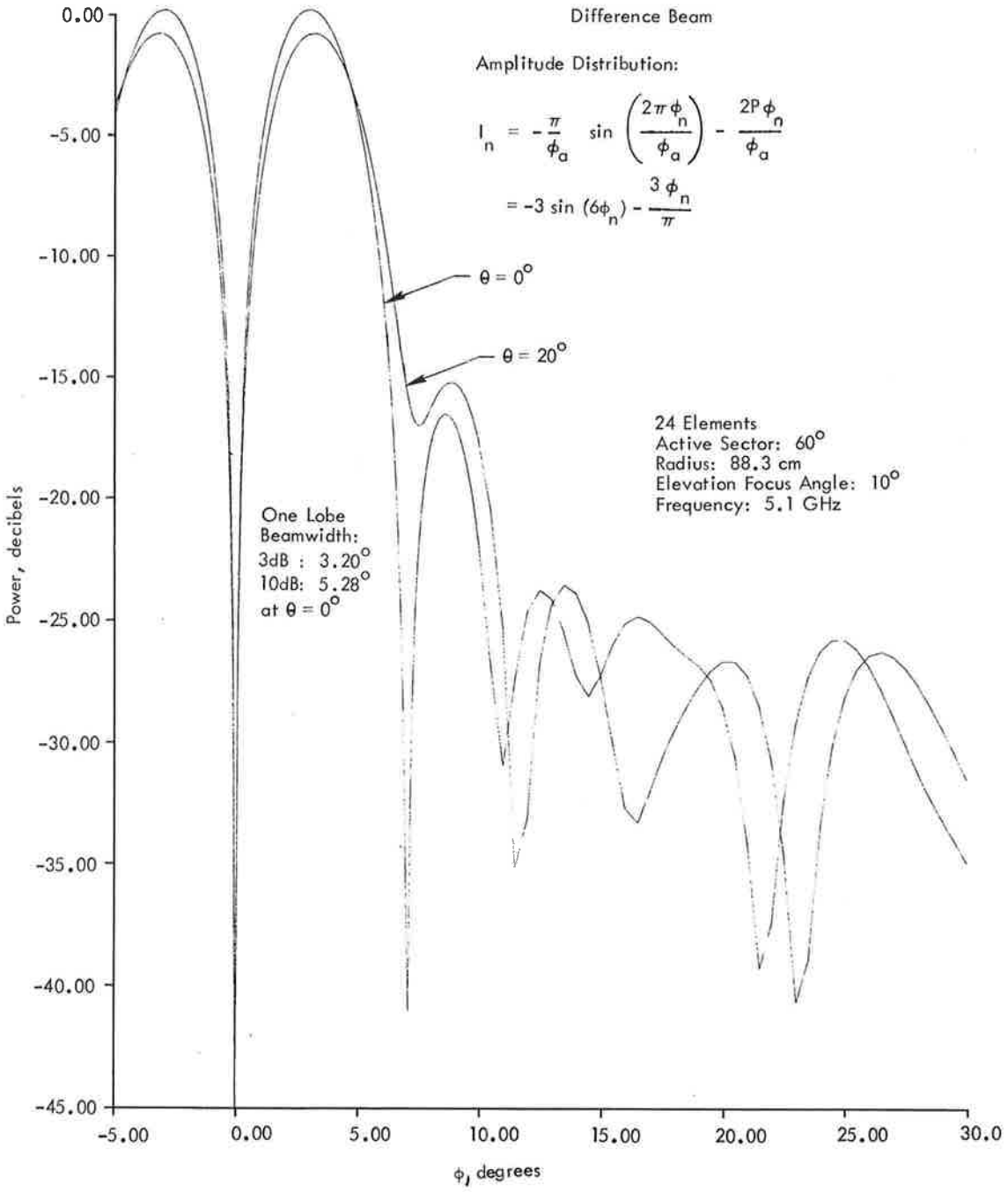

Figure 6.3.2 Calculated Difference Pattern of the Fine-Scan Attenuator-Fed Antenna

as closely as possible, the third memory is programmed to have the attenuators approximate a four-level "stepped" approximation to the exact amplitude distribution. This "stepped" distribution would be used if the coarse feed system was based on 4 x 4 transfer matrices instead of attenuators and incorporated the method employed by Hazeltine Corporation in the ATCRBS Electronic Scan Antenna contract.[1] Thus the third memory produces a set of amplitudes that allows a simulation of the results of using the 4 x 4 transfer matrix approach, shown in Figure 6.3.3, without actually building the complete feed network.

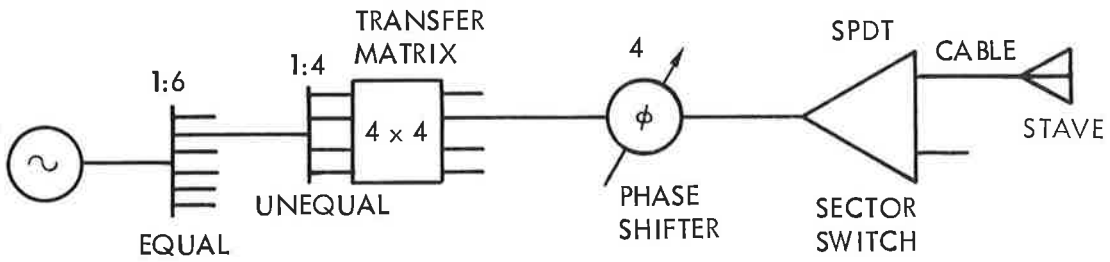

Figure 6.3.3 Transfer Matrix Distribution Network for Fine-Scan Azimuth Antenna

Calculations were performed to predict and compare the characteristics of sum beams generated with different approximations of the amplitude distribution, the results are presented in Table 6.3.2. The entries below the "exact" distribution represent the electronic attenuator approach, the transfer matrix approach, and the electronic attenuator approximation of the transfer matrix approach, (as would be generated by the third memory) respectively. The calculated performance of the attenuator approximation to the transfer matrix approach is slightly degraded from the calculated performance of the transfer matrix approach in terms of beamwidth, and significantly degraded in the terms of sidelobes. The third

1. Hazeltine Corp. "ATCRBS Electronic Scan Antenna Preliminary Design Review Data" Contract DOT-FAA 72 WA-2704, October 1971

TABLE 6.3.2 COMPARISON OF CALCULATED EFFECTS OF DIFFERENT METHODS OF APPROXIMATING THE AMPLITUDE DISTRIBUTION ON THE PERFORMANCE OF THE 4° BEAMWIDTH ANTENNA

24 Elements
Active Sector: 60°
Radius: 88.3 cm
Elevation Focus Angle: 10°
Frequency: 5.1 GHz

Amplitude Distribution	θ	3 dB BW	10 dB BW	SLL
EXACT (cosine^2 on a 0.5 pedestal)	0°	3.89°	6.69°	-25.1 dB*
	5	3.90	6.71	-25.2*
	10	3.94	6.79	-24.8*
	15	4.03	6.99	-22.2*
	20	4.19	7.39	-18.6**
3-bit Attenuator Approximation	0°	3.92°	6.75°	-24.8 dB*
	5	3.94	6.77	-24.9*
	10	3.98	6.86	-25.1*
	15	4.07	7.05	-22.4
	20	4.23	7.46	-18.6**
4-level "Stepped" Approximation	0°	3.87°	6.65°	-24.9 dB*
	5	3.89	6.68	-25.0*
	10	3.93	6.76	-24.4
	15	4.02	6.95	-22.0
	20	4.08	7.35	-18.5**
3-bit Attenuator Approximation of 4-level "Stepped" Approximation	0°	3.91°	6.73°	-22.0 dB
	5	3.93	6.76	-22.2
	10	3.96	6.84	-22.6
	15	4.06	7.04	-22.6
	20	4.22	7.45	-18.3**

* Quantization lobes about 22 dB down appear for this case at about 21° off boresight. These are reduced when the beam is scanned away from broadside.

** Appears as a shoulder, but is located where lobes exist at elevation focus angle. Lobing is down by more than 20 dB below main beam.

memory will thus allow a "worst case" test of the performance of the transfer matrix approach to coarse steering.

Since the method mentioned above requires only 4 x 4 matrices the transfer matrix method becomes competitive in terms of insertion loss. The only changes in system configuration from that shown in Figure 6.3.1 would be: 4 x 4 matrices would replace the attenuators, the 4-way power dividers would be "unequal" (see Figure 6.3.4 (a)), and the cabling to the antenna might have to be re-arranged. TSC has contracted to have a prototype 4 x 4 matrix designed and built for testing, using as a basis the work done on the 2 x 2 transfer switches which were incorporated in the lens feed. The TSC specification, (see Appendix B, Table B-11) calls for a 2.3 dB insertion loss for the 4 x 4 matrix. The 4-way "unequal" power divider would be likely to have a higher insertion loss than an "equal" power divider, however, this increased loss might be offset by designing the power divider and transfer matrix as a single unit (see Figure 6.3.4 (b)), as is possible due to the 3-layer construction of the matrix. Thus the transfer matrix approach is likely to have a total insertion loss that is 1.7 dB less than the total for the attenuator approach.

6.3.1.1 Calculated Performance of Range Test: Fine-Scan Antenna - Calculations have been performed which outline the anticipated performance of both sum and difference beams of the antenna that will be range tested as a function of frequency and elevation angle. These calculations are necessary because cylindrical arrays can only be perfectly collimated at one elevation angle at a particular frequency. If the elevation angle or frequency is changed, (assuming the settings of the phase shifters remain constant) the azimuth patterns deteriorate somewhat, exhibiting null filling, an increase in sidelobe levels, and beam broadening.

A measure of the deterioration of the pattern is given by Φ_{err}, the phase error at the edge of the active sector as seen from a far field point on boresight at an elevation angle other than the focus angle. As the defocusing error increases the sidelobes rise and the beam broadens.

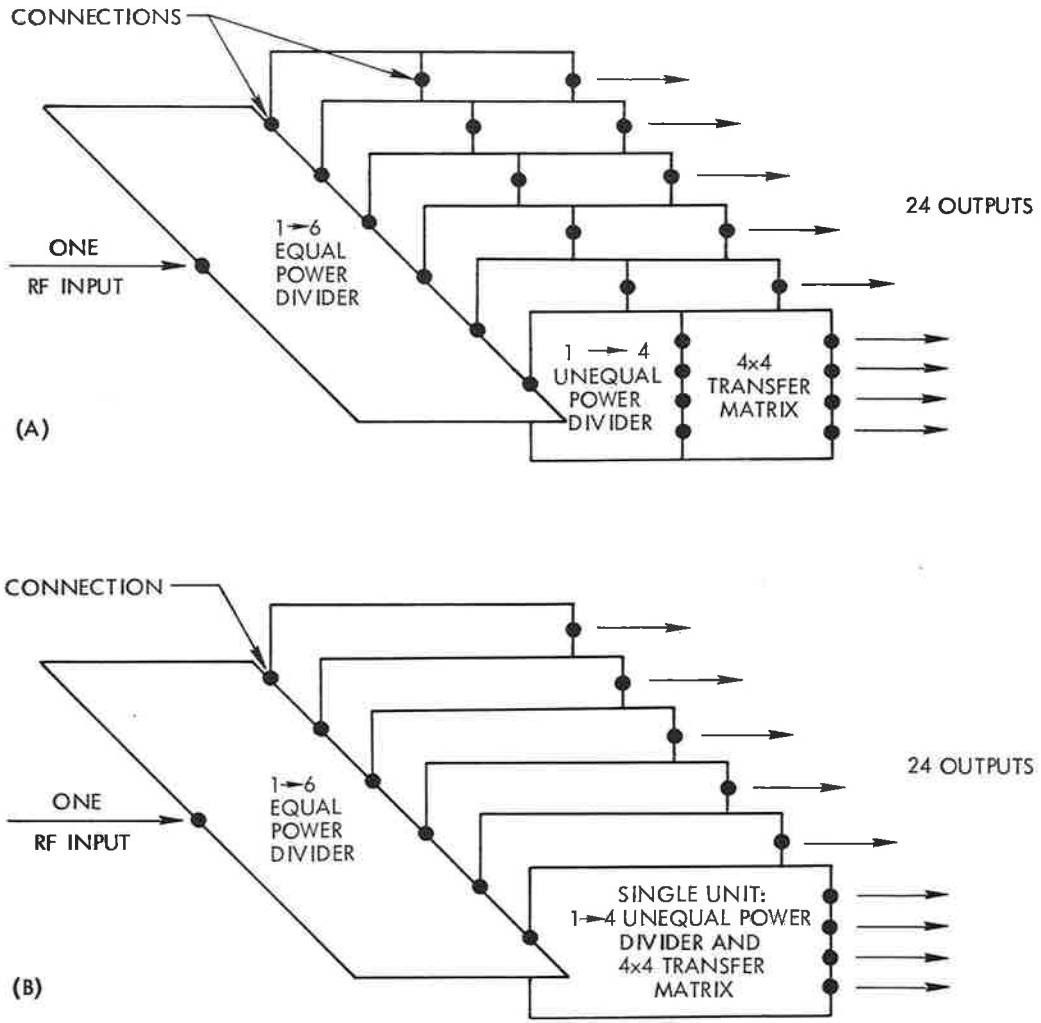

Figure 6.3.4 System Configuration for the Transfer Matrix Approach

A graph (Figure 6.3.5) has been prepared which shows how the distance to the focus point, the elevation focus angle and the defocusing error will change as a function of frequency in the actual range test antenna. It may be noted that for frequencies below a critical frequency the antenna is not focused at infinity but at a finite distance away. Furthermore, this focal distance varies with elevation angle. By lowering the operating frequency it will be possible, at a given elevation angle, to focus the antenna at $2D^2/\lambda$ or D^2/λ, which allows a receiver to be placed closer to the antenna before the beam broadens appreciably.

It can be observed from Figure 6.3.5 that the design point ($\theta_f = 10°$) has been moved up the frequency scale from 5.1 GHz to approximately 5.25 GHz. This is due to the fact that the test antenna has a slightly smaller radius that was used to calculate the phase shifter settings. Figures 6.3.6-6.3.10 show the calculated patterns of the actual range test antenna across and beyond the allowed frequency band. Table 6.3.3 compares the calculated beamwidth, sidelobe level and quantization lobe level of the actual range test antenna with the design.

Comparing the calculated performance of the antenna at 5.5 GHz and 5.25 GHz with the design suggests that the design could be improved by raising the elevation focus angle close to $\theta_f = 15°$ at mid-band. This would improve the performance at $\theta = 20°$ while it would not seriously degrade the performance at $\theta = 0°$. This could be accomplished (or the design point, $\theta_f = 10°$ at 5.1 GHz, restored) simply by re-calculating the phase shifter settings and re-programming the memories, but it is not necessary as the antenna performance within the allowed band should be more than adequate for evaluation purposes.

It is probable, (as mentioned in section 6.2.1) that the antenna elements will have their phase centers in front of the reflective surface of the antenna. This would increase the antenna's effective radius and move the design point back down the frequency scale somewhat.

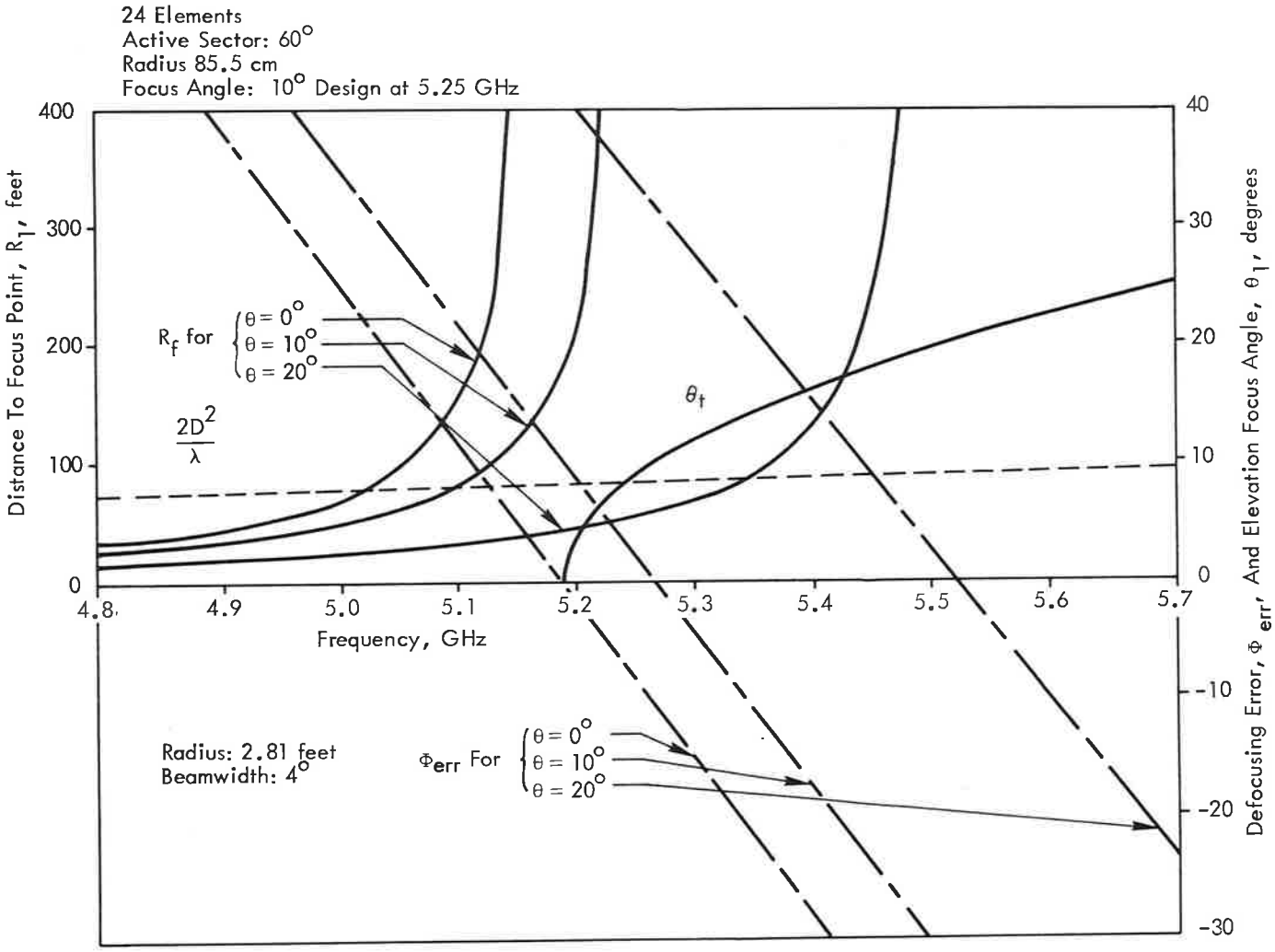

Figure 6.3.5 Effects of Frequency Variation on Performance Characteristics of Non-Collimating Cylindrical Array System

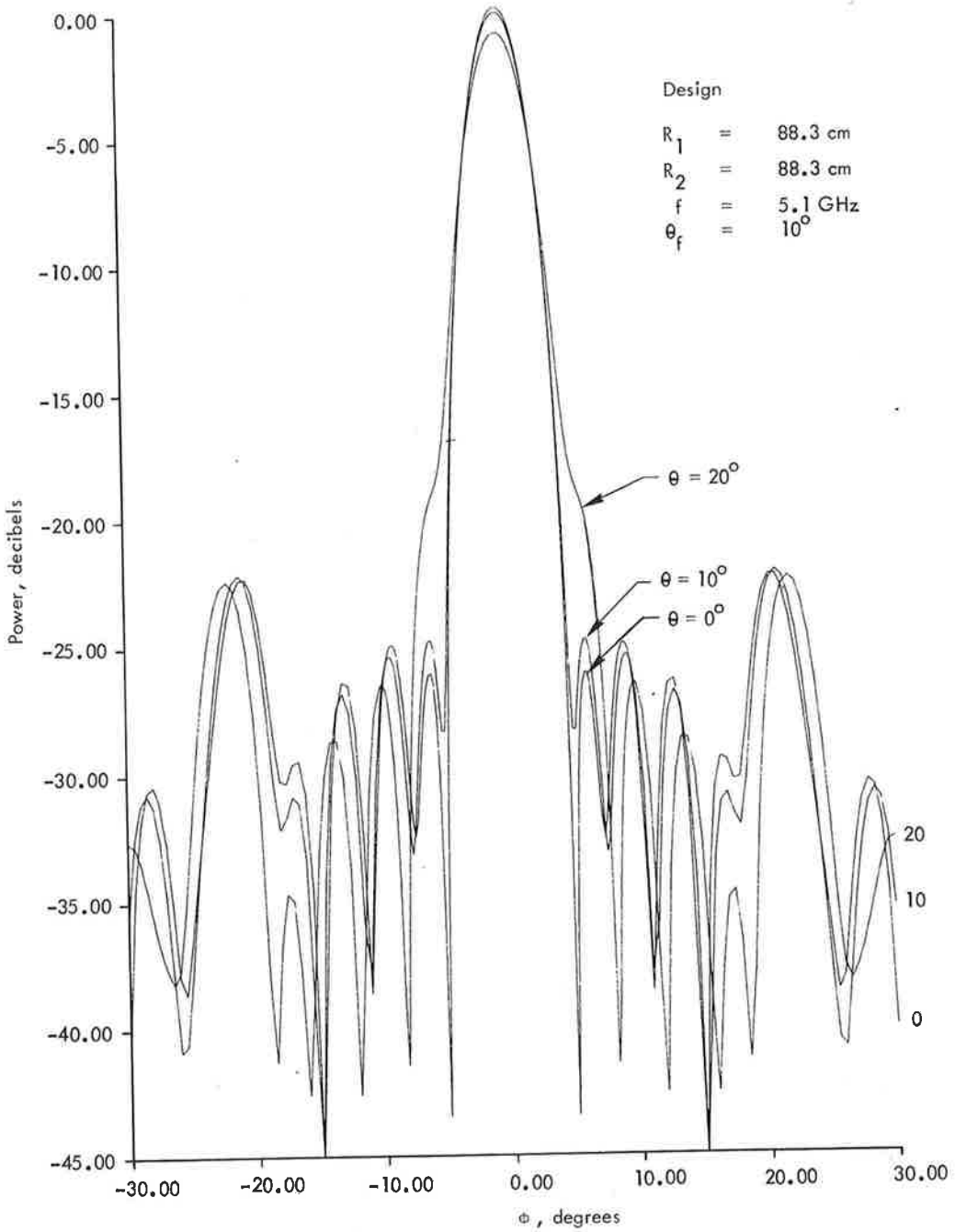

Figure 6.3.6 Design Pattern, Fine-Scan Antenna at 5.1 GHz

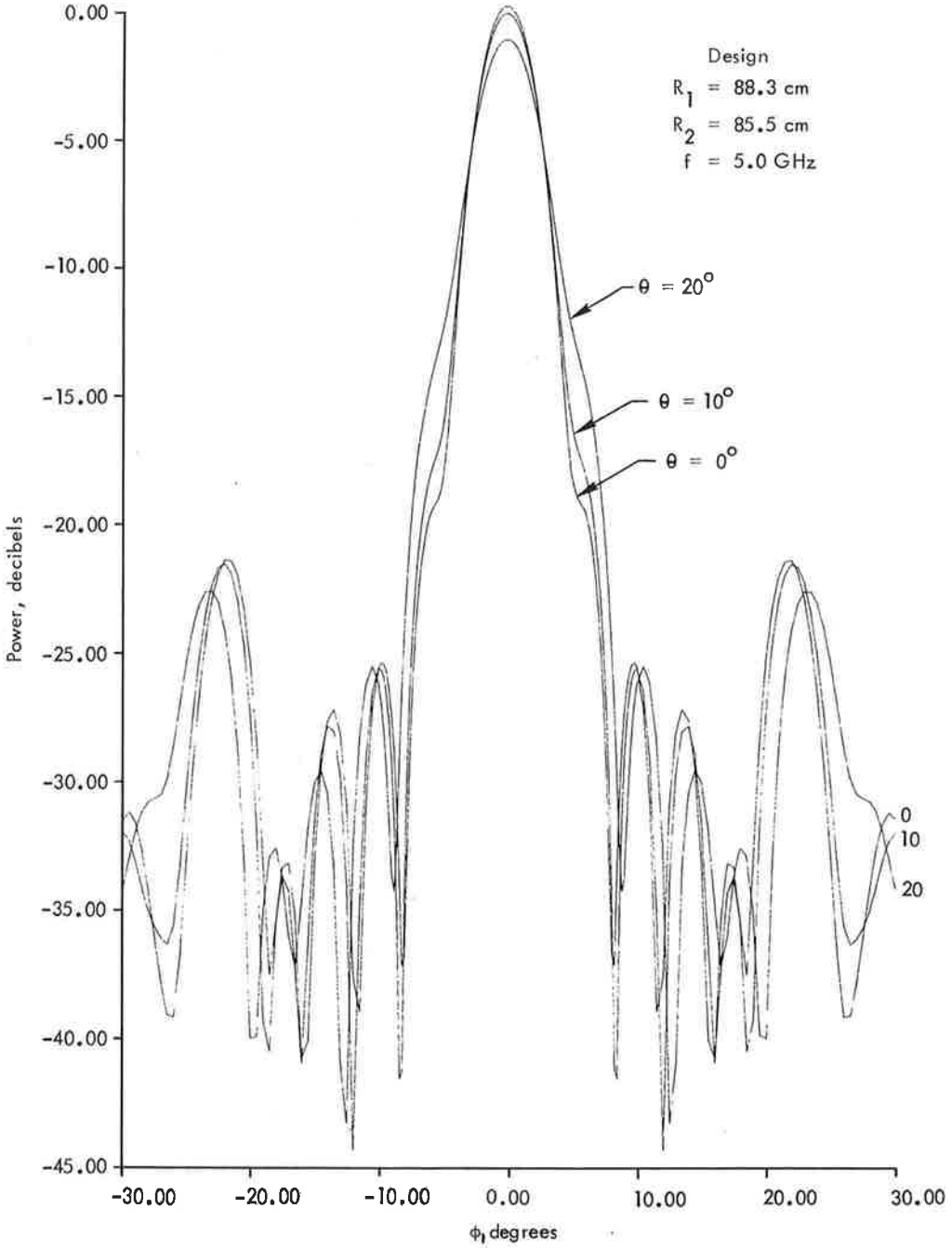

Figure 6.3.7 Calculated Pattern of Actual Range Test Antenna at 5.0 GHz

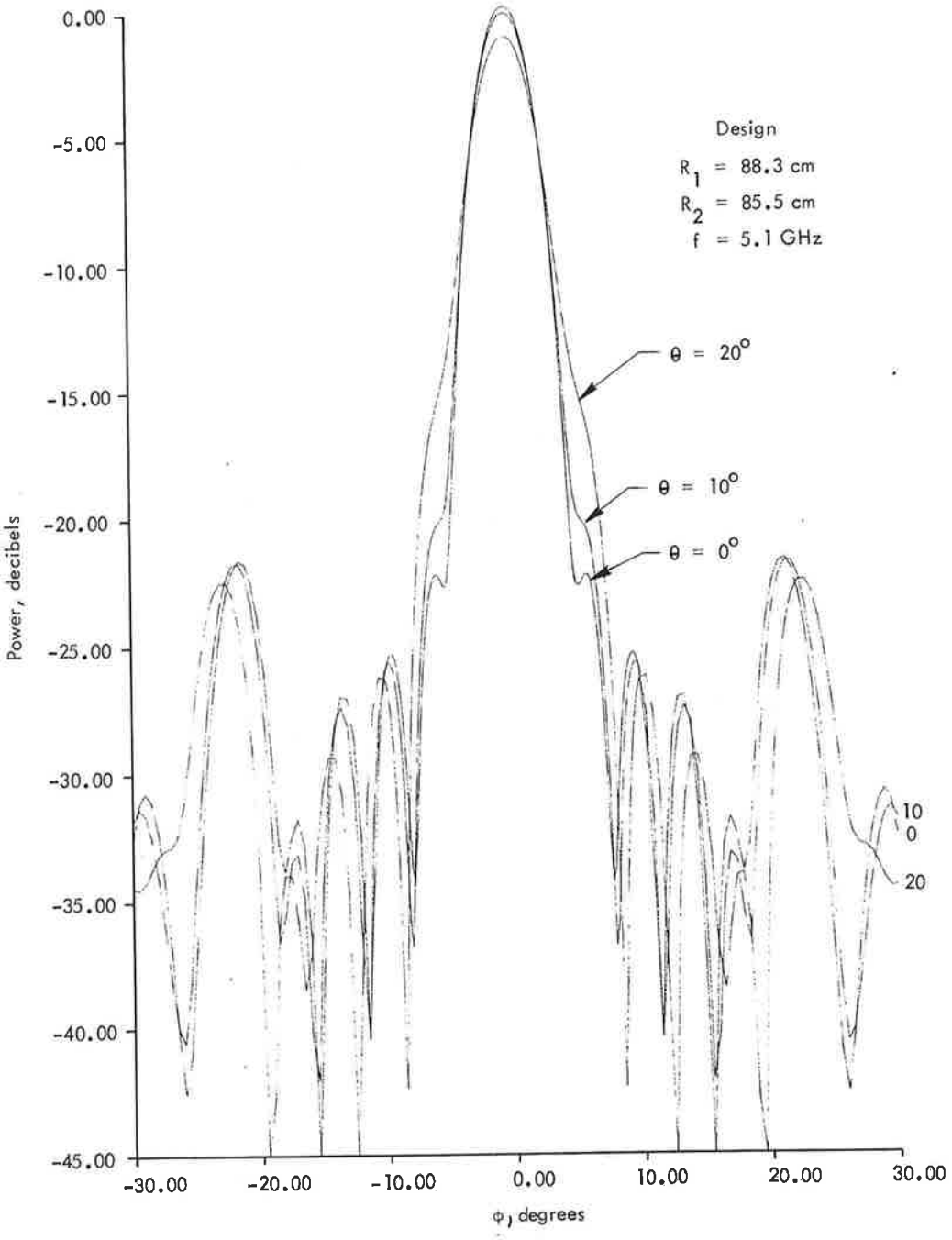

Figure 6.3.8 Calculated Pattern of Actual Range Test Antenna at 5.1 GHz

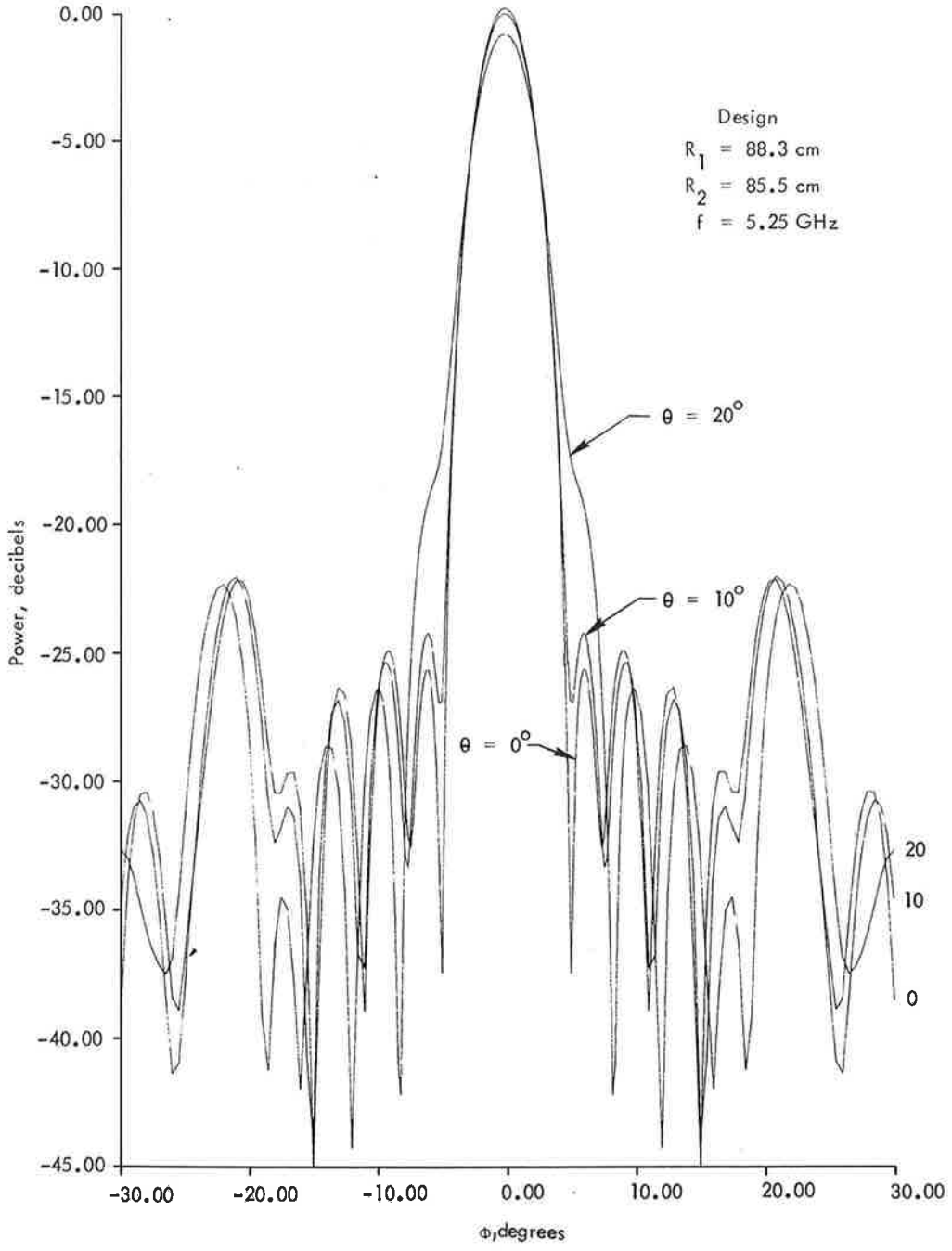

Figure 6.3.9 Calculated Pattern of Actual Range Test Antenna at 5.25 GHz

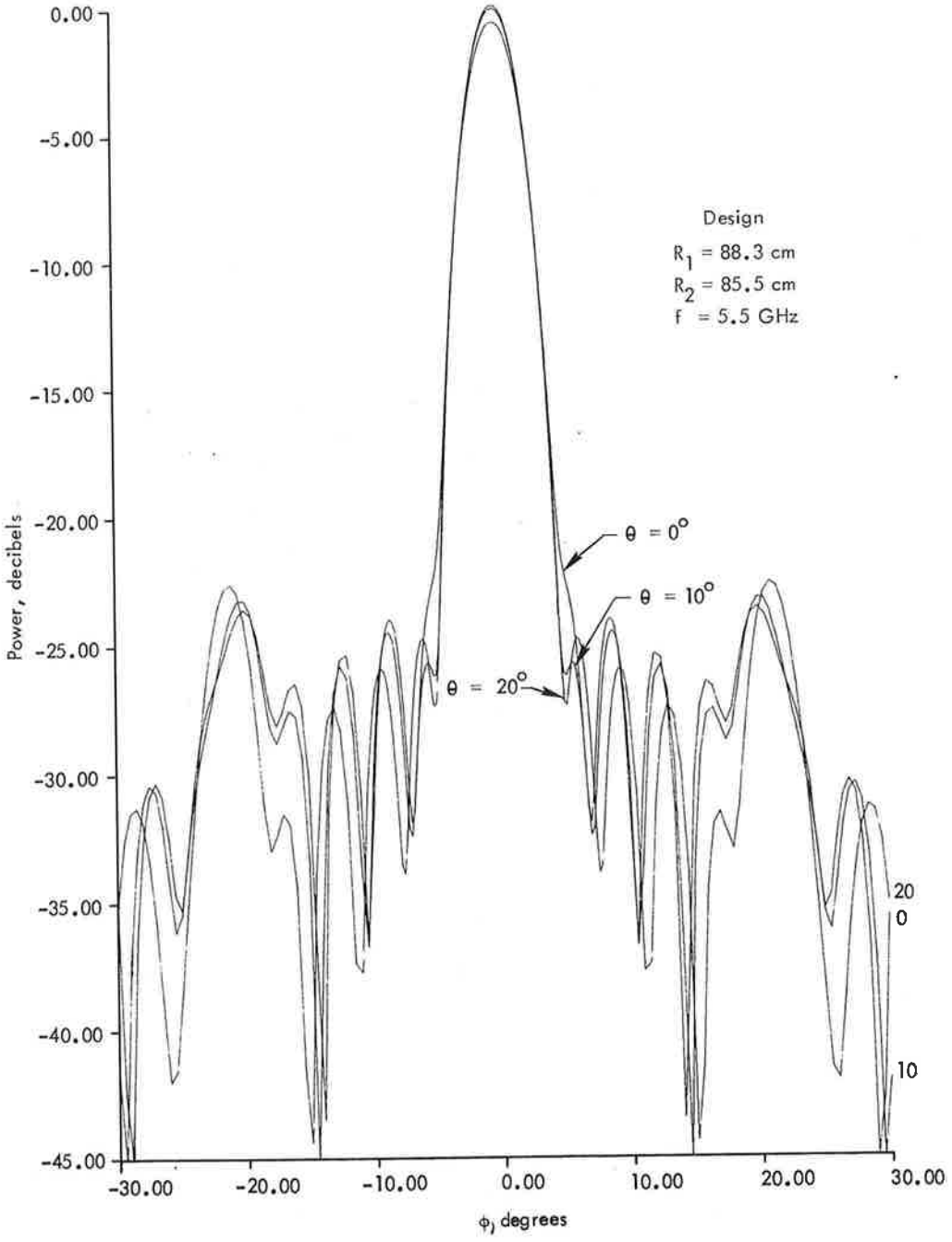

Figure 6.3.10 Calculated Pattern of Actual Range Test Antenna at 5.5 GHz

TABLE 6.3.3 COMPARISON OF CALCULATED RANGE TEST ANTENNA PERFORMANCE AT DIFFERENT FREQUENCIES WITH THE CALCULATED DESIGN PERFORMANCE

R_1: Antenna Radius Assumed in Calculating Phase Settings
R_2: Actual Radius of Antenna
f: Frequency
10 dB BW: Beamwidth Measured at the -10 dB Points
SLL: Sidelobe Level
QLL: Quantization Lobe Level

	R_1	R_2	f(GHz)	10 dB BW	SLL	QLL	
0°	88.3	88.3	5.1	6.69°	-25.1 dB	-22.1 dB	DESIGN
	88.3	85.5	5.0	7.22	-19.9	-21.7	
	88.3	85.5	5.1	6.95	-22.5	-21.9	
	88.3	85.5	5.25	6.70	-25.1	-22.4	
	88.3	85.5	5.5	6.60	-23.6	-23.7	
10°	88.3	88.3	5.1	6.80°	-24.8 dB	-22.1 dB	DESIGN
	88.3	85.5	5.0	7.50	-18.1	-21.5	
	88.3	85.5	5.1	7.15	-20.5	-21.7	
	88.3	85.5	5.25	6.81	-24.2	-22.0	
	88.3	85.5	5.5	6.59	-24.5	-23.2	
20°	88.3	88.3	5.1	7.40°	-18.7 dB	-21.6 dB	DESIGN
	88.3	85.5	5.0	8.94	-13.5	-21.6	
	88.3	85.5	5.1	8.17	-15.2	-21.5	
	88.3	85.5	5.25	7.45	-18.3	-22.5	
	88.3	85.5	5.5	6.82	-24.2	-22.0	

Figures 6.3.11-6.3.13 show that the calculated difference pattern does not deteriorate significantly over the allowed frequency band, nor does it deviate significantly from the design pattern.

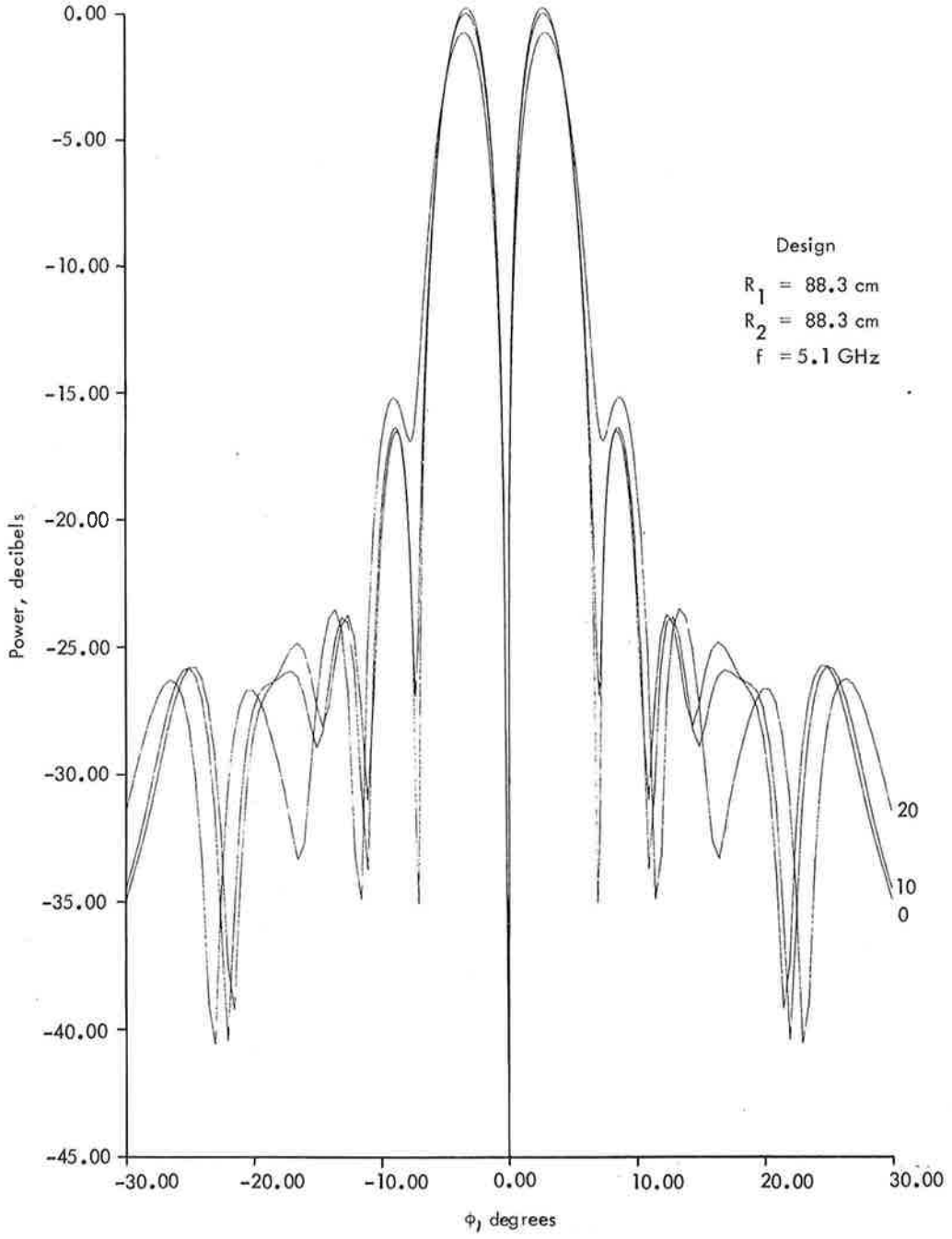

Figure 6.3.11 Design Difference for Fine-Scan Antenna at 5.1 GHz

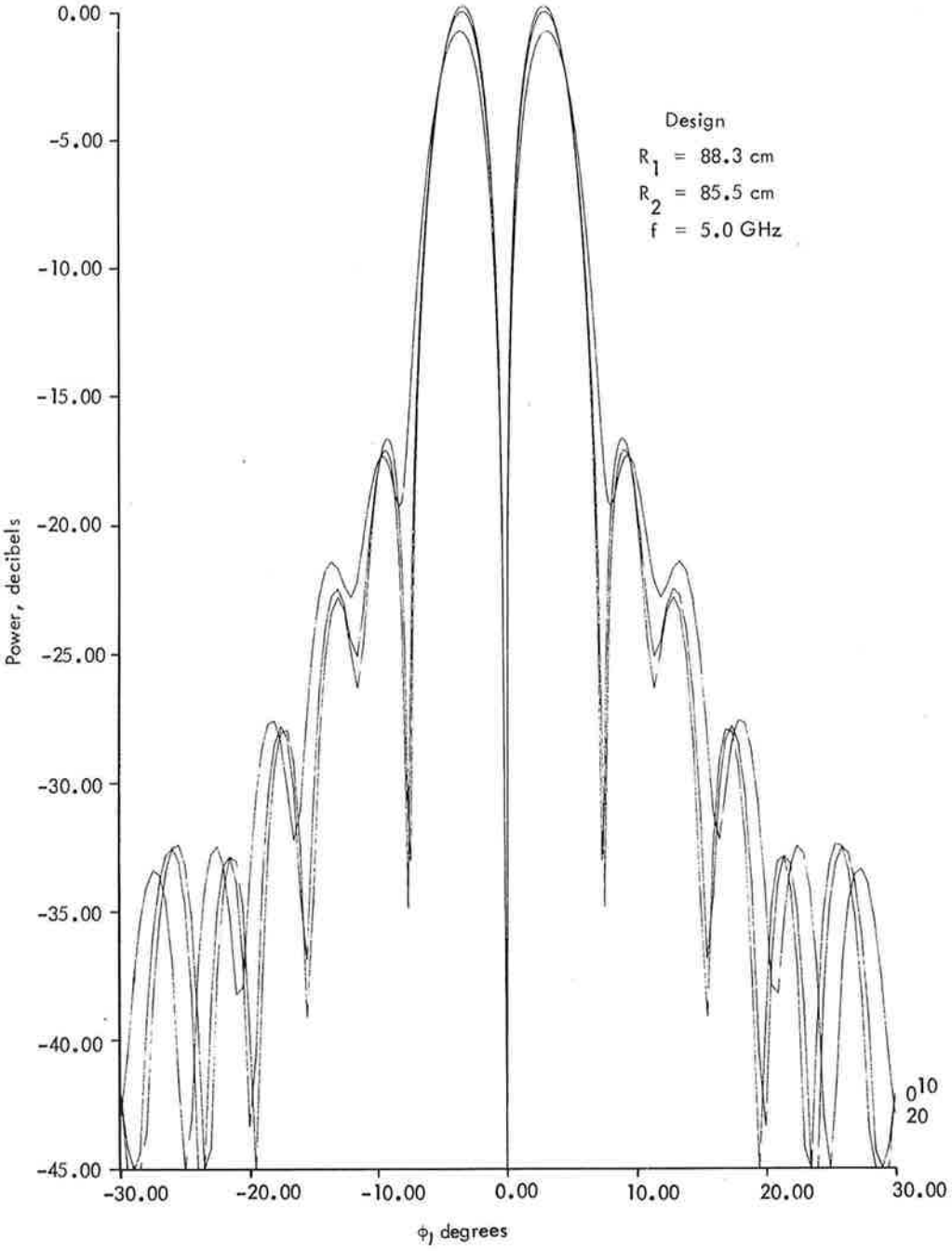

Figure 6.3.12 Calculated Difference Pattern of Actual Range Test Antenna at 5.0 GHz

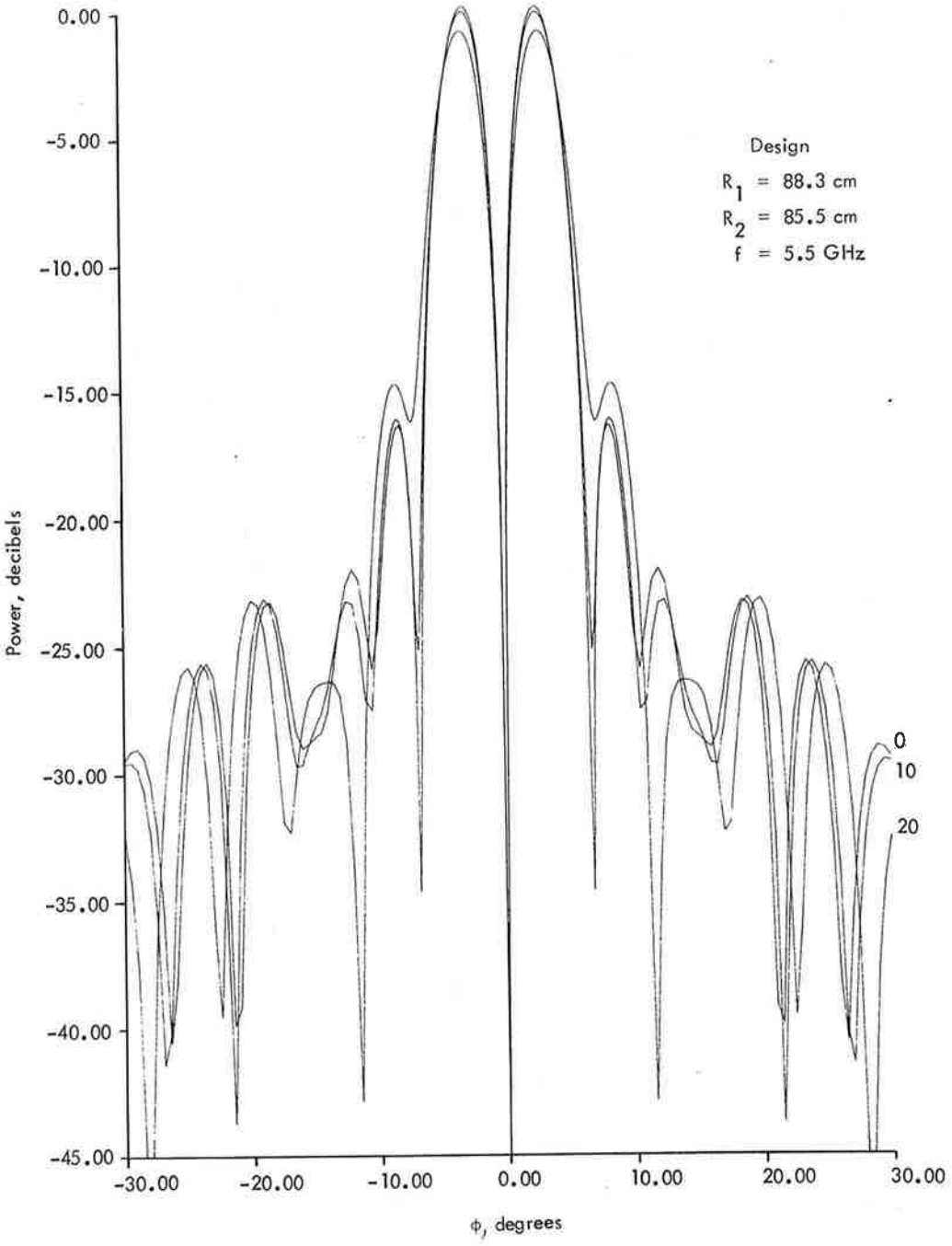

Figure 6.3.13 Calculated Difference Pattern of Actual Range Test Antenna at 5.5 GHz

6.3.2 MLS Attenuator Field Circular Array Beam Steering Computer

Introduction

The Azimuth Beam Steering Logic Computer for the most complex feed network, electronic attenuator feed, has been designed and fabricated. It will be used for electronically steering the microwave landing system cylindrical phased array antenna constructed at TSC and for experimental azimuth antenna beam pattern evaluation.

A major portion of the task was accomplished in-house. Installation and wiring of all logic components on printed circuit boards and cables for interconnecting logic racks and feed network components were performed in-house. Portions done elsewhere included interconnection cage wiring and display panel fabrication. The unit has been debugged and electrical performance checked.

The content of this section will be restricted to discussing the design criteria selection for the unit, explaining the logic functions, and describing the hardware. Section 6.3.2.1 deals with the design considerations and philosophy and section 6.3.2.2 will be devoted to explaining the logic functions and circuits and describing the hardware.

6.3.2.1 Design Criteria - In analyzing the design of the Beam Steering Computer for this application it was considered necessary to use a more flexible design to obtain the versatility required for an experimental antenna program. As a result, the design had to incorporate features such as a field programmable alterable Read-Only Memory, a manual override to enable the operator to position the beam in any selected location, and techniques for varying the number of fine scan positions for each coarse position setting. All of these features are needed for the experimental phase of the program but are certainly not required for a production system. The latter type system would employ simpler design and be less expensive.

Several techniques for implementing the logic were considered and discussed in the first annual report. Each had advantages and disadvantages in regard to complexity, cost, and performance. For example, the first approach was to use stored memory only, for storing all the commands. This would involve storage of a large number of memory bits (76,032), and would result in a more expensive system. A second approach would employ a switch matrix to rotate the phase settings. Although the memory storage capacity would be reduced to 5376 bits, the matrix would require five banks of switches to implement the commands and increases the complexity of the system. The third approach and the one selected for this application takes advantage of the fact that the phase commands are shifted with the coarse positions. Since only the phase settings are affected for each coarse position scanned, a design using a smaller capacity storage memory (5376 bits) and shift registers for rotating the phase settings for all fine positions was selected. A design based on the third approach was discussed in the first annual report. The design to be discussed in this report utilizes the same basic approach with several modifications. The modifications primarily involve improving techniques for implementing the logic and adding some useful features such as displays for monitoring binary data. As a result additional logic functions are needed and more hardware required.

In discussing the Azimuth Beam Steering Computer design, it is easier to separate the main unit into three subunits, explain each subunit function, and describe the logic circuits and hardware for each subunit.

The logic computer will thus be divided into three major subunits, the logic controller, the memory, and the logic shifting and buffering electronics. Each subunit performs a specific function related to generating commands, computing and processing information in the form of binary data for controlling and steering the antenna array in azimuth. Salient features of each subunit will be discussed in detail.

6.3.2.2 Logic Signal Controller - The logic signal controller generates the binary data bits which upon further processing are used to translate the appropriate commands to the drivers of the phase shifters, attenuators, and sector switches. In addition, this unit produces the timing and control pulses for performing the integrated circuit logic functions necessary to permit proper sequences of processing data through the system.

These pulses are generated by the Scan Rate Clock and the Sweep Frequency Clock and used to provide the timing for the Up/Down Counter, latches, granularity logic, memory, shift and buffer registers, etc. The Beam Steering Computer timing will be explained in detail later. The electrical operation of the logic unit can best be understood by a knowledge of the timing employed in the system.

A block diagram of the logic beam steering computer unit is shown in Figure 6.3.14. The logic signal controller unit encompasses all the logic circuits required to address the memory. A functional block diagram of the memory is also shown in Figure 6.3.14. The shift and buffer registers and buffering electronics on the output side of the memory completes the system. The timing diagram for the complete unit is shown in Figure 6.3.15. An explanation of the timing diagram will be given later. Figure 6.3.16 shows a more detailed schematic of the logic signal controller.

The logic signal controller unit was designed to allow an operator the flexibility of choosing between a manual or automatic mode of operation. In the manual mode it is possible to direct the beam to any selected location and step it on a position by position basis by depressing the manual push button switch on the controller. Initially, operation is set up by selecting a 10 bit binary word with ten toggle switches, called the Low Count Preset Limit Switches. The auto/manual switch on the control can be set to either mode of operation. If auto mode is selected all the Low Count Preset Limit Switches are set to zero and the High Count Preset Limit Switches to a binary value based on the

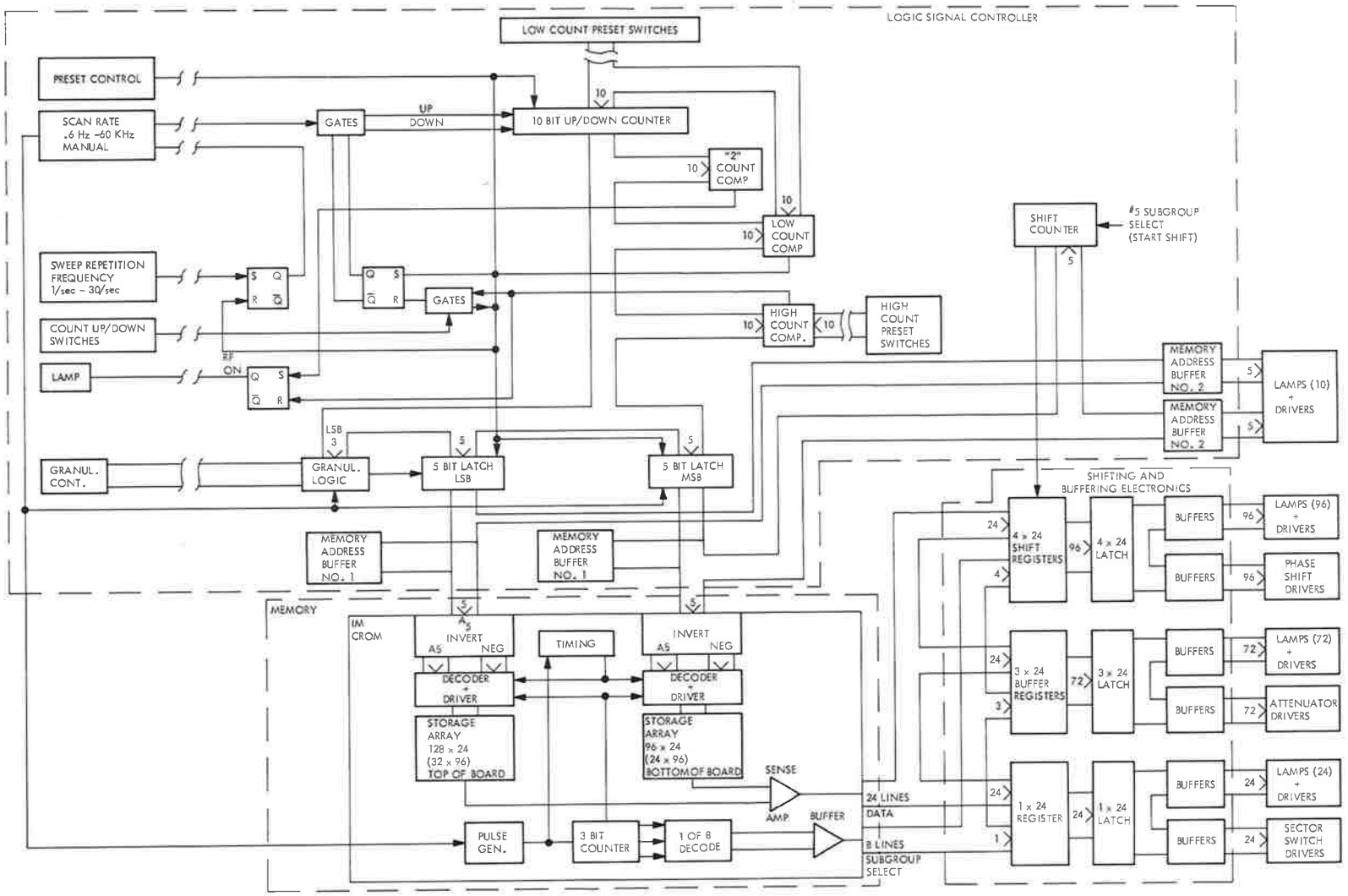

Figure 6.3.14 Microwave Landing System Beam Steering Unit Schematic for Electronic Attenuator-Fed Azimuth Antenna

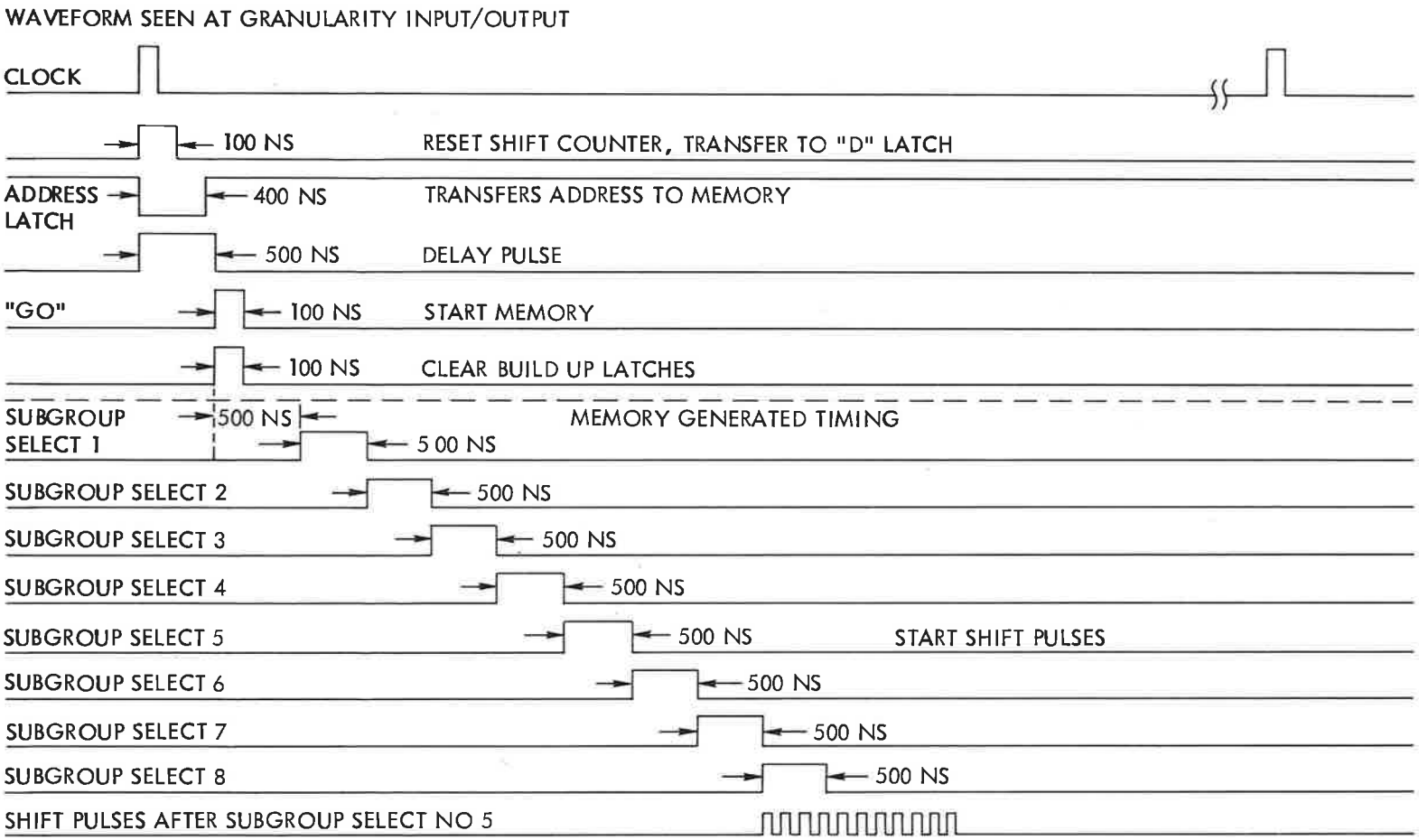

Figure 6.3.15 MLS Beam Steering Computer Unit Timing

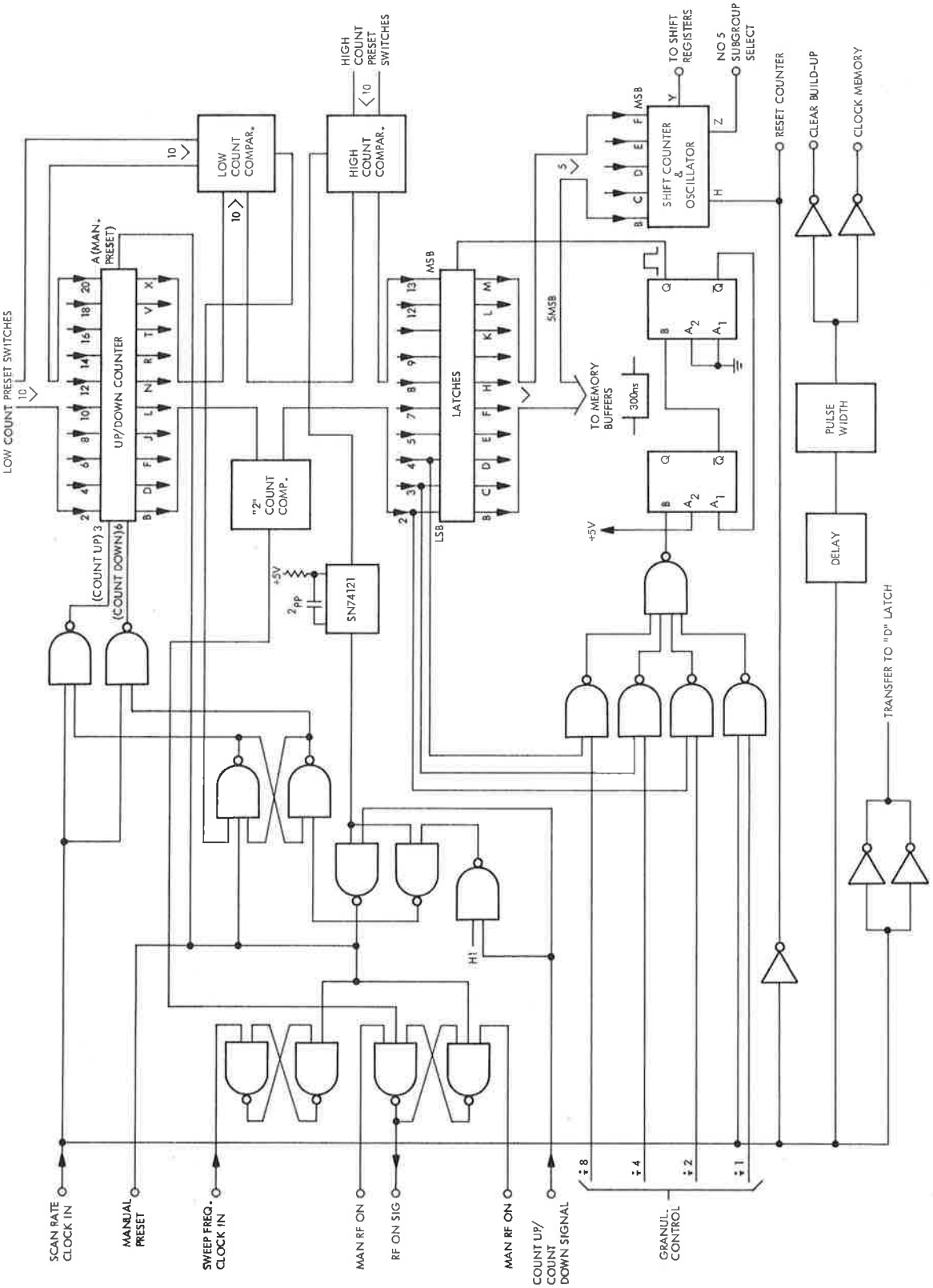

Figure 6.3.16 Microwave Landing System Azimuth Logic Signal Controller Unit Schematic

address desired for the memory. In any event, the switches will set upper and lower limits on the counter and in the automatic mode the counter will operate in its normal free running mode. In the manual mode the beam can be controlled on a position by position basis by simply actuating the manual push button on the control panel. This changes the memory address on a bit by bit basis. The counter direction can be controlled by a Count Up/Count Up-Down switch located on the panel. In the manual mode the operator can control the scan angle of the beam between any two predetermined locations or positions or change the position of the beam on a step by step basis in either direction. To load the bits into the counter it is necessary to depress the preset switch located on the panel.

Simultaneously, the ten bit binary data words selected by high and low count preset limit switch are loaded into the comparators. There are three comparator logic circuits each consisting of exclusive OR gates. On the block diagram they are listed as the low count, high count, and "2" count comparators. The "2" count comparator controls the RF signal condition. For the present; the low and high count comparators are of immediate concern. Upon loading the counter with the manual preset an output occurs on the counter. A comparison is made between the two signal inputs into the comparators, i.e., all the input bits are checked by the comparators. If they are the same, a "1" appears at the outputs of the comparators. The outputs from the comparators are fed to gates and flip-flops in the Up/Down Logic control board and control the counting direction of the Up/Down Counter.

In the auto mode the counter will count to its high limit, revert to the zero state, and repeat its count cycle. The counter which produces 1024 beam positions (2^{10}) can be set to automatically scan between two predetermined positions set by the high and low count preset switches and the comparators and Up/Down Logic.

The Up/Down counter is also controlled with the Scan Rate Clock and Sweep Frequency Clock. The Scan Rate Clock controls the stepping rate of the counter while the Sweep Frequency Clock

determines how often the Up-Down Counter cycles. The scan rate clock can be adjusted to vary between 0.6 Hz and 60 kHz. The sweep frequency clock can be varied from 0.1 Hz to 100 Hz. Both are oscillator controlled logic circuits using decade counters for dividing the basic oscillator frequency to the desired values.

The Up/Down Counter is a 10-bit synchronous counter consisting of three 4-bit SN74193 Integrated Circuits. Although twelve bits are available only ten are required here. The comparators are a series of SN7486 Quadruple 2-Input Exclusive-OR Gates, SN7404 Hex Inverters, and DTL (Diode Transistor Logic) 9930 gates with a 9933 Extender.

The output data from the Up/Down Counter is also loaded into latches as seen in Figure 6.3.16. The latches consist of three SN7475 4-bit Bis-table latches having a total capability to handle 12 bits of which only ten are used. The latch outputs provide the address to the memory.

Five MSB (Most Significant Bits) of the ten bit binary output from the latches are directed to the memory section containing a 96 x 24 storage array and the 5 LSB (Least Significant Bits) are steered to the storage section containing a 128 x 24 array. The latches act as a temporary hold circuit to allow proper organization of data being processed and allow updated counter data to be transferred to the memory at the proper interval. This function is controlled by the granularity logic which provides an enable signal to the latches.

Three LSB's of the ten-bit binary input word to the latches are used for controlling the granularity logic function which is used to derive the 32 fine positions between the coarse scanning positions. The Up/Down Counters divider capability is used for control. If only two positions are desired the circuit is set up so that only the left most significant bit is utilized. If four positions are desired, the 2nd least significant bit is used and so forth. If all 32 positions are needed the scan rate clock is the control (see Figure 6.3.16). The 3 LSB are fed to the granularity logic through an "anding" circuit and an oscillator

which provides a pulse to reset the latches to accomodate new data from the Up/Down Counter. The granularity logic board generates a number of output pulses used to strobe the latches, reset the shiftcounter, clear the "D" type latches in the Build-Up Register, transfer data from the shift registers to the "D" latches, and clock the memory. The output pulses are of a wide variety, negative and positive, delayed and shaped, and are used to control the sequence of timing events necessary to maintain orderly processing of binary data through the system. A schematic of the granularity logic is shown in Figure 6.3.17.

The granularity logic consists of a Quadruple-2 Input positive Nand Gate, a SN7420 Dual 4-Input Positive Nand Gate, three SN74121 Monostable Multivibrators (one shots), an oscillator, a SN7406 Hex Inverter and a SN7404 Hex Inverter. The SN7406 has Open-Collector High Voltage output and can handle heavier loads than the SN7404. The SN7406 can sink a maximum current of 40 ma. In cases where heavier loading is required the inverters can be paralleled.

The RF on signal is controlled from the "2" count comparator and other gates and circuits. The RF signal will be on when the "2" count comparator output is high and will remain on until the high limit count is reached and produces an output that inhibits the flip-flops that control the RF.

Since the output of the latch (at least the 5 MSB of the 10-bit output) are routed to the Shift Counter, primarily to control the shift register, the counter and oscillator will be described next. The Shift Counter and Oscillator consists of two SN7493 4-bit binary counters, two SN74121 one-shot multivibrators, several Nand gates (SN7400 and SN7430) and two Quadruple 2 Input Exclusive-OR gates. The 5 MSB from the latches control the counter. The counter is arranged to count to twenty-four. The fifth subgroup select pulse (start shift pulse) is used to enable the oscillator (two SN74121 multivibrators connected as an oscillator) in the Shift Counter and simultaneously actuate the shift registers and counter. The counter counts up to the binary value of

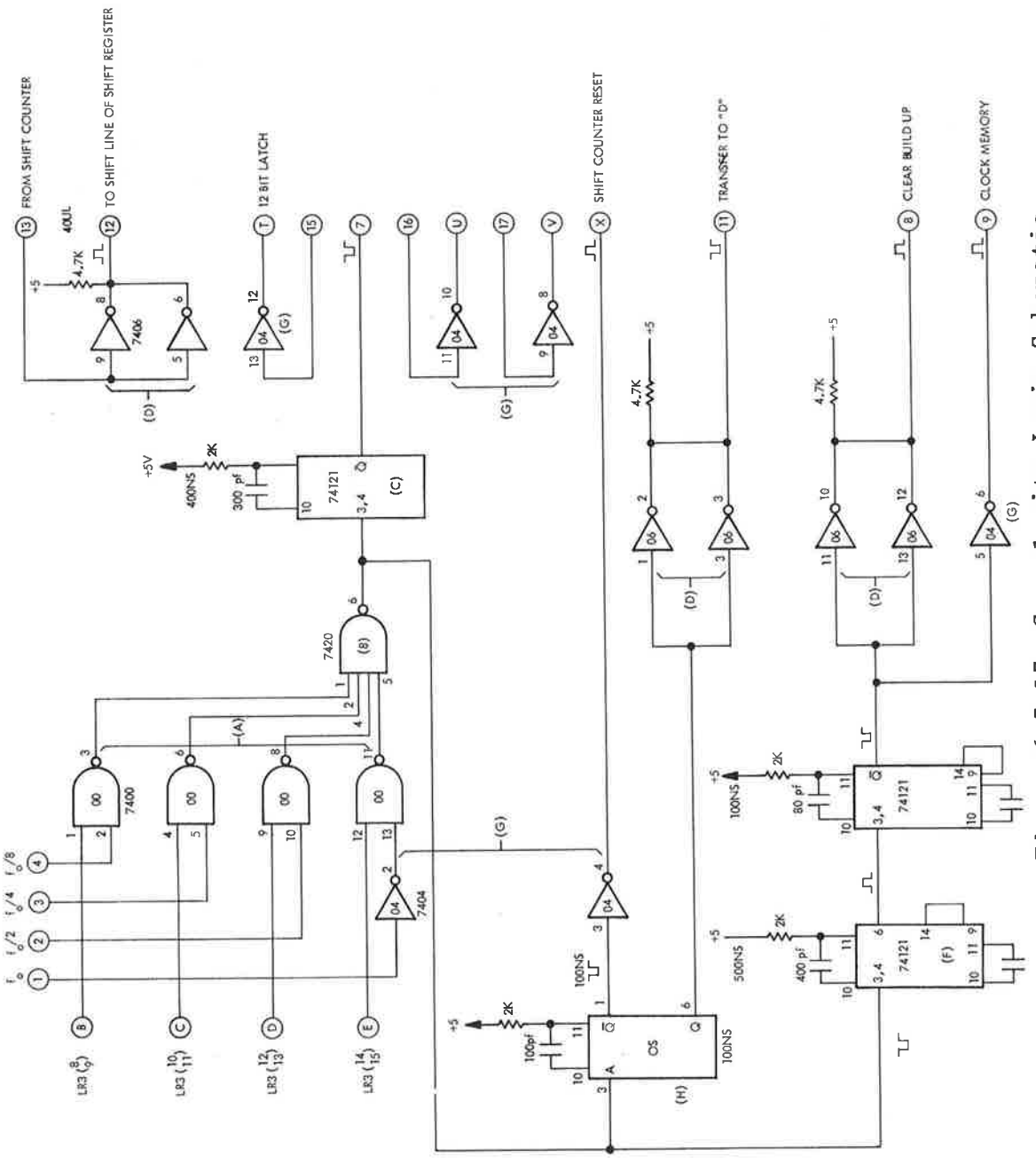

Figure 6.3.17 Granularity Logic Schematic

the 5 MSB at which point the counter is inhibited and the shifting action in the shift register is determined by the binary value of the 5 MSB. A gated direct reset line is provided on the counter which inhibits the counter inputs (5 MSB) and simultaneously returns the five flip-flops to a logical "0".

The logic signal controller unit was designed to provide extreme flexibility in operation of the system for the experimental application it is intended. It is intended to simplify the acquisition of experimental data required to determine the feasibility of a phased array cyclindrical antenna for electronic beam steering applications.

6.3.2.3 Memory - For this application it was decided that the memory must be of the field alterable programmable type, non-volatile, reasonably fast, and reasonably priced. After considering a number of memory types employing different technologies and comparing the advantages and disadvantages of each, it was decided that the Capacitive Read Only Memory (CROM) best met all the requirements stated above.

The CROM was purchased from an outside vendor based on specifications and requirements specified by TSC. The section containing the storage capacitors was laid out in two planes of memory (top and bottom of PC Board) in a 32 x 96 and 24 x 96 Array organized as 128 x 24 and 96 x 24. Total bit capacity is 5376. The overall dimensions of the PC board are 9 1/2 in. x 12 1/2 in. x 1/2 in. All the peripheral circuitry (Decoders, Drivers, Sensing, etc.) are mounted on the same PC board.

Since the memory is field alterable and programmable, minor program changes are easily implemented. Program revisions are implemented either by adding a capacitor to a sensing line or deleting one already attached to a sensing line by breaking the line connection. All the capacitors in the storage section of the CROM have available input and output lines. A capacitor which is connected to a sensing line represents a binary "1" whereas an unconnected capacitor is a binary "0". A capacitor can be connected to a sensing line merely by bridging the gap with silver paste.

The CROM is TTL compatible and has an Access Time equal to 100 ns and a cycle time of 100 ns. Thirty outputs are available, twenty-four of which are data lines and the other eight, subgroup select lines. The eight subgroup select lines act as data selectors. A group of four selects data for the shift registers or phase shifter information registers, three for the attenuator register and one for the sector switch register (See Figure 6.3.14). The data is loaded into the registers in the parallel entry mode.

The memory generates its own timing pulses upon triggering a "go" pulse. The triggering pulse is provided by the Scan Rate Clock and granularity logic. Pulses generated by the memory include the eight subgroup select pulses and internal memory peripheral circuit pulses.

6.3.2.4 Shifting and Buffering Electronics - This subsection's function is to receive the binary information in the form of 24 bit data words stored in the memory, arrange the proper word format, shift and/or store the information until on a stated command it is transferred to the drivers of the phase shifters , attenuators, and sector switches. The phase shifters require 4-bit digital words, the attenautors 3-bit words, and sector switches single bit words.

The Shifting and Buffering Electronics section consists of 5-bit registers, "D" type latches, and Hex Inverter Buffer/ Drivers. The registers, latches, and buffers are housed in two standard 19 inch rack card cages and account for the bulk of the hardware in the logic system. Each card in the Build-Up Register contains three SN7496 5-bit registers and four 4-bit bistable SN7475 "D" type latches. Each Buffer board contains three SN7406 Hex Inverters with open-collecter High-Voltage outputs. A single inverter can sink a maximum current of 40 ma and has a minimum breakdown voltage of 30 volts.

The 5-bit registers can be connected to perform parallel-to-serial or serial-to-parallel conversion. Since both inputs

and outputs to all flip-flops are accessible, parallel-in/parallel-out or serial-in/serial-out operation may be performed.

For our application the registers are used in the parallel-in/parallel-out configuration. They are categorized in Figure 6.3.14 as shift registers, buffer registers, and simply registers to clarify the function they perform.

To establish a new beam, all the commands are transferred from the registers to the latches to the driver circuits simultaneously. Information to establish a new beam must be in the proper order. The coarse steering position is established from the data steered into the buffer registers and registers and transferred to the attenuators and sector switches on a specified gating pulse. The fine beam position is derived from the information being shifted along the shift registers. When the proper number of shifts specified by the coarse positions is achieved, the shift cycle is halted and data stored in the shift register is in proper order for transfer to the drivers. All the data in the three registers can now be simultaneously transferred to the appropriate drivers through the "D" type latches and buffers.

The latch circuits consist of sixty four 4-bit bistable "D" type latches. The outputs from the registers are connected to the latch inputs. Data at the latch inputs is transferred to the Q output when the clock is high. The output of the latch will follow the input data as long as the clock remains high. When the clock goes low the information that was present at the data input at the time the transition occurred is retained at the Q output until the clock is permitted to go high. Thus, the latches allow the registers time to arrange the information in proper order and hold this information until a transfer to "D" pulse clocks the latches and releases the data. The clock pulses for clearing the latches are obtained from the granularity logic.

There are 16 P.C. Cards consisting of registers and latches. The interconnections from the memory outputs are arranged so that 15 data line outputs are connected to the 15 inputs of 3 registers on a P.C. Card and the other 9 data line outputs are connected to

two registers of another P.C. Card. The eight subgroup select line from the memory are connected to the registers in a similar way, i.e., each subgroup select line from the memory is connected to the same input pin (preset of SN7496) of each register group attached to a P.C. Card. With a subgroup select high, data from the memory is loaded in the registers through an Anding gate. This occurs after the old data in the register was transferred to the "D" latch and the register has been cleared and made ready to receive new data. The timing pulses required to maintain an orderly sequence of events for generating, steering, and implementing commands to the drivers play a vital role in operation of the system. A discussion of the timing will be given in the next section.

6.3.2.5 Logic Timing Pulses - Performance of the Azimuth Beam Steering Computer Unit is dependent on developing an orderly sequence of timing events to the logic circuits for generating, steering, and implementing the commands to the phase shifter, attenuator, and sector switch drivers. Logic sequential processing of data is maintained with appropriate timing pulses derived from a variety of pulse circuits. The circuits are clock pulse generators and provide timing pulses which perform logic functions such as memory clocking, strobing latches, stepping counter, shift clocking, etc.

The timing pulses used to electrically operate the MLS Azimuth beam steering computer are shown in Figure 6.3.15. It should be kept in mind that many of the timing events occur simultaneously to maintain an orderly flow of data through the system.

The top positive-going pulse (see Figure 6.3.15) is the Scan Rate Clock pulse. At time t_o with the granularity selector set to achieve 32 fine positions, the Scan Rate Clock pulse steps the Address or Up/Down Counter. On the leading edge of the Scan Rate Clock Pulse a 100 ns pulse from the granularity logic transfers data from the registers to the "D" type latches and also resets the shift counter. For this event to occur it is assumed that data has been "built up" in the Build-Up Registers. At the

same time (t_o), a 400 ns delay pulse generated in the granularity strobes the address data out of the address latch and transfers it to the Memory. At t_o, a 500 ns delay pulse generated by the granularity logic circuit initiates a 100 ns "Go" pulse and starts the memory. At the same time the memory is clocked a clear pulse generated by the granularity logic clears the build-up latches and releases the command signals to the phase shifter, attenuator, and sector switch drivers via the buffers. All the timing pulses discussed so far originate from the Scan Rate Clock and/or the granularity logic. After the memory is clocked, the remaining pulses are generated by the memory. These are the subgroup select pulses. Subgroup Select pulse 1 occurs 500 ns after the memory is started. All other subgroup select pulses are spaced at 500 ns intervals. There are eight subgroup select pulses. Subgroup Select pulse No. 5 which occurs 2.5 microseconds after the memory is clocked is the start shift pulse which enables the shift counter and regulates the number of positions the shift register should shift the binary bits representing phase shifter information.

In order to enter new data into the registers, the information in the registers must be first transferred to the "D" Latches, the registers cleared, and all flip-flops preset to "0". A preset enable pulse (subgroup select) performs the preset function and new data bits from the memory can be parallel loaded into the registers. This occurs for all registers for every coarse position change.

6.3.2.6 Display Controller Unit - To enable the operator to visually monitor a number of important logic functions a display controller unit has been added to the Beam Steering Computer. The display controller unit is shown in Figure 6.3.18. It consists of a display panel located at the top of the cabinet, a control panel in the middle, and power supplies at the bottom. Schematics of the logic controller can be seen in Figure 6.3.19 and Figure 6.3.20.

The display section contains a display mode which simulates the scanning beam. The lamps are arranged in an array of 12 columns x 8 rows and are fed through bundles of fiber optics. A

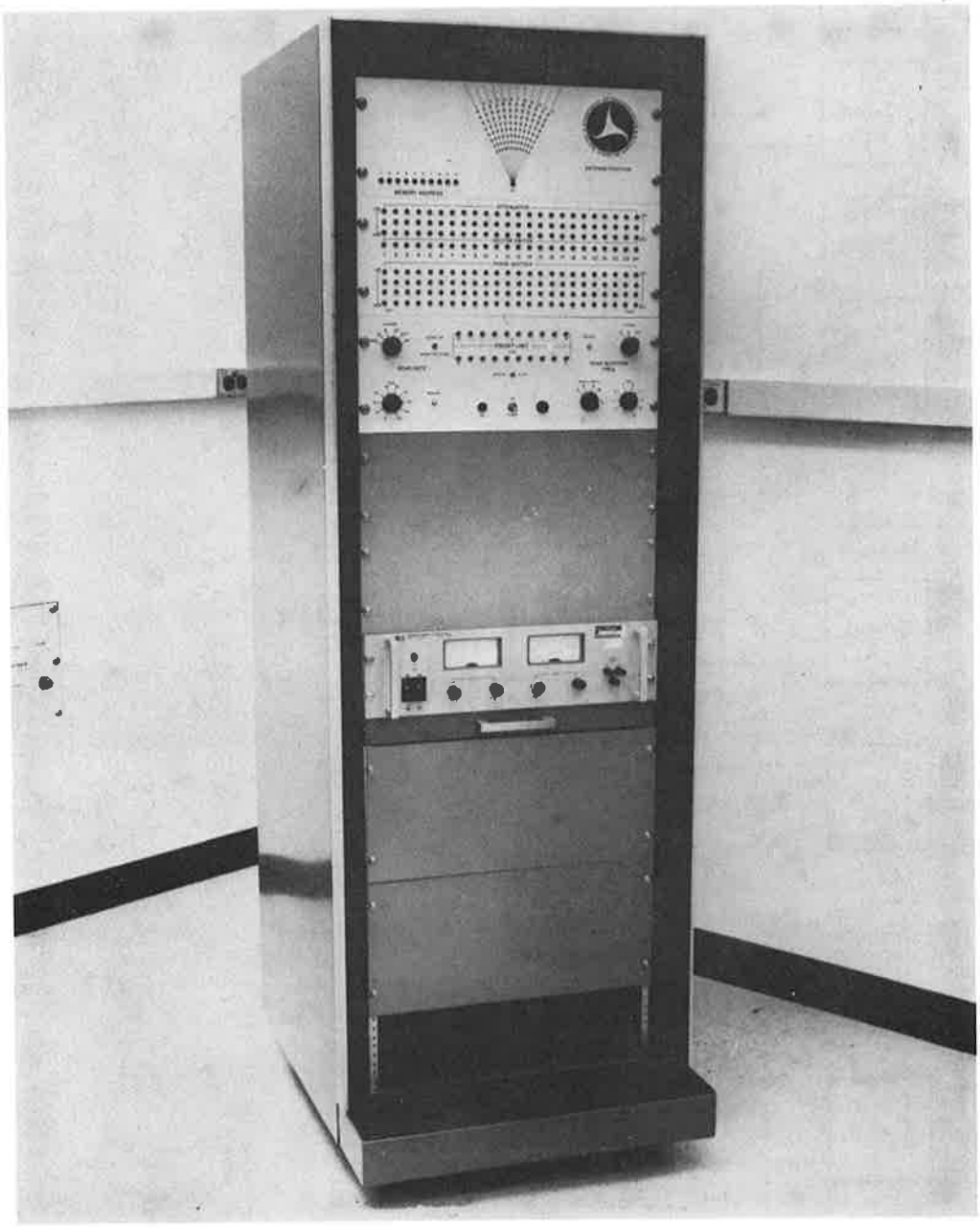

Figure 6.3.18 Display Controller Unit

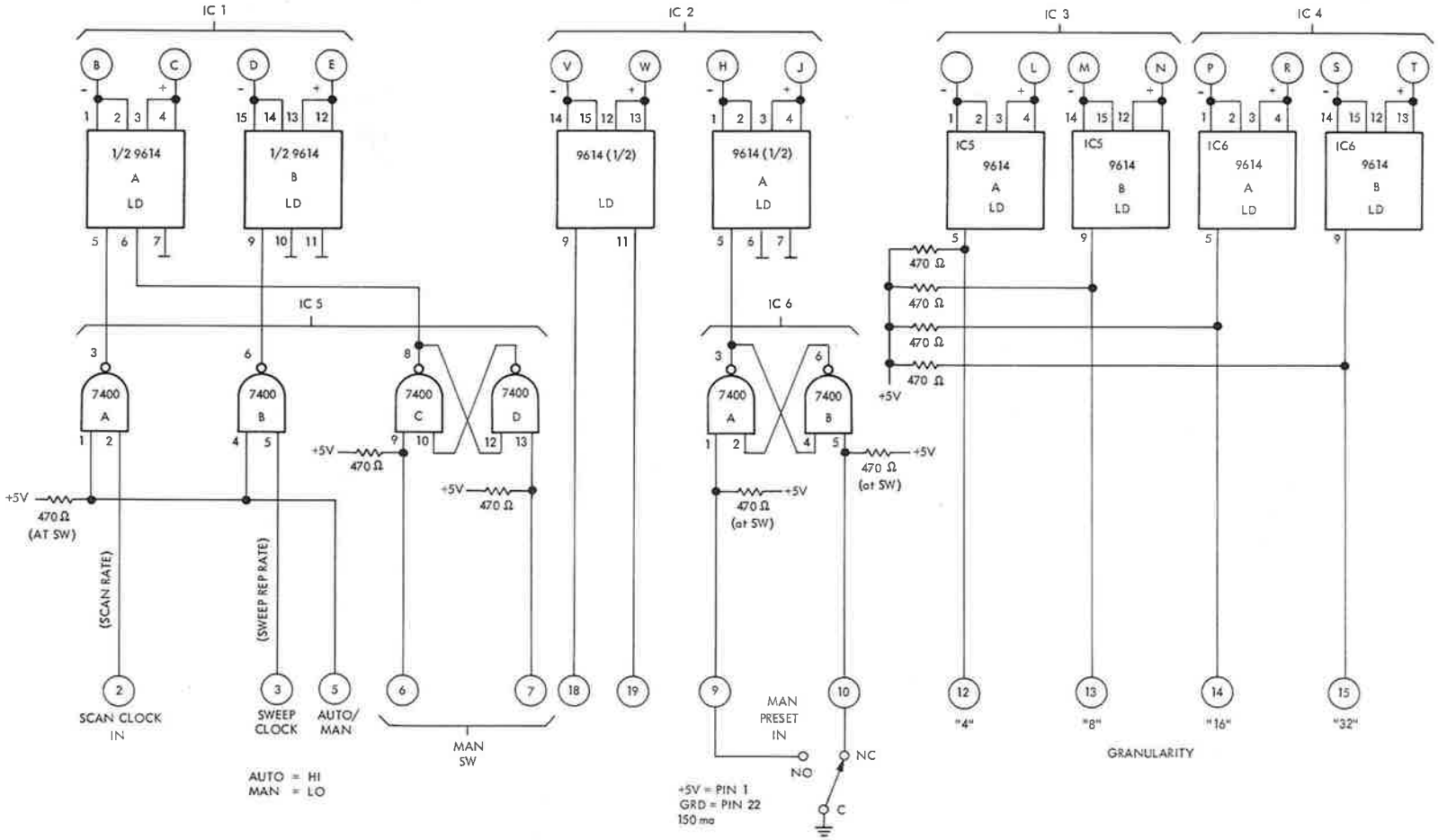

Figure 6.3.19 Control Logic Schematic

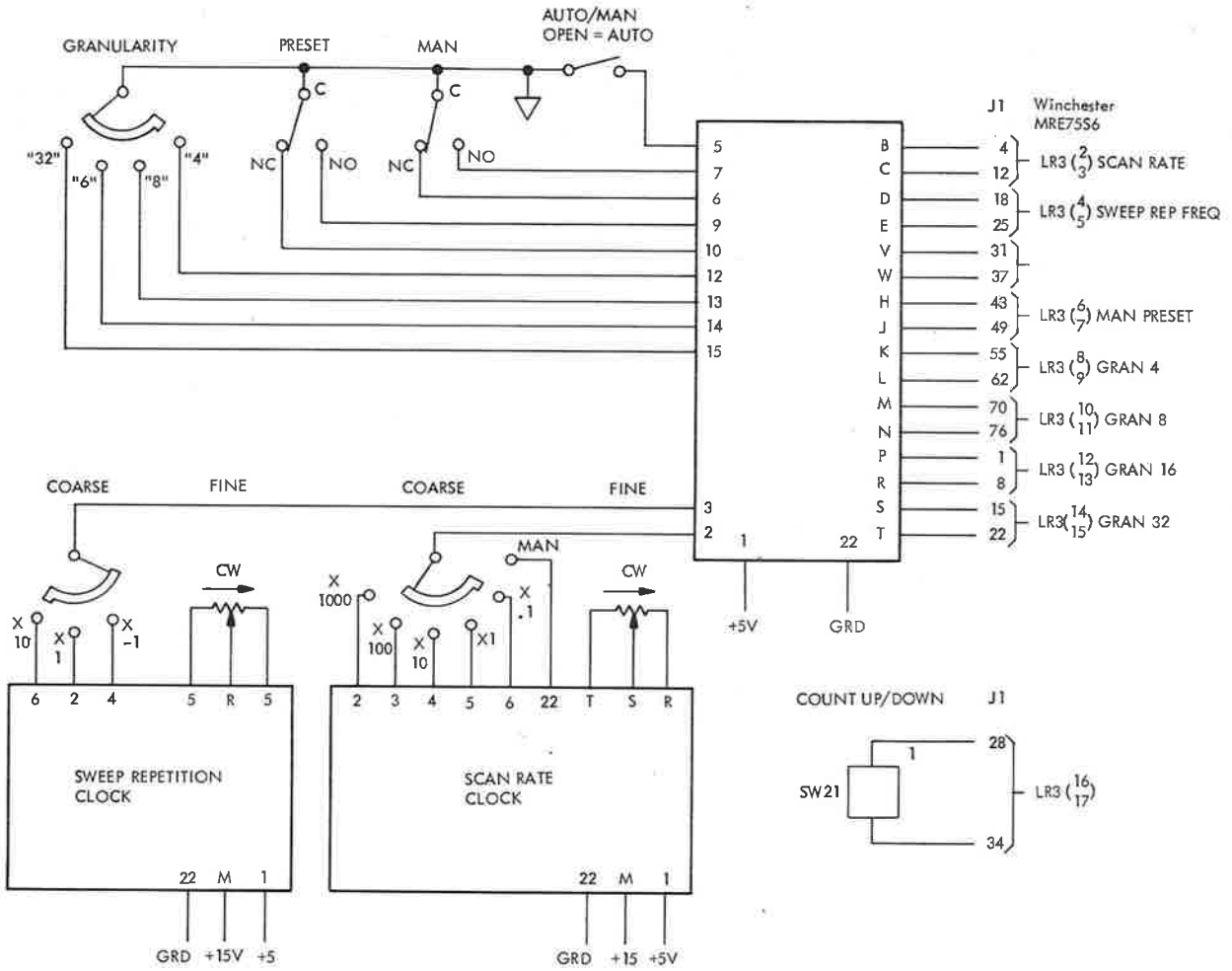

Figure 6.3.20 Control Logic Schematic

logic circuit consisting of an oscillator, counter, and 4-to-16 line decoder controls the VIP display. A lamp at the bottom of the VIP display is used to monitor the RF signal. Ten memory address lamps are located at the bottom left side of this panel and provide a display to observe the state of the counter and bits addressing the memory.

Located in another rack but still a part of the display panel are a total of 192 lamps for displaying the 192 bits to the phase shifters, attenuators, and sector switches. The lamps are arranged to display the twenty-four 4-bit words to the phase shifters, twenty-four 3-bit words to the attenuator and twenty-four single-bit words to the sector switches. One can visually monitor the data bits or commands to the phase shifters, attenuators, and sector switches.

The display controller unit also contains a rack called the control logic. The panel contains a variety of controls such as Preset Limit Switches (High and Low), Manual/Automatic Switch, Scan Rate Control, Scan Repetition Frequency Control, Granularity Control, Power ON/OFF switch, Manual pushbutton switch, and Preset switch. In addition to switches and potentiometers, there are P.C. Card logic circuits in the rack. One card contains the Scan Rate Clock; another, the Sweep Frequency Clock, and the third, a number of gates and 9614 differential line drivers. The latter card provides control logic signals in both the automatic and manual modes for the Up/Down Logic and Granularity Logic circuits.

The functions of the various controls are as follows:

1. Preset Limit Switches (High and Low) set the lower and upper limits on the Up/Down Counter. In manual operation the limits can be arbitrarily set to any desired value. In the count up position the low limit switches are set to binary bit "0", the high limit switches to a predetermined number set with the switches. The counter will count to the upper limit established by the settings on the high limit switches. The counter

must be enabled with the preset switch to begin operation. This loads the data into the counter. Step by step beam positioning can be obtained by depressing the manual pushbutton switch. If it is desired to count down from an established position the counter up-down switch must be engaged and the same procedure with the manual push button switch followed.

In the automatic mode, the counter will continue cycling, that is, count to 2^{10} and revert to zero and start counting again.

2. The Scan Rate Clock and Scan Repetition Frequency Clock control the speed at which the counter operates and how frequently it will count. Both the Scan Rate Clock and Scan Repetition Frequency Clock have coarse and fine control knobs on the panel. The Scan Rate Clock can be varied from 0.6 Hz to 60,000 Hz. The Scan Repetition Frequency Clock can be varied from 0.1 Hz to 100 Hz. Both clocks contain an oscillator whose frequency is subdivided into the frequency ranges mentioned above by SN7490 Decade Counters. Four such counters are required in the Scan Rate Clock to obtain a frequency range of 100,000 to 1. Three decade counters are used in the Scan Repetition Frequency clock to obtain a 1,000 to 1 frequency range.

3. Also located on the panel is a granularity control knob for adjusting the number of fine scan positions associated with each coarse position. The number of fine scan positions can be varied in increments of 2, 4, 8, 16 and 32 for each coarse position. Logic-wise this is accomplished by utilizing the inherent frequency dividing capability of the Up/Down Counter. The three LSB (Least Significant Bits) of the 10 bit binary word from the counter output along with the clock frequency of the Scan Rate Clock are fed to an Anding circuit in

the granularity logic, which in turn, triggers a one-shot multivibrator producing pulses which strobes the latch at the particular frequency controlled by the granularity knob settings.

The display controller unit will be located about 30 ft. from the antenna in a shelter. The cables connecting the display controller to the logic rack mounted on the antenna consist of twisted pairs with shielding, Kapton over Teflon, aluminized Kapton shield, 26 AWG, 7 strand wire. The use of this type shield and insulation has resulted in considerably reducing the cable bundle diameters.

The logic rack containing all the logic circuits comprising the logic signal controller, memory, and shifting and buffering electronics will be located on or near the antenna. A photograph of the logic rack with its wiring next is shown in Figure 6.3.21. Power Supplies to the MLS Beam Steering Computer are located in the Display Controller Unit. These consist of the following values:

Voltage	Current	Regulation
+5v	10 amps	equal to or < 0.05%
-5v	1 amp	equal to or < 0.05%
+15v	200 ma	equal to or < 0.05%
0 to +12v (Variable)	2 amps	non-regulated

6.4 ELEVATION ANTENNA DESIGN

ABSTRACT

The electrical design of the elevation antenna is presented and discussed.

The elevation antenna design incorporates mechanical attenuators so as to provide variable sidelobes. The schematic is shown in Figure 6.4.1. The height of the antenna is about 6 feet

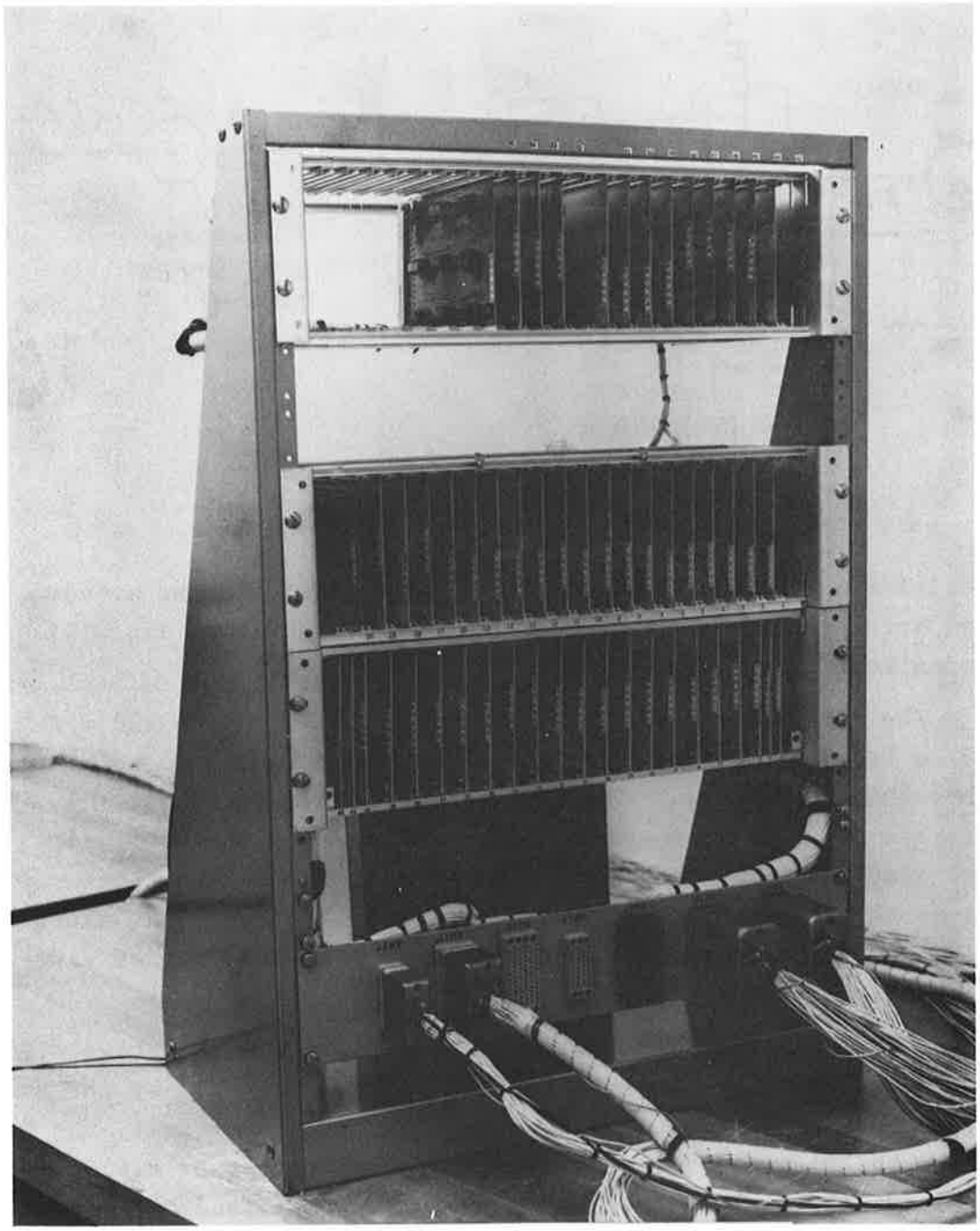

Figure 6.3.21 Logic Rack Photo

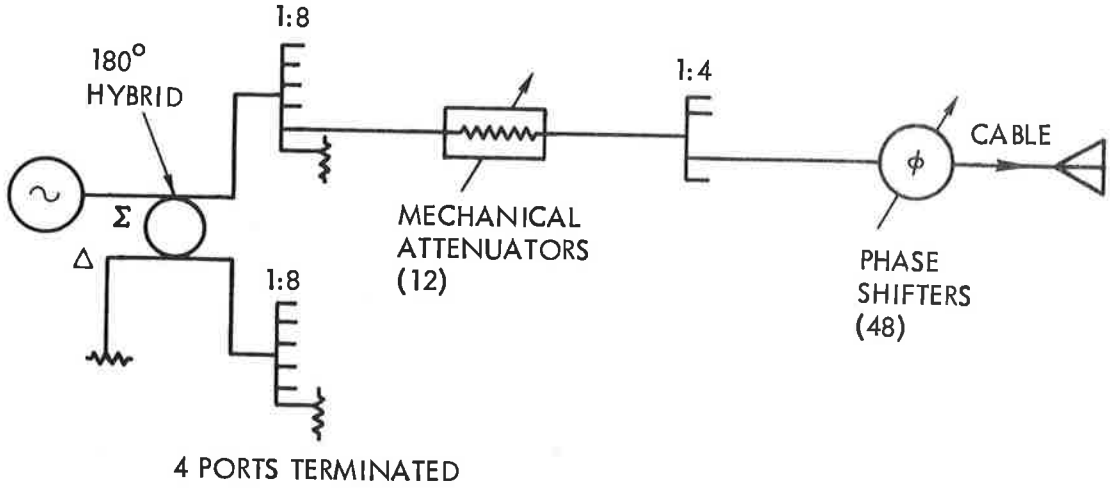

Figure 6.4.1 Schematic for Elevation Array

and yields a 2° beamwidth with 27 dB sidelobes. As the attenuators are adjusted to give lower sidelobes, the beamwidth will broaden somewhat, and conversely for high sidelobes.

The hybrid next to the source makes possible sum and difference beams, while the attenuators can be adjusted to optimize either kind of pattern. Amplitudes are grouped in fours; i.e., there are only 6, rather than 24, amplitude settings available which simplifies the work involved in changing distributions. Work on this project with stepped amplitude distributions shows that this causes no significant effect on beam accuracy or sidelobe levels.

It has not been determined whether equal length cables will be used; the choice of unequal cables is made possible by the fact that the phase shifters can compensate for them. However, the resulting bandwidth is much narrower. The source, power dividers, and phase shifters will all be found in one unit, and cables will run out to the stripline dipole elements.

The element design described in the first annual report[1] was fabricated and tested. The resulting VSWR and pattern shapes were satisfactory, but a significant cross-polarized component existed that would be troublesome near the edges of coverage (beyond $\pm 40°$). The elements will be redesigned to minimize this effect.

---

1 First Annual Report, pp. 85, 109.

7. ANTENNA TEST PROGRAM

CONTENTS

ILLUSTRATIONS

ILLUSTRATIONS (CONT.)

ILLUSTRATIONS (CONT.)

7.1 DISCUSSION

ABSTRACT

An R-2R Lens Fed Cylindrical Array Antenna was assembled and aligned for testing at the Lincoln Laboratory Antenna Test Range. Preliminary radiation patterns indicated that no gross problems existed with the system but that the input probes lying along the lens focal arc must be terminated with "matched loads" when not connected to the switching matrix. If this is not done, the energy reflected internally within the lens cavity will cause main beam asymmetries and increased side lobe levels.

7.1.1 Mechanical Considerations

An azimuth antenna design using an R-2R Lens fed cylindrical array was assembled for radiation pattern tests using some of the C-Band components which had been developed and purchased during the first year of the program. All components were separately checked for amplitude and phase balance over the 5.0 GHz to 5.25 GHz frequency range prior to assembly. The lens output cables which are required to have equal lengths were found to have phase variations between cables as large as 40°. Therefore a mechanical phase shifter had to be used with each cable to adjust for the equi-phase equal length condition on an Hewlett Packard Analyzer. The phase shifter also allowed some flexibility as to permit near field focusing and phase scanning measurements. The input cables did not require phase shifters since they were purchased from a different vendor and had been phased within $\pm$ 3° at 5.0 GHz. Furthermore, these cables had been stabilized so that they could be subjected to a moderate amount of bending without exceeding that tolerance.

The antenna was tested at the Lincoln Laboratory Antenna Test Range on an azimuth-over-elevation-over azimuth mount. This arrangement permitted the taking of "conical cuts" of the radiation patterns at various elevation angles by rotating the upper azimuth turntable at the desired elevation angle. Conical cuts of the azimuth radiation pattern are the patterns "seen" by an aircraft flying at a given altitude. Unless otherwise specified, the

radiation patterns taken at various elevation angles were conical cuts.

After the array had been assembled on the mount, it was optically aligned with the transmitting antenna, at 0° in azimuth and at 0° in elevation, by means of a right angle boresight telescope mounted on the antenna. The telescope mounting block could not be tilted so that alignment could only be checked at 0° elevation. A level was used to check for tilt but this is not as accurate as an optical alignment at several elevation angles. After alignment, the synchro indicators and chart recorder positioner were adjusted so that all subsequent angular data were referred to this optical alignment. Figures 7.1.1, 7.1.2, and 7.1.3 show different views of the antenna positioned on the mount.

The transmitting antenna was an 8 ft diameter parabolic dish located approximately 2,000 ft away from the antenna under test. The radiation patterns taken were receiving patterns. Since the antenna range is a ground reflection range, the precaution of adjusting the height of the transmitting antenna for a maximum signal at the test antenna was observed at each frequency. Furthermore the standard gain horn was positioned so that its maximum signal occurred at approximately (within 0.1 dB) the same transmitting antenna height.

7.1.2 Preliminary Tests

Prior to taking the array patterns of the antenna using the four element switching matrix to feed the lens input, preliminary patterns were taken in order to determine whether the antenna was operating properly. Far field receiving patterns were taken of a single antenna element in the center of the array and of a single element at the edge of the array. These element patterns were taken with adjacent probes terminated and are shown in Figures 7.1.4 and 7.1.5. As expected the patterns are very broad but with differences in their shapes due to the difference in mutual coupling at the two locations in the array.

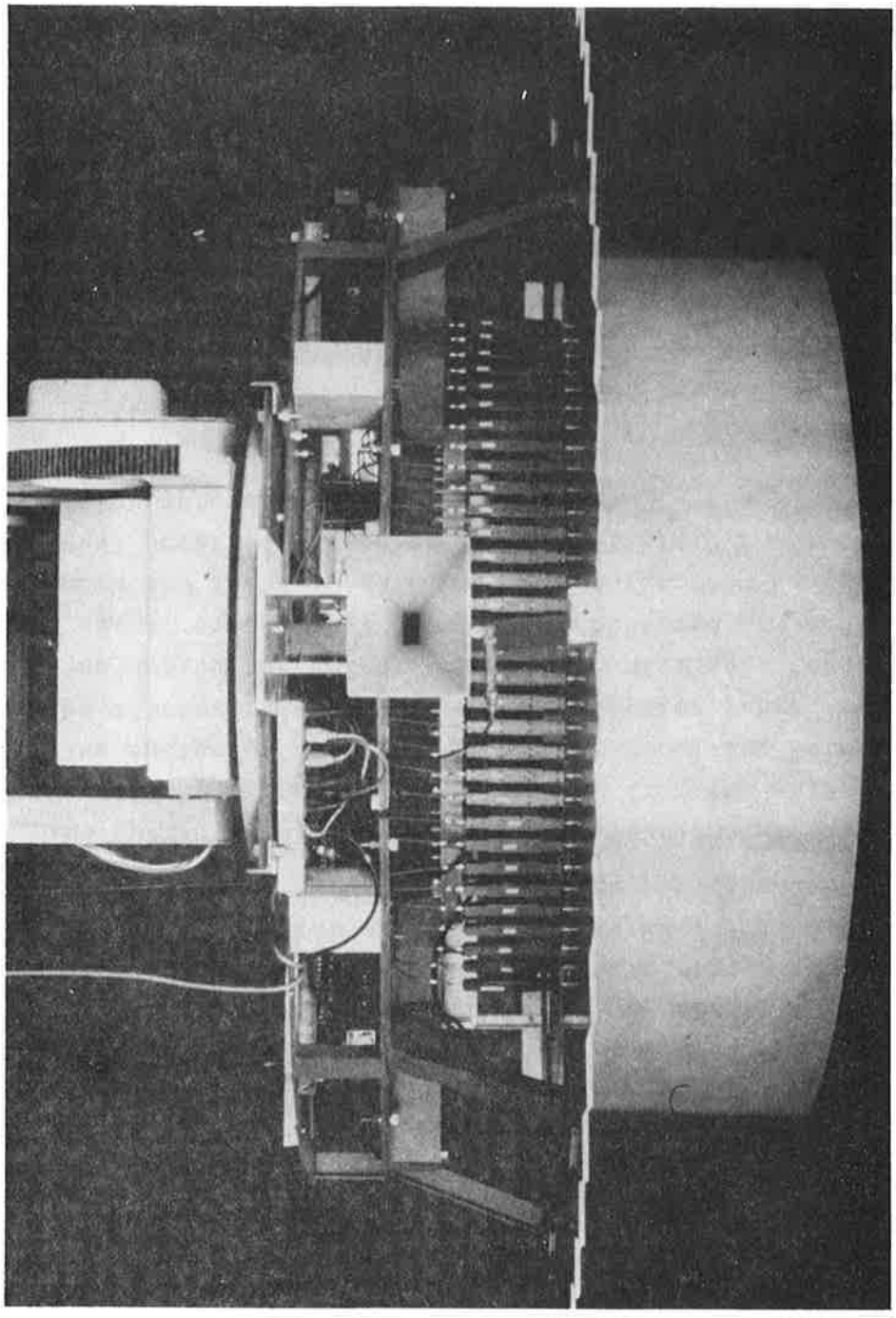

Figure 7.1.1 Antenna on Mount, Front View

Figure 7.1.2 Antenna on Mount, Side View

Figure 7.1.3 Antenna on Mount, Rear View

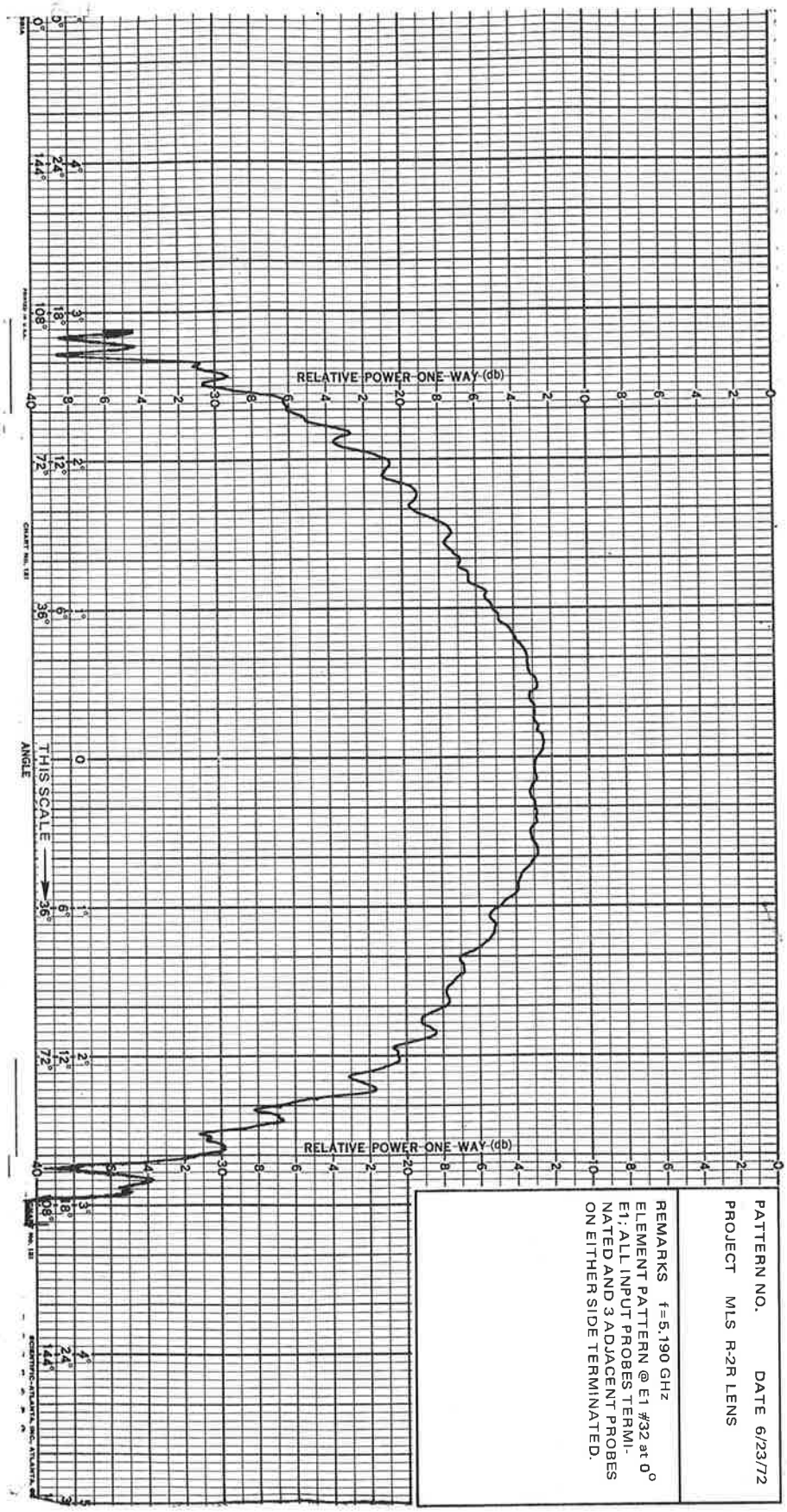

Figure 7.1.4 Element Pattern of Center Element in the Array at 0° Elevation

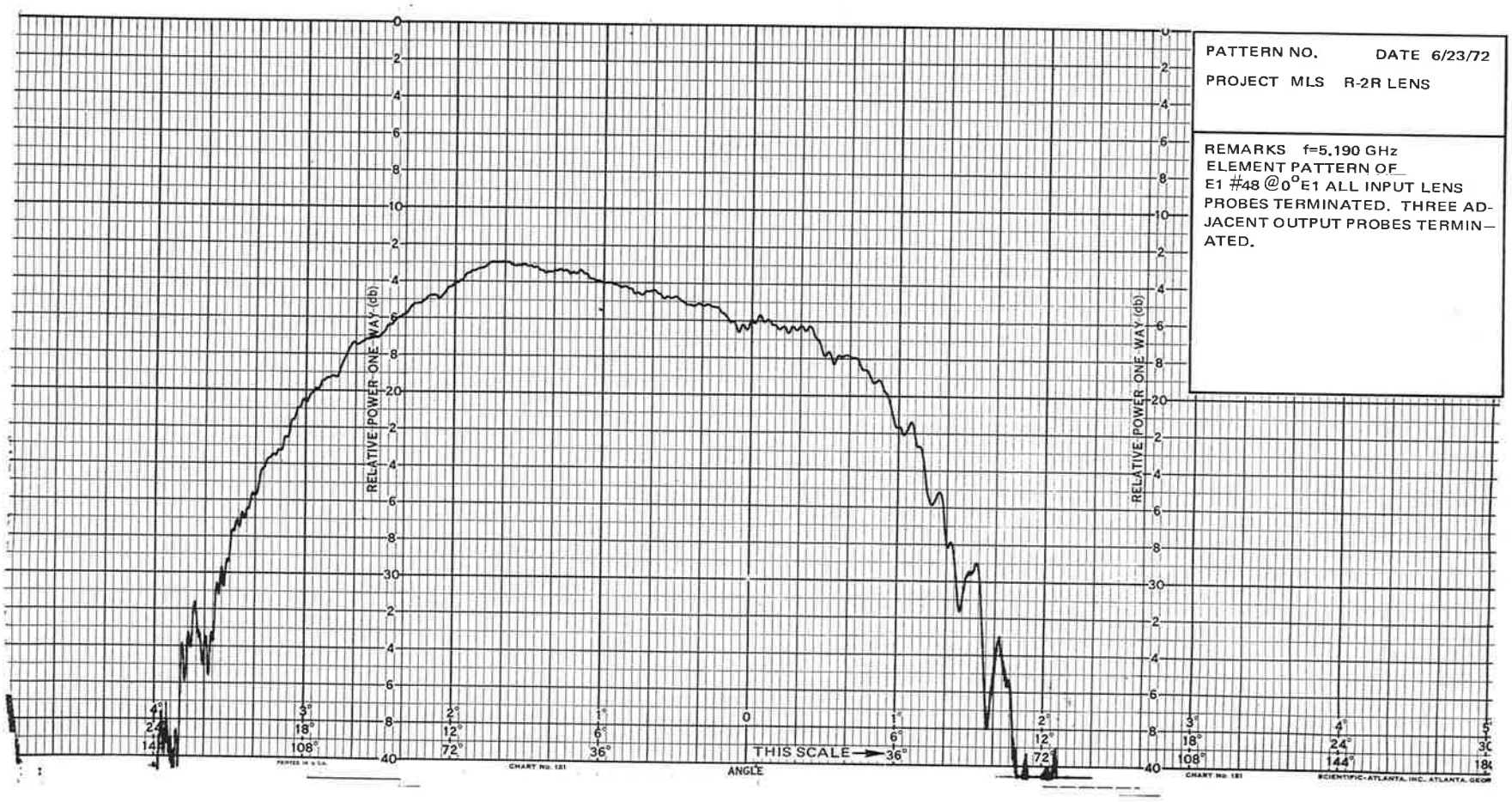

Figure 7.1.5 Element Pattern of End Element in the Array at 0° Elevation

Far-field azimuth array patterns were also taken at 0° in elevation for each of the lens input probe positions. These provided array patterns of the antenna at each of the 16 coarse azimuth beam positions determined by the angular location of the input probes along the lens focal arc. The beamwidth, and side lobe data of these patterns are summarized in Figures 7.1.6 and 7.1.7. Again the results were as expected and indicated that no gross problems existed with the antenna system. The relatively high side-lobe level (12.2 dB average) observed in these patterns was expected because illuminating the output surface of the lens by means of a single probe on the focal arc results in an almost uniform amplitude distribution along the array. For a uniform distribution the theoretical side lobe level is 13.2 dB.

An azimuth array radiation pattern was also taken of an equal amplitude equi-phase excitation of two probes on the lens focal arc. To show the effects on the far field radiation pattern of different focal arc excitations, Figures 7.1.8, 7.1.9, and 7.1.10 are presented. These are antenna patterns of one probe, two probe, and amplitude (-11 dB, 0 dB, 0 dB and -11 dB) tapered four probe excitation. The patterns subsequently taken for evaluating the antenna were of the four probe amplitude tapered excitation.

During this preliminary test phase, it was observed that the radiation patterns were seriously affected by the impedances appearing on the 'non-excited' probes along the focal arc. Open-circuited probes adjacent to the excited probes reflect sufficient energy to affect the radiation pattern. This posed a problem when taking array patterns using the four element switching matrix feed. The equi-phase tapered amplitude distribution is commutated along the input surface (focal arc) of the lens by means of transfer switches and SP4T sector switches. The output ports of these switches are not matched in the "off" or non-conducting state so that at any coarse beam position only four probes (those switches "on") along the focal arc are matched. RF energy incident on the unmatched probes is reflected back into the

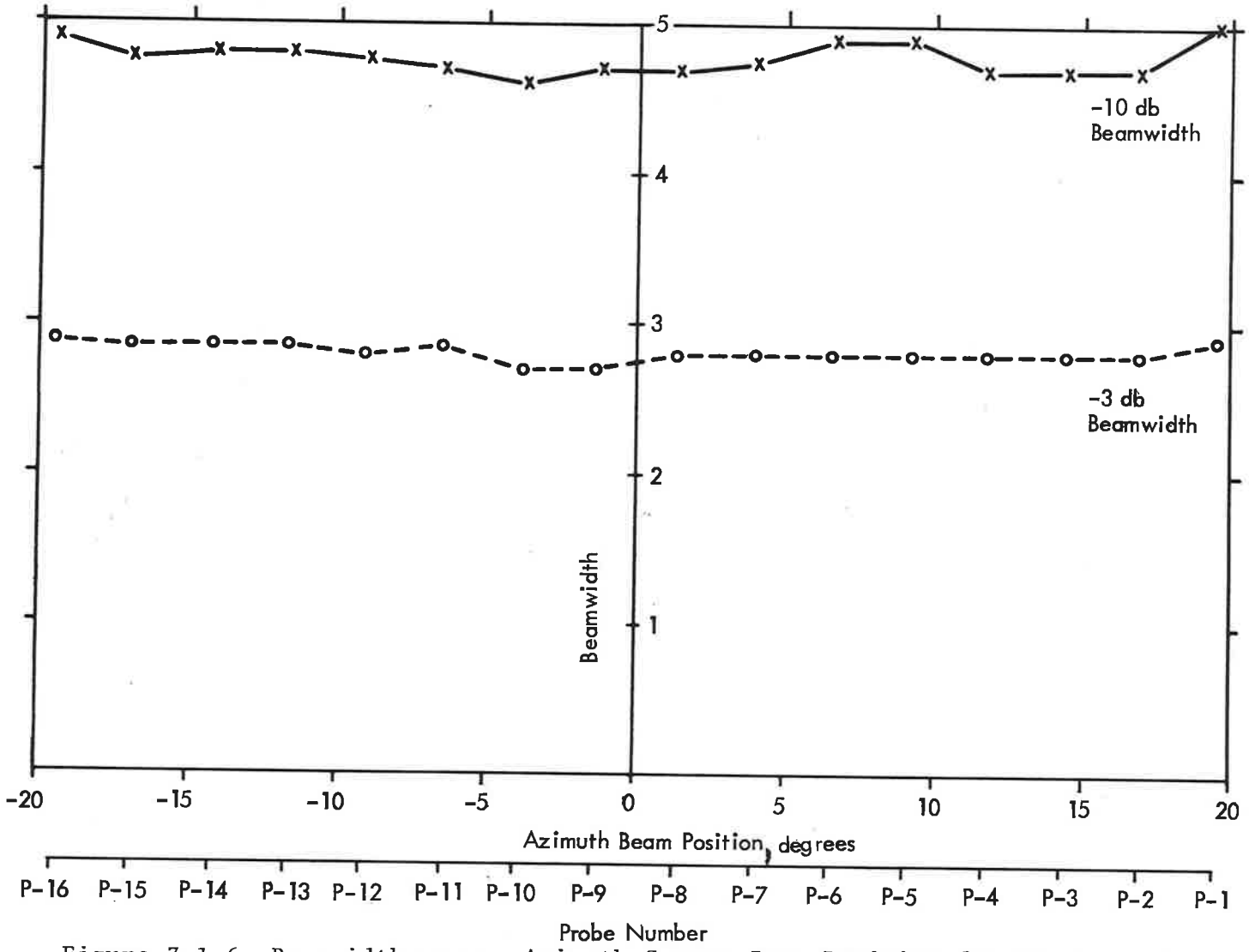

Figure 7.1.6 Beamwidth versus Azimuth Coarse Scan Position for Single Probe Illumination of R-2R Lens

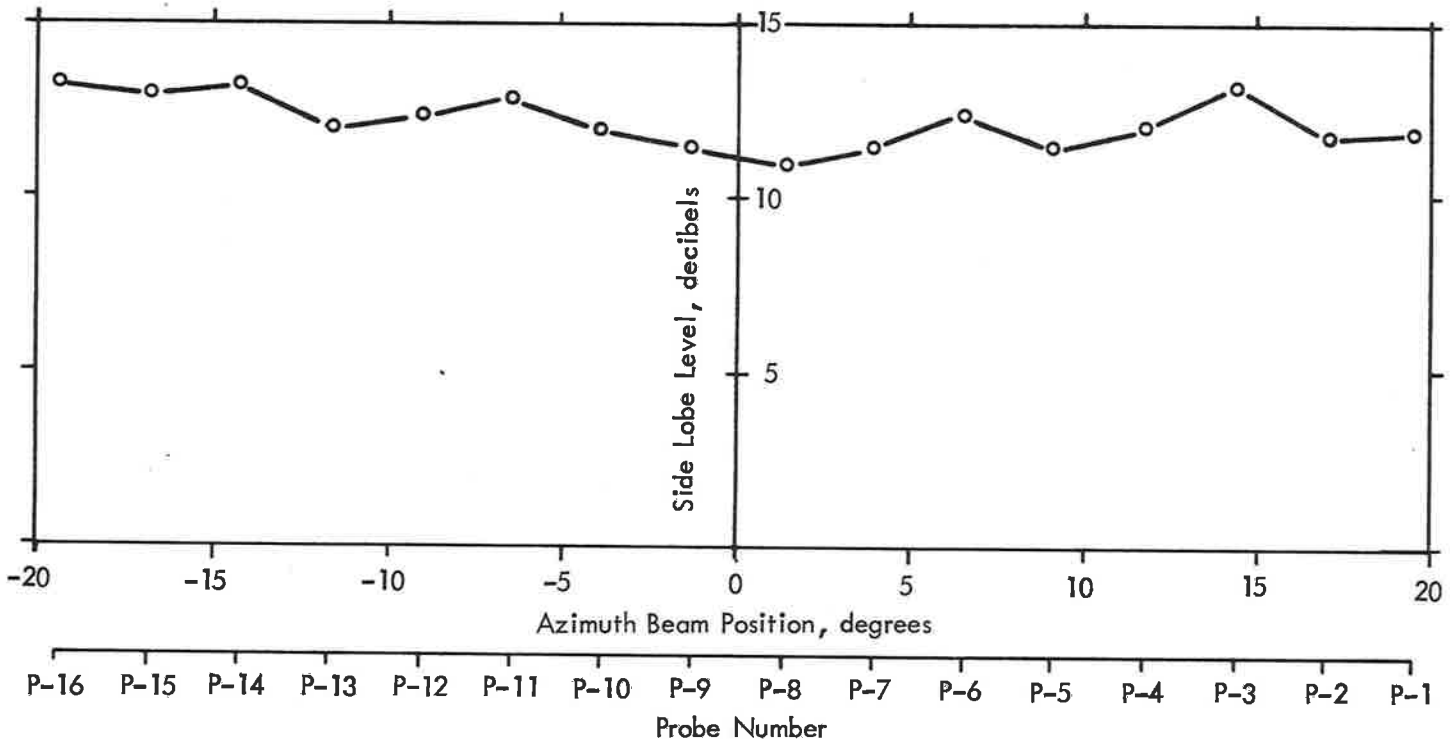

Figure 7.1.7 Side Lobe Level versus Azimuth Coarse Scan Position for Single Probe Illumination of R-2R Lens

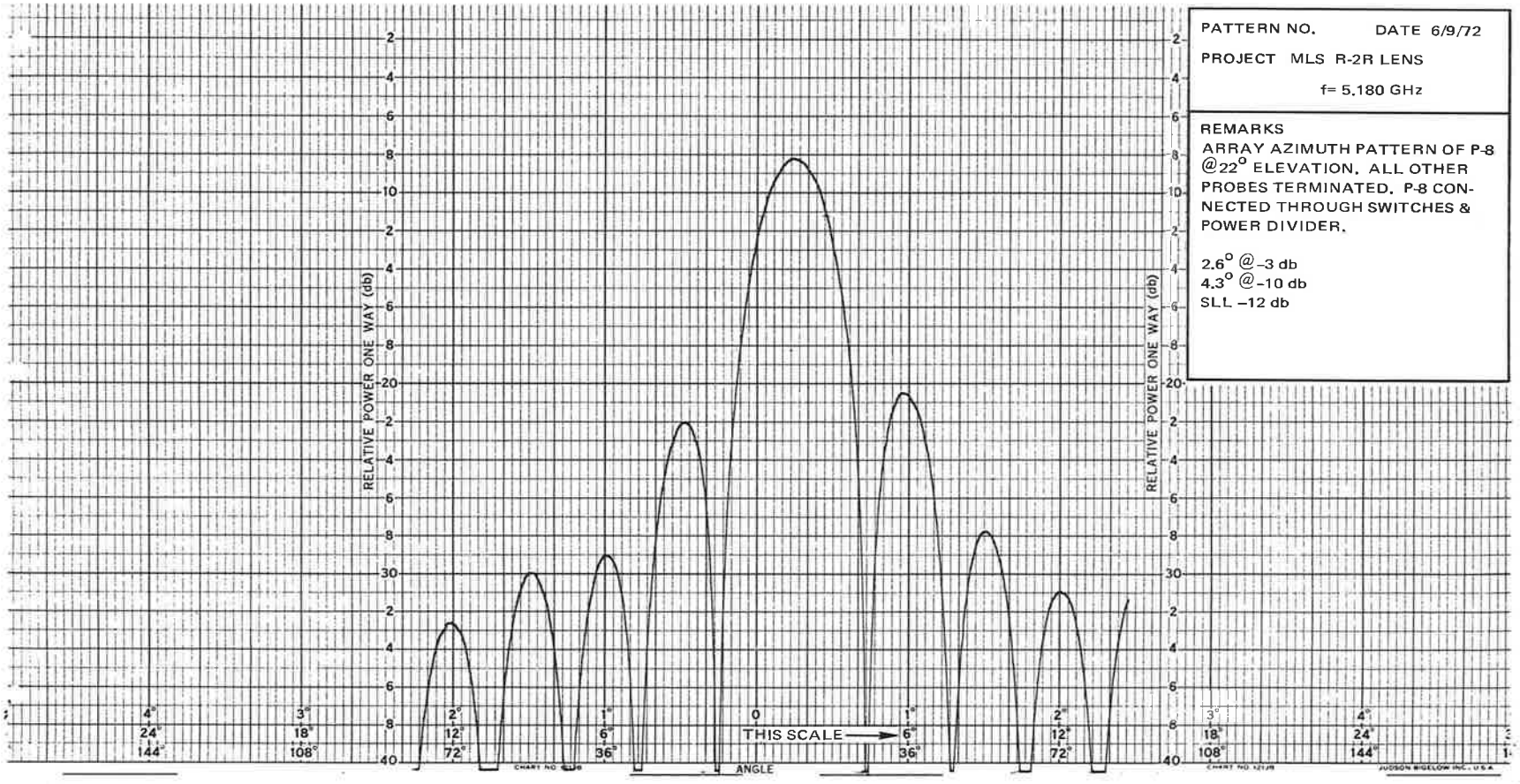

Figure 7.1.8 Far-Field Array Azimuth Pattern of Single Probe Excitation of Lens Focal Arc

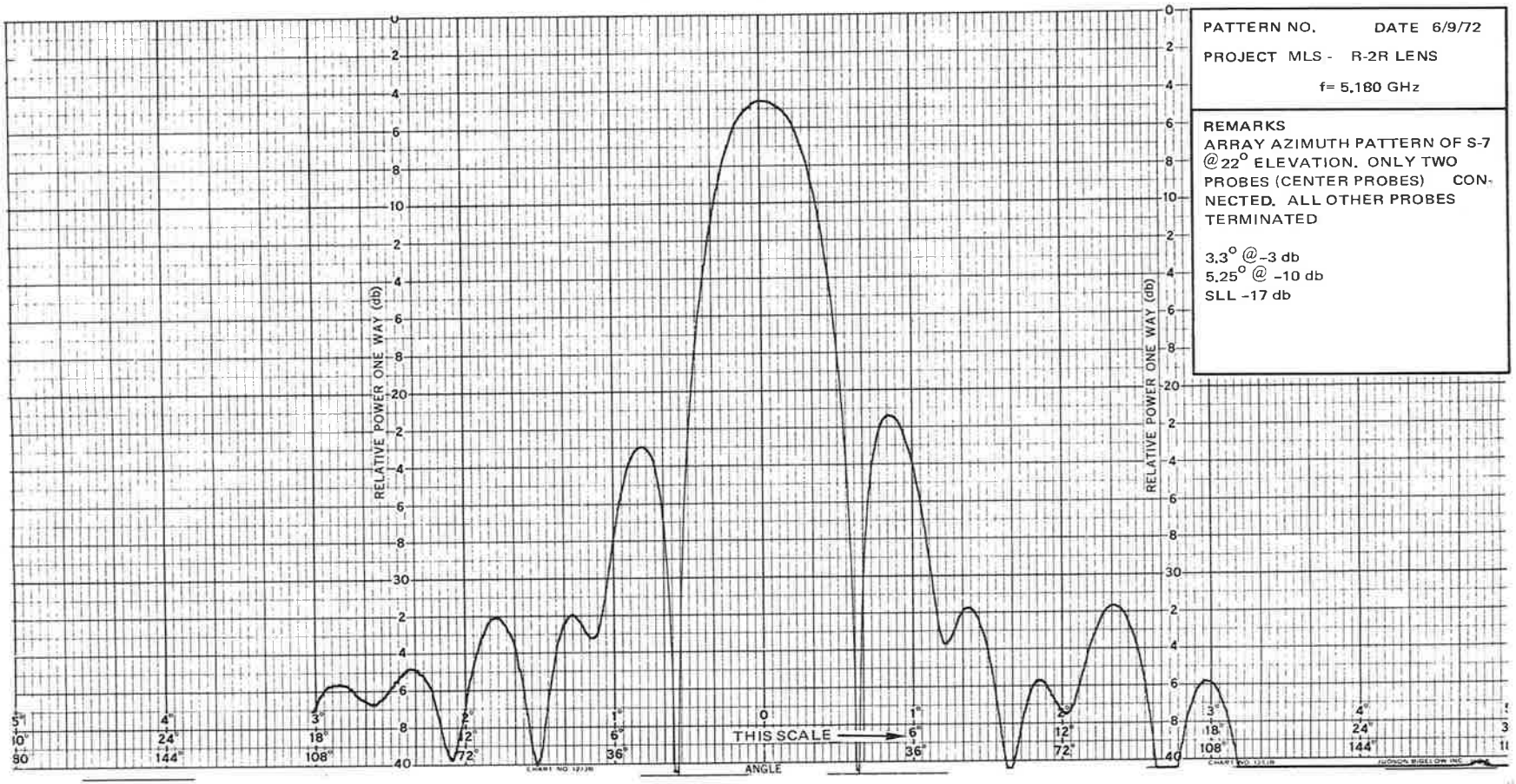

Figure 7.1.9 Far-Field Array Azimuth Pattern of Two Probe Equal Amplitude Equi-Phase Excitation of Lens Focal Arc

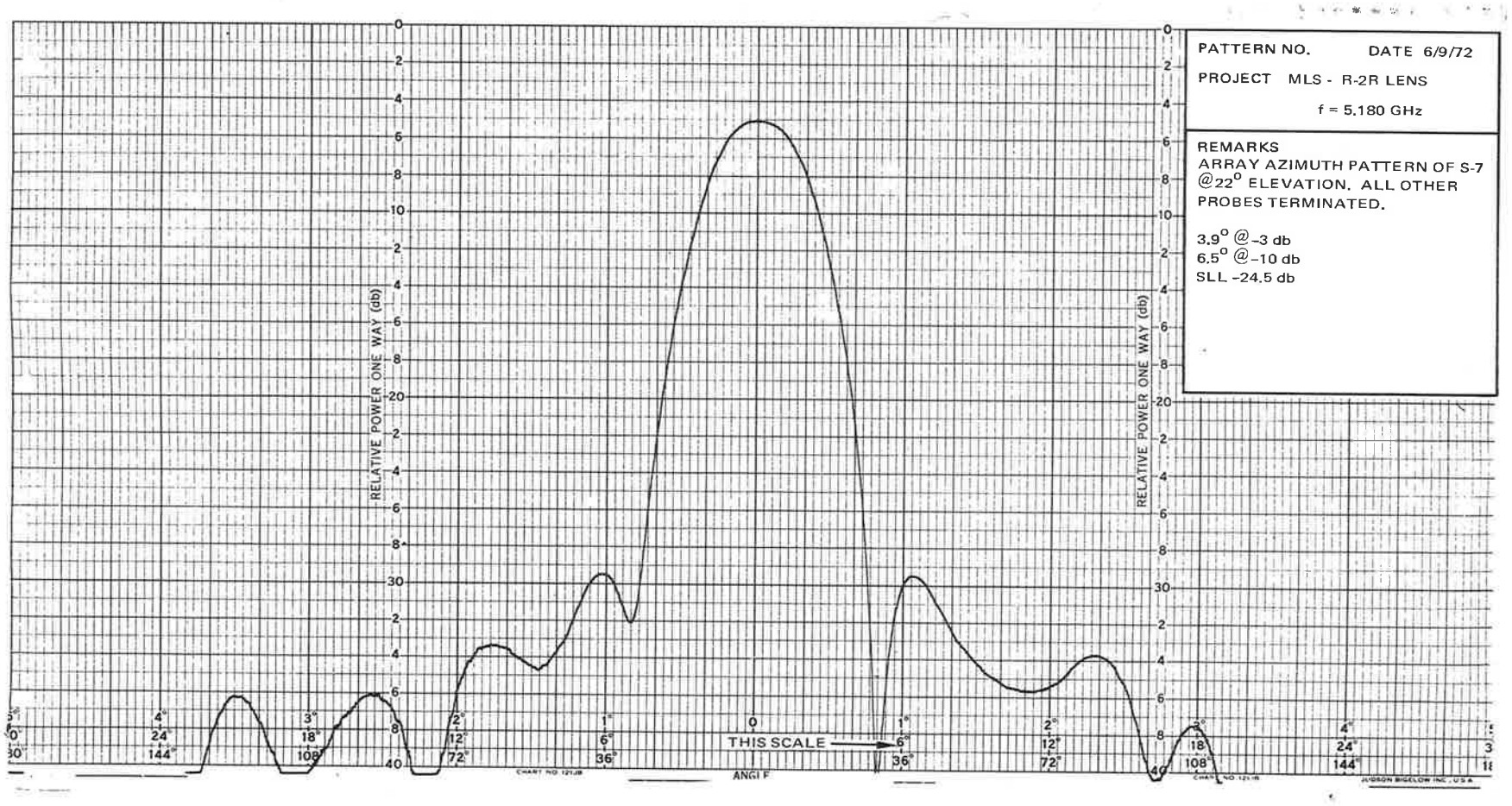

Figure 7.1.10 Far-Field Array Azimuth Pattern of Amplitude Tapered Four Probe Excitation of Lens Focal Arc

lens and eventually appears at these four probes. The phase of this reflected energy varies with the angle of incidence within the lens cavity and is determined by the array azimuth angle. The resultant effects are observed in the array radiation pattern as beam asymmetries and higher side lobes. The problem was solved by taking the array radiation patterns with input probes terminated in matched loads except those four that are switched "on". In a scanning system this can be implemented by means of a SPDT switch at each input probe terminal as shown below.

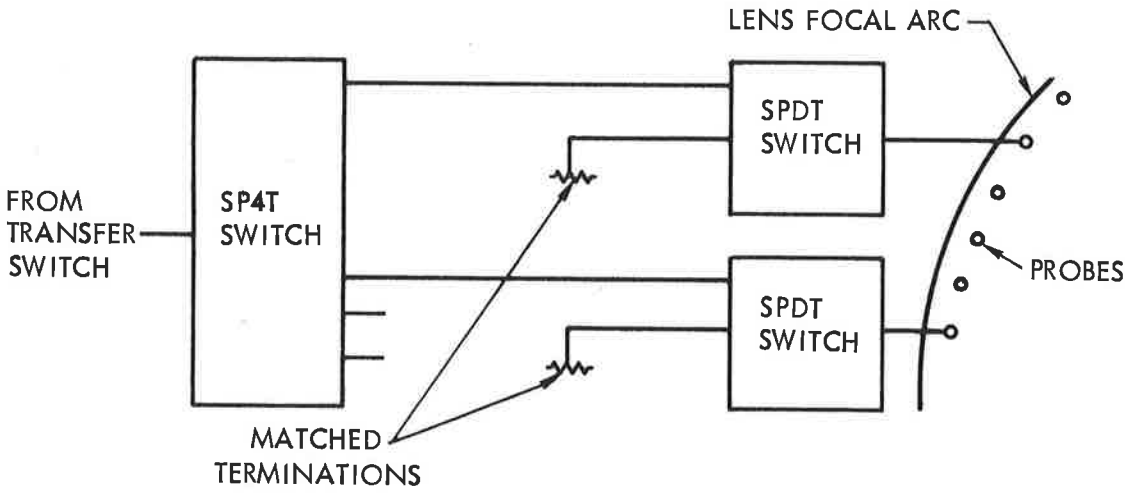

Figure 7.1.11 Possible Method of Terminating Inactive Input Probes

Typical radiation patterns for the "unterminated" and "terminated" inactive probes condition are shown in Figures 7.1.12 and 7.1.13 respectively.

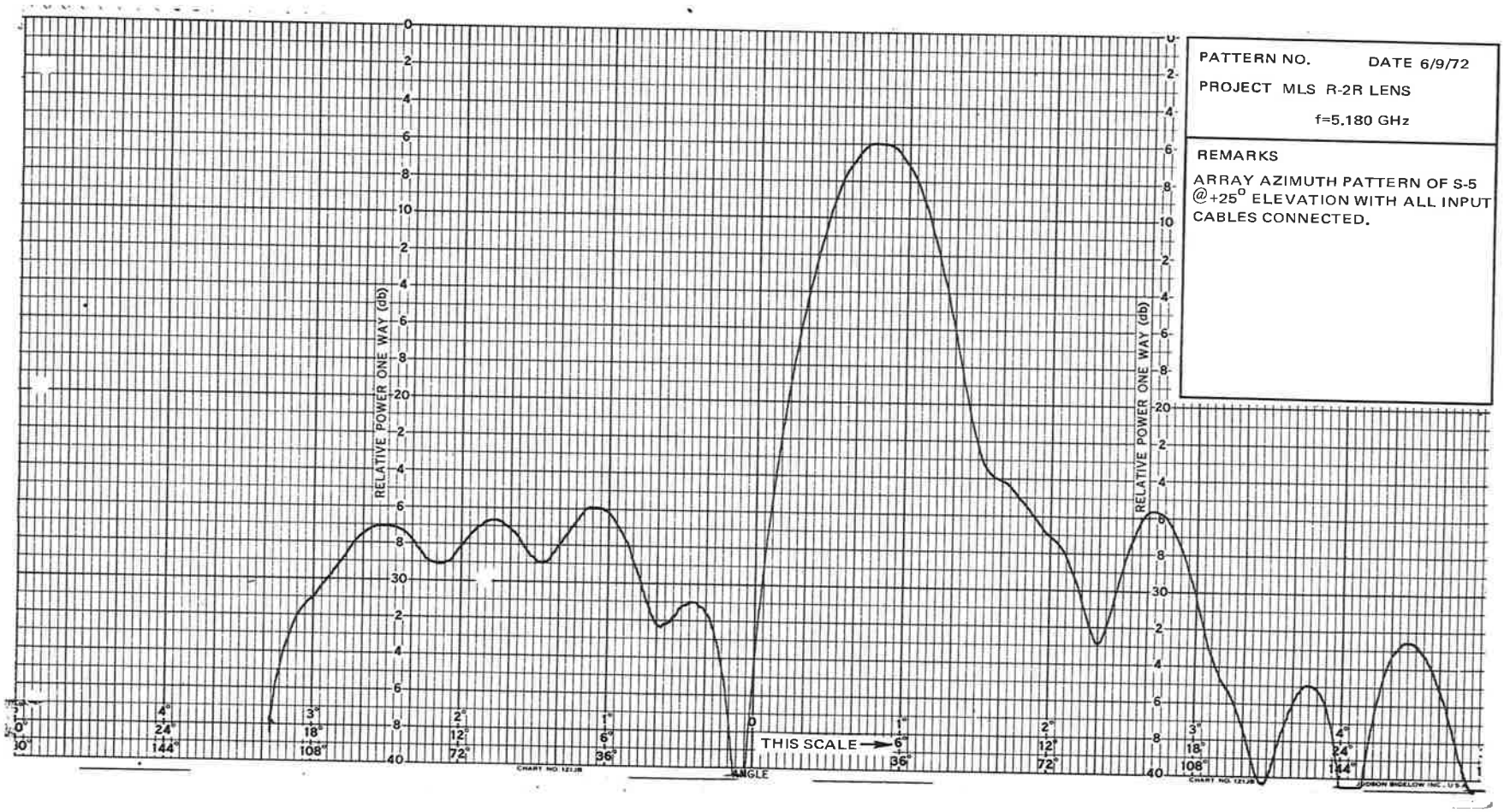

Figure 7.1.12 Far-Field Array Azimuth Pattern of Four Probe Amplitude Tapered Excitation with Inactive Probes Unterminated

Figure 7.1.13 Far-Field Array Azimuth Pattern of Four Probe Amplitude Tapered Excitation with Inactive Probes Terminated

7.2 RADIATION PATTERN TESTS

ABSTRACT

Antenna receiving patterns were taken at each coarse scan position at three frequencies and at various elevation angles. The data indicated good antenna performance with reference to beamwidth and side lobe level. Attempts to determine the exact value of θ_f, the array focus angle, resulted in verification that the effective radius of the array was greater than the actual radius, but the precision was not sufficient to determine this value accurately. Beam "skew" produced when phase scanning the array was verified and showed good agreement with the calculated values. Near field defocusing effects were also investigated and again the agreement with the predicted performance was good.

7.2.1. Scanning Beam Test Program

7.2.1.1 Description of Tests Performed - Once the preliminary tests had established a high confidence factor that the antenna was operating properly, array receiving patterns were taken at each of the 13 coarse scan positions. (The use of a four elemented tapered amplitude distribution for each of the coarse scan positions resulted in 3 less beams). For the reasons mentioned earlier only the four active probes remained connected to the switching matrix at each scan position. All other probes were terminated in matched loads. The tapered amplitude distribution was positioned along the lens focal arc by means of a static logic box through which the appropriate transfer and sector switches were manually switched. Each one of the logic states corresponded to a coarse beam position in space. Once a coarse position had been selected, the cables to the "non activated" probes were disconnected and matched loads attached manually.

Using this procedure for positioning the beam, array azimuth patterns were taken at each coarse position at three frequencies 5.0 GHz, 5.19 GHz and 5.25 GHz. These azimuth patterns were taken at 0° elevation (θ=0°) and at various other elevation angles. The patterns were taken through the switching matrix so that the relative gain of each pattern reflect the losses of these components. For each pattern the level of the standard gain horn

was recorded so that a gain value for the peak of each beam could be determined. Elevaticn patterns were also taken at a number of azimuth beam positions. A typical elevation pattern is shown in Figure 7.2.1. In this figure also are entered the relative gain values obtained from the azimuth patterns at the various elevation angles. As can be seen there is good agreement between the two data.

7.2.1.2 Results - The antenna patterns were subsequently analyzed. The beam width and side lobe level data are summarized in Figures 7.2.2 through 7.2.7. The plots of 3 dB and 10 dB beamwidths versus beam position show some change as a function of elevation angle. This is consistent with performance of a cylindrical array in which the beam spreading is caused by elevation defocusing. This will be discussed further in section 7.2.4. Figure 7.2.8 indicates that the antenna beam position varies with elevation angle. This "skew" was observed at all the frequencies tested and was always in the same direction. It is believed that this skew was caused by a slight tilt in the antenna mounting.

7.2.2 Elevation Focusing Tests

7.2.2.1 Discussion of Focusing Problem - The principal reason for taking array azimuth patterns of various elevation angles was to experimentally determine the elevation focus angle θ_f for this lens fed cylindrical array. It had been found during the bench testing of the lens, that the phase center of the probes radiating into the parallel plate cavity was at the probe circle rather than at the cavity wall. This difference resulted an effective lens radius that was 1/2" less than the physical radius. Due to the R-2R constraint on the relative radii of the lens with reference to the array radius, this difference would cause the antenna to be focused at an elevation angle of $\pm$14°

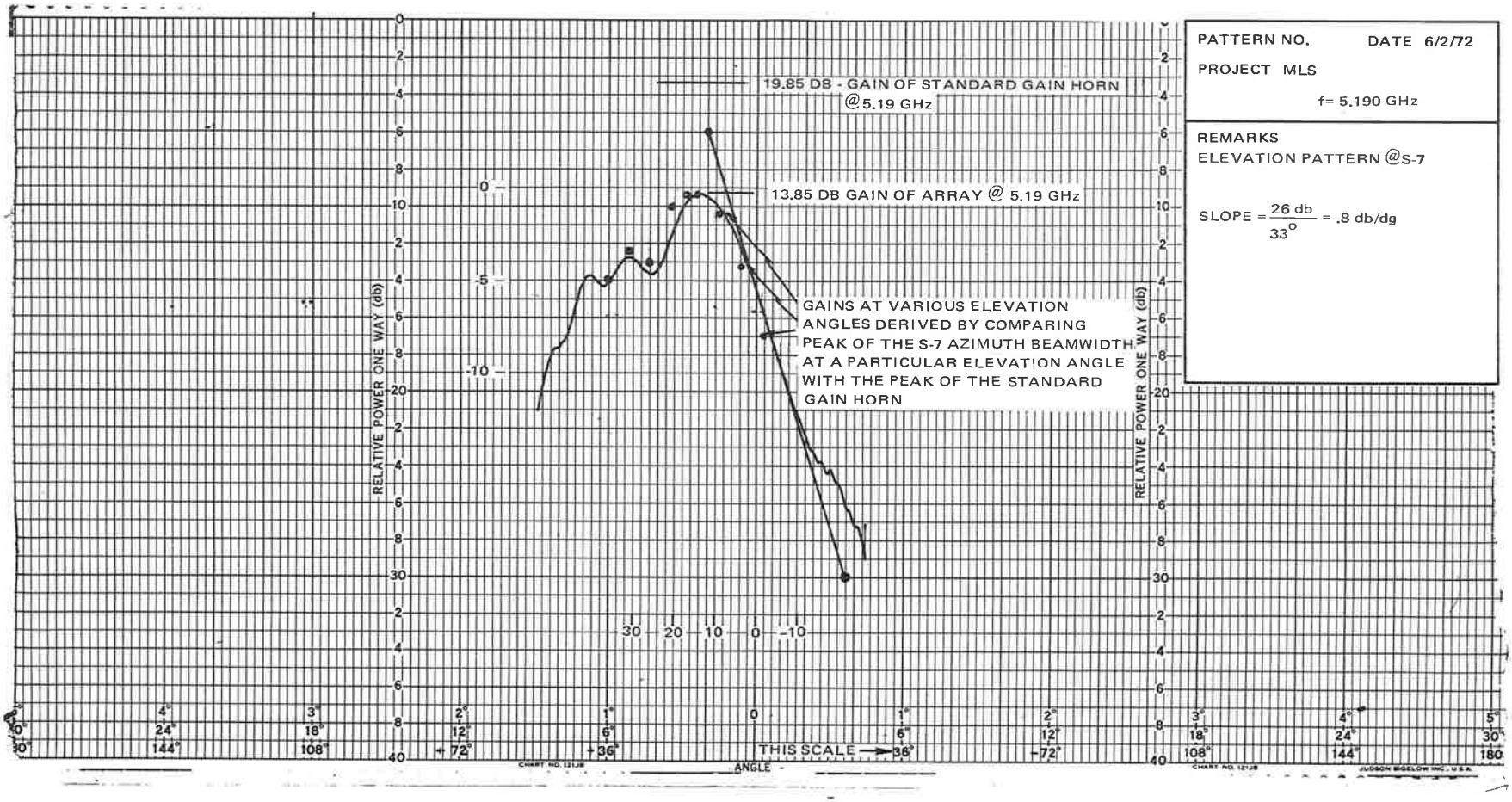

Figure 7.2.1 Elevation Pattern of Array at 0° Azimuth with Gain Values from Azimuth Patterns

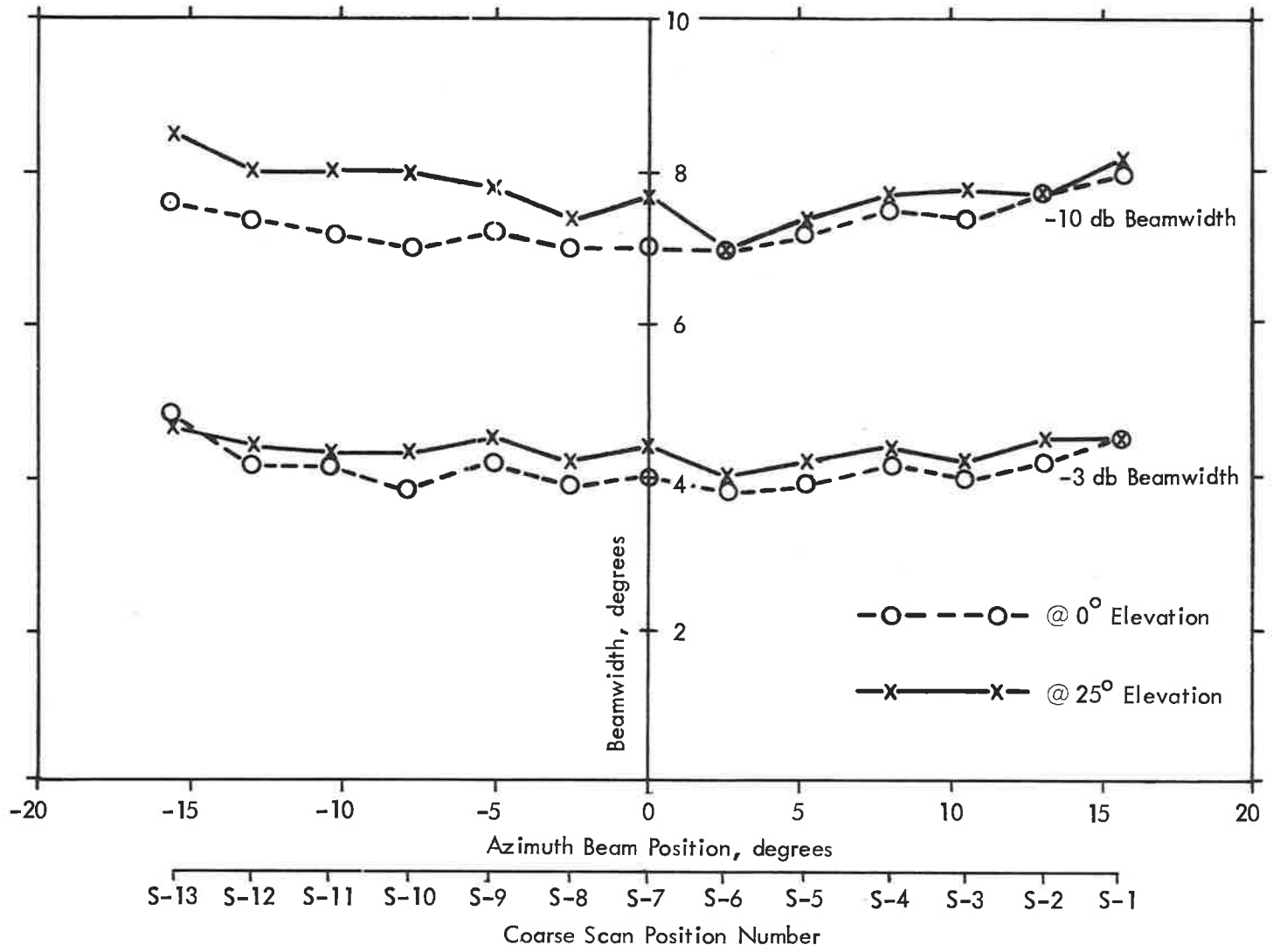

Figure 7.2.2 Array Azimuth Beamwidths versus Beam Position at 5.0 GHz

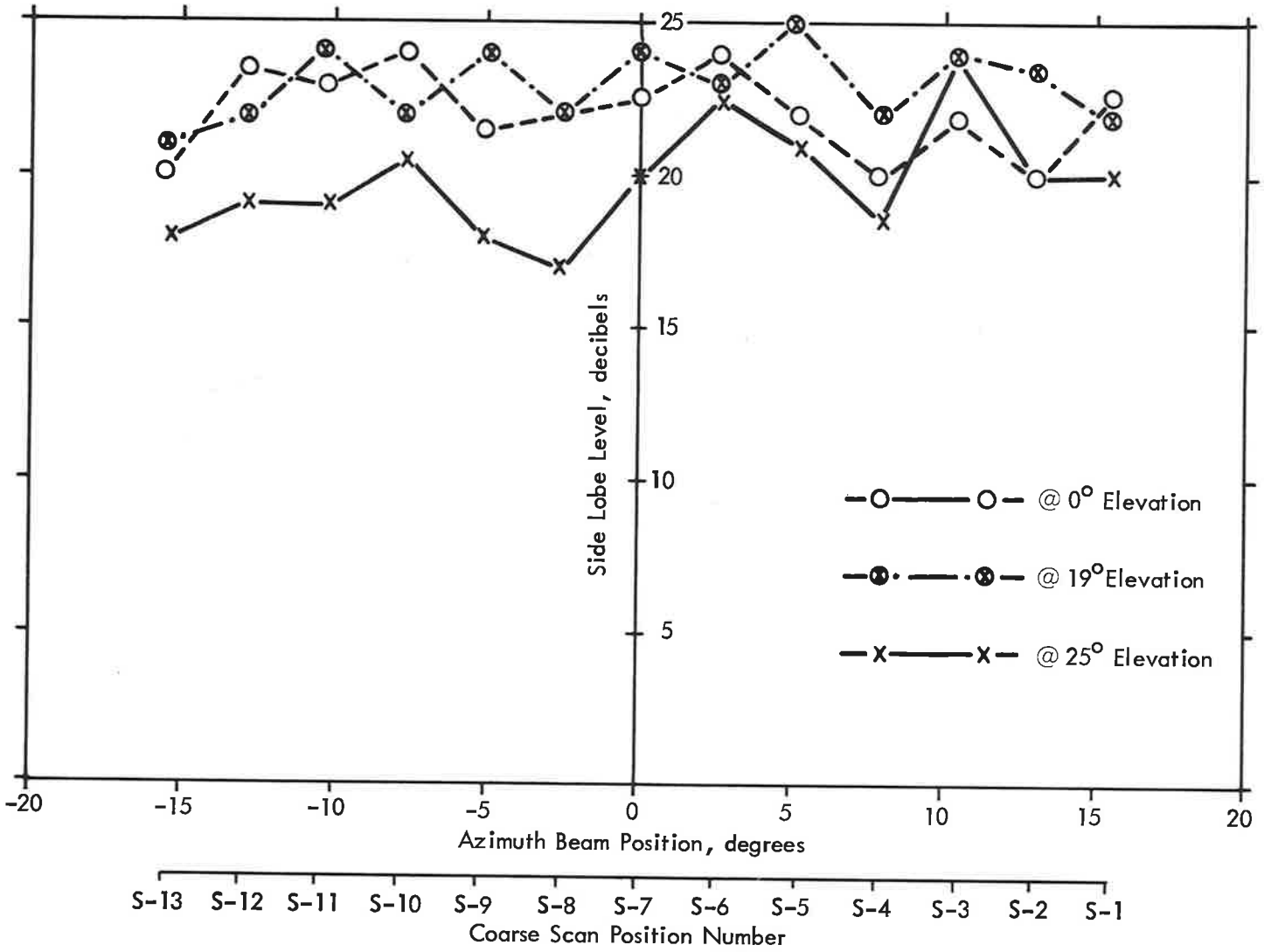

Figure 7.2.3 Array Azimuth Side Lobe Levels versus Beam Position at 5.0 GHz

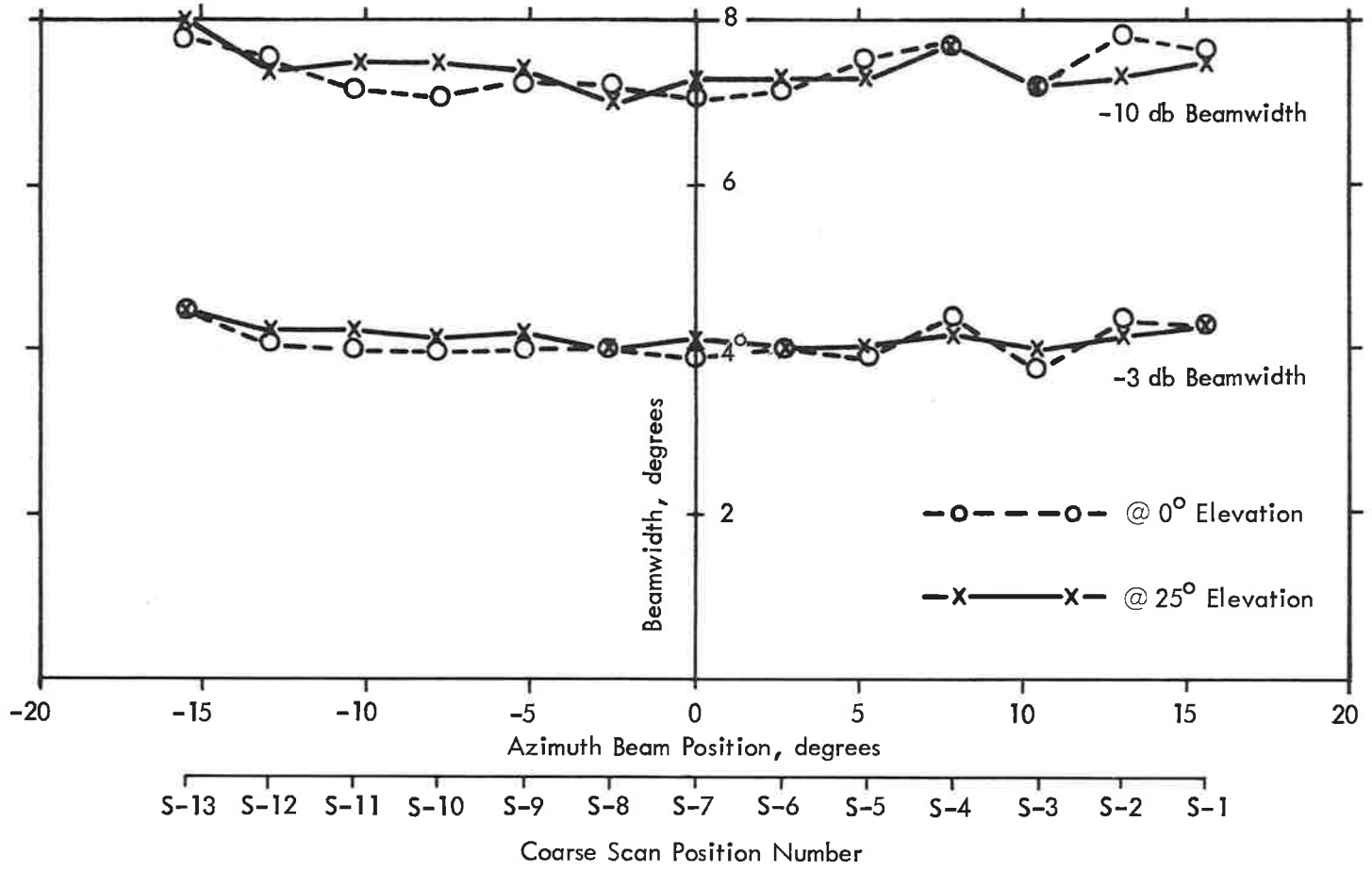

Figure 7.2.4 Array Azimuth Beamwidths versus Beam Position at 5.19 GHz

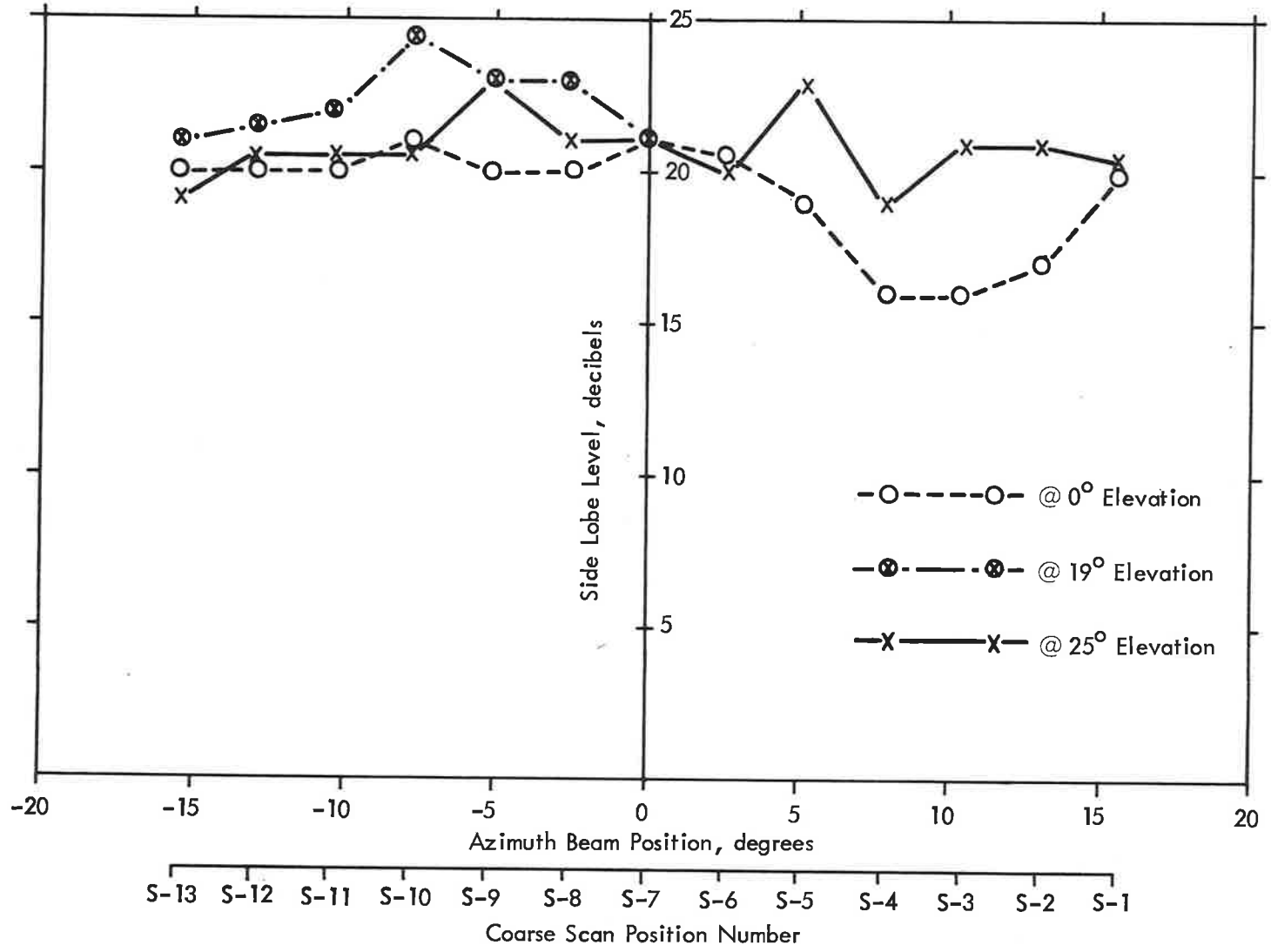

Figure 7.2.5 Array Azimuth Side Lobe Levels versus Beam Position at 5.19 GHz

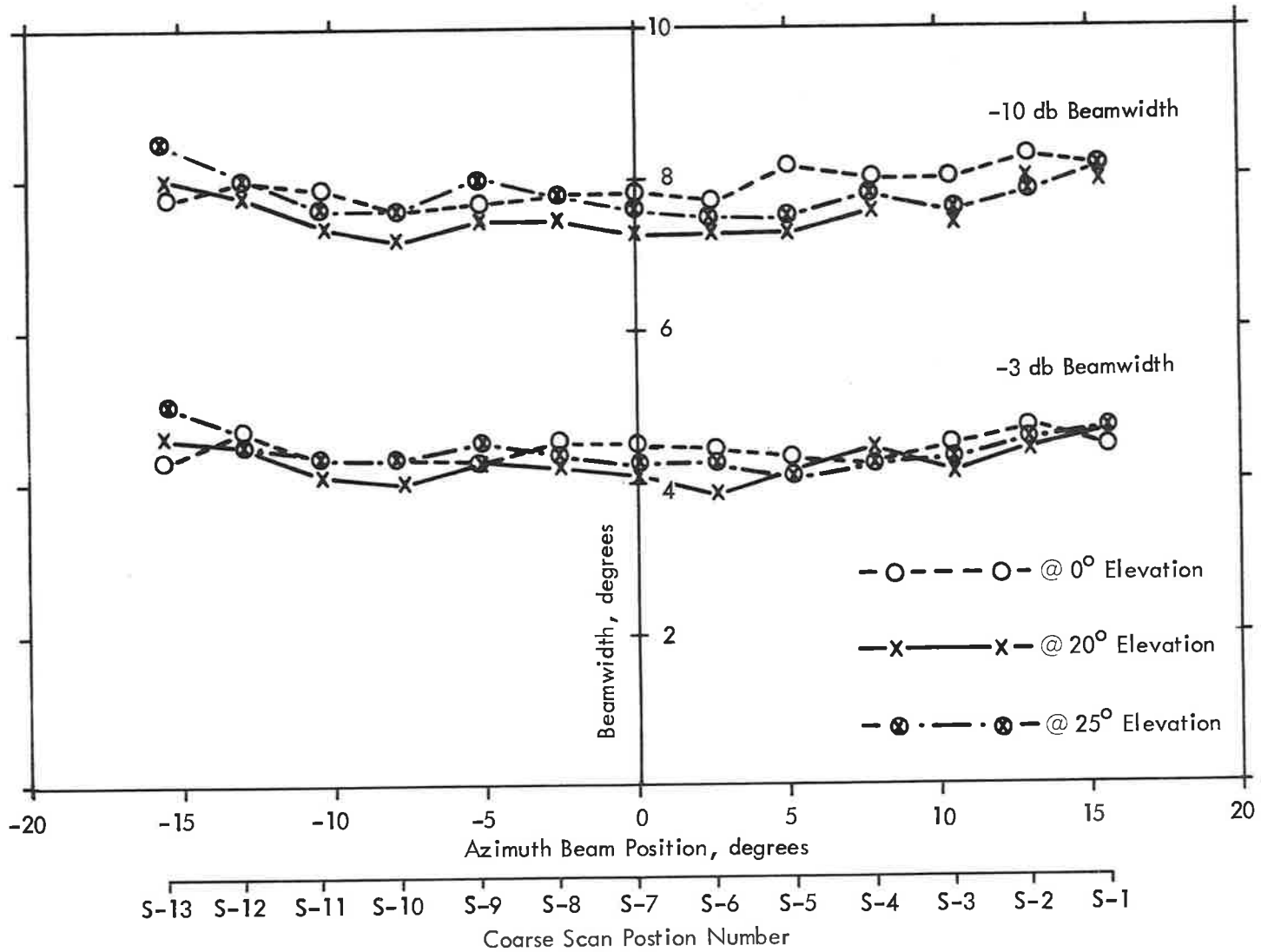

Figure 7.2.6 Array Azimuth Beamwidths versus Beam Position at 5.25 GHz

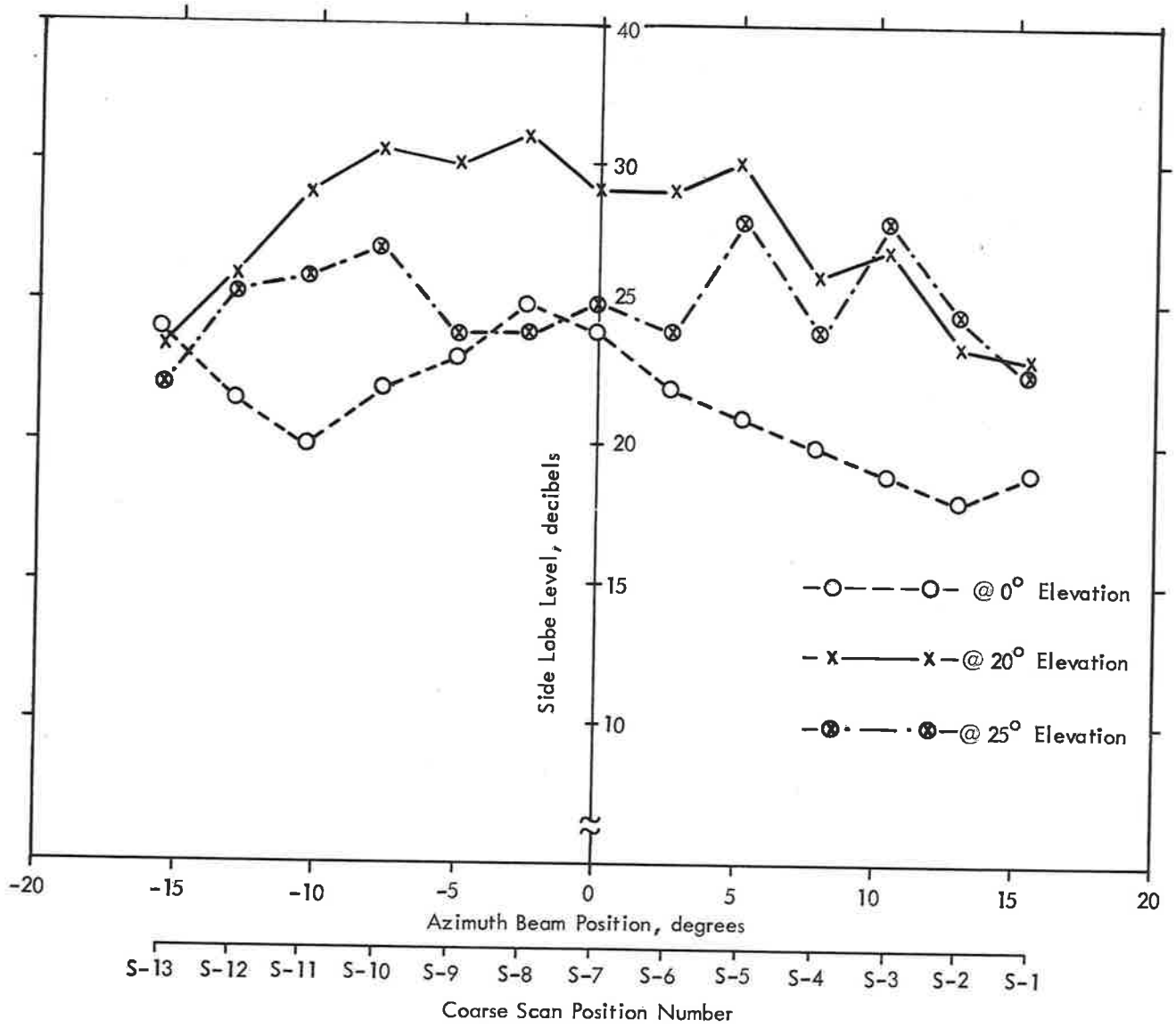

Figure 7.2.7 Array Azimuth Side Lobe Levels versus Beam Position at 5.25 GHz

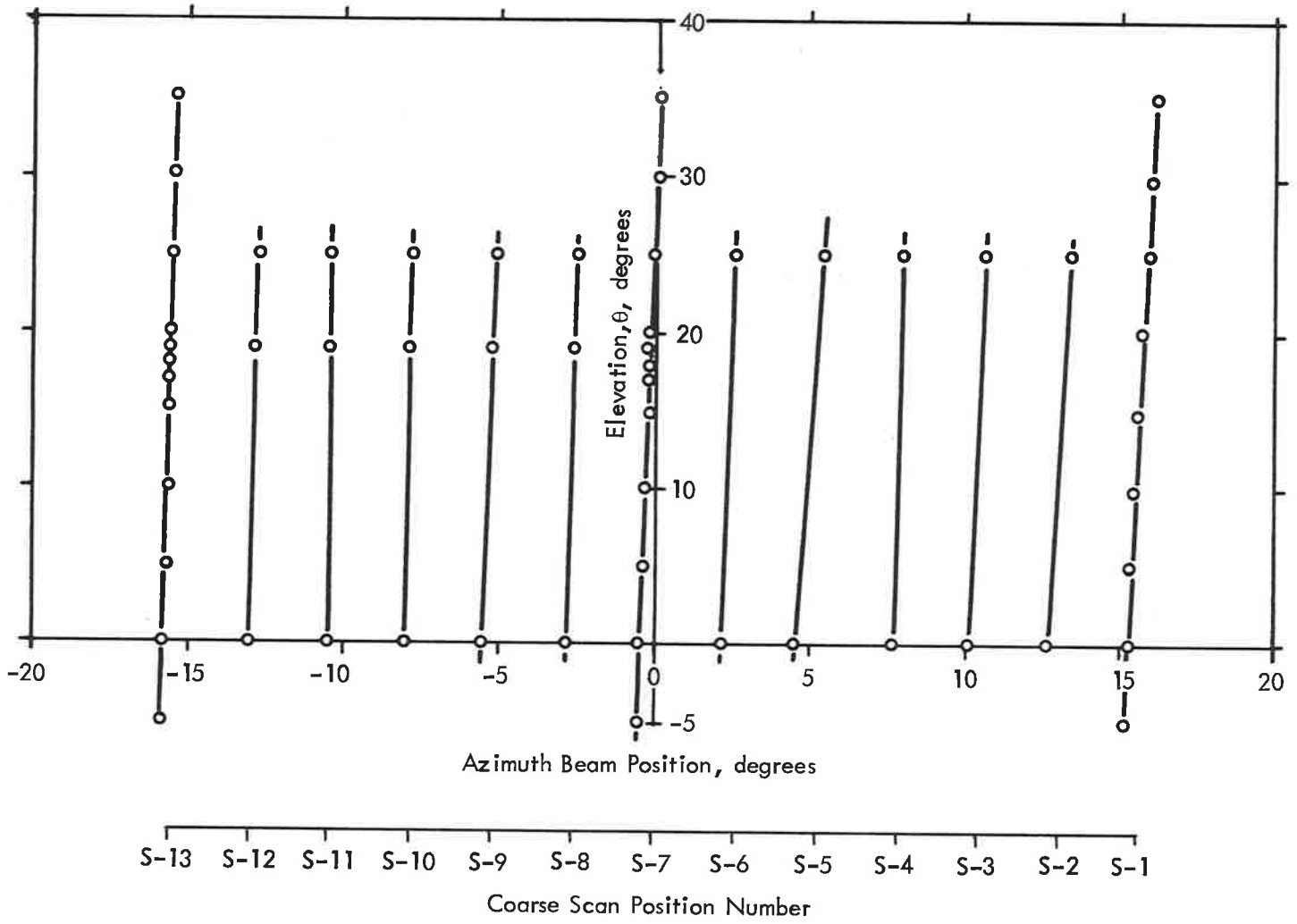

Figure 7.2.8 Measured Beam Position at Various Elevation Angles at 5.19 GHz

instead of 0°. Furthermore, since the radiating elements of the array are probes similar to the lens probes, the question arose whether a similar situation might not exist with reference to the array radius. In this case however the effective array radius would be 1/2" greater than the actual radius of the cylindrical reflector. If such were the case, the focus angle would be further increased to $\pm$19°.

7.2.2.2 Tests Performed and Results - Array azimuth patterns were taken at S-7 which is the 0° azimuth position where the effects of the reflector asymmetry would be minimal. (The antenna reflector is a half cylinder rather than a full cylinder). The patterns were taken at various values of the elevation angle and at very small increments of θ in the vicinity of θ=20°. Visual inspection of these data indicated that the array azimuth pattern at 19° elevation appeared to be the best focused. Criteria for determining this were depth of nulls, minimum beamwidth, and minimum side lobe level. Since these parameters tend to vary slowly in the vicinity of focus, a precise determination of θ_f is difficult. A quantitive measure which compares the ratio null depth to null beamwidth in the vicinity of focus appears to verify the value of θ =17°. However as Figure 7.2.9 indicates, this method is extremely sensitive to small errors in the vicinity of θ_f, because at focus the null depths approach infinity.

Attempts were subsequently made to refocus the antenna to 0° elevation by adjusting each of the output phase shifters. The values of the phase shift required to accomplish this were computed based on the assumption that the antenna was originally focused at 15° instead of 19°. With these values of phase shift, the focus angle θ_f would be changed from 19° to 15° instead of from 15° to 0° as had originally been planned. Array azimuth patterns were taken at various elevation angles to determine the elevation angle at which the antenna appeared to be in best focus. Visual inspection indicated that θ_f was indeed in the vicinity of 15°. Further verification was attempted by plotting the ratio of

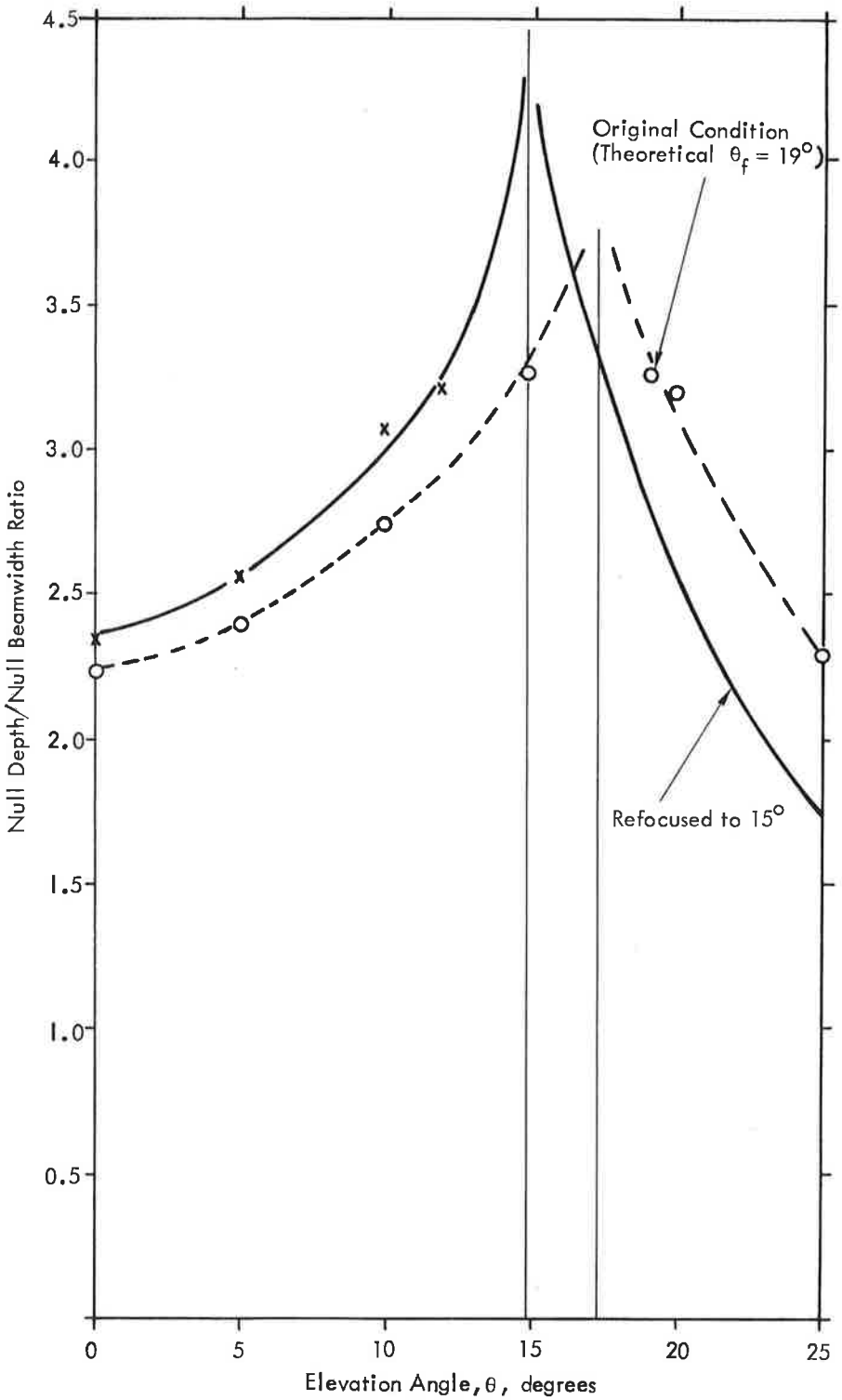

Figure 7.2.9 Null Depth/Null Beamwidth Ratio versus Elevation Angle

null depth and null beamwidth versus elevation angle θ. As shown in Figure 7.2.9, the plot appears to verify this value. Figure 7.2.10 and 7.2.11 are plots of beamwidth and side lobe levels respectively for the two different values of θ_f.

7.2.3 Phase Scanning Tests and Results

In order to show experimentally the skew that can occur when phase scanning even a cylindrical array, two phase scanned conditions were checked. The phase scanning was accomplished by adjusting the values of the output phase shifters in order to introduce the correct phase taper to scan the 0° azimuth beam or S-7 position. The first scan position was selected to show how well the antenna could "fine scan" to an intermediate position between two adjacent coarse beams, and to demonstrate that the skew for such a small interval would not be significant. Azimuth array patterns were taken at various elevation angles and the resulting data on beam position corrected to allow for the mechanical skew which was caused by the antenna tilt and which was mentioned in section 7.2.1.2. The corrected data is plotted in Figure 7.2.12. The resulting beam position agrees favorably with the position as calculated by the expression:

$$\sin \phi = \frac{\sin \phi_b}{\cos \theta}$$

where ϕ_b is the azimuth scan angle, at 0° elevation
θ is the elevation angle of interest
ϕ is the azimuth beam pointing angle seen at the elevation angle θ

The above formula applies to linear arrays but because the scanned angle was so small (ϕ_b = 1.15°) it was felt that this was a valid approximation.

The second scan position was one in which the 0° azimuth beam or S-7 position was phase scanned 17.45° from broadside. This would be sufficiently large so that an appreciable amount of skew could be observed. The data corrected for mechanical skew are

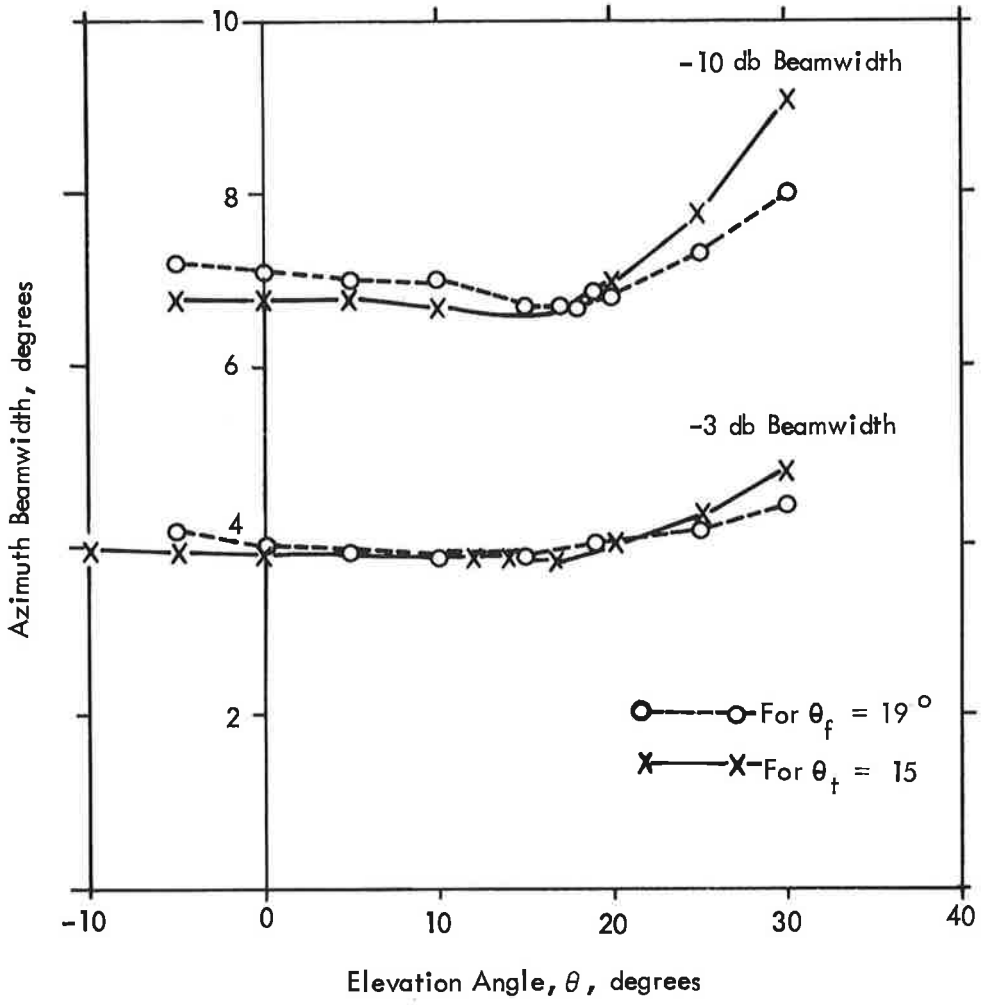

Figure 7.2.10 Beamwidth versus Elevation Angle of S-7 for Different Focus Angles

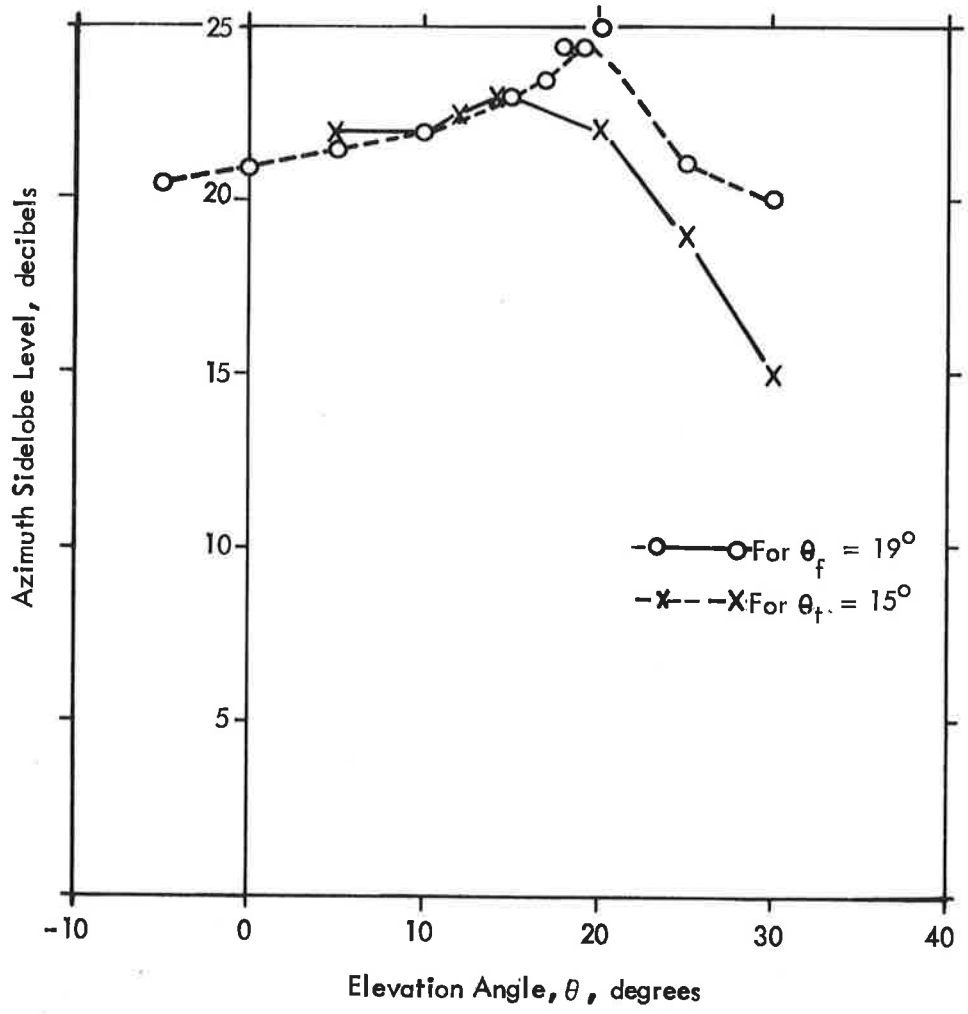

Figure 7.2.11 Side Lobe Level versus Elevation Angle of S-7 for Different Focus Angles

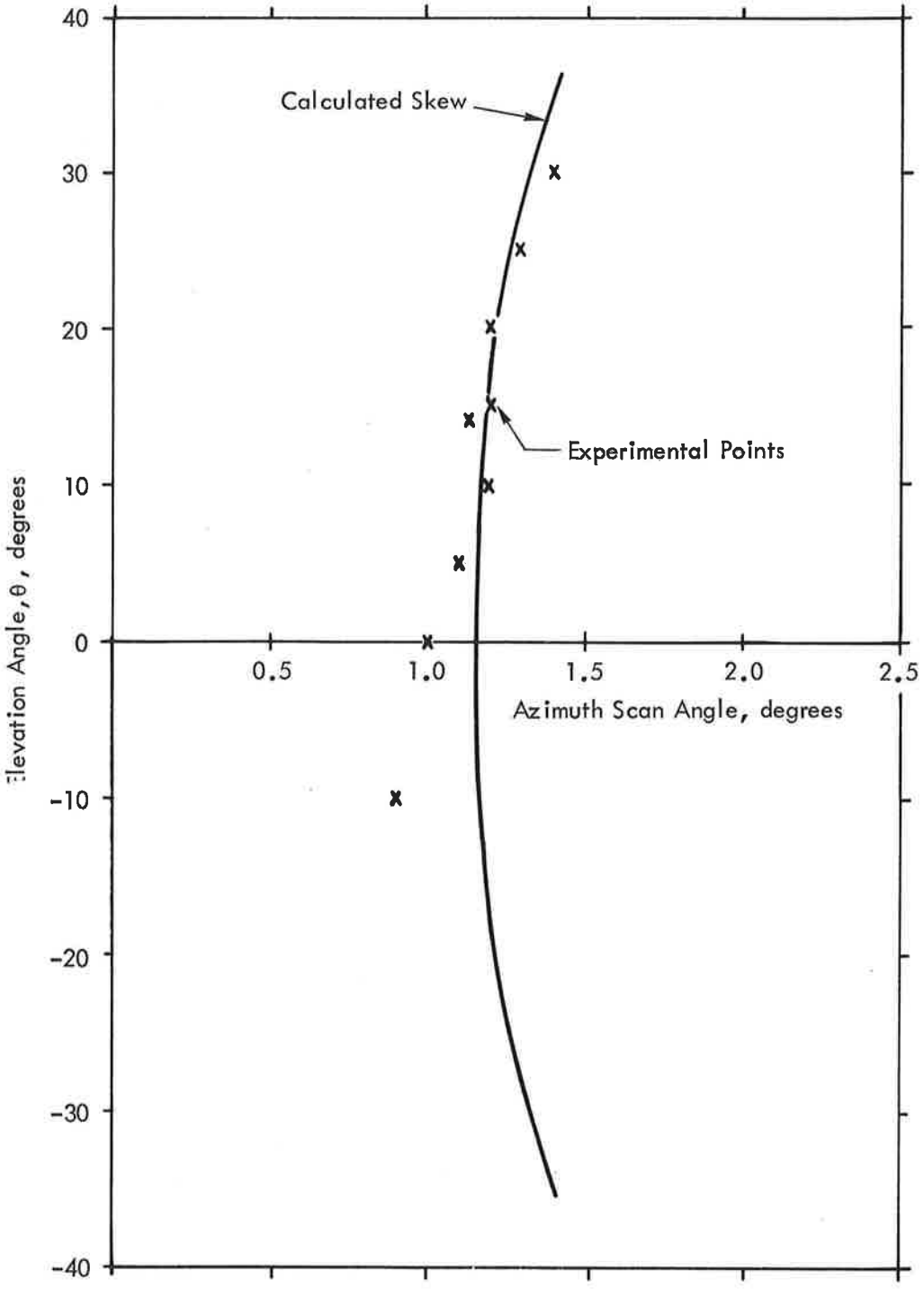

Figure 7.2.12 Beam Position versus Elevation Angle for an Azimuth Array Beam, Phase Scanned to + 1.15°

plotted in Figure 7.2.13.

Included on the same graph is the beam position as obtained from a series of computer calculated beam patterns of a cylindrical array which had been phase scanned to 17.45°. This was necessary to determine the theoretical beam position because no convenient formula exists for determining the beam peak at various elevation angles for a cylindrical array. In addition the theoretical beam position as calculated from the formula for a linear array is also plotted. It can be seen that for this particular phase scan condition, the linear array approximation holds, up to an elevation angle of about 15°.

7.2.4 Near-Field Refocusing Tests and Results

In order to determine the effects of near field refocusing on the far field radiation patterns two refocused antenna conditions were set-up. The output phase shifters were first adjusted to focus at D^2/λ and then after radiation patterns had been taken, readjusted to focus at D^2/λ for additional radiation patterns. For both conditions the values of phase shift required were computed for a frequency of 5.125 GHz and assuming that the antenna was originally focused at 15° instead of 19°. Azimuth array radiation patterns of S-7 were taken at various elevation angles. For the D^2/λ condition, the patterns were taken at 5.19 GHz and for the $D^2/2\lambda$ condition the patterns were taken at 5.0 GHz, and 5.25 GHz.

The patterns taken for the D^2/λ condition did not show the severe beam broadening associated with defocused antenna patterns. Some beam broadening did occur but it was not noticeable at the -3 dB or the -10 dB beamwidth levels. Furthermore the side lobe levels for this conditions were as good as the original focused condition. The beamwidth and sidelobe level data are summarized in Figures 7.2.14 and 7.2.15. Included for comparison is the data for the $\theta_f = 19°$ focused condition.

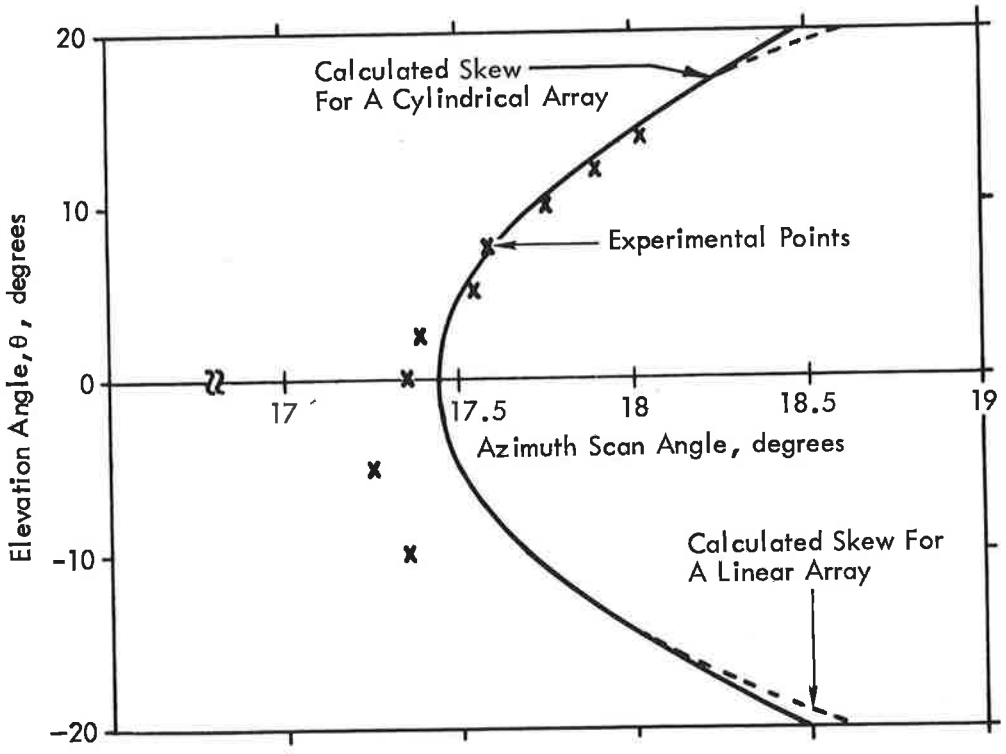

Figure 7.2.13 Beam Position versus Elevation Angle for an Azimuth Array Beam, Phase Scanned to +17.45°

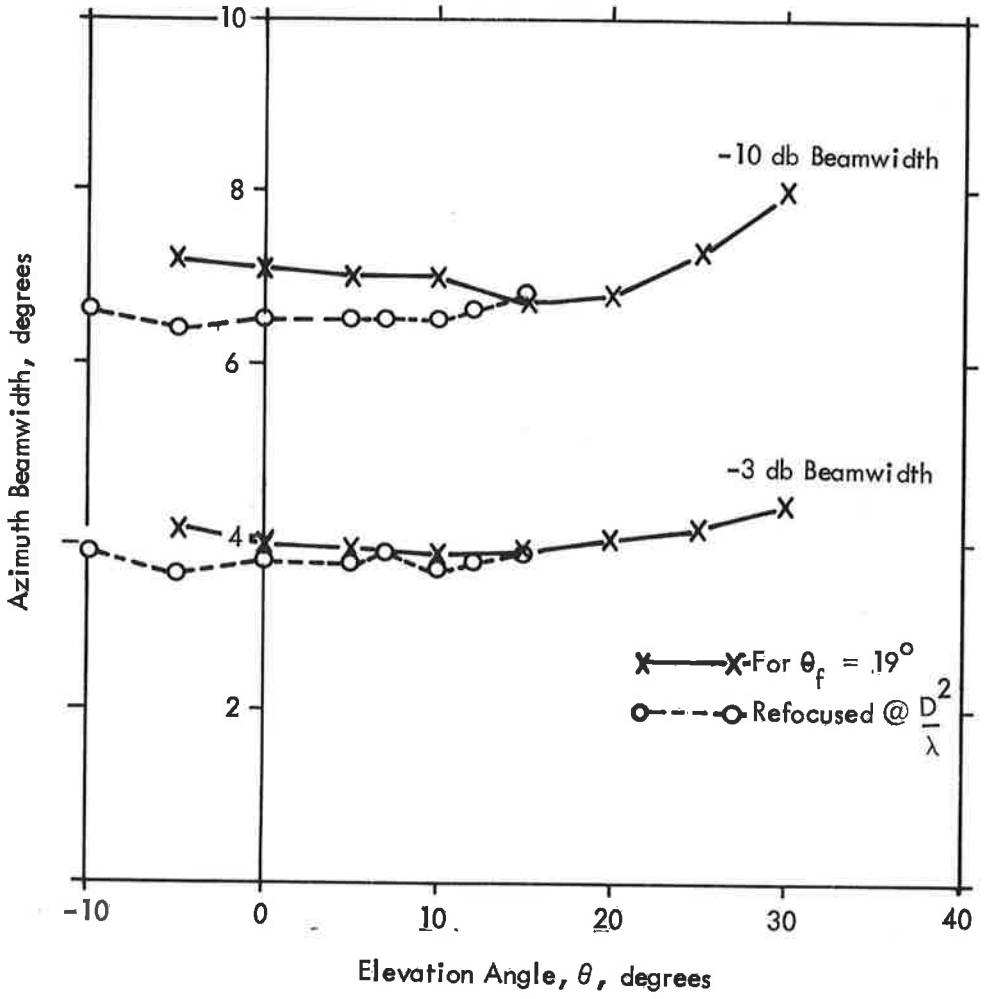

Figure 7.2.14 Array Azimuth Beamwidth versus Elevation Angle of S-7 at 5.19 GHz for the D^2/λ Refocused Condition

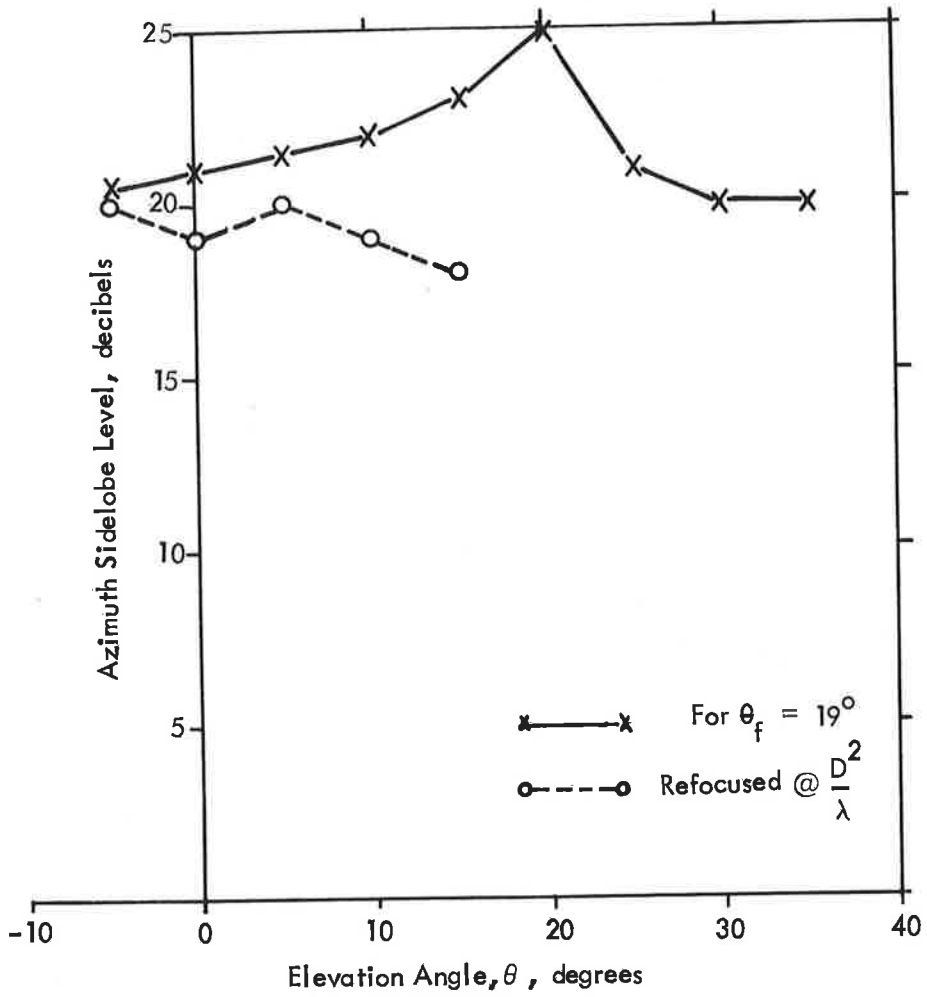

Figure 7.2.15 Array Azimuth Side Lobe Level versus Elevation Angle of S-7 at 5.19 GHz for the D^2/λ Refocused Condition

A possible explanation for these very slight effects on the radiation pattern could be the fact that the phase shifts required to refocus the antenna to D^2/λ were not too great and the resultant concave phase front was not much different from the phase front that would shift the focus to another elevation angle.

The patterns taken for the D^2/λ condition showed the effects of defocusing more markedly. There was considerable beam broadening caused by side lobes merging into the main lobe. However, if one disregards these "merged" sidelobes and considers only the "separated" lobes, the side lobe level is not too severe. Typical refocused antenna patterns are shown in Figures 7.2.16 through 7.2.18.

7.3 DISCUSSION OF THE ANTENNA TEST RESULTS

ABSTRACT

Analysis of the test data taken on the R-2R Lens fed cylindrical array verified that this type of antenna can be used to coarse scan a planar beam over wide angular sectors. Fine scanning is accomplished by the use of output phase shifters. The maximum skew introduced by this method was 0.05°. The measured gain of 13.85 dB compares favorably with the gain calculated by subtracting the antenna losses from the directive gain.

The R-2R Lens fed cylindrical array antenna tests served to verify experimentally those features which made it a possible choice for the azimuth antenna in the Microwave Landing System. The cylindrical array is capable of producing planar beams for the coarse beam scanning functions. The use of phase scanning for fine steering the beam between two adjacent coarse positions is feasible. The measured maximum value of skew caused by fine scanning this particular antenna amounted to 0.05° over the elevation range 0° to 20°. In terms of percentage beamwidth, this amounts to approximately 1.25% of the 3 dB beamwidth.

Since skew is symmetrical in elevation around 0°, this maximum value can be reduced by adjusting the phase shifters so that ϕ_b occurs at some intermediate elevation angle θ_i instead of 0°.

Figure 7.2.16 Typical Array Azimuth Pattern of S-7 at 5.0 GHz for the D^2/λ Refocused Condition

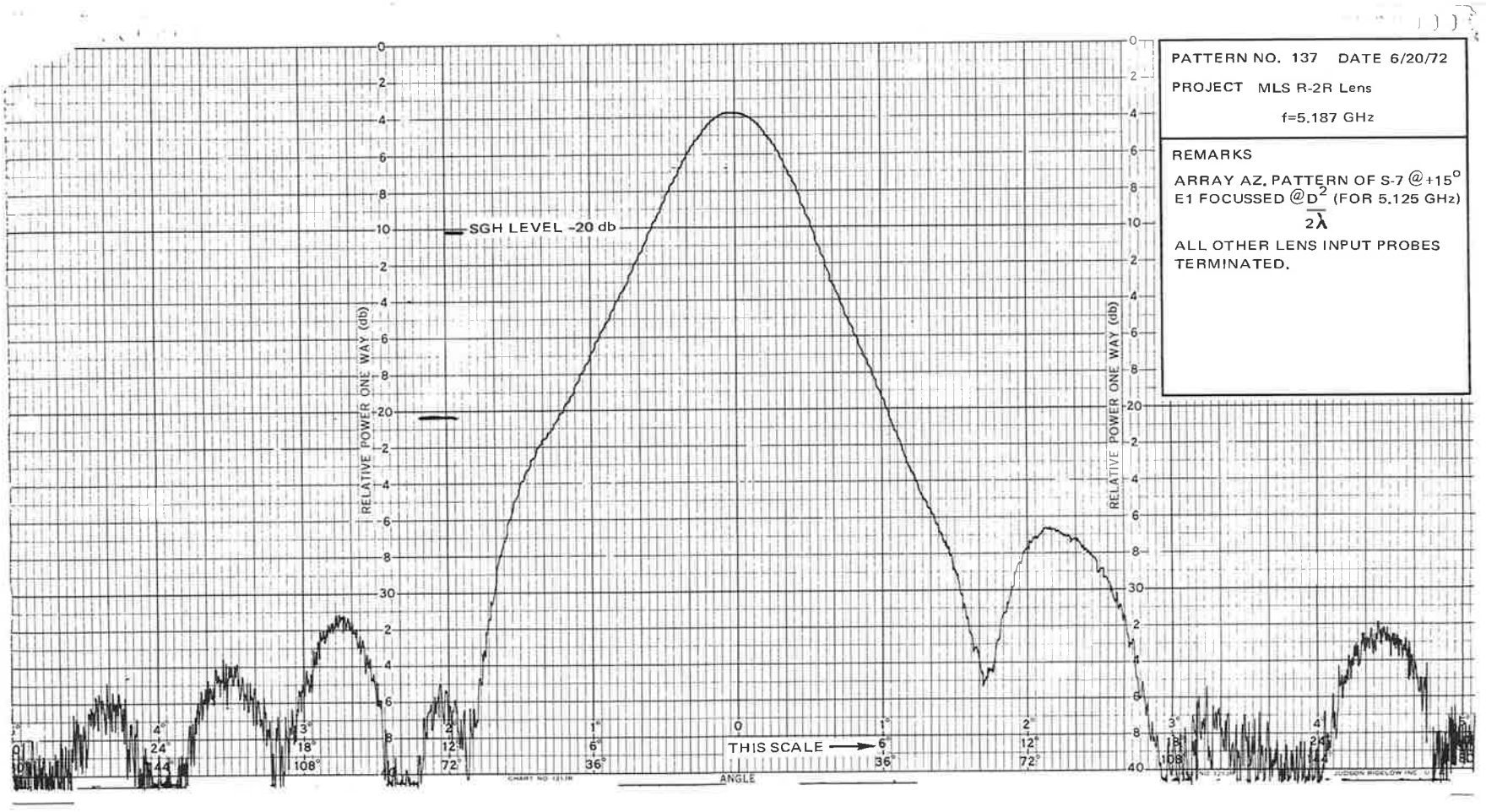

Figure 7.2.17 Typical Array Azimuth Pattern of S-7 at 5.19 GHz for the D^2/λ Refocused Condition

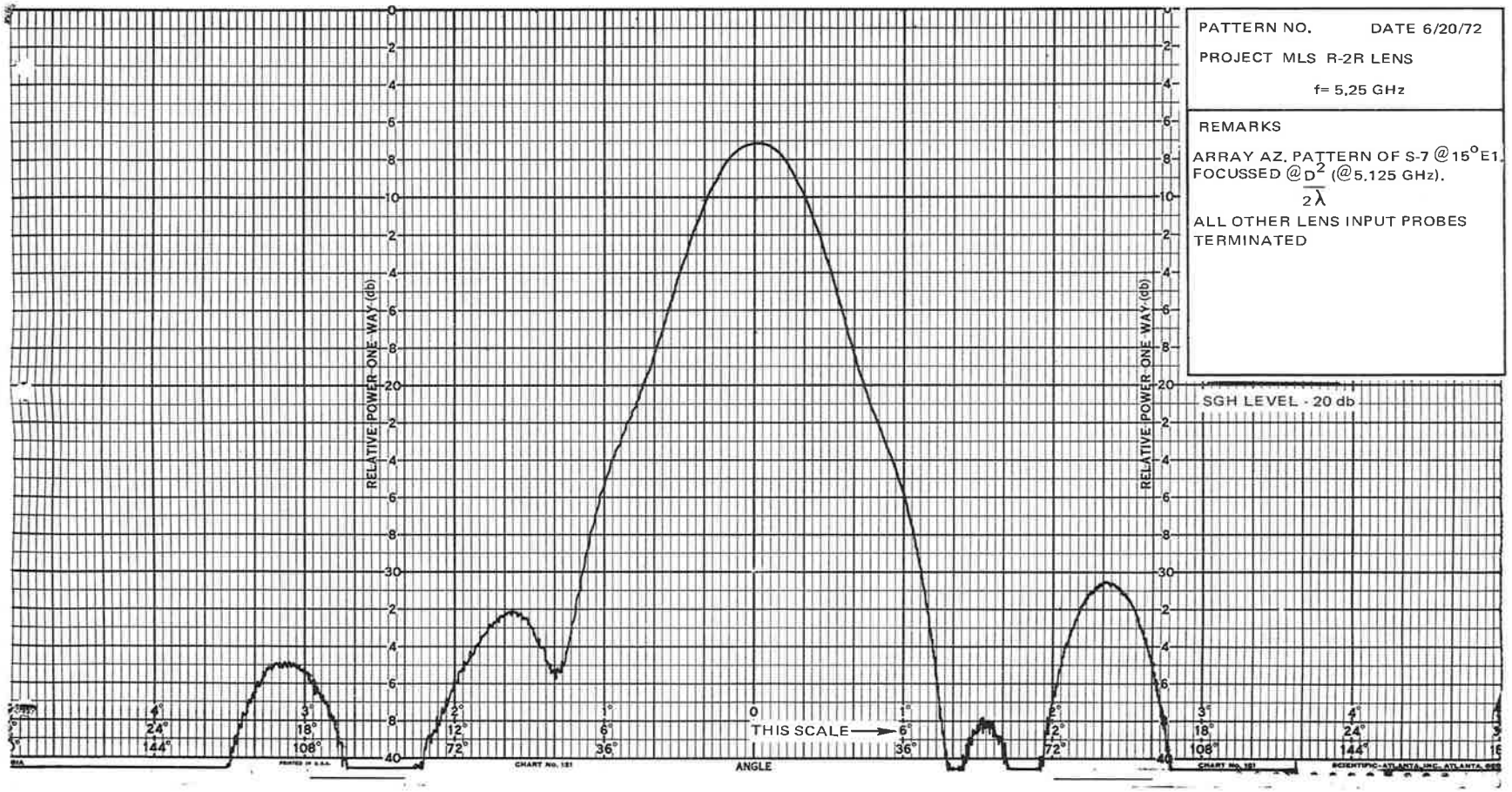

Figure 7.2.18 Typical Array Azimuth Pattern of S-7 at 5.25 GHz for the D^2/λ Refocused Condition

This allows one to select an elevation angle in order to reduce the maximum skew in a given elevation sector. The experimentally determined values of skew for the cylindrical array agree favorably with the calculated values, and for small scan angles is equal to the skew of a linear array. Furthermore, for small values of elevation angle (i.e., 15°) the linear array approximation can be applied to cylindrical arrays for computing the skew out to scan angles of $\pm 20°$ from broadside.

The use of the R-2R Lens as a possible feed for a cylindrical array was proved feasible. Two design problems with this feed system were observed and briefly studied. The first of these is the requirement of the lens input probes be always "matched" even when switched "off".

The second is the need for knowing the exact location of the radiation phase center of the probes in the lens cavity, and of the radiating elements on the array. This is necessary because the R-2R constraint on the lens radius and array radius is based on distances measured from the respective phase center, which are not necessarily the same as the mechanical radii. Errors in this area will result in the antenna to focus at some elevation angle. The relationship is a simple one and is given by:

$$\frac{2R_L}{R_A} = \cos \theta_f$$

where R_L = the effective radius of the lens
R_A = the effective radius of the array
θ_f = elevation focus angle

The results of the array pattern measurements appear to indicate that the elevation focus angle θ_f lies in the vicinity of 17° to 19°. This is consistent with the theoretical value of 17° but is

at variance with the 19° obtained by visually comparing the patterns in the vicinity of θ_f. Lack of time prevented further experimentation in this area.

With reference to the general antenna performance characteristics, the beamwidth and side lobe levels indicated that the design goals had been met reasonably well.

The measured -3 dB and -10 dB beamwidths agreed very well with the predicted values of 4.25° and 7.55° respectively. The average maximum side lobe levels at the three frequencies investigated were 23dB, were obtained from azimuth patterns taken at various elevation angles θ. The 27 dB average side lobe level was obtained at θ = 19° which is near the elevation focus angle and agrees very well with the theoretical design goal of 26.5 dB. The reason for the difference between experimental and theoretical side lobe levels at other two frequencies is not known but it is believed that the reason lies with the elevation focus problem. The limited range time available to us prevented further experimentation in this area.

The gain reading derived from standard gain horn measurements and plotted in Figure 7.2.1 for 5.19 GHz show excellent agreement between the relative values obtained at the various elevation angles and the elevation pattern contour as recorded on the chart in that figure. Furthermore if one calculates the directive gain by considering the -3 dB beamwidths in the two principal planes and subtracts the losses in the system there is also very good agreement. This calculation is included below together with a tabulation of the losses.

Elevation B.W. @ -3 dB 18°

Azimuth B.W. @ -3 dB 4°

$\frac{27000}{72} = 375$

10 log 375 = 25.74 = Directive Gain

Insertion Loss Budget for Lens Fed Cylindrical Array

1:4 Power Divider	0.8 dB
Mechanical Phase Shifter	0.5 dB
Mechanical Attenuator	5.0 dB
2x2 Transfer Switch	1.1 dB
SP4T Switch	1.6 dB
Lens	1.0 dB
Mechanical Phase Shifter	0.5 dB
Element VSWR	0.2 dB
Input Cable Loss	0.4 dB
Output Cable Loss	0.6 dB
	11.7 dB = TOTAL LOSSES

Directive Gain - Losses = Antenna Gain

25.74 - 11.7 = 14.07 dB

Gain obtained from comparison with Standard Gain Horn (Figure 7.2.1) = 13.85 dB

The near field refocused patterns served to verify experimentally the general far field pattern deterioration associated with defocused antennas.